An Introduction to Dynamic Meteorology

Fifth Edition

An Introduction to Dynamic Meteorology

Fifth Edition

James R. Holton
Gregory J. Hakim

ELSEVIER

AMSTERDAM • BOSTON • HEIDELBERG • LONDON
NEW YORK • OXFORD • PARIS • SAN DIEGO
SAN FRANCISCO • SINGAPORE • SYDNEY • TOKYO
Academic Press is an imprint of Elsevier

Academic Press is an imprint of Elsevier
225 Wyman Street, Waltham, MA 02451, USA
The Boulevard, Langford Lane, Kidlington, Oxford, OX5 1GB, UK

Library of Congress Cataloging-in-Publication Data

Holton, James R., and Hakim, Gregory J., authors.
An introduction to dynamic meteorology.—Fifth edition / Gregory J. Hakim.
pages cm
Includes bibliographical references and index. Revision of Fourth edition by Holton.
ISBN 978-0-12-384866-6 (hardback)
1. Dynamic meteorology. I. Title.
QC880.H65 2012
551.51'5—dc23 2012022179

British Library Cataloguing-in-Publication Data

A catalogue record for this book is available from the British Library.

For information on all Academic Press publications
visit our website at *http://store.elsevier.com*

Printed in the United States
12 13 14 15 16 10 9 8 7 6 5 4 3 2 1

Dedication

To the memory of James R. Holton (1938–2004)

Preface

When Jim Holton was making revisions for the Fourth Edition of this book, I served as a consultant on aspects of the material with which I was most familiar. Toward the end of the revision process, Jim asked whether I would like to join him as a coauthor for the next edition. Although I agreed to this wonderful opportunity and looked forward to the collaboration, it vanished when Jim Holton died on March 3, 2004. The shock of his sudden passing lingers in the dynamic meteorology community, where his influence is difficult to exaggerate. That sphere of influence includes this book on dynamic meteorology, which has served as the standard text on the subject for generations of students and practitioners in the atmospheric and related sciences. It was very difficult to take up revisions without Jim's guidance, but the situation also presented an opportunity to bring a fresh perspective to aspects of the material that had become dated, tracing their origin to lecture notes from classes taught at MIT during the 1960s.

This book serves three main communities: undergraduate and graduate students in the atmospheric sciences, practitioners in the field, and those in related physical sciences who want a definitive, and accessible, introduction to the subject matter. In making revisions, I have tried to draw on my experiences with the book as both a student and an instructor, to streamline and modernize aspects of the text to serve these communities. Major structural changes include Chapter 5 (on waves and the perturbation method, formerly Chapter 7), Chapter 7 (on baroclinic development, formerly Chapter 8), and Chapter 8 (on turbulence and the planetary boundary layer, formerly Chapter 5). The material now flows from the introduction of core concepts (Chapters 1–4) to the development of methods needed to understand the application of core concepts (Chapter 5) to understanding extratropical weather systems (Chapters 6 and 7), followed by advanced topics in later chapters.

In addition to numerous minor changes, specific substantial revisions include the following. In Chapter 1, the treatment of viscous effects and noninertial reference frames is streamlined, and a new section on kinematics is introduced. New sections in Chapter 2 are devoted to the Boussinesq approximation and thermodynamics of the moist atmosphere, which are used in several chapters later in the book. Potential vorticity (PV) is given an expanded treatment in Chapter 4, including a derivation of the Ertel PV as a special case of the Kelvin circulation theorem, a discussion of nonconservative effects, and an illustration of the use of PV to construct maps of the dynamical tropopause. Moreover, PV is used to motivate a derivation of the shallow-water and barotropic equations, which are used extensively in later chapters. In Chapter 5, the discussion of basic wave properties is extended to three dimensions, and a general strategy for solving wave problems is outlined. Stationary Rossby wave solutions are now discussed for both shallow-water and stratified atmospheres at rest, providing the reader with a deeper understanding of the basis for the quasi-geostrophic approximation that follows in the next chapter.

Chapter 6 is largely rewritten, with a novel, and simple, derivation of the quasi-geostrophic equations starting from the Ertel PV conservation equation. In contrast to previous editions, here standard height coordinates are used, which liberates the reader from the mental gymnastics associated with pressure coordinates. A MATLAB code for a quasi-geostrophic model is provided, along with a diagnostic package that allows the reader to simulate and diagnose extratropical weather systems; these codes are easily adapted for flow patterns different from those provided. Baroclinic development is covered in Chapter 7; the treatment is largely the same as in previous editions but offers a richer discussion of "generalized stability." Chapter 9 contains updated information on hurricanes, including a full derivation and discussion of potential intensity theory. A new section in Chapter 10 reviews climate sensitivity and feedbacks, which is a subject of increasing interest in the research community. Finally, Chapter 13 has been revised significantly to include a mathematical treatment of data assimilation, building up from simple examples for scalars to many variables. Kalman filters, variational techniques (3DVAR and 4DVAR), and ensemble Kalman filters are discussed. A new section reviews predictability and ensemble forecasting, including the Liouville equation and primary results on the theory of ensemble prediction. For other information about, and teaching aids for, this book, see booksite.academicpress.com/9780123848666.

I would like to thank Margaret Holton for her friendship and support in undertaking this project. Dale Durran and Cecilia Bitz maintained an excellent errata for the Fourth Edition, which was helpful when working on this revision. I am grateful to the following individuals for offering comments and suggestions on early chapter drafts: Hanin Binder, Bonnie Brown, Dale Durran, Luke Madaus, Max Menchaca, Dave Nolan, Ryan Torn, and Mike Wallace. Errors that remain are mine alone, and I would appreciate hearing about them at holton.hakim@gmail.com.

Greg Hakim
Seattle, WA

Chapter 1

Introduction

1.1 DYNAMIC METEOROLOGY

Dynamic meteorology is the study of air motion in the Earth's atmosphere that is associated with weather and climate. These motions organize into coherent circulation features that affect human activity primarily through wind, temperature, clouds, and precipitation patterns. Short-lived features, lasting from a few minutes to a few days, are related to weather, and some familiar weather examples that we will examine in this book include tropical and extratropical cyclones, organized thunderstorms, and local wind patterns such as those that occur near mountains. Figure 1.1 illustrates the mixing effect of larger weather patterns in the atmosphere, from large areas of convective cloud in the tropics to extratropical cyclones in the higher latitudes of the Northern and Southern Hemispheres. These weather elements occur in the *troposphere*, which is the portion of the atmosphere in contact with the surface. The troposphere normally exhibits a drop in temperature with elevation and contains most of the water vapor, clouds, and precipitation found in the atmosphere. On average, the troposphere extends vertically about 10 kilometers, where the *tropopause* is located. Above the tropopause is the stratosphere, where the temperature increases with elevation due to heating of the air by absorption of ultraviolet radiation by ozone. Most of the topics addressed in this book concern the dynamics of the troposphere and stratosphere.

Over longer time periods, the realm of climate, circulation features may persist from seasons to years over large regions of Earth. Examples of climate variability include shifts in the locations where storms occur, oscillations in large-scale pressure patterns, and planetary patterns of variability associated with the El Niño Southern Oscillation (ENSO) phenomenon of the tropical Pacific Ocean. ENSO reminds us that although dynamic meterology involves the study of air motion in the atmosphere, this motion links to other parts of Earth's system, including the oceans, biosphere, and cryosphere, and plays an active role in the transport of chemical species. Moreover, many of the ideas we present here also apply to the atmospheres of other planets.

Before we set off to explore the landscape of dynamic meteorology, we devote this first chapter to introducing fundamental concepts that will guide the

An Introduction to Dynamic Meteorology. DOI: 10.1016/B978-0-12-384866-6.00001-5

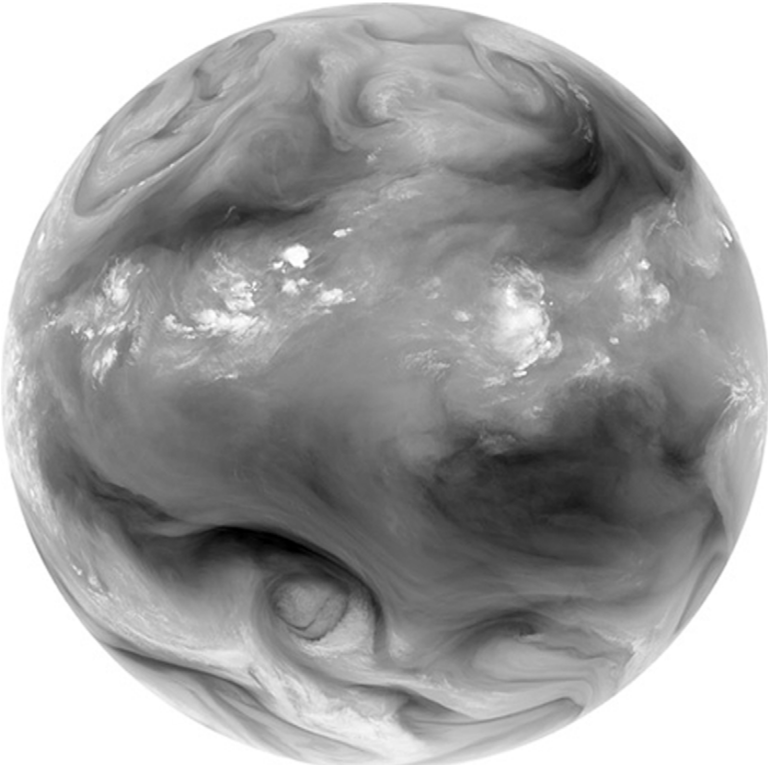

FIGURE 1.1 Infrared satellite image near a wavelength of 6.7 μm, which is known as the "water vapor" channel since it captures the distribution of that field in a layer roughly 5 to 10 km above Earth's surface. Because water vapor is continuously distributed, in contrast to clouds, atmospheric motion is especially well captured. Here we see the convective clouds in the tropics and the mixing effects of eddies at higher latitude. (*Source: NASA.*)

journey. First, note that the laws that govern atmospheric motion satisfy the principle of *dimensional homogeneity*, which means that all terms in the equations expressing these laws must have the same physical dimensions. These dimensions can be expressed in terms of multiples and ratios of four dimensionally independent properties: length, time, mass, and thermodynamic temperature. To measure and compare the scales of terms in the laws of motion, a set of units of measure must be defined for these four fundamental properties. In this text the international system of units (SI) will be used almost exclusively. The four fundamental properties are measured in terms of the SI *base units* shown in Table 1.1. All other properties are measured in terms of SI *derived units*, which are units formed from products or ratios of the base units. For example, velocity has the derived units of meter per second (m s^{-1}).

TABLE 1.1 SI Base Units

Property	Name	Symbol
Length	Meter (meter)	m
Mass	Kilogram	kg
Time	Second	s
Temperature	Kelvin	K

TABLE 1.2 SI Derived Units with Special Names

Property	Name	Symbol
Frequency	Hertz	$\mathrm{Hz(s^{-1})}$
Force	Newton	$\mathrm{N(kg\ m\ s^{-2})}$
Pressure	Pascal	$\mathrm{Pa(N\ m^{-2})}$
Energy	Joule	J (N m)
Power	Watt	$\mathrm{W(J\ s^{-1})}$

A number of important derived units have special names and symbols. Those that are commonly used in dynamic meteorology are indicated in Table 1.2. In addition, the supplementary unit designating a plane angle, the radian (rad), is required for expressing angular velocity (rad s^{-1}) in the SI system.[1] Finally, Table 1.3 lists the symbols frequently used in this book for some of the basic physical quantities. Note that the full three-dimensional velocity vector, $\mathbf{U}$, is related to the horizontal velocity vector, $\mathbf{V}$, by $\mathbf{U} = (\mathbf{V}, w)$ and $\mathbf{U} = (\mathbf{V}, \omega)$ in height and pressure vertical coordinates, respectively. We shall use the term "zonal" to refer to the East–West direction and "meridional" to refer to the North–South direction.

Dynamic meteorology applies the conservation laws of classical physics for momentum (Newton's laws of motion), mass, and energy (First law of thermodynamics) to the atmosphere. An essential aspect of this application involves the *continuum* approximation, whereby the properties of discrete molecules are ignored in favor of a continuous representation involving a local average over a blob of molecules. This approximation is common to all fluids, including liquids and gases, and allows atmospheric properties (e.g., pressure, density, temperature), or "field variables," to be represented as smooth functions taking on unique values

[1]Note that *Hertz* measures frequency in *cycles* per second, not in radians per second.

TABLE 1.3 Symbols and Units of Basic Physical Quantities

Quantity	Symbol	Units
Three-dimensional velocity vector	$\mathbf{U}$	$\mathrm{m\ s^{-1}}$
Horizontal velocity vector	$\mathbf{V}$	$\mathrm{m\ s^{-1}}$
Eastward component of velocity	u	$\mathrm{m\ s^{-1}}$
Northward component of velocity	v	$\mathrm{m\ s^{-1}}$
Upward component of velocity	w (ω)	$\mathrm{m\ s^{-1}}$ ($\mathrm{Pa\ s^{-1}}$)
Pressure	P	$\mathrm{N\ m^{-2}}$
Density	ρ	$\mathrm{kg\ m^{-3}}$
Temperature	T	K (or °C)

in the independent variables of space and time. A "point" in the continuum is regarded as a volume element that is very small compared with the volume of atmosphere under consideration, but that still contains a large number of molecules. The expressions *air parcel* and *air particle* are both commonly used to refer to such a point. In Chapter 2, the fundamental conservation laws are applied to a small volume element of the atmosphere subject to the continuum approximation in order to obtain the governing equations. Our goal here is to provide a survey of the main forces that influence atmospheric motions.

1.2 CONSERVATION OF MOMENTUM

Newton's first law states that an object at rest or moving with a constant velocity remains so unless acted upon by an external unbalanced force. Once the forces are identified, Newton's second law states that the temporal change of momentum (i.e., acceleration) is a vector having direction given by the net force (the sum over all forces) and magnitude given by the size of the net force divided by the object's mass. These forces can be classified as either *body forces* or *surface forces*. Body forces act on the center of mass of a fluid parcel and have magnitudes proportional to the mass of the parcel; gravity is an example of a body force. Surface forces act across the boundary surface separating a fluid parcel from its surroundings and have magnitudes independent of the mass of the parcel; the pressure force is an example.

For atmospheric motions of meteorological interest, the forces that are of primary concern are the pressure gradient force, the gravitational force, and the frictional force. These *fundamental* forces determine acceleration as measured relative to coordinates fixed in space. If, as is the usual case, the motion is referred to a coordinate system rotating with Earth, Newton's second law may still be applied provided that certain *apparent* forces, the centrifugal force and the Coriolis force, are included. The fundamental forces are discussed subsequently, and the apparent forces are introduced in Section 1.3.

1.2.1 Pressure Gradient Force

Pressure is defined as the force per unit area acting normal to a surface. In a gas such as the atmosphere, pressure at a point acts equally in all directions due to random molecular motion. Therefore, the magnitude of the net force due to molecules colliding with a surface is independent of the orientation of the surface; note that the *direction* of the net force changes with the orientation of the surface, but the magnitude does not. Placing a wall in a gas, with the pressure on one side different from that on the other, yields a net force that will accelerate the wall toward the side having lower pressure; this net force associated with pressure differences is the essence of the pressure *gradient* force.

Consider now an infinitesimal volume element of air, $\delta V = \delta x \delta y \delta z$, centered at the point x_0, y_0, z_0, as illustrated in Figure 1.2. Due to random molecular motions, momentum is continually imparted to the walls of the volume element by the surrounding air. This momentum transfer per unit time per unit area is just the pressure exerted on the walls of the volume element by the surrounding air. If the pressure at the center of the volume element is designated by p_0, then the pressure on the wall labeled A in Figure 1.2 can be expressed in a Taylor series expansion as

$$p_0 + \frac{\partial p}{\partial x}\frac{\delta x}{2} + \text{higher-order terms}$$

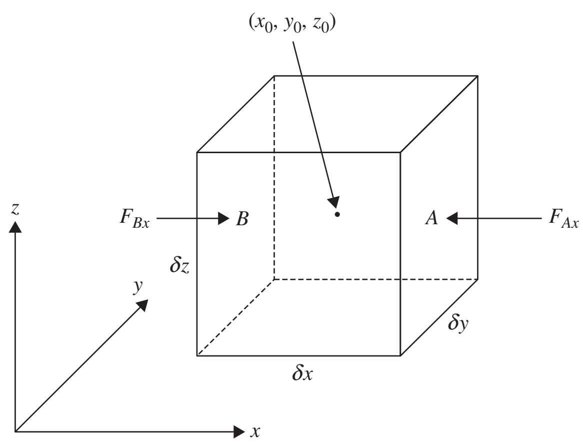

FIGURE 1.2 The x component of the pressure gradient force acting on a fluid element.

Neglecting the higher-order terms in this expansion, the pressure force acting on the volume element at wall A is

$$F_{Ax} = -\left(p_0 + \frac{\partial p}{\partial x}\frac{\delta x}{2}\right)\delta y\,\delta z$$

where $\delta y \delta z$ is the area of wall A. Similarly, the pressure force acting on the volume element at wall B is just

$$F_{Bx} = +\left(p_0 - \frac{\partial p}{\partial x}\frac{\delta x}{2}\right)\delta y\,\delta z$$

Therefore, the net x component of this force acting on the volume is

$$F_x = F_{Ax} + F_{Bx} = -\frac{\partial p}{\partial x}\,\delta x\,\delta y\,\delta z$$

Because the net force is proportional to the derivative of pressure, it is referred to as the *pressure gradient force*. The mass m of the differential volume element is simply the density ρ times the volume: $m = \rho\delta x\delta y\delta z$. Thus, the x component of the pressure gradient force per unit mass is

$$\frac{F_x}{m} = -\frac{1}{\rho}\frac{\partial p}{\partial x}$$

Similarly, it can easily be shown that the y and z components of the pressure gradient force per unit mass are

$$\frac{F_y}{m} = -\frac{1}{\rho}\frac{\partial p}{\partial y} \qquad \text{and} \qquad \frac{F_z}{m} = -\frac{1}{\rho}\frac{\partial p}{\partial z}$$

so that the total pressure gradient force per unit mass is the vector given by

$$\frac{\mathbf{F}}{m} = -\frac{1}{\rho}\nabla p \tag{1.1}$$

The gradient operator $\nabla = \left(\mathbf{i}\frac{\partial}{\partial x}, \mathbf{j}\frac{\partial}{\partial y}, \mathbf{k}\frac{\partial}{\partial z}\right)$ acts on functions to its right to yield vectors that point toward higher values of the function. It is important to note that (1) the pressure gradient points from low to high pressure, but the pressure gradient *force* points from high to low pressure, and (2) the pressure gradient force is proportional to the *gradient* of the pressure field, not to the pressure itself.

1.2.2 Viscous Force

Any real fluid is subject to internal friction, called viscosity, which causes it to resist the tendency to flow. Viscosity arises when the fluid velocity varies spatially so that random molecular motion accomplishes a net transport of momentum from molecules in faster-moving air parcels to molecules in nearby slower-moving air parcels. This momentum exchange between parcels may be expressed as a viscous force, F, acting *along* the face of the air parcel, which produces a *shear* stress, τ, on the parcel per area, A,

$$\tau = \frac{F}{A} \tag{1.2}$$

Therefore, the viscous force is given by $F = \tau A$. For a Newtonian fluid, we assume that the shear stress depends linearly on the fluid speed, which is a very good approximation for air. In the vertical direction, for example, variation in the x component of the wind, u, produces the stress

$$\tau \approx \mu \frac{\partial u}{\partial z} \tag{1.3}$$

where μ is the viscosity coeficient, which depends on the fluid. As in the pressure gradient force discussion, we need the net force acting on the air parcel from viscous effects. Following a similar Taylor-approximation approach as for the pressure gradient derivation, but noting that the force is directed *along* rather than *normal* to the face of the parcel volume, we find that the viscous force per unit mass due to vertical shear of the component of motion in the x direction is

$$\frac{1}{\rho}\frac{\partial \tau_{zx}}{\partial z} = \frac{1}{\rho}\frac{\partial}{\partial z}\left(\mu \frac{\partial u}{\partial z}\right) \tag{1.4}$$

For constant μ, the right side may be simplified to $\nu \partial^2 u/\partial z^2$, where $\nu = \mu/\rho$ is the *kinematic viscosity coefficient*. For standard atmosphere[2] conditions at sea level, $\nu = 1.46 \times 10^{-5}\,\mathrm{m^2\,s^{-1}}$. Note that (1.4) represents only the contribution from x momentum shear stress in the z direction, and the net force in the x direction, F_{rx}, also includes contributions from the x and y directions. The net frictional force components per unit mass in the three Cartesian coordinate directions are

$$\begin{aligned}
F_{rx} &= \nu\left[\frac{\partial^2 u}{\partial x^2} + \frac{\partial^2 u}{\partial y^2} + \frac{\partial^2 u}{\partial z^2}\right] \\
F_{ry} &= \nu\left[\frac{\partial^2 v}{\partial x^2} + \frac{\partial^2 v}{\partial y^2} + \frac{\partial^2 v}{\partial z^2}\right] \\
F_{rz} &= \nu\left[\frac{\partial^2 w}{\partial x^2} + \frac{\partial^2 w}{\partial y^2} + \frac{\partial^2 w}{\partial z^2}\right]
\end{aligned} \tag{1.5}$$

Each component frictional force represents diffusion of momentum in that coordinate direction, since, for example, $\frac{\partial^2 u}{\partial x^2} + \frac{\partial^2 u}{\partial y^2} + \frac{\partial^2 u}{\partial z^2} = \nabla \cdot \nabla u = \nabla^2 u$. For any

[2] The U.S. standard atmosphere is a specified vertical profile of atmospheric structure.

vector **A**, $\nabla \cdot \mathbf{A}$ is a scalar quantity called the *divergence* of **A**, since it is positive when vectors diverge away from a point; negative divergence is called *convergence.* At a local maximum in u, ∇u points toward (converges on) the maximum, and therefore $\nabla^2 u < 0$, resulting in a loss of momentum from the maximum value to the surrounding region. This process is called *downgradient diffusion*, since momentum diffuses down the gradient, from large to small values.

For the atmosphere below 100 km, ν is so small that molecular viscosity is negligible except in a thin layer within a few centimeters of Earth's surface, where the vertical shear is very large. Away from this surface molecular boundary layer, momentum is transferred primarily by turbulent eddy motions, which are discussed in Chapter 8.

1.2.3 Gravitational Force

The sole body force on atmospheric air parcels is due to gravity. Newton's law of universal gravitation states that any two elements of mass in the universe attract each other with a force proportional to their masses and inversely proportional to the square of the distance separating them. Thus, if two mass elements M and m are separated by a distance $r \equiv |\mathbf{r}|$ (with the vector **r** directed toward m as shown in Figure 1.3), then the force exerted by mass M on mass m due to gravitation is

$$\mathbf{F}_g = -\frac{GMm}{r^2}\left(\frac{\mathbf{r}}{r}\right) \tag{1.6}$$

where G is a universal constant called the gravitational constant. The law of gravitation as expressed in (1.6) actually applies only to hypothetical "point" masses, since for objects of finite extent **r** will vary from one part of the object to another. However, for finite bodies, (1.6) may still be applied if $|\mathbf{r}|$ is interpreted

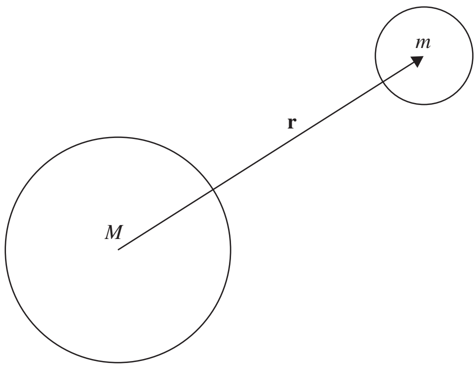

FIGURE 1.3 Two spherical masses whose centers are separated by a distance r.

as the distance between the centers of mass of the bodies. Thus, if Earth is designated as mass M, and m is a mass element of the atmosphere, then the force per unit mass exerted on the atmosphere by the gravitational attraction of Earth is

$$\frac{\mathbf{F}_g}{m} \equiv \mathbf{g}^* = -\frac{GM}{r^2}\left(\frac{\mathbf{r}}{r}\right) \tag{1.7}$$

In dynamic meteorology it is customary to use the height above mean sea level as a vertical coordinate. If the mean radius of Earth is designated by a and the distance above mean sea level is designated by z, then neglecting the small departure of the shape of Earth from sphericity, $r = a + z$. Therefore, Eq. (1.7) can be rewritten as

$$\mathbf{g}^* = \frac{\mathbf{g}_0^*}{(1 + z/a)^2} \tag{1.8}$$

where $\mathbf{g}_0^* = -(GM/a^2)(\mathbf{r}/r)$ is the gravitational force at mean sea level. For meteorological applications, $z \ll a$, so that with negligible error we can let $\mathbf{g}^* = \mathbf{g}_0^*$ and simply treat the gravitational force as a constant. Note that this treatment of the gravitational force will be modified in Section 1.3.2 to account for centrifugal forces due to Earth's rotation.

1.3 NONINERTIAL REFERENCE FRAMES AND "APPARENT" FORCES

In formulating the laws of atmospheric dynamics, it is natural to use a *geocentric* reference frame—that is, a frame of reference at rest with respect to rotating Earth. Newton's first law of motion states that a mass in uniform motion relative to a coordinate system fixed in space will remain in uniform motion in the absence of any forces. Such motion is referred to as *inertial motion*, and the fixed reference frame is an inertial, or absolute, frame of reference. It is clear, however, that an object at rest or in uniform motion with respect to rotating Earth is not at rest or in uniform motion relative to a coordinate system fixed in space.

Therefore, motion that appears to be inertial motion to an observer in a geocentric reference frame is really accelerated motion. Hence, a geocentric reference frame is a *noninertial* reference frame. Newton's laws of motion can only be applied in such a frame if the acceleration of the coordinates is taken into account. The most satisfactory way of including the effects of coordinate acceleration is to introduce "apparent" forces in the statement of Newton's second law. These apparent forces are the inertial reaction terms that arise because of the coordinate acceleration. For a coordinate system in uniform rotation, two such apparent forces are required: the centrifugal force and the Coriolis force.

1.3.1 Centripetal Acceleration and Centrifugal Force

To illustrate the essential aspects of noninertial frames, we consider a ball of mass m attached to a string and whirled through a circle of radius r at a constant angular velocity ω. From the point of view of an observer in inertial space the speed of the ball is constant, but its direction of travel is continuously changing so that its velocity is not constant. To compute the acceleration we consider the change in velocity $\delta\mathbf{V}$ that occurs for a time increment δt during which the ball rotates through an angle $\delta\theta$ as shown in Figure 1.4. Because $\delta\theta$ is also the angle between the vectors $\mathbf{V}$ and $\mathbf{V} + \delta\mathbf{V}$, the magnitude of $\delta\mathbf{V}$ is just $|\delta\mathbf{V}| = |\mathbf{V}|\,\delta\theta$. If we divide by δt and note that in the limit $\delta t \to 0$, $\delta\mathbf{V}$ is directed toward the axis of rotation, we obtain

$$\frac{D\mathbf{V}}{Dt} = |\mathbf{V}|\frac{D\theta}{Dt}\left(-\frac{\mathbf{r}}{r}\right)$$

However, $|\mathbf{V}| = \omega r$ and $D\theta/Dt = \omega$, so that

$$\frac{D\mathbf{V}}{Dt} = -\omega^2\mathbf{r} \tag{1.9}$$

Therefore, viewed from fixed coordinates, the motion is one of uniform acceleration directed toward the axis of rotation at a rate equal to the square of the angular velocity times the distance from the axis of rotation. This acceleration is called *centripetal acceleration*. It is caused by the force of the string pulling the ball.

Now suppose that we observe the motion in a coordinate system rotating with the ball. In this rotating system the ball is stationary, but there is still a force acting on the ball—namely, the pull of the string. Therefore, in order to apply Newton's second law to describe the motion relative to this rotating

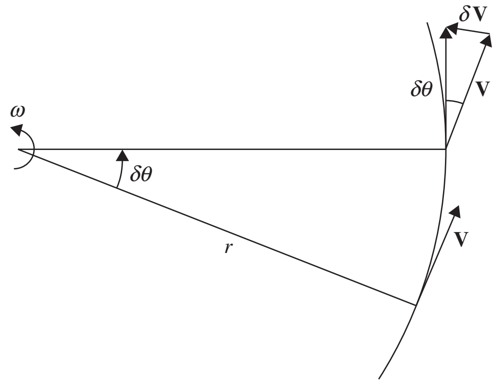

FIGURE 1.4 Centripetal acceleration is given by the rate of change of the direction of the velocity vector, which is directed toward the axis of rotation, as illustrated here by $\delta\mathbf{V}$.

coordinate system, we must include an additional apparent force, the *centrifugal force*, which just balances the force of the string on the ball. Thus, the centrifugal force is equivalent to the inertial reaction of the ball on the string and just equal and opposite to the centripetal acceleration.

To summarize, observed from a fixed system, the rotating ball undergoes a uniform centripetal acceleration in response to the force exerted by the string. Observed from a system rotating along with it, the ball is stationary and the force exerted by the string is balanced by a centrifugal force.

1.3.2 Gravity Revisited

An object at rest on the surface of Earth is not at rest or in uniform motion relative to an inertial reference frame except at the poles. Rather, an object of unit mass at rest on the surface of Earth is subject to a centripetal acceleration directed toward the axis of rotation of Earth given by $-\Omega^2\mathbf{R}$, where $\mathbf{R}$ is the position vector from the axis of rotation to the object and $\Omega = 7.292 \times 10^{-5}\,\mathrm{rad\,s^{-1}}$ is the angular speed of rotation of Earth.[3] Since, except at the equator and poles, the centripetal acceleration has a component directed poleward along the horizontal surface of Earth (i.e., along a surface of constant *geopotential*), there must be a net horizontal force directed poleward along the horizontal to sustain the horizontal component of the centripetal acceleration.

This force arises because rotating Earth is not a sphere but has assumed the shape of an oblate spheroid in which there is a poleward component of gravitation along a constant geopotential surface just sufficient to account for the poleward component of the centripetal acceleration at each latitude for an object at rest on the surface of Earth. In other words, from the point of view of an observer in an inertial reference frame, geopotential surfaces slope upward toward the equator (Figure 1.5). As a consequence, the equatorial radius of Earth is about 21 km larger than the polar radius.

Viewed from a frame of reference rotating with Earth, however, a geopotential surface is everywhere normal to the sum of the true force of gravity, $\mathbf{g}^*$, and the centrifugal force $\Omega^2\mathbf{R}$ (which is just the reaction force of the centripetal acceleration). A geopotential surface is thus experienced as a level surface by an object at rest on rotating Earth. Except at the poles, the weight of an object of mass m at rest on such a surface, which is just the reaction force of Earth on the object, will be slightly less than the gravitational force $m\mathbf{g}^*$ because, as illustrated in Figure 1.5, the centrifugal force partly balances the gravitational force. It is, therefore, convenient to combine the effects of the gravitational force and centrifugal force by defining *gravity* $\mathbf{g}$ such that

$$\mathbf{g} \equiv -g\mathbf{k} \equiv \mathbf{g}^* + \Omega^2\mathbf{R} \tag{1.10}$$

---

[3]Earth revolves around its axis once every *sidereal* day, which is equal to 23 h 56 min 4 s (86,164 s). Thus, $\Omega = 2\pi/(86{,}164\,\mathrm{s}) = 7.292 \times 10^{-5}\,\mathrm{rad\,s^{-1}}$.

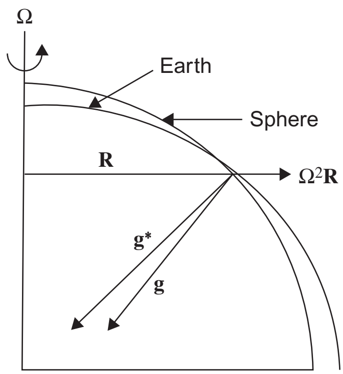

FIGURE 1.5 Relationship between the true gravitation vector $\mathbf{g}^*$ and gravity $\mathbf{g}$. For an idealized homogeneous spherical Earth, $\mathbf{g}^*$ would be directed toward the center of Earth. In reality, $\mathbf{g}^*$ does not point exactly to the center except at the equator and the poles. Gravity, $\mathbf{g}$, is the vector sum of $\mathbf{g}^*$ and the centrifugal force and is perpendicular to the level surface of Earth, which approximates an oblate spheroid.

where $\mathbf{k}$ designates a unit vector parallel to the local vertical. Gravity, g, sometimes referred to as "apparent gravity," will here be taken as a constant ($g = 9.81\,\mathrm{m\,s^{-2}}$). Except at the poles and the equator, $\mathbf{g}$ is not directed toward the center of Earth, but is perpendicular to a geopotential surface as indicated by Figure 1.5. True gravity $\mathbf{g}^*$, however, is not perpendicular to a geopotential surface, but has a horizontal component just large enough to balance the horizontal component of $\Omega^2\mathbf{R}$.

Gravity can be represented in terms of the gradient of a potential function Φ, which is just the geopotential referred to before:

$$\nabla\Phi = -\mathbf{g}$$

However, because $\mathbf{g} = -g\mathbf{k}$, where $g \equiv |\mathbf{g}|$, it is clear that $\Phi = \Phi(z)$ and $d\Phi/dz = g$. Thus, horizontal surfaces on Earth are surfaces of constant geopotential. If the value of dz should be dz', where dz' is a dummy variable of integration, geopotential is set to zero at mean sea level, the geopotential $\Phi(z)$ at height z is just the work required to raise a unit mass to height z from mean sea level:

$$\Phi = \int_0^z g dz \tag{1.11}$$

Despite the fact that the surface of Earth bulges toward the equator, an object at rest on the surface of rotating Earth does not slide "downhill" toward the pole because, as indicated previously, the poleward component of gravitation is balanced by the equatorward component of the centrifugal force. However, if the object is put into motion relative to Earth, this balance will be disrupted. Consider a frictionless object located initially at the North Pole. Such an object has zero angular momentum about the axis of Earth. If it is displaced away from the pole in the absence of a zonal torque, it will not acquire rotation and thus will feel a restoring force due to the horizontal component of true gravity, which, as indicated before, is equal and opposite to the horizontal component of the centrifugal force for an object at rest on the surface of Earth. Letting R be the distance from the pole, the horizontal restoring force for a small displacement is thus $-\Omega^2 R$, and the object's acceleration viewed in the inertial coordinate system satisfies the equation for a simple harmonic oscillator:

$$\frac{d^2R}{dt^2} + \Omega^2 R = 0 \tag{1.12}$$

The object will undergo an oscillation of period $2\pi/\Omega$ along a path that will appear as a straight line passing through the pole to an observer in a fixed coordinate system, but will appear as a closed circle traversed in 1/2 day to an observer rotating with Earth (Figure 1.6). From the point of view of an Earth-bound observer, there is an apparent deflection force that causes the object to deviate to the right of its direction of motion at a fixed rate.

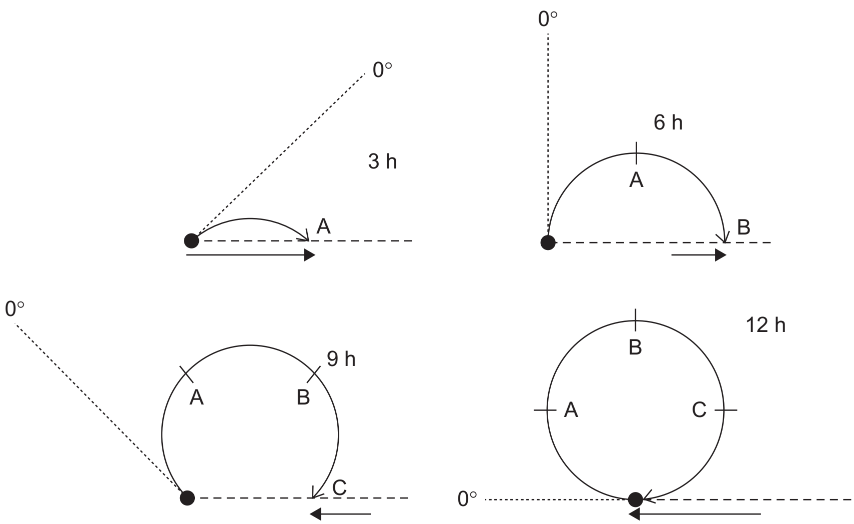

FIGURE 1.6 Motion of a frictionless object launched from the North Pole along the 0° longitude meridian at $t = 0$, as viewed in fixed and rotating reference frames at 3, 6, 9, and 12 h after launch. The *horizontal dashed line* marks the position that the 0° longitude meridian had at $t = 0$, and the short dashed lines show its position in the fixed reference frame at subsequent 3-h intervals. The *horizontal arrows* show 3-h displacement vectors as seen by an observer in the fixed reference frame. *Heavy curved arrows* show the trajectory of the object as viewed by an observer in the rotating system. Labels A, B, and C show the position of the object relative to the rotating coordinates at 3-h intervals. In the fixed coordinate frame, the object oscillates back and forth along a straight line under the influence of the restoring force provided by the horizontal component of gravitation. The period for a complete oscillation is 24 h (only 1/2 period is shown). To an observer in rotating coordinates, however, the motion appears to be at constant speed and describes a complete circle in a clockwise direction in 12 h.

1.3.3 The Coriolis Force and the Curvature Effect

Newton's second law of motion expressed in coordinates rotating with Earth can be used to describe the force balance for an object at rest on the surface of Earth, provided that an apparent force, the centrifugal force, is included among the forces acting on the object. If, however, the object is in motion along the surface of Earth, additional apparent forces are required in the statement of Newton's second law. The Coriolis force will be given a more formal mathematical treatment in Chapter 2, and our purpose here is to deduce the effect by building upon the centrifugal force discussion of the previous section.

Angular momentum, $\mathbf{m} = \mathbf{r} \times \mathbf{p}$, provides a measures of the rotation traced by the linear momentum vector $\mathbf{p}$ with respect to a set of coordinates, the origin of which defines the position vector $\mathbf{r}$. We note that the dynamically important piece of the angular momentum vector lies parallel to Earth's rotational axis, $m = \mathbf{m} \cos\phi$. For now, assume that the linear momentum vector points eastward, having contributions from eastward air motion, u, and from the planetary rotation, $R\Omega$, where $R = r\cos\phi$ is the distance of the air parcel from the axis of rotation (Figure 1.7). If there is no torque in the east–west direction (i.e., no pressure gradient or viscous forces), then m is conserved following the motion,

$$\frac{Dm}{Dt} = \frac{DR}{Dt}(2R\Omega + u) + R\frac{Du}{Dt} = 0 \tag{1.13}$$

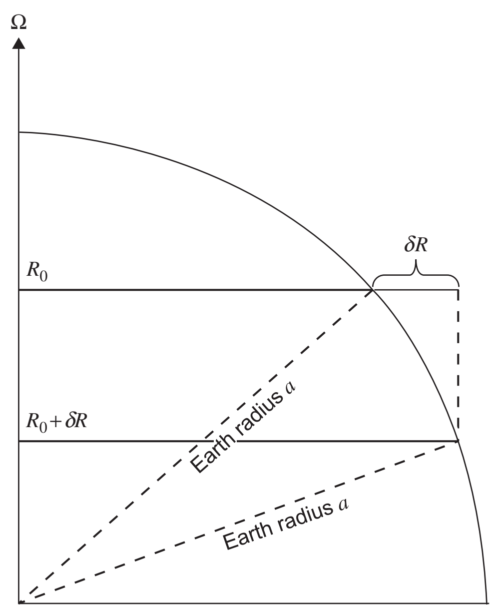

FIGURE 1.7 For poleward motion, air parcels move closer to the axis of rotation and, through angular momentum conservation, the zonal wind accelerates.

so that

$$\frac{Du}{Dt} = -\frac{(2\Omega R + u)}{R}\frac{DR}{Dt} \tag{1.14}$$

Figure 1.7 shows that moving an air parcel closer to the axis of rotation, $\frac{DR}{Dt} < 0$, while conserving angular momentum, increases the westerly linear momentum, analagous to an ice skater spinning faster as the person's arms are drawn inward.

We expand the right side of (1.14) by first noting that

$$\frac{DR}{Dt} = \frac{Dr}{Dt}\cos\phi + r\frac{D}{Dt}\cos\phi = w\cos\phi - v\sin\phi \tag{1.15}$$

where v and w are the northward and upward velocity components, respectively. With this relation, (1.14) becomes

$$\frac{Du}{Dt} = (2\Omega\sin\phi)v - (2\Omega\cos\phi)w - \frac{uw}{r} + \frac{uv}{r}\tan\phi \tag{1.16}$$

The first two terms on the right in (1.16) are the zonal component of the *Coriolis force* due to meridional and vertical motion, respectively. The last two terms on the right are referred to as *metric terms* or *curvature effects* because they arise from the curvature of Earth's surface; since r is large, these terms are negligibly small except near large u.

Suppose now that the object is set in motion in the eastward direction by an impulsive force. Axial angular momentum is not conserved in this case, but considering again the centrifugal force will help expose the meridional component of the Coriolis force. Because the object is now rotating faster than Earth, the centrifugal force on the object will be increased. The excess of the centrifugal force over that for an object at rest is

$$\left(\Omega + \frac{u}{R}\right)^2\mathbf{R} - \Omega^2\mathbf{R} = \frac{2\Omega u\mathbf{R}}{R} + \frac{u^2\mathbf{R}}{R^2}$$

The terms on the right represent *deflecting* forces, which act outward along the vector $\mathbf{R}$ (i.e., perpendicular to the axis of rotation). The meridional and vertical components of these forces are obtained by taking meridional and vertical components of $\mathbf{R}$, as shown in Figure 1.8, to yield

$$\frac{Dv}{Dt} = -2\Omega u\sin\phi - \frac{u^2}{a}\tan\phi \tag{1.17}$$

$$\frac{Dw}{Dt} = 2\Omega u\cos\phi + \frac{u^2}{a} \tag{1.18}$$

The first terms on the right are the meridional and vertical components, respectively, of the Coriolis forces for zonal motion; the second terms on the right are curvature effects.

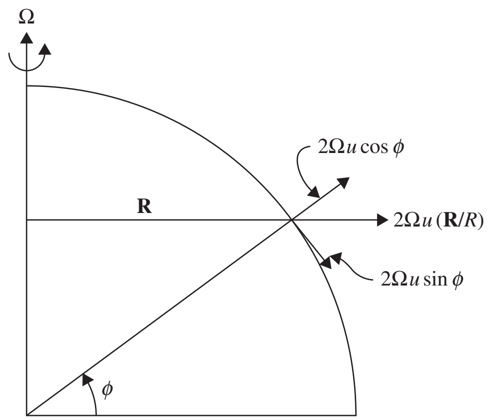

FIGURE 1.8 Components of the Coriolis force due to relative motion along a latitude circle.

For larger-scale motions, the curvature terms can be neglected as an approximation. Therefore, relative horizontal motion produces a horizontal acceleration perpendicular to the direction of motion given by

$$\frac{Du}{Dt} = 2\Omega v \sin\phi = fv \tag{1.19}$$

$$\frac{Dv}{Dt} = -2\Omega u \sin\phi = -fu \tag{1.20}$$

where $f \equiv 2\Omega \sin\phi$ is the *Coriolis parameter*.

Thus, for example, an object moving eastward in the horizontal is deflected equatorward by the Coriolis force, whereas a westward moving object is deflected poleward. In either case the deflection is to the right of the direction of motion in the Northern Hemisphere and to the left in the Southern Hemisphere. The vertical component of the Coriolis force in (1.18) is ordinarily much smaller than the gravitational force so that its only effect is to cause a very minor change in the apparent weight of an object depending on whether the object is moving eastward or westward.

The Coriolis force is negligible for motions with time scales that are very short compared to the period of Earth's rotation (a point that is illustrated by several problems at the end of the chapter). Thus, the Coriolis force is not important for the dynamics of individual cumulus clouds but is essential for an understanding of longer time scale phenomena such as synoptic scale systems. The Coriolis force must also be taken into account when computing long-range missile or artillery trajectories.

As an example, suppose that a ballistic missile is fired due eastward at 43°N latitude ($f = 10^{-4}\ \mathrm{s}^{-1}$ at 43°N). If the missile travels 1000 km at a horizontal speed $u_0 = 1000\ \mathrm{m\,s}^{-1}$, by how much is the missile deflected from its eastward path by the Coriolis force? Integrating (1.20) with respect to time, we find that

$$v = -fu_0 t \tag{1.21}$$

where it is assumed that the deflection is sufficiently small so that we may let f and u_0 be constants. To find the total displacement, we must integrate (1.13) with respect to time:

$$\int_0^t v dt = \int_{y_0}^{y_0+\delta y} dy = -fu_0 \int_0^t t dt$$

Thus, the total displacement is

$$\delta y = -fu_0 t^2/2 = -50\,\text{km}$$

Therefore, the missile is deflected southward by 50 km due to the Coriolis effect. Further examples of the deflection of objects by the Coriolis force are given in some of the problems at the end of the chapter.

The x and y components given in (1.19) and (1.20) can be combined in vector form as

$$\left(\frac{D\mathbf{V}}{Dt}\right)_{Co} = -f\mathbf{k} \times \mathbf{V} \tag{1.22}$$

where $\mathbf{V} \equiv (u, v)$ is the horizontal velocity, $\mathbf{k}$ is a vertical unit vector, and the subscript Co indicates that the acceleration is due solely to the Coriolis force. Since $-\mathbf{k} \times \mathbf{V}$ is a vector rotated 90° to the right of $\mathbf{V}$, (1.22) clearly shows the deflection character of the Coriolis force. The Coriolis force can only change the direction of motion, not the speed.

1.3.4 Constant Angular Momentum Oscillations

Suppose an object initially at rest on Earth at the point (x_0, y_0) is impulsively propelled along the x axis with a speed V at time $t = 0$. Then, from (1.19) and (1.20), the time evolution of the velocity is given by $u = V\cos ft$ and $v = -V\sin ft$. However, because $u = Dx/Dt$ and $v = Dy/Dt$, integration with respect to time gives the position of the object at time t as

$$x - x_0 = \frac{V}{f}\sin ft \quad \text{and} \quad y - y_0 = \frac{V}{f}(\cos ft - 1) \tag{1.23}$$

where the variation of f with latitude is neglected. Equations (1.23) show that in the Northern Hemisphere, where f is positive, the object orbits clockwise (anticyclonically) in a circle of radius $R = V/f$ about the point $(x_0, y_0 - V/f)$ with a period given by

$$\tau = 2\pi R/V = 2\pi/f = \pi/(\Omega\sin\phi) \tag{1.24}$$

Thus, an object displaced horizontally from its equilibrium position on the surface of Earth under the influence of the force of gravity will oscillate about its equilibrium position with a period that depends on latitude and is equal to one sidereal day at 30° latitude and 1/2 sidereal day at the pole. Constant angular momentum oscillations (often referred to as "inertial oscillations") are commonly observed in the oceans, but are apparently not of importance in the atmosphere.

1.4 STRUCTURE OF THE STATIC ATMOSPHERE

The thermodynamic state of the atmosphere at any point is determined by the values of pressure, temperature, and density (or specific volume) at that point. These field variables are related to one an other by the equation of state for an ideal gas. Letting p, T, ρ, and $\alpha(\equiv \rho^{-1})$ denote pressure, temperature, density, and specific volume, respectively, we can express the equation of state for dry air as

$$p\alpha = RT \quad \text{or} \quad p = \rho RT \tag{1.25}$$

where R is the gas constant for dry air ($R = 287\,\mathrm{J\,kg^{-1}\,K^{-1}}$).

1.4.1 The Hydrostatic Equation

In the absence of atmospheric motions, the gravity force must be exactly balanced by the vertical component of the pressure gradient force. Thus, as illustrated in Figure 1.9,

$$dp/dz = -\rho g \tag{1.26}$$

This condition of *hydrostatic balance* provides an excellent approximation for the vertical dependence of the pressure field in the real atmosphere. Only for intense small-scale systems, such as squall lines and tornadoes, is it necessary to consider departures from hydrostatic balance. Integrating (1.26) from a height z to the top of the atmosphere, we find that

$$p(z) = \int_z^\infty \rho g dz \tag{1.27}$$

so that the pressure at any point is simply equal to the weight of the unit cross-section column of air overlying the point. Thus, mean sea level pressure $p(0) = 1013.25\,\mathrm{hPa}$ is simply the average weight per square meter of the total atmospheric column.[4] It is often useful to express the hydrostatic equation in

[4]For computational convenience, the mean surface pressure is often assumed to equal 1000 hPa.

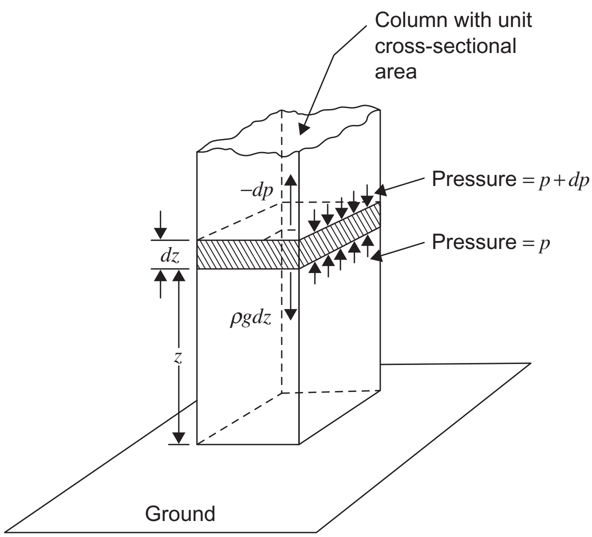

FIGURE 1.9 Balance of forces for hydrostatic equilibrium. *Small arrows* show the upward and downward forces exerted by air pressure on the air mass in the shaded block. The downward force exerted by gravity on the air in the block is given by ρgdz, whereas the net pressure force given by the difference between the upward force across the lower surface and the downward force across the upper surface is $-dp$. Note that dp is negative, as pressure decreases with height. (*After Wallace and Hobbs, 2006.*)

terms of the geopotential rather than the geometric height. Noting from (1.11) that $d\Phi = gdz$ and from (1.25) that $\alpha = RT/p$, we can express the hydrostatic equation in the form

$$gdz = d\Phi = -(RT/p)dp = -RTd\ln p \tag{1.28}$$

Thus, the variation in geopotential with respect to pressure depends only on temperature. Integration of (1.28) in the vertical yields a form of the *hypsometric equation*:

$$\Phi(z_2) - \Phi(z_1) = g_0(Z_2 - Z_1) = R\int_{p_2}^{p_1} Td\ln p \tag{1.29}$$

Here $Z \equiv \Phi(z)/g_0$ is the *geopotential height*, where $g_0 \equiv 9.80665\,\mathrm{m\,s^{-2}}$ is the global average of gravity at mean sea level. Thus, in the troposphere and lower stratosphere, Z is numerically almost identical to the geometric height z. In terms of Z the hypsometric equation becomes

$$Z_T \equiv Z_2 - Z_1 = \frac{R}{g_0}\int_{p_2}^{p_1} Td\ln p \tag{1.30}$$

where Z_T is the *thickness* of the atmospheric layer between the pressure surfaces p_2 and p_1. Defining a layer mean temperature

$$\langle T \rangle = \left[\int_{p_2}^{p_1} d \ln p \right]^{-1} \int_{p_2}^{p_1} T d \ln p$$

and a layer mean scale height $H \equiv R\langle T \rangle / g_0$, we have from Eq. (1.30)

$$Z_T = H \ln(p_1/p_2) \tag{1.31}$$

Thus, the thickness of a layer bounded by isobaric surfaces is proportional to the mean temperature of the layer. Pressure decreases more rapidly with height in a cold layer than in a warm layer. It also follows immediately from (1.31) that in an isothermal atmosphere of temperature T, the geopotential height is proportional to the natural logarithm of pressure normalized by the surface pressure clearer:

$$Z = H \ln(p_0/p) \tag{1.32}$$

where p_0 is the pressure at $Z = 0$. Thus, in an isothermal atmosphere the pressure decreases exponentially with geopotential height by a factor of e^{-1} per scale height:

$$p(Z) = p(0)e^{-Z/H}$$

1.4.2 Pressure as a Vertical Coordinate

From the hydrostatic equation (1.26), it is clear that a single-valued monotonic relationship exists between pressure and height in each vertical column of the atmosphere. Thus, we may use pressure as the independent vertical coordinate and height (or geopotential) as a dependent variable. The thermodynamic state of the atmosphere is then specified by the fields of $\Phi(x, y, p, t)$ and $T(x, y, p, t)$.

Now the horizontal components of the pressure gradient force given by Eq. (1.1) are evaluated by partial differentiation holding z constant. However, when pressure is used as the vertical coordinate, horizontal partial derivatives must be evaluated holding p constant. Transformation of the horizontal pressure gradient force from height to pressure coordinates may be carried out with the aid of Figure 1.10. Considering only the x, z plane, we see from Figure 1.10 that

$$\left[\frac{(p_0 + \delta p) - p_0}{\delta x} \right]_z = \left[\frac{(p_0 + \delta p) - p_0}{\delta z} \right]_x \left(\frac{\delta z}{\delta x} \right)_p$$

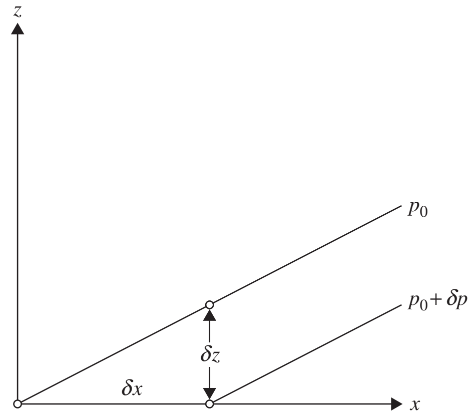

FIGURE 1.10 Slope of pressure surfaces in the x, z plane.

where subscripts indicate variables that remain constant in evaluating the differentials. For example, in the limit $\delta z \to 0$

$$\left[\frac{(p_0+\delta p)-p_0}{\delta z}\right]_x \to \left(-\frac{\partial p}{\partial z}\right)_x$$

where the minus sign is included because $\delta z < 0$ for $\delta p > 0$.

Taking the limits $\delta x, \delta z \to 0$, we obtain[5]

$$\left(\frac{\partial p}{\partial x}\right)_z = -\left(\frac{\partial p}{\partial z}\right)_x \left(\frac{\partial z}{\partial x}\right)_p$$

which after substitution from the hydrostatic equation (1.26) yields

$$-\frac{1}{\rho}\left(\frac{\partial p}{\partial x}\right)_z = -g\left(\frac{\partial z}{\partial x}\right)_p = -\left(\frac{\partial \Phi}{\partial x}\right)_p \tag{1.33}$$

Similarly, it is easy to show that

$$-\frac{1}{\rho}\left(\frac{\partial p}{\partial y}\right)_z = -\left(\frac{\partial \Phi}{\partial y}\right)_p \tag{1.34}$$

Thus, in the *isobaric* coordinate system the horizontal pressure gradient force is measured by the gradient of geopotential at constant pressure. Density no longer appears explicitly in the pressure gradient force; this is a distinct advantage of the isobaric system.

[5]It is important to note the minus sign on the right in this expression!

1.4.3 A Generalized Vertical Coordinate

Any single-valued monotonic function of pressure or height may be used as the independent vertical coordinate. For example, in many numerical weather prediction models, pressure normalized by the pressure at the ground, $\sigma \equiv p(x, y, z, t)/p_s(x, y, t)$, is used as a vertical coordinate. This choice guarantees that the ground is a coordinate surface ($\sigma \equiv 1$) even in the presence of spatial and temporal surface pressure variations. Thus, this so-called σ coordinate system is particularly useful in regions of strong topographic variations.

We now obtain a general expression for the horizontal pressure gradient, which is applicable to any vertical coordinate $s = s(x, y, z, t)$ that is a single-valued monotonic function of height. Referring to Figure 1.11 we see that for a horizontal distance δx, the pressure difference evaluated along a surface of constant s is related to that evaluated at constant z by the relationship

$$\frac{p_C - p_A}{\delta x} = \frac{p_C - p_B}{\delta z}\frac{\delta z}{\delta x} + \frac{p_B - p_A}{\delta x}$$

Taking the limits as $\delta x, \delta z \to 0$, we obtain

$$\left(\frac{\partial p}{\partial x}\right)_s = \frac{\partial p}{\partial z}\left(\frac{\partial z}{\partial x}\right)_s + \left(\frac{\partial p}{\partial x}\right)_z \tag{1.35}$$

Using the identity $\partial p/\partial z = (\partial s/\partial z)(\partial p/\partial s)$, we can express (1.35) in the alternate form

$$\left(\frac{\partial p}{\partial x}\right)_s = \left(\frac{\partial p}{\partial x}\right)_z + \frac{\partial s}{\partial z}\left(\frac{\partial z}{\partial x}\right)_s \left(\frac{\partial p}{\partial s}\right) \tag{1.36}$$

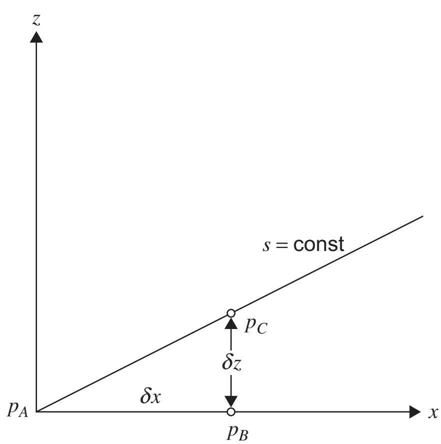

FIGURE 1.11 Transformation of the pressure gradient force to s coordinates.

In later chapters we will apply (1.35) or (1.36) and similar expressions for other fields to transform the dynamical equations to several different vertical coordinate systems.

1.5 KINEMATICS

Kinematics involves the analysis of motion without reference to forces that change the motion in time. It provides a diagnosis of motion at a particular instant in time, which may in turn prove useful for understanding the dynamics of the flow as it evolves in time. There are many aspects of kinematics, but usually one is interested in the structure of the flow, and here we will limit attention to the horizontal flow. One way to quantify flow structure is to examine linear variations in the flow near an arbitrary point (x_0, y_0). A leading-order Taylor approximation to the wind near the point is

$$u(x_0 + dx, y_0 + dy) \approx u(x_0, y_0) + \left.\frac{\partial u}{\partial x}\right|_{(x_0,y_0)} dx + \left.\frac{\partial u}{\partial y}\right|_{(x_0,y_0)} dy \tag{1.37a}$$

$$v(x_0 + dx, y_0 + dy) \approx v(x_0, y_0) + \left.\frac{\partial v}{\partial x}\right|_{(x_0,y_0)} dx + \left.\frac{\partial v}{\partial y}\right|_{(x_0,y_0)} dy \tag{1.37b}$$

Making the following definitions

$$\frac{\partial u}{\partial x} + \frac{\partial v}{\partial y} = \delta \tag{1.38a}$$

$$\frac{\partial v}{\partial x} - \frac{\partial u}{\partial y} = \zeta \tag{1.38b}$$

$$\frac{\partial u}{\partial x} - \frac{\partial v}{\partial y} = d_1 \tag{1.38c}$$

$$\frac{\partial v}{\partial x} + \frac{\partial u}{\partial y} = d_2 \tag{1.38d}$$

allows the derivatives in (1.37a,b) to be replaced in favor of the elemental quanties δ, ζ, d_1, and d_2:

$$u(x_0 + dx, y_0 + dy) \approx u(x_0, y_0) + \frac{1}{2}(\delta + d_1)dx + \frac{1}{2}(d_2 - \zeta)dy \tag{1.39a}$$

$$v(x_0 + dx, y_0 + dy) \approx v(x_0, y_0) + \frac{1}{2}(\zeta + d_2)dx + \frac{1}{2}(\delta - d_1)dy \tag{1.39b}$$

The advantage of this manipulation is that we can now think about the wind near a point as a linear combination of the elemental fluid properties. The vorticity, ζ, represents pure rotation (about the vertical direction); δ represents pure divergence; and $\delta < 0$ is called convergence. Pure deformation is represented by d_1

and d_2, where the wind field contracts, or is *confluent* in one direction, called the axis of contraction, and the wind field stretches in the normal direction, called the axis of dilatation. d_2 represents a 45° rotation of d_1, and therefore they are not independent patterns. The leading, constant, terms in (1.39a,b) represent uniform translation.

By setting all elemental quantities in (1.39a,b) except one to zero, we visualize the spatial distribution of the horizontal wind associated with one elemental quantity (Figure 1.12). Note that the pure deformation pattern represents d_1 only and that, although the vectors appear to converge and diverge, the divergence is exactly zero in this field. This is an important example of the fact that confluence (difluence) in vector fields is not the same as convergence (divergence). In the lower right panel of Figure 1.12, we see a linear combination of vorticity

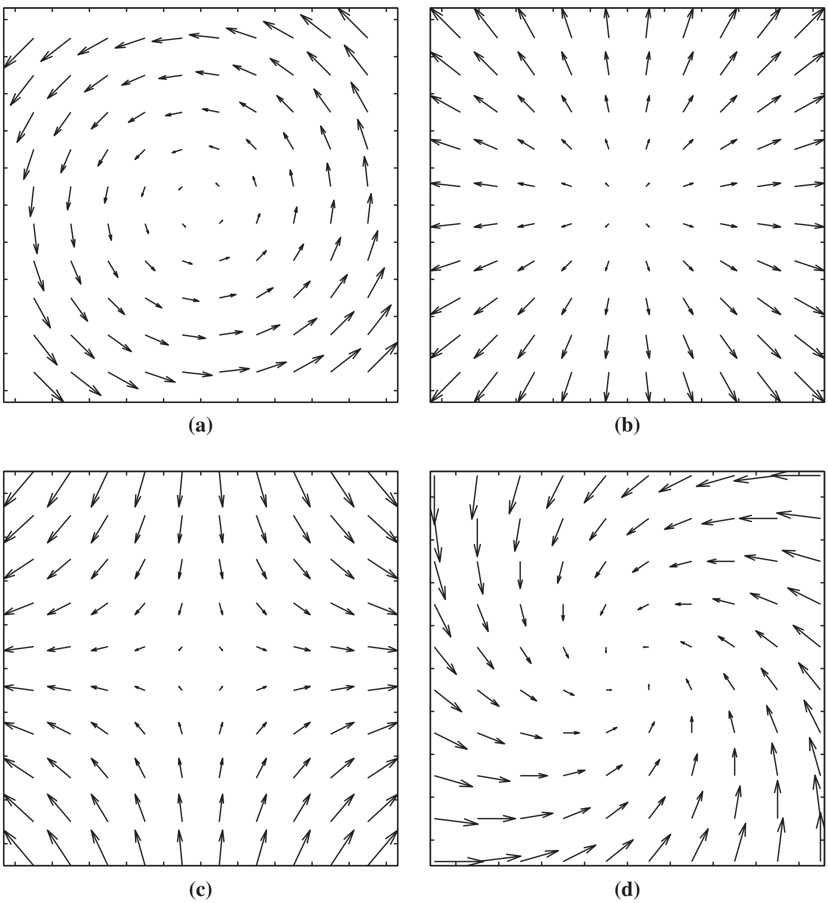

FIGURE 1.12 Velocity fields associated with pure vorticity (a), pure divergence (b), pure deformation (c), and a mixture of vorticity and convergence (d).

and divergence, illustrating a more complicated pattern than the elemental fields in isolation. By computing the elemental variables at a point, one can visualize the linear variation of the flow near that point through (1.39a,b).

This taste of kinematics highlights the importance of certain properties of the wind field that will be explored in greater depth in future chapters. Divergence is connected to vertical motion by mass conservation, as will be discussed in Chapter 2. Vorticity is fundamental to understanding dynamic meteorology and will be explored in detail in Chapter 3. Deformation is important for creating and destroying boundaries in fluids, such as horizontal temperature contrasts known as *frontal zones*, which will be explored in Chapter 9.

1.6 SCALE ANALYSIS

Scale analysis, or scaling, is a convenient technique for estimating the magnitudes of various terms in the governing equations for a particular type of motion. In scaling, typical expected values of the following quantities are specified:

1. Magnitudes of the field variables
2. Amplitudes of fluctuations in the field variables
3. Characteristic length, depth, and time scales on which the fluctuations occur

These typical values are then used to compare the magnitudes of various terms in the governing equations. For example, in a typical midlatitude synoptic[6] cyclone, the surface pressure might fluctuate by 10 hPa over a horizontal distance of 1000 km. Designating the amplitude of the horizontal pressure fluctuation by δp, the horizontal coordinates by x and y, and the horizontal scale by L, the magnitude of the horizontal pressure gradient may be estimated by dividing δp by the length L to get

$$\left(\frac{\partial p}{\partial x}, \frac{\partial p}{\partial y}\right) \sim \frac{\delta p}{L} = 10\,\text{hpa}/10^3\text{ km}\ \left(10^{-3}\text{ Pa m}^{-1}\right)$$

Pressure fluctuations of similar magnitudes occur in other motion systems of vastly different scale such as tornadoes, squall lines, and hurricanes. Thus, the horizontal pressure gradient can range over several orders of magnitude for systems of meteorological interest. Similar considerations are also valid for derivative terms involving other field variables. Therefore, the nature of the dominant terms in the governing equations is crucially dependent on the horizontal scale of the motions. In particular, motions with horizontal scales of only a few kilometers tend to have short time scales so that terms involving the rotation of Earth are negligible, while for larger scales they become very

---

[6]The term *synoptic* designates the branch of meteorology that deals with the analysis of observations taken over a wide area at or near the same time. This term is commonly used (as here) to designate the characteristic scale of the disturbances that are depicted on weather maps.

TABLE 1.4 Scales of Atmospheric Motions

Type of Motion	Horizontal Scale (m)
Molecular mean free path	10^{-7}
Minute turbulent eddies	10^{-2} to 10^{-1}
Small eddies	10^{-1} to 1
Dust devils	1 to 10
Gusts	10 to 10^2
Tornadoes	10^2
Cumulonimbus clouds	10^3
Fronts, squall lines	10^4 to 10^5
Hurricanes	10^5
Synoptic cyclones	10^6
Planetary waves	10^7

important. Because the character of atmospheric motions depends so strongly on the horizontal scale, this scale provides a convenient method for the classification of motion systems. Table 1.4 classifies examples of various types of motions by horizontal scale for the spectral region from 10^{-7} to 10^7 m. In the following chapters, scaling arguments are used extensively in developing simplifications of the governing equations for use in modeling various types of motion systems.

SUGGESTED REFERENCES

Complete reference information is provided in the Bibliography at the end of the book.

Curry and Webster, *Thermodynamics of Atmospheres and Oceans*, contains a more advanced discussion of atmospheric statistics.

Durran (1993) discusses the constant angular momentum oscillation in detail.

Wallace and Hobbs, *Atmospheric Science: An Introductory Survey*, discuss much of the material in this chapter at an elementary level.

PROBLEMS

1.1. Neglecting the latitudinal variation in the radius of Earth, calculate the angle between the gravitational force and gravity vectors at the surface of Earth as a function of latitude. What is the maximum value of this angle?

1.2. Calculate the altitude at which an artificial satellite orbiting in the equatorial plane can be a synchronous satellite (i.e., can remain above the same spot on the surface of Earth).

1.3. An artificial satellite is placed in a natural synchronous orbit above the equator and is attached to Earth below by a wire. A second satellite is attached to the first by a wire of the same length and is placed in orbit directly above the first at the same angular velocity. Assuming that the wires have zero mass, calculate the tension in the wires per unit mass of satellite. Could this tension be used to lift objects into orbit with no additional expenditure of energy?

1.4. A train is running smoothly along a curved track at the rate of 50 $\mathrm{m\,s^{-1}}$. A passenger standing on a set of scales observes that his weight is 10% greater than when the train is at rest. The track is banked so that the force acting on the passenger is normal to the floor of the train. What is the radius of curvature of the track?

1.5. If a baseball player throws a ball a horizontal distance of 100 m at 30° latitude in 4 s, by how much is the ball deflected laterally as a result of the rotation of Earth?

1.6. Two balls 4 cm in diameter are placed 100 m apart on a frictionless horizontal plane at 43°N. If the balls are impulsively propelled directly at each other with equal speeds, at what speed must they travel so that they just miss each other?

1.7. A locomotive of mass 2×10^5 kg travels 50 $\mathrm{m\,s^{-1}}$ along a straight horizontal track at 43°N. What lateral force is exerted on the rails? Compare the magnitudes of the upward reaction force exerted by the rails for cases where the locomotive is traveling eastward and westward, respectively.

1.8. Find the horizontal displacement of a body dropped from a fixed platform at a height h at the equator, neglecting the effects of air resistance. What is the numerical value of the displacement for $h = 5$ km?

1.9. A bullet is fired directly upward with initial speed w_0 at latitude ϕ. Neglecting air resistance, by what distance will it be displaced horizontally when it returns to the ground? (Neglect $2\Omega u \cos\phi$ compared to g in the vertical momentum equation.)

1.10. A block of mass $M = 1$ kg is suspended from the end of a weightless string. The other end of the string is passed through a small hole in a horizontal platform and a ball of mass $m = 10$ kg is attached. At what angular velocity must the ball rotate on the horizontal platform to balance the weight of the block if the horizontal distance of the ball from the hole is 1 m? While the ball is rotating, the block is pulled down 10 cm. What is the new angular velocity of the ball? How much work is done in pulling down the block?

1.11. A particle is free to slide on a horizontal frictionless plane located at a latitude ϕ on Earth. Find the equation governing the path of the particle if it is given an impulsive northward velocity $v = V_0$ at $t = 0$. Give the solution for the position of the particle as a function of time. (Assume that the latitudinal excursion is sufficiently small that f is constant.)

1.12. Calculate the 1000 to 500 hPa thickness for isothermal conditions with temperatures of 273 and 250 K, respectively.

1.13. Isolines of 1000 to 500 hPa thickness are drawn on a weather map using a contour interval of 60 m. What is the corresponding layer mean temperature interval?

1.14. Show that a homogeneous atmosphere (density independent of height) has a finite height that depends only on the temperature at the lower boundary. Compute the height of a homogeneous atmosphere with surface temperature $T_0 = 273$ K and surface pressure 1000 hPa. (Use the ideal gas law and hydrostatic balance.)

1.15. For the conditions of the previous problem, compute the variation of the temperature with respect to height.

1.16. Show that in an atmosphere with uniform *lapse rate* γ (where $\gamma \equiv -dT/dz$) the geopotential height at pressure level p_1 is given by

$$Z = \frac{T_0}{\gamma}\left[1 - \left(\frac{p_0}{p_1}\right)^{-R\gamma/g}\right]$$

where T_0 and p_0 are the sea-level temperature and pressure, respectively.

1.17. Calculate the 1000 to 500 hPa thickness for a constant lapse rate atmosphere with $\gamma = 6.5\,\mathrm{K\,km^{-1}}$ and $T_0 = 273\,\mathrm{K}$. Compare your results with the results in Problem 1.12.

1.18. Derive an expression for the variation in density with respect to height in a constant lapse rate atmosphere.

1.19. Derive an expression for the altitude variation in the pressure change δp that occurs when an atmosphere with a constant lapse rate is subjected to a height-independent temperature change δT while the surface pressure remains constant. At what height is the magnitude of the pressure change a maximum if the lapse rate is 6.5 K km^{-1}, $T_0 = 300$, and $\delta T = 2\,\mathrm{K}$?

MATLAB Exercises

M1.1. This exercise investigates the role of the curvature terms for high-latitude constant angular momentum trajectories.

(a) Run the **coriolis.m** script with the following initial conditions: initial latitude 60°, initial velocity $u = 0$, $v = 40\,\mathrm{m\,s^{-1}}$, run time = 5 days. Compare the appearance of the trajectories for the case with the curvature terms included and the case with the curvature terms neglected. Qualitatively explain the difference that you observe. Why is the trajectory not a closed circle as described in Eq. (1.15) of the text? [*Hint*: Consider the separate effects of the term proportional to tan ϕ and of the spherical geometry.]

(b) Run **coriolis.m** with latitude 60°, $u = 0$, $v = 80$ m/s. What is different from case (a)? By varying the run time, see if you can determine how long it takes for the particle to make a full circuit in each case, and compare this to the time given in Eq. (1.24) for $\phi = 60°$.

M1.2. Using the MATLAB script from Problem M1.1, compare the magnitudes of the lateral deflection for ballistic missiles fired eastward and westward at 43° latitude. Each missile is launched at a velocity of 1000 m s^{-1} and travels 1000 km. Explain your results. Can the curvature term be neglected in these cases?

M1.3. This exercise examines the strange behavior of constant angular momentum trajectories near the equator. Run the **coriolis.m** script for the following contrasting cases: (a) latitude $0.5°$, $u = 20\ \mathrm{m\,s^{-1}}$, $v = 0$, run time = 20 days and (b) latitude $0.5°$, $u = -20\ \mathrm{m\,s^{-1}}$, $v = 0$, run time = 20 days. Obviously, eastward and westward motion near the equator leads to very different behavior. Briefly explain why the trajectories are so different in these two cases. By running different time intervals, determine the approximate period of oscillation in each case (i.e., the time to return to the original latitude).

M1.4. More strange behavior near the equator. Run the script **const_ang_mom_traj1.m** by specifying initial conditions of latitude = 0, $u = 0$, $v = 50\ \mathrm{m\,s^{-1}}$, and a time of about 5 or 10 days. Notice that the motion is symmetric about the equator and that there is a net eastward drift. Why does providing a parcel with an initial poleward velocity at the equator lead to an eastward average displacement? By trying different initial meridional velocities in the range of 50 to $250\ \mathrm{m\,s^{-1}}$, determine the approximate dependence of the maximum latitude reached by the ball on the initial meridional velocity. Also determine how the net eastward displacement depends on the initial meridional velocity. Show your results in a table, or plot them using MATLAB.

Chapter 2

Basic Conservation Laws

Atmospheric motions are governed by three fundamental physical principles: conservation of mass, conservation of momentum, and conservation of energy. The mathematical relations that express these laws may be derived by considering the budgets of mass, momentum, and energy for an infinitesimal *control volume* in the fluid. Two types of control volume are commonly used in fluid dynamics. In the *Eulerian* frame of reference, the control volume consists of a parallelepiped of sides δx, δy, and δz, whose position is fixed relative to the coordinate axes. Mass, momentum, and energy budgets will depend on fluxes caused by the flow of fluid through the boundaries of the control volume. (This type of control volume was used in Section 1.2.1.) In the *Lagrangian* frame, however, the control volume consists of an infinitesimal mass of "tagged" fluid particles; thus, the control volume moves about following the motion of the fluid, always containing the same fluid particles.

The Lagrangian frame is particularly useful for deriving conservation laws, since such laws may be stated most simply in terms of a particular mass element of the fluid. The Eulerian system is, however, more convenient for solving most problems because in that system the field variables are related by a set of partial differential equations in which the independent variables are the coordinates x, y, z, and t. In the Lagrangian system, however, it is necessary to follow the time evolution of the fields for various individual fluid parcels. Thus, the independent variables are x_0, y_0, z_0, and t, where x_0, y_0, and z_0 designate the position that a particular parcel passed through at a reference time t_0.

2.1 TOTAL DIFFERENTIATION

The conservation laws to be derived in this chapter contain expressions for the rates of change of density, momentum, and thermodynamic energy following the motion of particular fluid parcels. In order to apply these laws in the Eulerian frame, it is necessary to derive a relationship between the rate of change of a field variable following the motion and its rate of change at a fixed point. The former is called the *substantial*, the *total*, or the *material* derivative (it will be denoted D/Dt). The latter is called the *local* derivative (it is merely the partial derivative with respect to time).

An Introduction to Dynamic Meteorology. DOI: 10.1016/B978-0-12-384866-6.00002-7

To derive a relationship between the total derivative and the local derivative, it is convenient to refer to a particular field variable (temperature, for example). For a given air parcel the location (x, y, z) is a function of t so that $x = x(t)$, $y = y(t)$, $z = z(t)$. Following the parcel, T may then be considered as truly a function only of time, and its rate of change is just the total derivative DT/Dt. To relate the total derivative to the local rate of change at a fixed point, we consider the temperature measured on a balloon that moves with the wind. Suppose that this temperature is T_0 at the point x_0, y_0, z_0 and time t_0. If the balloon moves to the point $x_0+\delta x$, $y_0+\delta y$, $z_0+\delta z$ in a time increment δt, then the temperature change recorded on the balloon, δT, can be expressed in a Taylor series expansion as

$$\delta T = \left(\frac{\partial T}{\partial t}\right)\delta t + \left(\frac{\partial T}{\partial x}\right)\delta x + \left(\frac{\partial T}{\partial y}\right)\delta y + \left(\frac{\partial T}{\partial z}\right)\delta z + \text{(higher-order terms)}$$

Dividing through by δt and noting that δT is the change in temperature following the motion so that

$$\frac{DT}{Dt} \equiv \lim_{\delta t \to 0} \frac{\delta T}{\delta t}$$

we find that in the limit $\delta t \to 0$

$$\frac{DT}{Dt} = \frac{\partial T}{\partial t} + \left(\frac{\partial T}{\partial x}\right)\frac{Dx}{Dt} + \left(\frac{\partial T}{\partial y}\right)\frac{Dy}{Dt} + \left(\frac{\partial T}{\partial z}\right)\frac{Dz}{Dt}$$

is the rate of change of T following the motion.

If we now let

$$\frac{Dx}{Dt} \equiv u, \quad \frac{Dy}{Dt} \equiv v, \quad \frac{Dz}{Dt} \equiv w$$

then u, v, w are the velocity components in the x, y, z directions, respectively, and

$$\frac{DT}{Dt} = \frac{\partial T}{\partial t} + \left(u\frac{\partial T}{\partial x} + v\frac{\partial T}{\partial y} + w\frac{\partial T}{\partial z}\right) \tag{2.1}$$

Using vector notation, this expression may be rewritten as

$$\frac{\partial T}{\partial t} = \frac{DT}{Dt} - \mathbf{U} \cdot \nabla T$$

where $\mathbf{U} = \mathbf{i}u + \mathbf{j}v + \mathbf{k}w$ is the velocity vector. The term $-\mathbf{U} \cdot \nabla T$ is called the temperature *advection*. It gives the contribution to the local temperature change due to air motion. For example, if the wind is blowing from a cold region toward a warm region, $-\mathbf{U} \cdot \nabla T$ will be negative (cold advection) and the advection term will contribute negatively to the local temperature change. Thus, the local rate of change of temperature equals the rate of change of temperature following the motion (i.e., the heating or cooling of individual air parcels) plus the advective rate of change of temperature.

The relationship between the total derivative and the local derivative given for temperature in (2.1) holds for any of the field variables. Furthermore, the total derivative can be defined following a motion field other than the actual wind field.

Example

We may wish to relate the pressure change measured by a barometer on a moving ship to the local pressure change. The surface pressure decreases by 3 hPa per 180 km in the eastward direction. A ship steaming eastward at 10 km/h measures a pressure fall of 1 hPa per 3 h.

What is the pressure change on an island that the ship is passing? If we take the x axis oriented eastward, then the local rate of change of pressure on the island is

$$\frac{\partial p}{\partial t} = \frac{Dp}{Dt} - u\frac{\partial p}{\partial x}$$

where Dp/Dt is the pressure change observed by the ship and u is the velocity of the ship. Thus,

$$\frac{\partial p}{\partial t} = \frac{-1\ \text{hPa}}{3\ \text{h}} - \left(10\frac{\text{km}}{\text{h}}\right)\left(\frac{-3\ \text{hPa}}{180\ \text{km}}\right) = -\frac{1\ \text{hPa}}{6\ \text{h}}$$

so that the rate of pressure fall on the island is only half the rate measured on the moving ship.

If the total derivative of a field variable is zero, then that variable is a conservative quantity following the motion. The local change is then entirely due to advection. As shown later, field variables that are approximately conserved following the motion play an important role in dynamic meteorology.

2.1.1 Total Differentiation of a Vector in a Rotating System

The conservation law for momentum (Newton's second law of motion) relates the rate of change of the absolute momentum following the motion in an inertial reference frame to the sum of the forces acting on the fluid. For most applications in meteorology it is desirable to refer the motion to a reference frame rotating with Earth. Transformation of the momentum equation to a rotating coordinate system requires a relationship between the total derivative of a vector in an inertial reference frame and the corresponding total derivative in a rotating system.

To derive this relationship, we let $\mathbf{A}$ be an arbitrary vector whose Cartesian components in an inertial frame are given by

$$\mathbf{A} = \mathbf{i}'A'_x + \mathbf{j}'A'_y + \mathbf{k}'A'_z$$

and whose components in a frame rotating with an angular velocity $\boldsymbol{\Omega}$ are

$$\mathbf{A} = \mathbf{i}A_x + \mathbf{j}A_y + \mathbf{k}A_z$$

Letting $D_a\mathbf{A}/Dt$ be the total derivative of $\mathbf{A}$ in the inertial frame, we can write

$$\begin{aligned}\frac{D_a\mathbf{A}}{Dt} &= \mathbf{i}'\frac{DA'_x}{Dt} + \mathbf{j}'\frac{DA'_y}{Dt} + \mathbf{k}'\frac{DA'_z}{Dt} \\ &= \mathbf{i}\frac{DA_x}{Dt} + \mathbf{j}\frac{DA_y}{Dt} + \mathbf{k}\frac{DA_z}{Dt} + \frac{D_a\mathbf{i}}{Dt}A_x + \frac{D_a\mathbf{j}}{Dt}A_y + \frac{D_a\mathbf{k}}{Dt}A_z\end{aligned}$$

The first three terms on the preceding line can be combined to give

$$\frac{D\mathbf{A}}{Dt} \equiv \mathbf{i}\frac{DA_x}{Dt} + \mathbf{j}\frac{DA_y}{Dt} + \mathbf{k}\frac{DA_z}{Dt}$$

which is just the total derivative of $\mathbf{A}$ as viewed in the rotating coordinates (i.e., the rate of change in $\mathbf{A}$ following the relative motion).

The last three terms arise because the directions of the unit vectors ($\mathbf{i}$, $\mathbf{j}$, $\mathbf{k}$) change their orientation in space as Earth rotates. These terms have a simple form for a rotating coordinate system. For example, consider the eastward directed unit vector:

$$\delta\mathbf{i} = \frac{\partial\mathbf{i}}{\partial\lambda}\delta\lambda + \frac{\partial\mathbf{i}}{\partial\phi}\delta\phi + \frac{\partial\mathbf{i}}{\partial z}\delta z$$

For solid-body rotation $\delta\lambda = \Omega\delta t$, $\delta\phi = 0$, $\delta z = 0$, so that $\delta\mathbf{i}/\delta t = (\partial\mathbf{i}/\partial\lambda)\,(\delta\lambda/\delta t)$ and taking the limit $\delta t \to 0$,

$$\frac{D_a\mathbf{i}}{Dt} = \Omega\frac{\partial\mathbf{i}}{\partial\lambda}$$

But from Figures 2.1 and 2.2, the longitudinal derivative of $\mathbf{i}$ can be expressed as

$$\frac{\partial\mathbf{i}}{\partial\lambda} = \mathbf{j}\sin\phi - \mathbf{k}\cos\phi$$

However, $\boldsymbol{\Omega} = (0, \Omega\cos\phi, \Omega\sin\phi)$ so that

$$\frac{D_a\mathbf{i}}{Dt} = \Omega(\mathbf{j}\sin\phi - \mathbf{k}\cos\phi) = \boldsymbol{\Omega}\times\mathbf{i}$$

In a similar fashion, it can be shown that $D_a\mathbf{j}/Dt = \boldsymbol{\Omega}\times\mathbf{j}$ and $D_a\mathbf{k}/Dt = \boldsymbol{\Omega}\times\mathbf{k}$. Therefore, the total derivative for a vector in an inertial frame is related to that in a rotating frame by the expression

$$\frac{D_a\mathbf{A}}{Dt} = \frac{D\mathbf{A}}{Dt} + \boldsymbol{\Omega}\times\mathbf{A} \tag{2.2}$$

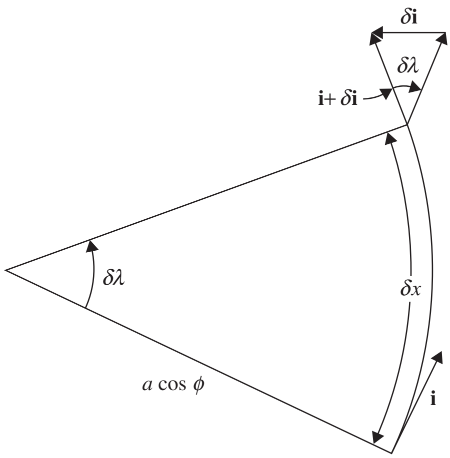

FIGURE 2.1 Longitudinal dependence of the unit vector **i**.

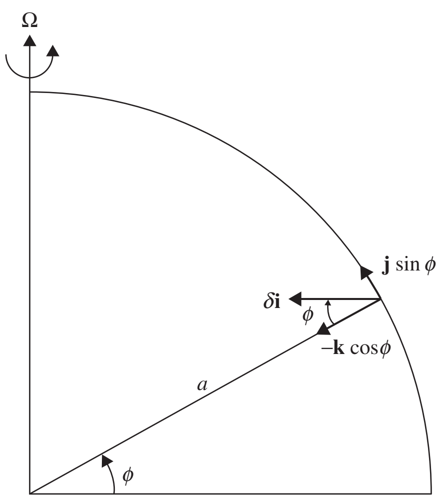

FIGURE 2.2 Resolution of $\delta\mathbf{i}$ in Figure 2.1 into northward and vertical components.

2.2 THE VECTORIAL FORM OF THE MOMENTUM EQUATION IN ROTATING COORDINATES

In an inertial reference frame, Newton's second law of motion may be written symbolically as

$$\frac{D_a \mathbf{U}_a}{Dt} = \sum \mathbf{F} \tag{2.3}$$

The left side represents the rate of change of the absolute velocity $\mathbf{U}_a$, following the motion as viewed in an inertial system. The right side represents the sum of the real forces acting per unit mass. In Section 1.3 we found through simple physical reasoning that when the motion is viewed in a rotating coordinate system, certain additional apparent forces must be included if Newton's second law is to be valid. The same result may be obtained by a formal transformation of coordinates in (2.3).

In order to transform this expression into rotating coordinates, we must first find a relationship between $\mathbf{U}_a$ and the velocity relative to the rotating system, which we will designate $\mathbf{U}$. This relationship is obtained by applying (2.2) to the position vector $\mathbf{r}$ for an air parcel on rotating Earth:

$$\frac{D_a\mathbf{r}}{Dt} = \frac{D\mathbf{r}}{Dt} + \boldsymbol{\Omega} \times \mathbf{r} \tag{2.4}$$

but $D_a\mathbf{r}/Dt \equiv \mathbf{U}_a$ and $D\mathbf{r}/Dt \equiv \mathbf{U}$; therefore, (2.4) may be written as

$$\mathbf{U}_a = \mathbf{U} + \boldsymbol{\Omega} \times \mathbf{r} \tag{2.5}$$

which states simply that the absolute velocity of an object on rotating Earth is equal to its velocity relative to Earth plus the velocity due to the rotation of Earth.

Now we apply (2.2) to the velocity vector $\mathbf{U}_a$ and obtain

$$\frac{D_a\mathbf{U}_a}{Dt} = \frac{D\mathbf{U}_a}{Dt} + \boldsymbol{\Omega} \times \mathbf{U}_a \tag{2.6}$$

Substituting from (2.5) into the right side of (2.6) gives

$$\begin{aligned}\frac{D_a\mathbf{U}_a}{Dt} &= \frac{D}{Dt}(\mathbf{U} + \boldsymbol{\Omega} \times \mathbf{r}) + \boldsymbol{\Omega} \times (\mathbf{U} + \boldsymbol{\Omega} \times \mathbf{r}) \\ &= \frac{D\mathbf{U}}{Dt} + 2\boldsymbol{\Omega} \times \mathbf{U} - \Omega^2\mathbf{R}\end{aligned} \tag{2.7}$$

where $\boldsymbol{\Omega}$ is assumed to be constant. Here $\mathbf{R}$ is a vector perpendicular to the axis of rotation, with magnitude equal to the distance to the axis of rotation, so that with the aid of a vector identity,

$$\boldsymbol{\Omega} \times (\boldsymbol{\Omega} \times \mathbf{r}) = \boldsymbol{\Omega} \times (\boldsymbol{\Omega} \times \mathbf{R}) = -\Omega^2\mathbf{R}$$

Equation (2.7) states that the acceleration following the motion in an inertial system equals the rate of change in relative velocity following the relative motion in the rotating frame plus the Coriolis acceleration due to relative motion in the rotating frame plus the centripetal acceleration caused by the rotation of the coordinates.

If we assume that the only real forces acting on the atmosphere are the pressure gradient force, gravitation, and friction, we can rewrite Newton's second law (2.3) with the aid of (2.7) as

$$\frac{D\mathbf{U}}{Dt} = -2\boldsymbol{\Omega} \times \mathbf{U} - \frac{1}{\rho}\nabla p + \mathbf{g} + \mathbf{F}_r \tag{2.8}$$

where $\mathbf{F}_r$ designates the frictional force (see Section 1.2.2), and the centrifugal force has been combined with gravitation in the gravity term $\mathbf{g}$ (see Section 1.3.2). Equation (2.8) is the statement of Newton's second law for motion relative to a rotating coordinate frame. It states that the acceleration following the relative motion in the rotating frame equals the sum of the Coriolis force, the pressure gradient force, effective gravity, and friction. This form of the momentum equation is basic to most work in dynamic meteorology.

2.3 COMPONENT EQUATIONS IN SPHERICAL COORDINATES

For purposes of theoretical analysis and numerical prediction, it is necessary to expand the vectorial momentum equation (2.8) into its scalar components. Since the departure of the shape of Earth from sphericity is entirely negligible for meteorological purposes, it is convenient to expand (2.8) in spherical coordinates so that the (level) surface of Earth corresponds to a coordinate surface. The coordinate axes are then (λ, ϕ, z), where λ is longitude, ϕ is latitude, and z is the vertical distance above the surface of Earth. If the unit vectors $\mathbf{i}$, $\mathbf{j}$, and $\mathbf{k}$ are now taken to be directed eastward, northward, and upward, respectively, the relative velocity becomes

$$\mathbf{U} \equiv \mathbf{i}u + \mathbf{j}v + \mathbf{k}w$$

where the components u, v, and w are defined as

$$u \equiv r\cos\phi\,\frac{D\lambda}{Dt}, \quad v \equiv r\frac{D\phi}{Dt}, \quad w \equiv \frac{Dz}{Dt} \tag{2.9}$$

Here, r is the distance to the center of Earth, which is related to z by $r = a + z$, where a is the radius of Earth. Traditionally, the variable r in (2.9) is replaced by the constant a. This is a very good approximation, since $z \ll a$ for the regions of the atmosphere with which meteorologists are concerned.

For notational simplicity, it is conventional to define x and y as eastward and northward distance, such that $Dx = a\cos\phi\, D\lambda$ and $Dy = a\, D\phi$. Thus, the horizontal velocity components are $u \equiv Dx/Dt$ and $v \equiv Dy/Dt$ in the eastward and northward directions, respectively. The (x, y, z) coordinate system defined in this way is not, however, a Cartesian coordinate system because the directions of the $\mathbf{i}, \mathbf{j}, \mathbf{k}$ unit vectors are not constant but are functions of position on spherical Earth. This position dependence of the unit vectors must be taken into account when the acceleration vector is expanded into its components on the sphere. Thus, we write

$$\frac{D\mathbf{U}}{Dt} = \mathbf{i}\frac{Du}{Dt} + \mathbf{j}\frac{Dv}{Dt} + \mathbf{k}\frac{Dw}{Dt} + u\frac{D\mathbf{i}}{Dt} + v\frac{D\mathbf{j}}{Dt} + w\frac{D\mathbf{k}}{Dt} \tag{2.10}$$

To obtain the component equations, it is necessary first to evaluate the rates of change of the unit vectors following the motion. We first consider $D\mathbf{i}/Dt$. Expanding the total derivative as in (2.1) and noting that $\mathbf{i}$ is a function only of x (i.e., an eastward-directed vector does not change its orientation if the motion is in the north–south or vertical directions), we get

$$\frac{D\mathbf{i}}{Dt} = u\frac{\partial \mathbf{i}}{\partial x}$$

From Figure 2.1 we see by similarity of triangles,

$$\lim_{\delta x \to 0} \frac{|\delta \mathbf{i}|}{\delta x} = \left|\frac{\partial \mathbf{i}}{\partial x}\right| = \frac{1}{a\cos\phi}$$

and that the vector $\partial \mathbf{i}/\partial x$ is directed toward the axis of rotation. Thus, as is illustrated in Figure 2.2,

$$\frac{\partial \mathbf{i}}{\partial x} = \frac{1}{a\cos\phi}(\mathbf{j}\ \sin\phi - \mathbf{k}\cos\phi)$$

Therefore,

$$\frac{D\mathbf{i}}{Dt} = \frac{u}{a\cos\phi}(\mathbf{j}\ \sin\phi - \mathbf{k}\cos\phi) \tag{2.11}$$

Considering now $D\mathbf{j}/Dt$, we note that $\mathbf{j}$ is a function only of x and y. Thus, with the aid of Figure 2.3 we see that for eastward motion $|\delta\mathbf{j}| = \delta x/(a/\tan\phi)$. Because the vector $\partial\mathbf{j}/\partial x$ is directed in the negative x direction, we then have

$$\frac{\partial \mathbf{j}}{\partial x} = -\frac{\tan\phi}{a}\mathbf{i}$$

From Figure 2.4 it is clear that for northward motion $|\delta\mathbf{j}| = \delta\phi$, but $\delta y = a\delta\phi$, and $\delta\mathbf{j}$ is directed downward so that

$$\frac{\partial \mathbf{j}}{\partial y} = -\frac{\mathbf{k}}{a}$$

Hence,

$$\frac{D\mathbf{j}}{Dt} = -\frac{u\tan\phi}{a}\mathbf{i} - \frac{v}{a}\mathbf{k} \tag{2.12}$$

Finally, by similar arguments it can be shown that

$$\frac{D\mathbf{k}}{Dt} = \mathbf{i}\frac{u}{a} + \mathbf{j}\frac{v}{a} \tag{2.13}$$

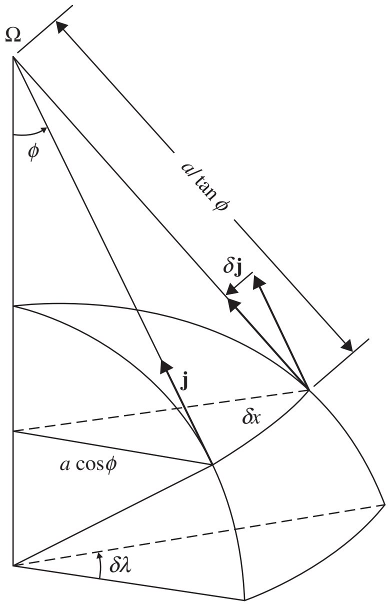

FIGURE 2.3 Dependence of unit vector **j** on longitude.

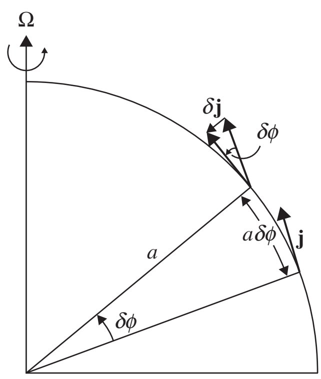

FIGURE 2.4 Dependence of unit vector **j** on latitude.

Substituting (2.11), (2.12), and (2.13) into (2.10) and rearranging the terms, we obtain the spherical polar coordinate expansion of the acceleration following the relative motion

$$\frac{D\mathbf{U}}{Dt} = \left(\frac{Du}{Dt} - \frac{uv\tan\phi}{a} + \frac{uw}{a}\right)\mathbf{i} + \left(\frac{Dv}{Dt} + \frac{u^2\tan\phi}{a} + \frac{vw}{a}\right)\mathbf{j} + \left(\frac{Dw}{Dt} - \frac{u^2+v^2}{a}\right)\mathbf{k} \tag{2.14}$$

We next turn to the component expansion of the force terms in (2.8). The Coriolis force is expanded by noting that $\mathbf{\Omega}$ has no component parallel to $\mathbf{i}$ and that its components parallel to $\mathbf{j}$ and $\mathbf{k}$ are $2\Omega\cos\phi$ and $2\Omega\sin\phi$, respectively. Thus, using the definition of the vector cross-product,

$$\begin{aligned} -2\mathbf{\Omega}\times\mathbf{U} &= -2\Omega\begin{vmatrix}\mathbf{i} & \mathbf{j} & \mathbf{k}\\ 0 & \cos\phi & \sin\phi\\ u & v & w\end{vmatrix} \\ &= -(2\Omega w\cos\phi - 2\Omega v\sin\phi)\,\mathbf{i} - 2\Omega u\sin\phi\,\mathbf{j} + 2\Omega u\cos\phi\,\mathbf{k} \end{aligned} \tag{2.15}$$

The pressure gradient may be expressed as

$$\nabla p = \mathbf{i}\frac{\partial p}{\partial x} + \mathbf{j}\frac{\partial p}{\partial y} + \mathbf{k}\frac{\partial p}{\partial z} \tag{2.16}$$

and gravity is conveniently represented as

$$\mathbf{g} = -g\,\mathbf{k} \tag{2.17}$$

where g is a positive scalar ($g \cong 9.8$ m s^{-2} at Earth's surface). Finally, recall from Section 1.2.2 that

$$\mathbf{F}_r = \mathbf{i}F_{rx} + \mathbf{j}F_{ry} + \mathbf{k}F_{rz} \tag{2.18}$$

Substituting (2.14) through (2.18) into the equation of motion (2.8) and equating all terms in the $\mathbf{i}$, $\mathbf{j}$, and $\mathbf{k}$ directions, respectively, we obtain

$$\frac{Du}{Dt} - \frac{uv\tan\phi}{a} + \frac{uw}{a} = -\frac{1}{\rho}\frac{\partial p}{\partial x} + 2\Omega v\sin\phi - 2\Omega w\cos\phi + F_{rx} \tag{2.19}$$

$$\frac{Dv}{Dt} + \frac{u^2\tan\phi}{a} + \frac{vw}{a} = -\frac{1}{\rho}\frac{\partial p}{\partial y} - 2\Omega u\sin\phi + F_{ry} \tag{2.20}$$

$$\frac{Dw}{Dt} - \frac{u^2+v^2}{a} = -\frac{1}{\rho}\frac{\partial p}{\partial z} - g + 2\Omega u\cos\phi + F_{rz} \tag{2.21}$$

which are the eastward, northward, and vertical component momentum equations, respectively. The terms proportional to $1/a$ on the left sides in (2.19), (2.20), and (2.21) are called *curvature* terms; they are due to the curvature the Earth.[1] Because they are nonlinear (i.e., they are quadratic in the dependent variables), they are difficult to handle in theoretical analyses. Fortunately, as shown in the next section, the curvature terms are unimportant for midlatitude synoptic-scale motions. However, even when the curvature terms are neglected,

[1] It can be shown that when r is replaced by a, as here (the traditional approximation) the Coriolis terms proportional to $\cos\phi$ in (2.19) and (2.21) must be neglected if the equations are to satisfy angular momentum conservation.

(2.19), (2.20), and (2.21) are still nonlinear partial differential equations, as can be seen by expanding the total derivatives into their local and advective parts:

$$\frac{Du}{Dt} = \frac{\partial u}{\partial t} + u\frac{\partial u}{\partial x} + v\frac{\partial u}{\partial y} + w\frac{\partial u}{\partial z}$$

with similar expressions for Dv/Dt and Dw/Dt. In general, the advective acceleration terms are comparable in magnitude to the local acceleration term. The presence of nonlinear advection processes is one reason that dynamic meteorology is an interesting and challenging subject.

2.4 SCALE ANALYSIS OF THE EQUATIONS OF MOTION

Section 1.6 discussed the basic notion of scaling the equations of motion in order to determine whether some terms in the equations are negligible for motions of meteorological concern. Elimination of terms on scaling considerations have the advantage of simplifying the mathematics; as shown in later chapters, the elimination of small terms in some cases has the very important property of completely eliminating or *filtering* an unwanted type of motion. The complete equations of motion—(2.19), (2.20), and (2.21)—describe all types and scales of atmospheric motions. Sound waves, for example, are a perfectly valid class of solutions to these equations. However, sound waves are of negligible importance in dynamical meteorology. Therefore, it will be a distinct advantage if, as turns out to be true, we can neglect the terms that lead to the production of sound waves and filter out this unwanted class of motions.

To simplify (2.19), (2.20), and (2.21) for synoptic-scale motions, we define the following characteristic scales of the field variables based on observed values for midlatitude synoptic systems.

$U \sim 10\,\mathrm{m\,s^{-1}}$	horizontal velocity scale
$W \sim 1\,\mathrm{cm\,s^{-1}}$	vertical velocity scale
$L \sim 10^6\,\mathrm{m}$	length scale [$\sim 1/(2\pi)$ wavelength]
$H \sim 10^4\,\mathrm{m}$	depth scale
$\delta P/\rho \sim 10^3\,\mathrm{m^2\,s^{-2}}$	horizontal pressure fluctuation scale
$L/U \sim 10^5\,\mathrm{s}$	time scale

Horizontal pressure fluctuation δP is normalized by the density ρ in order to produce a scale estimate that is valid at all heights in the troposphere, despite the approximate exponential decrease with height of both δP and ρ. Note that $\delta P/\rho$ has units of a geopotential. Referring back to (1.31), we see that indeed the magnitude of the fluctuation of $\delta P/\rho$ on a surface of constant height must equal the magnitude of the fluctuation of the geopotential on an isobaric surface. The time scale here is an advective one, which is appropriate for pressure systems

TABLE 2.1 Scale Analysis of the Horizontal Momentum Equations

	A	B	C	D	E	F	G
$x-$ Eq.	$\frac{Du}{Dt}$	$-2\Omega v \sin\phi$	$+2\Omega w \cos\phi$	$+\frac{uw}{a}$	$-\frac{uv\tan\phi}{a}$	$=-\frac{1}{\rho}\frac{\partial p}{\partial x}$	$+F_{rx}$
$y-$ Eq.	$\frac{Dv}{Dt}$	$+2\Omega u \sin\phi$		$+\frac{vw}{a}$	$+\frac{u^2\tan\phi}{a}$	$=-\frac{1}{\rho}\frac{\partial p}{\partial y}$	$+F_{ry}$
Scales	U^2/L	$f_0 U$	$f_0 W$	$\frac{UW}{a}$	$\frac{U^2}{a}$	$\frac{\delta P}{\rho L}$	$\frac{\nu U}{H^2}$
(m s^{-2})	10^{-4}	10^{-3}	10^{-6}	10^{-8}	10^{-5}	10^{-3}	10^{-12}

that move at approximately the speed of the horizontal wind, as is observed for synoptic-scale motions. Thus, L/U is the time required to travel a distance L at a speed U, and the substantial differential operator scales as $D/Dt \sim U/L$ for such motions.

It should be pointed out here that the synoptic-scale vertical velocity is not a directly measurable quantity. However, as shown in Chapter 3, the magnitude of w can be deduced from knowledge of the horizontal velocity field.

We can now estimate the magnitude of each term in (2.19) and (2.20) for synoptic-scale motions at a given latitude. It is convenient to consider a disturbance centered at latitude $\phi_0 = 45°$ and introduce the notation

$$f_0 = 2\Omega \sin\phi_0 = 2\Omega \cos\phi_0 \cong 10^{-4}\mathrm{s}^{-1}$$

Table 2.1 shows the characteristic magnitude of each term in (2.19) and (2.20) based on the scaling considerations given before. The molecular friction term is so small that it may be neglected for all motions except the smallest-scale turbulent motions near the ground, where vertical wind shears shear can become very large and the molecular friction term must be retained, as discussed in Chapter 8.

2.4.1 Geostrophic Approximation and Geostrophic Wind

It is apparent from Table 2.1 that for midlatitude synoptic-scale disturbances the Coriolis force (term B) and the pressure gradient force (term F) are in approximate balance. Retaining only these two terms in (2.19) and (2.20) gives as a first approximation the *geostrophic* relationship

$$-fv \approx -\frac{1}{\rho}\frac{\partial p}{\partial x}; \qquad fu \approx -\frac{1}{\rho}\frac{\partial p}{\partial y} \tag{2.22}$$

where $f \equiv 2\Omega \sin\phi$ is called the *Coriolis parameter*. The geostrophic balance is a *diagnostic* expression that gives the approximate relationship between the pressure field and horizontal velocity in large-scale extratropical systems. The approximation (2.22) contains no reference to time and therefore cannot be used to predict the evolution of the velocity field. It is for this reason that the geostrophic relationship is called a diagnostic relationship.

By analogy to the geostrophic approximation (2.22), it is possible to define a horizontal velocity field, $\mathbf{V}_g \equiv \mathbf{i}u_g + \mathbf{j}v_g$, called the *geostrophic wind*, that satisfies (2.22) identically. In vectorial form,

$$\mathbf{V}_g \equiv \mathbf{k} \times \frac{1}{\rho f} \nabla p \tag{2.23}$$

Thus, knowledge of the pressure distribution at any time determines the geostrophic wind. It should be kept clearly in mind that (2.23) always defines the geostrophic wind; however, only for large-scale motions away from the equator should the geostrophic wind be used as an approximation to the actual horizontal wind field. For the scales used in Table 2.1, the geostrophic wind approximates the true horizontal velocity to within 10 to 15% in midlatitudes.

2.4.2 Approximate Prognostic Equations: The Rossby Number

To obtain prediction equations, it is necessary to retain the acceleration (term A) in (2.19) and (2.20). The resulting approximate horizontal momentum equations are

$$\frac{Du}{Dt} = fv - \frac{1}{\rho}\frac{\partial p}{\partial x} = f\left(v - v_g\right) = fv_a \tag{2.24}$$

$$\frac{Dv}{Dt} = -fu - \frac{1}{\rho}\frac{\partial p}{\partial y} = -f\left(u - u_g\right) = -fu_a \tag{2.25}$$

where (2.23) is used to rewrite the pressure gradient force in terms of the geostrophic wind. Because the acceleration terms in (2.24) and (2.25) are proportional to the difference between the actual wind and the geostrophic wind, they are about an order of magnitude smaller than the Coriolis force and the pressure gradient force, in agreement with our scale analysis. In the final equalities of (2.24) and (2.25) we define the difference between the actual wind and the geostrophic wind as the *ageostrophic wind.*

The fact that the horizontal flow is in approximate geostrophic balance is helpful for diagnostic analysis. However, it makes actual applications of these equations in weather prognosis difficult because acceleration (which must be measured accurately) is given by the small difference between two large terms. Thus, a small error in measurement of either velocity or pressure gradient will lead to very large errors in estimating the acceleration. This problem of numerical weather prediction is discussed in Chapter 13, and the problem of simplifying the equations for physical understanding based on the smallness of the ageostrophic wind will be taken up in Chapter 6.

A convenient measure of the magnitude of the acceleration compared to the Coriolis force may be obtained by forming the ratio of the characteristic scales for the acceleration and Coriolis force terms: $(U^2/L)/(f_0U)$. This ratio is a nondimensional number called the *Rossby number* after the Swedish meteorologist C. G. Rossby (1898–1957) and is designated by

$$\mathrm{Ro} \equiv U/(f_0 L)$$

Thus, the smallness of the Rossby number is a measure of the validity of the geostrophic approximation.

2.4.3 The Hydrostatic Approximation

A similar scale analysis can be applied to the vertical component of the momentum equation (2.21). Because pressure decreases by about an order of magnitude from the ground to the tropopause, the vertical pressure gradient may be scaled by P_0/H, where P_0 is the surface pressure and H is the depth of the troposphere. The terms in (2.21) may then be estimated for synoptic-scale motions and are shown in Table 2.2. As with the horizontal component equations, we consider motions centered at 45° latitude and neglect friction. The scaling indicates that to a high degree of accuracy the pressure field is in *hydrostatic equilibrium*; that is, the pressure at any point is simply equal to the weight of a unit cross-section column of air above that point.

The preceding analysis of the vertical momentum equation is, however, somewhat misleading. It is not sufficient to show merely that the vertical acceleration is small compared to g. Because only that part of the pressure field that varies horizontally is directly coupled to the horizontal velocity field, it is actually necessary to show that the horizontally varying pressure component is itself in hydrostatic equilibrium with the horizontally varying density field. To show this, it is convenient to first define a standard pressure $p_0(z)$, which is the horizontally averaged pressure at each height, and a corresponding standard density $\rho_0(z)$, defined so that $p_0(z)$ and $\rho_0(z)$ are in *exact* hydrostatic balance:

$$\frac{1}{\rho_0}\frac{dp_0}{dz} \equiv -g \tag{2.26}$$

TABLE 2.2 Scale Analysis of the Vertical Momentum Equation

$z-$ Eq.	Dw/Dt	$-2\Omega u\cos\phi$	$-(u^2+v^2)/a$	$= -\rho^{-1}\partial p/\partial z$	$-g$	$+\mathrm{F}_{rz}$
Scales	UW/L	f_0U	U^2/a	$P_0/(\rho H)$	g	νWH^{-2}
m s^{-2}	10^{-7}	10^{-3}	10^{-5}	10	10	10^{-15}

We may then write the total pressure and density fields as

$$
\begin{aligned}
p(x, y, z, t) &= p_0(z) + p'(x, y, z, t) \\
\rho(x, y, z, t) &= \rho_0(z) + \rho'(x, y, z, t)
\end{aligned}
\tag{2.27}
$$

where p' and ρ' are deviations from the standard values of pressure and density, respectively. For an atmosphere at rest, p' and ρ' would thus be zero. Using the definitions of (2.26) and (2.27) and assuming that ρ'/ρ_0 is much less than unity in magnitude so that $(\rho_0 + \rho')^{-1} \cong \rho_0^{-1}$ $(1 - \rho'/\rho_0)$, we find that

$$
\begin{aligned}
-\frac{1}{\rho}\frac{\partial p}{\partial z} - g &= -\frac{1}{(\rho_0 + \rho')}\frac{\partial}{\partial z}\left(p_0 + p'\right) - g \\
&\approx \frac{1}{\rho_0}\left[\frac{\rho'}{\rho_0}\frac{dp_0}{dz} - \frac{\partial p'}{\partial z}\right] = -\frac{1}{\rho_0}\left[\rho' g + \frac{\partial p'}{\partial z}\right]
\end{aligned}
\tag{2.28}
$$

For synoptic-scale motions, the terms in (2.28) have the magnitudes

$$
\frac{1}{\rho_0}\frac{\partial p'}{\partial z} \sim \left[\frac{\delta P}{\rho_0 H}\right] \sim 10^{-1}\mathrm{m\ s^{-2}}, \qquad \frac{\rho' g}{\rho_0} \sim 10^{-1}\mathrm{m\ s^{-2}}
$$

Comparing these with the magnitudes of other terms in the vertical momentum equation (refer to Table 2.2), we see that to a very good approximation the perturbation pressure field is in hydrostatic equilibrium with the perturbation density field so that

$$
\frac{\partial p'}{\partial z} + \rho' g = 0 \tag{2.29}
$$

Therefore, for synoptic-scale motions, vertical accelerations are negligible and the vertical velocity cannot be determined from the vertical momentum equation. However, we show in Chapter 3 that it is, nevertheless, possible to deduce the vertical motion field indirectly. Moreover, in Chapter 6 we show that the vertical motion field may be estimated, and physically understood, from knowledge of the pressure field alone.

2.5 THE CONTINUITY EQUATION

We turn now to the second of the three fundamental conservation principles: conservation of mass. The mathematical relationship that expresses conservation of mass for a fluid is called the *continuity equation*. This section develops the continuity equation using two alternative methods. The first method is based on an Eulerian control volume, whereas the second is based on a Lagrangian control volume.

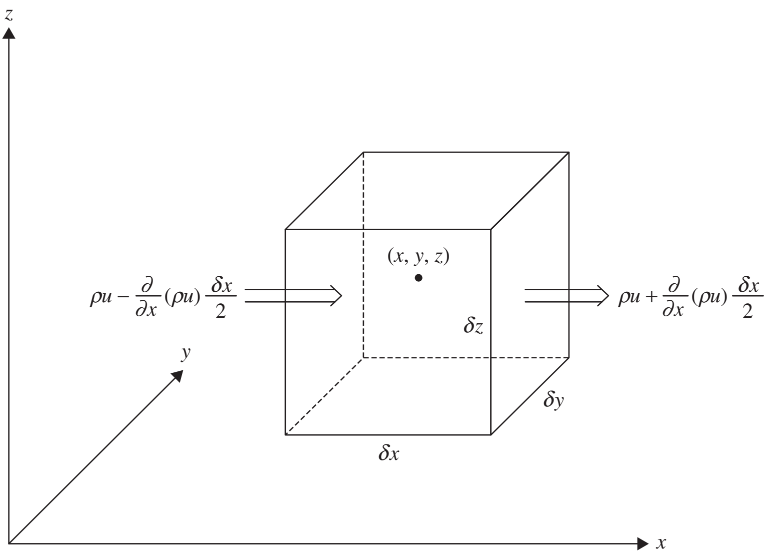

FIGURE 2.5 Mass inflow into a fixed (Eulerian) control volume as a result of motion parallel to the x axis.

2.5.1 A Eulerian Derivation

We consider a volume element $\delta x \delta y \delta z$ that is fixed in a Cartesian coordinate frame as shown in Figure 2.5. For such a fixed control volume, the net rate of mass inflow through the sides must equal the rate of accumulation of mass within the volume. The rate of inflow of mass through the left face per unit area is

$$\left[\rho u - \frac{\partial}{\partial x}(\rho u)\frac{\delta x}{2}\right]$$

whereas the rate of outflow per unit area through the right face is

$$\left[\rho u + \frac{\partial}{\partial x}(\rho u)\frac{\delta x}{2}\right]$$

Because the area of each of these faces is $\delta y \delta z$, the net rate of flow into the volume due to the x velocity component is

$$\left[\rho u - \frac{\partial}{\partial x}(\rho u)\frac{\delta x}{2}\right]\delta y \delta z - \left[\rho u + \frac{\partial}{\partial x}(\rho u)\frac{\delta x}{2}\right]\delta y \delta z = -\frac{\partial}{\partial x}(\rho u)\delta x \delta y \delta z$$

Similar expressions obviously hold for the y and z directions. Thus, the net rate of mass inflow is

$$-\left[\frac{\partial}{\partial x}(\rho u) + \frac{\partial}{\partial y}(\rho v) + \frac{\partial}{\partial z}(\rho w)\right]\delta x \delta y \delta z$$

and the mass inflow per unit volume is just $-\nabla \cdot (\rho \mathbf{U})$, which must equal the rate of mass increase per unit volume. Now the increase of mass per unit volume is just the local density change $\partial\rho/\partial t$. Therefore,

$$\frac{\partial \rho}{\partial t} + \nabla \cdot (\rho \mathbf{U}) = 0 \qquad (2.30)$$

Equation (2.30) is the mass divergence form of the continuity equation.

An alternative form of the continuity equation is obtained by applying the vector identity

$$\nabla \cdot (\rho \mathbf{U}) \equiv \rho \nabla \cdot \mathbf{U} + \mathbf{U} \cdot \nabla \rho$$

and the relationship

$$\frac{D}{Dt} \equiv \frac{\partial}{\partial t} + \mathbf{U} \cdot \nabla$$

to get

$$\frac{1}{\rho}\frac{D\rho}{Dt} + \nabla \cdot \mathbf{U} = 0 \qquad (2.31)$$

Equation (2.31) is the velocity divergence form of the continuity equation. It states that the fractional rate of increase of the density *following the motion* of an air parcel is equal to minus the velocity divergence (i.e., convergence). This should be clearly distinguished from (2.30), which states that the *local* rate of change of density is equal to minus the mass divergence.

2.5.2 A Lagrangian Derivation

The physical meaning of divergence can be illustrated by the following alternative derivation of (2.31). Consider a control volume of fixed mass δM that moves with the fluid. Letting $\delta V = \delta x \delta y \delta z$ be the volume, we find that because $\delta M = \rho \delta V = \rho \delta x \delta y \delta z$ is conserved following the motion, we can write

$$\frac{1}{\delta M}\frac{D}{Dt}(\delta M) = \frac{1}{\rho \delta V}\frac{D}{Dt}(\rho \delta V) = \frac{1}{\rho}\frac{D\rho}{Dt} + \frac{1}{\delta V}\frac{D}{Dt}(\delta V) = 0 \qquad (2.32)$$

but

$$\frac{1}{\delta V}\frac{D}{Dt}(\delta V) = \frac{1}{\delta x}\frac{D}{Dt}(\delta x) + \frac{1}{\delta y}\frac{D}{Dt}(\delta y) + \frac{1}{\delta z}\frac{D}{Dt}(\delta z)$$

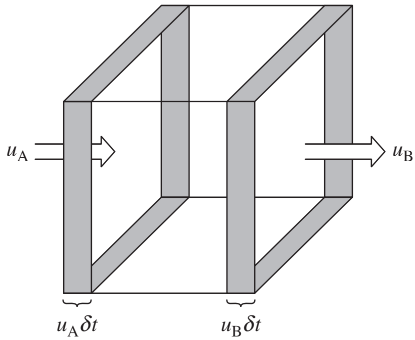

FIGURE 2.6 Change in Lagrangian control volume (shown by shading) as a result of fluid motion parallel to the x axis.

Referring to Figure 2.6, we see that the faces of the control volume in the y, z plane (designated A and B) are advected with the flow in the x direction at speeds $u_A = Dx/Dt$ and $u_B = D(x + \delta x)/Dt$, respectively. Thus, the difference in speeds of the two faces is $\delta u = u_B - u_A = D(x + \delta x)/Dt - Dx/Dt$ or $\delta u = D(\delta x)/Dt$. Similarly, $\delta v = D(\delta y)/Dt$ and $\delta w = D(\delta z)/Dt$. Therefore,

$$\lim_{\delta x, \delta y, \delta z \to 0} \left[\frac{1}{\delta V} \frac{D}{Dt}(\delta V) \right] = \frac{\partial u}{\partial x} + \frac{\partial v}{\partial y} + \frac{\partial w}{\partial z} = \nabla \cdot \mathbf{U}$$

so that in the limit $\delta V \to 0$, (2.32) reduces to the continuity equation (2.31); the divergence of the three-dimensional velocity field is equal to the fractional rate of change of the volume of a fluid parcel in the limit $\delta V \to 0$. It is left as a problem for the student to show that the divergence of the *horizontal* velocity field is equal to the fractional rate of change of the horizontal area δA of a fluid parcel in the limit $\delta A \to 0$.

2.5.3 Scale Analysis of the Continuity Equation

Following the technique developed in Section 2.4.3, and again assuming that $|\rho'/\rho_0| \ll 1$, we can approximate the continuity (2.31) as

$$\underset{\text{A}}{\frac{1}{\rho_0}\left(\frac{\partial \rho'}{\partial t} + \mathbf{U} \cdot \nabla \rho'\right)} + \underset{\text{B}}{\frac{w}{\rho_0}\frac{d\rho_0}{dz}} + \underset{\text{C}}{\nabla \cdot \mathbf{U}} \approx 0 \tag{2.33}$$

where ρ' designates the local deviation of density from its horizontally averaged value, $\rho_0(z)$. For synoptic-scale motions, $\rho'/\rho_0 \sim 10^{-2}$ so that, using the characteristic scales given in Section 2.4, we find that term A has magnitude

$$\frac{1}{\rho_0}\left(\frac{\partial \rho'}{\partial t} + \mathbf{U} \cdot \nabla \rho'\right) \sim \frac{\rho'}{\rho_0}\frac{U}{L} \approx 10^{-7}\text{s}^{-1}$$

For motions in which the depth scale H is comparable to the density scale height, $d \ln \rho_0/dz \sim H^{-1}$, so that term B scales as

$$\frac{w}{\rho_0}\frac{d\rho_0}{dz} \backsim \frac{W}{H} \approx 10^{-6}\text{s}^{-1}$$

Expanding term C in Cartesian coordinates, we have

$$\nabla \cdot \mathbf{U} = \frac{\partial u}{\partial x} + \frac{\partial v}{\partial y} + \frac{\partial w}{\partial z}$$

For synoptic-scale motions, the terms $\partial u/\partial x$ and $\partial v/\partial y$ tend to be of equal magnitude but opposite sign. Thus, they tend to balance so that

$$\left(\frac{\partial u}{\partial x} + \frac{\partial v}{\partial y}\right) \backsim 10^{-1}\frac{U}{L} \approx 10^{-6}\,\text{s}^{-1}$$

In addition,

$$\frac{\partial w}{\partial z} \sim \frac{W}{H} \approx 10^{-6}\,\text{s}^{-1}$$

Thus, terms B and C are each an order of magnitude greater than term A, and, to a first approximation, terms B and C balance in the continuity equation. To a good approximation, then

$$\frac{\partial u}{\partial x} + \frac{\partial v}{\partial y} + \frac{\partial w}{\partial z} + w\frac{d}{dz}(\ln \rho_0) = 0$$

or, alternatively, in vector form

$$\nabla \cdot (\rho_0 \mathbf{U}) = 0 \tag{2.34}$$

Thus, for synoptic-scale motions the mass flux computed using the basic state density ρ_0 is nondivergent. This approximation is similar to the idealization of incompressibility, which is often used in fluid mechanics. However, an *incompressible* fluid has a density constant following the motion

$$\frac{D\rho}{Dt} = 0$$

Thus, by (2.31) the velocity divergence vanishes ($\nabla \cdot \mathbf{U} = 0$) in an incompressible fluid, which is not the same as (2.34). Our approximation (2.34) shows that for purely horizontal flow the atmosphere behaves as though it were an incompressible fluid. However, when there is vertical motion, the compressibility associated with the height dependence of ρ_0 must be taken into account.

2.6 THE THERMODYNAMIC ENERGY EQUATION

We now turn to the third fundamental conservation principle: the conservation of energy as applied to a moving fluid element. The first law of thermodynamics is usually derived by considering a system in thermodynamic equilibrium—that is, a system that is initially at rest and, after exchanging heat with its surroundings and doing work on the surroundings, is again at rest. For such a system the first law states that *the change in internal energy of the system is equal to the difference between the heat added to the system and the work done by the system*. A Lagrangian control volume consisting of a specified mass of fluid may be regarded as a thermodynamic system. However, unless the fluid is at rest, it will not be in thermodynamic equilibrium. Nevertheless, the first law of thermodynamics still applies.

To show that this is the case, we note that the total thermodynamic energy of the control volume is considered to consist of the sum of the internal energy (due to the kinetic energy of the individual molecules) and the kinetic energy due to the macroscopic motion of the fluid. The rate of change of this total thermodynamic energy is equal to the rate of diabatic heating plus the rate at which work is done on the fluid parcel by external forces.

If we let e designate the internal energy per unit mass, then the total thermodynamic energy contained in a Lagrangian fluid element of density ρ and volume δV is $\rho\,[e + (1/2)\mathbf{U}\cdot\mathbf{U}]\,\delta V$. The external forces that act on a fluid element may be divided into surface forces, such as pressure and viscosity, and body forces, such as gravity or the Coriolis force. The rate at which work is done on the fluid element by the x component of the pressure force is illustrated in Figure 2.7. Recalling that pressure is a force per unit area and that the rate at which a force does work is given by the dot product of the force and velocity

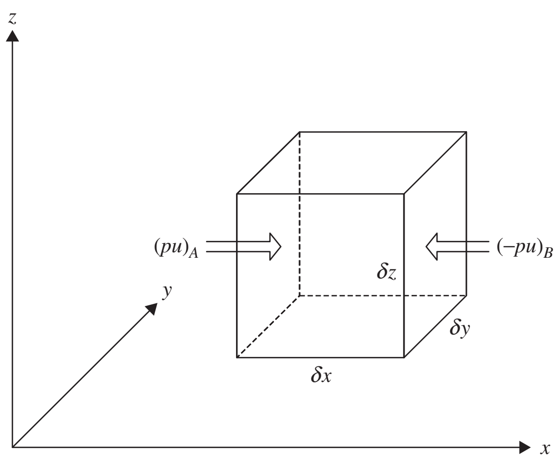

FIGURE 2.7 Rate of working on a fluid element due to the x component of the pressure force.

vectors, we see that the rate at which the surrounding fluid does work on the element due to the pressure force on the two boundary surfaces in the y, z plane is given by

$$(pu)_A \delta y \delta z - (pu)_B \delta y \delta z$$

(The negative sign is needed before the second term because the work done on the fluid element is positive if u is negative across face B.) Now, by expanding in a Taylor series, we can write

$$(pu)_B = (pu)_A + \left[\frac{\partial}{\partial x}(pu)\right]_A \delta x + \cdots$$

Thus, the net rate at which the pressure force does work due to the x component of motion is

$$\left[(pu)_A - (pu)_B\right] \delta y \delta z = -\left[\frac{\partial}{\partial x}(pu)\right]_A \delta V$$

where $\delta V = \delta x \delta y \delta z$.

Similarly, we can show that the net rates at which the pressure force does work due to the y and z components of motion are

$$-\left[\frac{\partial}{\partial y}(pv)\right] \delta V \text{ and } -\left[\frac{\partial}{\partial z}(pw)\right] \delta V$$

respectively. Hence, the total rate at which work is done by the pressure force is simply

$$-\nabla \cdot (p\mathbf{U})\delta V$$

The only body forces of meteorological significance that act on an element of mass in the atmosphere are the Coriolis force and gravity. However, because the Coriolis force, $-2\boldsymbol{\Omega} \times \mathbf{U}$, is perpendicular to the velocity vector, it can do no work. Thus, the rate at which body forces do work on the mass element is just $\rho\mathbf{g} \cdot \mathbf{U}\, \delta V$.

Applying the principle of energy conservation to our Lagrangian control volume (neglecting effects of molecular viscosity), we thus obtain

$$\frac{D}{Dt}\left[\rho\left(e + \frac{1}{2}\mathbf{U}\cdot\mathbf{U}\right)\delta V\right] = -\nabla \cdot (p\mathbf{U})\delta V + \rho\mathbf{g}\cdot\mathbf{U}\delta V + \rho J \delta V \qquad (2.35)$$

Here J is the rate of heating per unit mass due to radiation, conduction, and latent heat release. With the aid of the chain rule of differentiation, we can rewrite (2.35) as

$$\begin{aligned} \rho\delta V \frac{D}{Dt}\left(e + \frac{1}{2}\mathbf{U}\cdot\mathbf{U}\right) + \left(e + \frac{1}{2}\mathbf{U}\cdot\mathbf{U}\right)\frac{D(\rho\delta V)}{Dt} \\ = -\mathbf{U}\cdot\nabla p\, \delta V - p\nabla\cdot\mathbf{U}\, \delta V - \rho g w\, \delta V + \rho J\, \delta V \end{aligned} \qquad (2.36)$$

where we have used $\mathbf{g} = -g\mathbf{k}$. Now, from (2.32), the second term on the left in (2.36) vanishes so that

$$\rho\frac{De}{Dt} + \rho\frac{D}{Dt}\left(\frac{1}{2}\mathbf{U}\cdot\mathbf{U}\right) = -\mathbf{U}\cdot\nabla p - p\nabla\cdot\mathbf{U} - \rho g w + \rho J \tag{2.37}$$

This equation can be simplified by noting that if we take the dot product of $\mathbf{U}$ with the momentum equation (2.8), we obtain (neglecting friction)

$$\rho\frac{D}{Dt}\left(\frac{1}{2}\mathbf{U}\cdot\mathbf{U}\right) = -\mathbf{U}\cdot\nabla p - \rho g w \tag{2.38}$$

Subtracting (2.38) from (2.37), we obtain

$$\rho\frac{De}{Dt} = -p\nabla\cdot\mathbf{U} + \rho J \tag{2.39}$$

The terms in (2.37) that were eliminated by subtracting (2.38) represent the balance of mechanical energy due to the motion of the fluid element; the remaining terms represent the thermal energy balance.

Using the definition of geopotential (1.11), we have

$$gw = g\frac{Dz}{Dt} = \frac{D\Phi}{Dt}$$

so that (2.38) can be rewritten as

$$\rho\frac{D}{Dt}\left(\frac{1}{2}\mathbf{U}\cdot\mathbf{U} + \Phi\right) = -\mathbf{U}\cdot\nabla p \tag{2.40}$$

which is referred to as the *mechanical energy equation*. The sum of the kinetic energy plus the gravitational potential energy is called the *mechanical energy*. Thus, (2.40) states that following the motion, the rate of change of mechanical energy per unit volume equals the rate at which work is done by the pressure gradient force.

The thermal energy equation (2.39) can be written in more familiar form by noting from (2.31) that

$$\frac{1}{\rho}\nabla\cdot\mathbf{U} = -\frac{1}{\rho^2}\frac{D\rho}{Dt} = \frac{D\alpha}{Dt}$$

and that for dry air the internal energy per unit mass is given by $e = c_v T$, where $c_v (= 717\ \mathrm{J\ kg^{-1}\ K^{-1}})$ is the specific heat at constant volume. We then obtain

$$c_v\frac{DT}{Dt} + p\frac{D\alpha}{Dt} = J \tag{2.41}$$

which is the usual form of the thermodynamic energy equation. Thus, the first law of thermodynamics indeed is applicable to a fluid in motion. The second term on the left, representing the rate of working by the fluid system (per unit mass), represents a conversion between thermal and mechanical energy. This conversion process enables the solar heat energy to drive the motions of the atmosphere.

2.7 THERMODYNAMICS OF THE DRY ATMOSPHERE

Taking the total derivative of the equation of state (1.25), we obtain

$$p\frac{D\alpha}{Dt} + \alpha\frac{Dp}{Dt} = R\frac{DT}{Dt}$$

Substituting for $pD\alpha/Dt$ in (2.41) and using $c_p = c_v + R$, where $c_p(= 1004$ J kg^{-1} K^{-1}) is the specific heat at constant pressure, we can rewrite the first law of thermodynamics as

$$c_p\frac{DT}{Dt} - \alpha\frac{Dp}{Dt} = J \tag{2.42}$$

Dividing through by T and again using the equation of state, we obtain the entropy form of the first law of thermodynamics:

$$c_p\frac{D\ln T}{Dt} - R\frac{D\ln p}{Dt} = \frac{J}{T} \equiv \frac{Ds}{Dt} \tag{2.43}$$

Equation (2.43) gives the rate of change of entropy per unit mass following the motion for a thermodynamically *reversible* process. A reversible process is one in which a system changes its thermodynamic state and then returns to the original state without changing its surroundings. For such a process the entropy s defined by (2.43) is a field variable that depends only on the state of the fluid. Thus, Ds is a perfect differential, and Ds/Dt is to be regarded as a total derivative. However, "heat" is not a field variable, so the heating rate J is not a total derivative.[2]

2.7.1 Potential Temperature

For an ideal gas that is undergoing an *adiabatic* process (i.e., a reversible process in which no heat is exchanged with the surroundings), the first law of thermodynamics can be written in differential form as

$$c_p D\ln T - RD\ln p = D\left(c_p \ln T - R\ln p\right) = 0$$

Integrating this expression from a state at pressure p and temperature T to a state in which the pressure is p_s and the temperature is θ, we obtain, after taking the antilogarithm,

$$\theta = T\,(p_s/p)^{R/c_p} \tag{2.44}$$

[2]For a discussion of entropy and its role in the second law of thermodynamics, see Curry and Webster (1999), for example.

This relationship in (2.44) is referred to as Poisson's equation, and the temperature θ defined by (2.44) is called the *potential temperature*. θ is simply the temperature that a parcel of dry air at pressure p and temperature T would have if it were expanded or compressed adiabatically to a standard pressure p_s (usually taken to be 1000 hPa). Thus, every air parcel has a unique value of potential temperature, and this value is conserved for dry adiabatic motion. Because synoptic-scale motions are approximately adiabatic outside regions of active precipitation, θ is a quasi-conserved quantity for such motions.

Taking the logarithm of (2.44) and differentiating, we find that

$$c_p \frac{D \ln \theta}{Dt} = c_p \frac{D \ln T}{Dt} - R \frac{D \ln p}{Dt} \tag{2.45}$$

Comparing (2.43) and (2.45), we obtain

$$c_p \frac{D \ln \theta}{Dt} = \frac{J}{T} = \frac{Ds}{Dt} \tag{2.46}$$

Thus, for reversible processes, changes in fractional potential temperature are indeed proportional to entropy changes. A parcel that conserves entropy following the motion must move along an isentropic (constant θ) surface.

2.7.2 The Adiabatic Lapse Rate

A relationship between the *lapse rate* of temperature (i.e., the rate of *decrease* of temperature with respect to height) and the rate of change of potential temperature with respect to height can be obtained by taking the logarithm of (2.44) and differentiating with respect to height. Using the hydrostatic equation and the ideal gas law to simplify the result gives

$$\frac{T}{\theta} \frac{\partial \theta}{\partial z} = \frac{\partial T}{\partial z} + \frac{g}{c_p} \tag{2.47}$$

For an atmosphere in which the potential temperature is constant with respect to height, the lapse rate is thus

$$-\frac{dT}{dz} = \frac{g}{c_p} \equiv \Gamma_d \tag{2.48}$$

Thus, the dry adiabatic lapse rate is approximately constant throughout the lower atmosphere.

2.7.3 Static Stability

If potential temperature is a function of height, the atmospheric lapse rate, $\Gamma \equiv -\partial \mathrm{T}/\partial z$, will differ from the adiabatic lapse rate and

$$\frac{T}{\theta} \frac{\partial \theta}{\partial z} = \Gamma_d - \Gamma \tag{2.49}$$

If $\Gamma < \Gamma_d$ so that θ increases with height, an air parcel that undergoes an adiabatic displacement from its equilibrium level will be positively buoyant when displaced downward and negatively buoyant when displaced upward, so that it will tend to return to its equilibrium level and the atmosphere is said to be statically stable or *stably stratified*.

Adiabatic oscillations of a fluid parcel about its equilibrium level in a stably stratified atmosphere are referred to as *buoyancy oscillations*. The characteristic frequency of such oscillations can be derived by considering a parcel that is displaced vertically a small distance δz without disturbing its environment. If the environment is in hydrostatic balance, $\rho_0 g = -dp_0/dz$, where p_0 and ρ_0 are the pressure and density of the environment, respectively. The vertical acceleration of the parcel is

$$\frac{Dw}{Dt} = \frac{D^2}{Dt^2}(\delta z) = -g - \frac{1}{\rho}\frac{\partial p}{\partial z} \tag{2.50}$$

where p and ρ are the pressure and density of the parcel, respectively. In the parcel method it is assumed that the pressure of the parcel adjusts instantaneously to the environmental pressure during the displacement: $p = p_0$. This condition must be true if the parcel is to leave the environment undisturbed. Thus, with the aid of the hydrostatic relationship, pressure can be eliminated in (2.50) to give

$$\frac{D^2}{Dt^2}(\delta z) = g\left(\frac{\rho_0 - \rho}{\rho}\right) = g\frac{\theta}{\theta_0} \tag{2.51}$$

where (2.44) and the ideal gas law have been used to express the buoyancy force in terms of potential temperature. Here θ designates the deviation of the potential temperature of the parcel from its basic state (environmental) value $\theta_0(z)$. If the parcel is initially at level $z = 0$ where the potential temperature is $\theta_0(0)$, then for a small displacement δz, we can represent the environmental potential temperature as

$$\theta_0(\delta z) \approx \theta_0(0) + (d\theta_0/dz)\,\delta z$$

If the parcel displacement is adiabatic, the potential temperature of the parcel is conserved. Thus, $\theta(\delta z) = \theta_0(0) - \theta_0(\delta z) = -(d\theta_0/dz)\delta z$, and (2.51) becomes

$$\frac{D^2}{Dt^2}(\delta z) = -N^2 \delta z \tag{2.52}$$

where

$$N^2 = g\frac{d \ln \theta_0}{dz}$$

is a measure of the static stability of the environment. Equation (2.52) has a general solution of the form $\delta z = A\exp(iNt)$. Therefore, if $N^2 > 0$, the parcel will oscillate about its initial level with a period $\tau = 2\pi/N$. The corresponding frequency N is the *buoyancy frequency*.[3] For average tropospheric conditions, $N \approx 1.2 \times 10^{-2}\,\mathrm{s}^{-1}$ so that the period of a buoyancy oscillation is about 8 min.

In the case of $N = 0$, examination of (2.52) indicates that no accelerating force will exist and the parcel will be in neutral equilibrium at its new level. However, if $N^2 < 0$ (potential temperature decreasing with height), the displacement will increase exponentially with time. We thus arrive at the familiar gravitational or static stability criteria for dry air:

$d\theta_0/dz > 0$	statically stable
$d\theta_0/dz = 0$	statically neutral
$d\theta_0/dz < 0$	statically unstable

On the synoptic-scale the atmosphere is always stably stratified because any unstable regions that develop are stabilized quickly by convective overturning.

2.7.4 Scale Analysis of the Thermodynamic Energy Equation

If potential temperature is divided into a basic state $\theta_0(z)$ and a deviation $\theta\,(x, y, z, t)$ so that the total potential temperature at any point is given by $\theta_{\mathrm{tot}} = \theta_0\,(z) + \theta\,(x, y, z, t)$, the first law of thermodynamics (2.46) can be written approximately for synoptic scaling as

$$\frac{1}{\theta_0}\left(\frac{\partial \theta}{\partial t} + u\frac{\partial \theta}{\partial x} + v\frac{\partial \theta}{\partial y}\right) + w\frac{d \ln \theta_0}{dz} = \frac{J}{c_p T} \tag{2.53}$$

where we have used the facts that for $|\theta/\theta_0| \ll 1$, $|d\theta/dz| \ll d\theta_0/dz$, and

$$\ln \theta_{\mathrm{tot}} = \ln\left[\theta_0\,(1 + \theta/\theta_0)\right] \approx \ln \theta_0 + \theta/\theta_0$$

Outside regions of active precipitation, diabatic heating is due primarily to net radiative heating. In the troposphere, radiative heating is quite weak so that typically $J/c_p \leq 1^\circ\mathrm{C\,d^{-1}}$ (except near cloud tops, where substantially larger cooling can occur due to thermal emission by the cloud particles). The typical amplitude of horizontal potential temperature fluctuations in a midlatitude synoptic system (above the boundary layer) is $\theta \sim 4^\circ\mathrm{C}$. Thus,

$$\frac{T}{\theta_0}\left(\frac{\partial \theta}{\partial t} + u\frac{\partial \theta}{\partial x} + v\frac{\partial \theta}{\partial y}\right) \sim \frac{\theta U}{L} \sim 4^\circ\mathrm{C\,d^{-1}}$$

The cooling due to vertical advection of the basic state potential temperature (usually called adiabatic cooling) has a typical magnitude of

$$w\left(\frac{T}{\theta_0}\frac{d\theta_0}{dz}\right) = w\,(\Gamma_d - \Gamma) \sim 4^\circ\mathrm{C\,d^{-1}}$$

[3] N is often referred to as the Brunt–Väisälä frequency.

where $w \sim 1$ cm s^{-1}, and $\Gamma_d - \Gamma$, the difference between dry adiabatic and actual lapse rates, is $\sim 4°$ C km^{-1}.

Thus, in the absence of strong diabatic heating, the rate of change in the perturbation potential temperature is equal to the adiabatic heating or cooling due to vertical motion in the statically stable basic state, and (2.54) can be approximated as

$$\left(\frac{\partial \theta}{\partial t} + u\frac{\partial \theta}{\partial x} + v\frac{\partial \theta}{\partial y}\right) + w\frac{d\theta_0}{dz} \approx 0 \tag{2.54}$$

Alternatively, if the temperature field is divided into a basic state $T_0(z)$ and a deviation $T(x, y, z, t)$, then, since $\theta/\theta_0 \approx T/T_0$, (2.54) can be expressed to the same order of approximation in terms of temperature as

$$\left(\frac{\partial T}{\partial t} + u\frac{\partial T}{\partial x} + v\frac{\partial T}{\partial y}\right) + w(\Gamma_d - \Gamma) \approx 0 \tag{2.55}$$

2.8 THE BOUSSINESQ APPROXIMATION

In some situations, air parcel vertical displacements are relatively small, so the density change following the motion is also small. The *Boussinesq approximation* yields a simplified form of the dynamical equations that are appropriate to this situation. In this approximation, density is replaced by a constant mean value, ρ_0, everywhere except in the buoyancy term in the vertical momentum equation. The horizontal momentum equations (2.24) and (2.25) can then be expressed in Cartesian coordinates as

$$\frac{Du}{Dt} = -\frac{1}{\rho_0}\frac{\partial p}{\partial x} + fv + F_{rx} \tag{2.56}$$

and

$$\frac{Dv}{Dt} = -\frac{1}{\rho_0}\frac{\partial p}{\partial y} - fu + F_{ry} \tag{2.57}$$

while, with the aid of equations (2.28) and (2.51), the vertical momentum equation becomes

$$\frac{Dw}{Dt} = -\frac{1}{\rho_0}\frac{\partial p}{\partial z} + g\frac{\theta}{\theta_0} + F_{rz} \tag{2.58}$$

Here, as in Section 2.7.3 θ designates the perturbation departure of potential temperature from its basic state value $\theta_0(z)$. Thus, the total potential temperature field is given by $\theta_{tot} = \theta(x, y, z, t) + \theta_0(z)$, and the adiabatic thermodynamic energy equation has a form similar to (2.54),

$$\frac{D\theta}{Dt} = -w\frac{d\theta_0}{dz} \tag{2.59}$$

except, from the full material derivative, we see that the vertical advection of perturbation potential temperature is formally included. Finally, the continuity equation (2.34) under the Boussinesq approximation is

$$\frac{\partial u}{\partial x} + \frac{\partial v}{\partial y} + \frac{\partial w}{\partial z} = 0 \tag{2.60}$$

2.9 THERMODYNAMICS OF THE MOIST ATMOSPHERE

Although it is convenient as a first approximation to neglect the role of water vapor in atmospheric dynamics, it sometimes plays an important, if not essential, role. Most often it is the change in phase of water, and the accompanying latent heat release, that affects the dynamics, but even just the presence of water vapor can be critical to the buoyancy acceleration. Water vapor is a highly variable constituent in the atmosphere and as such presents a challenge to the ideal gas law, since the gas constant depends on the molecular composition of air. For dry air the ideal gas law is

$$p_d = \rho_d R_d T \tag{2.61}$$

where p_d and ρ_d are the dry air pressure and density, respectively, and R_d is the dry air gas constant. For pure water vapor, the ideal gas law is

$$e = \rho_v R_v T \tag{2.62}$$

where e and ρ_v are the vapor pressure and density, respectively, and R_v is the water vapor gas constant. For moist air (a mixture of dry air and water vapor) we choose

$$p = \rho R_d T_v \tag{2.63}$$

where p and ρ are the pressure and density, respectively, and T_v is the *virtual temperature*, which represents the temperature dry air needs to have the same pressure and density as moist air. This formulation allows use of the dry air gas constant everywhere. By adding (2.61) and (2.62), it can be shown that the virtual temperature is given by

$$T_v = \frac{T}{1 - \frac{e}{p}\left(1 - \frac{R_d}{R_v}\right)} \tag{2.64}$$

We see that $T_v \geq T$, and the difference is typically on the order of a few degrees Celsius or less; nevertheless, even these small changes can make the difference between an air parcel being stable or unstable.

There are many measures of water vapor in the atmosphere, and we summarize here some of the most common. A measure used earlier in the ideal gas law is the vapor pressure that by Dalton's Law is simply the contribution to the total pressure from water vapor. Saturation vapor pressure is determined solely by temperature as given by the Clausius–Clapeyron equation[4]

$$\frac{1}{e_s}\frac{de_s}{dT} = \frac{L}{R_v T^2} \tag{2.65}$$

For water vapor over a plane surface of liquid water (ice), L represents the latent heat of condensation (sublimation). Saturation vapor pressure depends approximately exponentially on temperature and, for temperatures below freezing, is larger above water surfaces than ice. Relative humidity may be defined as the percentage

$$RH = 100 \times \frac{e}{e_s} \tag{2.66}$$

and e_s may apply to either water or ice saturation; if unspecified, the former may be assumed with confidence.

The water vapor mixing ratio is given by the ratio of the mass of water vapor to the mass of dry air in a volume of air, which takes units of either kg/kg or, more commonly, g/kg. From (2.61) and (2.62), the mixing ratio is given by

$$q = 0.622\frac{e}{p - e} \tag{2.67}$$

where the leading coefficient 0.622 reflects the ratio of the molecular weight of water vapor to dry air.

There are several ways to bring moist air to saturation, one of which is by cooling the air at constant pressure without addition or removal of water vapor. Saturation achieved in this manner gives the dew point temperature.

2.9.1 Equivalent Potential Temperature

We previously applied the parcel method to discuss the vertical stability of a dry atmosphere. We found that the stability of a dry parcel with respect to a vertical displacement depends on the lapse rate of potential temperature in the environment such that a parcel displacement is stable, provided that $\partial\theta/\partial z > 0$ (i.e., the actual lapse rate is less than the adiabatic lapse rate). The same condition also applies to parcels in a moist atmosphere when the relative humidity is less than 100%. If, however, a parcel of moist air is forced to rise, it will eventually

[4] For a derivation see, for example, Curry and Webster (1999, p. 108).

become saturated at a level called the lifting condensation level (LCL). A further forced rise will then cause condensation and latent heat release, and the parcel will then cool at the saturated adiabatic lapse rate. If the environmental lapse rate is greater than the saturated adiabatic lapse rate, and the parcel is forced to continue to rise, it will reach a level at which it becomes buoyant relative to its surroundings. It can then freely accelerate upward. The level at which this occurs is called the level of free convection (LFC).

Discussion of parcel dynamics in a moist atmosphere is facilitated by defining a thermodynamic field called the *equivalent potential temperature*. Equivalent potential temperature, designated θ_e, is the potential temperature that a parcel of air would have if all its moisture were condensed and the resultant latent heat used to warm the parcel. The temperature of an air parcel can be brought to its equivalent potential value by raising the parcel from its original level until all the water vapor in the parcel has condensed and fallen out, and then compressing the parcel adiabatically to a pressure of 1000 hPa. Because the condensed water is assumed to fall out, the temperature increase during the compression will be at the dry adiabatic rate and the parcel will arrive back at its original level with a temperature that is higher than its original temperature. Thus, the process is irreversible. Ascent of this type, in which all condensation products are assumed to fall out, is called *pseudoadiabatic* ascent. (It is not a truly adiabatic process because the liquid water that falls out carries a small amount of heat with it.)

A complete derivation of the mathematical expression relating θ_e to the other variables of state is rather involved and will be relegated to Appendix D. For most purposes, however, it is sufficient to use an approximate expression for θ_e that can be immediately derived from the entropy form of the first law of thermodynamics (2.46). If we let q_s denote the mass of water vapor per unit mass of dry air in a saturated parcel (the saturation mixing ratio), then the rate of diabatic heating per unit mass is

$$J = -L_c \frac{Dq_s}{Dt}$$

where L_c is the latent heat of condensation. Therefore, from the first law of thermodynamics

$$c_p \frac{D \ln \theta}{Dt} = -\frac{L_c}{T} \frac{Dq_s}{Dt} \tag{2.68}$$

For a saturated parcel undergoing pseudoadiabatic ascent, the rate of change in q_s following the motion is much larger than the rate of change in T or L_c. Therefore,

$$d \ln \theta \approx -d\left(L_c q_s / c_p T\right) \tag{2.69}$$

Integrating (2.69) from the initial state (θ, q_s, T) to a state where $q_s \approx 0$, we obtain

$$\ln(\theta/\theta_e) \approx -L_c q_s / c_p T$$

where θ_e, the potential temperature in the final state, is approximately the equivalent potential temperature defined earlier. Thus, θ_e, for a saturated parcel is given by

$$\theta_e \approx \theta \exp\left(L_c q_s / c_p T\right) \tag{2.70}$$

The expression in (2.70) may also be used to compute θ_e for an unsaturated parcel provided that the temperature used in the formula is the temperature that the parcel would have if expanded adiabatically to saturation (i.e., T_{LCL}) and the saturation mixing ratio were replaced by the *actual* mixing ratio of the initial state. Thus, equivalent potential temperature is conserved for a parcel during both dry adiabatic and pseudoadiabatic displacements.

An alternative to θ_e, which is sometimes used in studies of convection, is the *moist static energy*, defined as $h \equiv s + L_c q$, where $s \equiv c_p T + gz$ is the *dry static energy*. It can be shown (Problem 2.10) that

$$c_p T d \ln \theta_e \approx dh \tag{2.71}$$

Thus, moist static energy is approximately conserved when θ_e is conserved.

2.9.2 The Pseudoadiabatic Lapse Rate

The first law of thermodynamics (2.68) can be used to derive a formula for the rate of change in temperature with respect to height for a saturated parcel undergoing pseudoadiabatic ascent. Using the definition of θ (2.44), we can rewrite (2.68) for vertical ascent as

$$\frac{d \ln T}{dz} - \frac{R}{c_p}\frac{d \ln p}{dz} = -\frac{L_c}{c_p T}\frac{dq_s}{dz}$$

which, upon noting that $q_s \equiv q_s(T, p)$ and applying the hydrostatic equation and equation of state, can be expressed as

$$\frac{dT}{dz} + \frac{g}{c_p} = -\frac{L_c}{c_p}\left[\left(\frac{\partial q_s}{\partial T}\right)_p \frac{dT}{dz} - \left(\frac{\partial q_s}{\partial p}\right)_T \rho g\right]$$

Thus, as shown in detail in Appendix D, following the ascending saturated parcel

$$\Gamma_s \equiv -\frac{dT}{dz} = \Gamma_d \frac{\left[1 + L_c q_s / (RT)\right]}{\left[1 + \varepsilon L_c^2 q_s / \left(c_p R T^2\right)\right]} \tag{2.72}$$

where $\varepsilon = 0.622$ is the ratio of the molecular weight of water to that of dry air, $\Gamma_d \equiv g/c_p$ is the dry adiabatic lapse rate, and Γ_s is the *pseudoadiabatic lapse rate,* which is always less than Γ_d. Observed values of Γ_s range from $\sim$4 K km^{-1} in warm, humid air masses in the lower troposphere to $\sim$6–7 K km^{-1} in the midtroposphere.

2.9.3 Conditional Instability

Section 2.7.3 showed that for dry adiabatic motions the atmosphere is statically stable provided that the lapse rate is less than the dry adiabatic lapse rate (i.e., the potential temperature increases with height). If the lapse rate Γ lies between dry adiabatic and pseudoadiabatic values ($\Gamma_s < \Gamma < \Gamma_d$), the atmosphere is stably stratified with respect to dry adiabatic displacements but unstable with respect to pseudoadiabatic displacements. Such a situation is referred to as *conditional instability* (i.e., the instability is conditional to saturation of the air parcel).

The conditional stability criterion can also be expressed in terms of the gradient of a field variable θ_e^*, defined as the equivalent potential temperature of a hypothetically saturated atmosphere that has the thermal structure of the actual atmosphere.[5] Thus,

$$d \ln \theta_e^* = d \ln \theta + d\left(L_c q_s / c_p T\right) \tag{2.73}$$

where T is the actual temperature, not the temperature after adiabatic expansion to saturation as in (2.70). To derive an expression for conditional instability, we consider the motion of a saturated parcel in an environment in which the potential temperature is θ_0 at the level z_0. At the level $z_0 - \delta z$ the undisturbed environmental air thus has potential temperature

$$\theta_0 - (\partial\theta/\partial z)\,\delta z$$

Suppose that a saturated parcel that has the environmental potential temperature at $z_0 - \delta z$ is raised to the level z_0. When it arrives at z_0, the parcel will have the potential temperature

$$\theta_1 = \left(\theta_0 - \frac{\partial\theta}{\partial z}\delta z\right) + \delta\theta$$

where $\delta\theta$ is the change in parcel potential temperature due to condensation during ascent through vertical distance δz. Assuming a pseudoadiabatic ascent, we see from (2.69) that

$$\frac{\delta\theta}{\theta} \approx -\delta\left(\frac{L_c q_s}{c_p T}\right) \approx -\frac{\partial}{\partial z}\left(\frac{L_c q_s}{c_p T}\right)\delta z$$

[5]Note that θ_e^* is *not* the same as θ_e except in a saturated atmosphere.

so that the buoyancy of the parcel when it arrives at z_0 is proportional to

$$\frac{(\theta_1 - \theta_0)}{\theta_0} \approx -\left[\frac{1}{\theta}\frac{\partial \theta}{\partial z} + \frac{\partial}{\partial z}\left(\frac{L_c q_s}{c_p T}\right)\right]\delta z \approx -\frac{\partial \ln \theta_e^*}{\partial z}\delta z$$

where the last expression arises from the application of (2.73).

The saturated parcel will be warmer than its environment at z_0 provided that $\theta_1 > \theta_0$. Thus, the conditional stability criterion for a saturated parcel is

$$\frac{\partial \theta_e^*}{\partial z}\begin{cases} < 0 & \text{conditionally unstable} \\ = 0 & \text{saturated neutral} \\ > 0 & \text{conditionally stable} \end{cases} \tag{2.74}$$

In Figure 2.8 the vertical profiles of θ, θ_e, and θ_e^* for a typical sounding in the vicinity of an extratropical thunderstorm are shown. It is obvious from

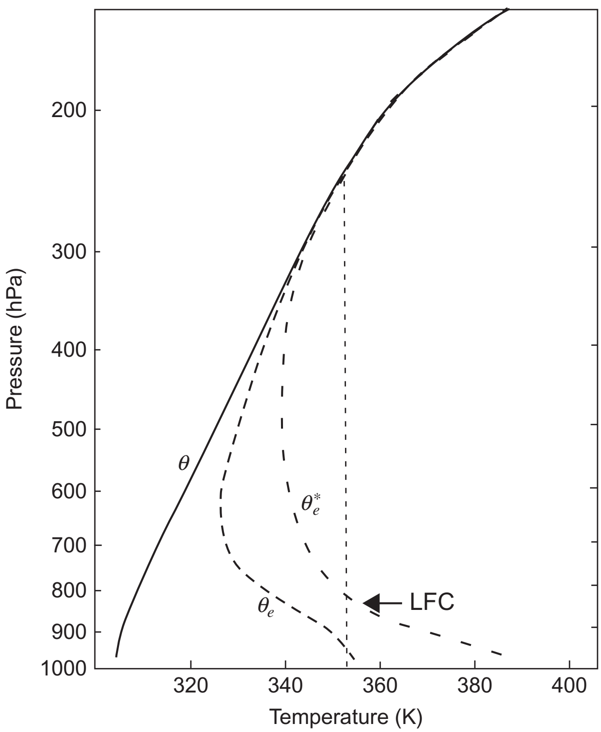

FIGURE 2.8 Schematic sounding for a conditionally unstable environment, characteristic of midwestern North American thunderstorm conditions, showing the vertical profiles of potential temperature θ, equivalent potential temperature θ_e, and equivalent temperature θ_e^* of a hypothetically saturated atmosphere with the same temperature profile. The *dotted line* shows θ_e for a nonentraining parcel raised from the surface. The *arrow* denotes the LFC for the parcel.

this figure that the sounding is conditionally unstable in the lower troposphere. However, this observed profile does not imply that convective overturning will occur spontaneously. The release of conditional instability requires not only that $\partial\theta_e^*/\partial z < 0$, but also parcel saturation at the environmental temperature of the level where the convection begins (i.e., the parcel must reach the LFC). The mean relative humidity in the troposphere is well below 100%, even in the boundary layer. Thus, low-level convergence with resultant forced layer ascent or vigorous vertical turbulent mixing in the boundary layer is required to produce saturation.

The amount of ascent necessary to raise a parcel to its LFC can be estimated simply from Figure 2.8. A parcel rising pseudoadiabatically from a level $z_0 - \delta z$ will conserve the value of θ_e characteristic of the environment at $z_0 - \delta z$. However, the buoyancy of a parcel depends only on the difference in density between the parcel and its environment. Thus, in order to compute the buoyancy of the parcel at z_0, it is not correct simply to compare θ_e of the environment at z_0 to $\theta_e(z_0 - \delta z)$ because if the environment is unsaturated, the difference in θ_e between the parcel and the environment may be due primarily to the difference in mixing ratios, not to any temperature (density) difference. To estimate the buoyancy of the parcel, $\theta_e(z_0 - \delta z)$ should instead be compared to $\theta_e^*(z_0)$, which is the equivalent potential temperature that the environment at z_0 would have if it were isothermally brought to saturation. The parcel will thus become buoyant when raised to the level z_0 if $\theta_e(z_0 - \delta z) > \theta_e^*(z_0)$, for then the parcel temperature will exceed the temperature of the environment at z_0.

From Figure 2.8, we see that θ_e for a parcel raised from about 960 hPa will intersect the θ_e^* curve near 850 hPa, whereas a parcel raised from any level much above 850 hPa will not intersect θ_e^* no matter how far it is forced to ascend. It is for this reason that low-level convergence is usually required to initiate convective overturning over the oceans. Only air near the surface has a sufficiently high value of θ_e to become buoyant when it is forcibly raised. Convection over continental regions, however, can be initiated without significant boundary layer convergence, as strong surface heating can produce positive parcel buoyancy all the way to the surface. Sustained deep convection, however, requires mean low-level moisture convergence.

SUGGESTED REFERENCES

Curry and Webster's *Thermodynamics of Atmospheres and Oceans* contains an excellent treatment of atmospheric thermodynamics.

Pedlosky, *Geophysical Fluid Dynamics*, discusses the equations of motion for a rotating coordinate system and has a thorough discussion of scale analysis at a graduate level.

Salby's *Fundamentals of Atmospheric Physics* contains a thorough development of the basic conservation laws at the graduate level.

PROBLEMS

2.1. A ship is steaming northward at a rate of 10 km h^{-1}.The surface pressure increases toward the northwest at the rate of 5 Pa km^{-1}. What is the pressure tendency recorded at a nearby island station if the pressure aboard the ship decreases at a rate of 100 Pa/3 h?

2.2. The temperature at a point 50 km north of a station is 3°C cooler than at the station. If the wind is blowing from the northeast at 20 m s^{-1} and the air is being heated by radiation at the rate of 1°C h^{-1}, what is the local temperature change at the station?

2.3. Derive the relationship

$$\mathbf{\Omega} \times (\mathbf{\Omega} \times \mathbf{r}) = -\Omega^2 \mathbf{R}$$

which was used in Eq. (2.7).

2.4. Derive the expression given in Eq. (2.13) for the rate of change of **k** following the motion.

2.5. Suppose a 1-kg parcel of dry air is rising at a constant vertical velocity. If the parcel is being heated by radiation at the rate of 10^{-1}W kg^{-1}, what must the speed of rise be to maintain the parcel at a constant temperature?

2.6. Derive an expression for the density ρ that results when an air parcel initially at pressure p_s and density ρ_s expands adiabatically to pressure p.

2.7. An air parcel that has a temperature of 20°C at the 1000-hPa level is lifted dry adiabatically. What is its density when it reaches the 500-hPa level?

2.8. Suppose an air parcel starts from rest at the 800-hPa level and rises vertically to 500 hPa while maintaining a constant 1°C temperature excess over the environment. Assuming that the mean temperature of the 800- to 500-hPa layer is 260 K, compute the energy released due to the work of the buoyancy force. Assuming that all the released energy is realized as kinetic energy of the parcel, what will the vertical velocity of the parcel be at 500 hPa?

2.9. Show that for an atmosphere with an adiabatic lapse rate (i.e., constant potential temperature) the geopotential height is given by

$$Z = H_\theta \left[1 - (p/p_0)^{R/c_p}\right]$$

where p_0 is the pressure at $Z = 0$ and $H_\theta \equiv c_p\,\theta/g_0$ is the total geopotential height of the atmosphere.

2.10. The azimuthal velocity component in some hurricanes is observed to have a radial dependence given by $v_\lambda = V_0(r_0/r)^2$ for distances from the center given by $r \geq r_0$. Letting $V_0 = 50\,\mathrm{m\,s^{-1}}$ and $r_0 = 50\,\mathrm{km}$, find the total geopotential difference between the far field ($r \to \infty$) and $r = r_0$, assuming gradient wind balance and $f_0 = 5 \times 10^{-5}\ \mathrm{s^{-1}}$. At what distance from the center does the Coriolis force equal the centrifugal force?

2.11. In the *isentropic* coordinate system (see Section 4.6), potential temperature is used as the vertical coordinate. Because potential temperature in adiabatic flow is conserved following the motion, isentropic coordinates are useful for tracing the actual paths of travel of individual air parcels. Show that the transformation of the horizontal pressure gradient force from z to θ coordinates is given by

$$\frac{1}{\rho}\nabla_z p = \nabla_\theta M$$

where $M \equiv c_p\, T + \Phi$ is the *Montgomery streamfunction*.

2.12. French scientists have developed a high-altitude balloon that remains at constant potential temperature as it circles Earth. Suppose such a balloon is in the lower equatorial stratosphere where the temperature is isothermal at 200 K. If the balloon were displaced vertically from its equilibrium level by a small distance δz, it would tend to oscillate about the equilibrium level. What would be the period of this oscillation?

2.13. Derive the approximate thermodynamic energy equation (2.55) using the scaling arguments of Sections 2.4 and 2.7.

MATLAB Exercises

M2.1. The MATLAB script **standard_T_p.m** defines and plots the temperature and the lapse rate associated with the U.S. Standard Atmosphere as functions of height. Modify this script to compute the pressure and potential temperature, and plot these in the same format used for temperature and lapse rate. [*Hint*: To compute pressure, integrate the hydrostatic equation from the surface upward in increments of δz.] Show that if we define a mean scale height for the layer between z and $z + \delta z$ by letting $H = R\,[T\,(z) + T\,(z + \delta z)]/(2g)$, then $p\,(z + \delta z) = p\,(z)\exp[-\delta z/H]$. (Note that as you move upward layer by layer, you must use the local height-dependent value of H in this formula.)

M2.2. The MATLAB script **thermo_profile.m** is a simple script to read in data giving pressure and temperature for a tropical mean sounding. Run this script to plot temperature versus pressure for data in the file **tropical_temp.dat**. Use the hypsometric equation to compute the geopotential height corresponding to each pressure level of the data file. Compute the corresponding potential temperature and plot graphs of the temperature and potential temperature variations with pressure and with geopotential height.

Chapter 3

Elementary Applications of the Basic Equations

In addition to the geostrophic wind, which was discussed in Chapter 2, there are other approximate expressions for the relationships among velocity, pressure, and temperature fields that are useful in the analysis of weather systems. We consider estimates of the wind that derive from fundamental force balances, trajectory and streamline analysis, the thermal wind, and estimates for vertical motion and surface pressure tendency.

3.1 BASIC EQUATIONS IN ISOBARIC COORDINATES

The topics are discussed most conveniently using a coordinate system in which pressure is the vertical coordinate. Thus, before introducing the elementary applications of the present chapter, it is useful to present the dynamical equations in isobaric coordinates.

3.1.1 The Horizontal Momentum Equation

The approximate horizontal momentum equations (2.24) and (2.25) may be written in vectorial form as

$$\frac{D\mathbf{V}}{Dt} + f\,\mathbf{k} \times \mathbf{V} = -\frac{1}{\rho}\nabla p \tag{3.1}$$

where $\mathbf{V} = \mathbf{i}u + \mathbf{j}v$ is the *horizontal* velocity vector. In order to express (3.1) in isobaric coordinate form, we transform the pressure gradient force using (1.33) and (1.34) to obtain

$$\frac{D\mathbf{V}}{Dt} + f\,\mathbf{k} \times \mathbf{V} = -\nabla_p \Phi \tag{3.2}$$

where ∇_p is the horizontal gradient operator applied with pressure held constant.

An Introduction to Dynamic Meteorology. DOI: 10.1016/B978-0-12-384866-6.00003-9

Because p is the independent vertical coordinate, we must expand the total derivative as

$$\begin{aligned}\frac{D}{Dt} &\equiv \frac{\partial}{\partial t} + \frac{Dx}{Dt}\frac{\partial}{\partial x} + \frac{Dy}{Dt}\frac{\partial}{\partial y} + \frac{Dp}{Dt}\frac{\partial}{\partial p} \\ &= \frac{\partial}{\partial t} + u\frac{\partial}{\partial x} + v\frac{\partial}{\partial y} + \omega\frac{\partial}{\partial p}\end{aligned} \tag{3.3}$$

Here $\omega \equiv Dp/Dt$ (usually called the "omega" vertical motion) is the pressure change following the motion, which plays the same role in the isobaric coordinate system that $w \equiv Dz/Dt$ plays in height coordinates. We note that the partial derivatives with respect to x and y are taken with pressure held constant—that is, on isobaric surfaces.

From (3.2) we see that the isobaric coordinate form of the geostrophic relationship is

$$f\mathbf{V}_g = \mathbf{k} \times \nabla_p \Phi \tag{3.4}$$

One advantage of isobaric coordinates is easily seen by comparing (2.23) and (3.4). In the latter equation, density does not appear. Thus, a given geopotential gradient implies the same geostrophic wind at any height, whereas a given horizontal pressure gradient implies different values of the geostrophic wind depending on the density. Furthermore, if f is regarded as a constant, the horizontal divergence of the geostrophic wind at constant pressure is zero:

$$\nabla_p \cdot \mathbf{V}_g = 0$$

3.1.2 The Continuity Equation

It is possible to transform the continuity equation (2.31) from height coordinates to pressure coordinates. However, it is simpler to directly derive the isobaric form by considering a Lagrangian control volume $\delta V = \delta x \delta y \delta z$ and applying the hydrostatic equation $\delta p = -\rho g \delta z$ (note that $\delta p < 0$) to express the volume element as $\delta V = -\delta x \delta y \delta p/(\rho g)$. The mass of this fluid element, which is conserved following the motion, is then $\delta M = \rho \delta V = -\delta x \delta y \delta p/g$. Thus,

$$\frac{1}{\delta M}\frac{D}{Dt}(\delta M) = \frac{g}{\delta x \delta y \delta p}\frac{D}{Dt}\left(\frac{\delta x \delta y \delta p}{g}\right) = 0$$

After differentiating, using the chain rule, and changing the order of the differential operators, we obtain[1]

$$\frac{1}{\delta x}\delta\left(\frac{Dx}{Dt}\right) + \frac{1}{\delta y}\delta\left(\frac{Dy}{Dt}\right) + \frac{1}{\delta p}\delta\left(\frac{Dp}{Dt}\right) = 0$$

[1] From now on g will be regarded as a constant.

or

$$\frac{\delta u}{\delta x} + \frac{\delta v}{\delta y} + \frac{\delta \omega}{\delta p} = 0$$

Taking the limit δx, δy, $\delta p \to 0$ and observing that δx and δy are evaluated at constant pressure, we obtain the continuity equation in the isobaric system:

$$\left(\frac{\partial u}{\partial x} + \frac{\partial v}{\partial y}\right)_p + \frac{\partial \omega}{\partial p} = 0 \tag{3.5}$$

This form of the continuity equation contains no reference to the density field and does not involve time derivatives. The simplicity of (3.5) is one of the chief advantages of the isobaric coordinate system.

3.1.3 The Thermodynamic Energy Equation

The first law of thermodynamics (2.43) can be expressed in the isobaric system by letting $Dp/Dt = \omega$ and expanding DT/Dt using (3.3):

$$c_p\left(\frac{\partial T}{\partial t} + u\frac{\partial T}{\partial x} + v\frac{\partial T}{\partial y} + \omega\frac{\partial T}{\partial p}\right) - \alpha\omega = J$$

This may be rewritten as

$$\left(\frac{\partial T}{\partial t} + u\frac{\partial T}{\partial x} + v\frac{\partial T}{\partial y}\right) - S_p\omega = \frac{J}{c_p} \tag{3.6}$$

where, with the aid of the equation of state and Poisson's equation (2.44), we have

$$S_p \equiv \frac{RT}{c_p p} - \frac{\partial T}{\partial p} = -\frac{T}{\theta}\frac{\partial \theta}{\partial p} \tag{3.7}$$

which is the static stability parameter for the isobaric system. Using (2.49) and the hydrostatic equation, (3.7) may be rewritten as

$$S_p = (\Gamma_d - \Gamma)/\rho g$$

Thus, S_p is positive provided that the lapse rate is less than dry adiabatic. However, because density decreases approximately exponentially with height, S_p increases rapidly with height. This strong height dependence of the stability measure S_p is a minor disadvantage of isobaric coordinates.

3.2 BALANCED FLOW

Despite the apparent complexity of atmospheric motion systems as depicted on synoptic weather charts, the pressure (or geopotential height) and velocity distributions in meteorological disturbances are actually related by rather simple approximate force balances. In order to gain a qualitative understanding of the horizontal balance of forces in atmospheric motions, we idealize by considering flows that are steady state (i.e., time independent) and have no vertical component of velocity. Furthermore, it is useful to describe the flow field by expanding the isobaric form of the horizontal momentum equation (3.2) into its components in a so-called *natural* coordinate system.

3.2.1 Natural Coordinates

The natural coordinate system is defined by the orthogonal set of unit vectors **t**, **n**, and **k**. Unit vector **t** is oriented parallel to the horizontal velocity at each point; unit vector **n** is normal to the horizontal velocity and is oriented so that it is positive to the left of the flow direction; and unit vector **k** is directed vertically upward. In this system the horizontal velocity may be written $\mathbf{V} = V\mathbf{t}$, where V, the horizontal speed, is a nonnegative scalar defined by $V \equiv Ds/Dt$, where $s(x, y, t)$ is the distance along the curve followed by a parcel moving in the horizontal plane. The acceleration following the motion is thus

$$\frac{D\mathbf{V}}{Dt} = \frac{D(V\mathbf{t})}{Dt} = \mathbf{t}\frac{DV}{Dt} + V\frac{D\mathbf{t}}{Dt}$$

The rate of change of **t** following the motion may be derived from geometrical considerations with the aid of Figure 3.1:

$$\delta\psi = \frac{\delta s}{|R|} = \frac{|\delta\mathbf{t}|}{|\mathbf{t}|} = |\delta\mathbf{t}|$$

Here R is the *radius of curvature* following the parcel motion, and we have used the fact that $|\mathbf{t}| = 1$. By convention, R is taken to be positive when the center of curvature is in the positive **n** direction. Thus, for $R > 0$, the air parcels turn

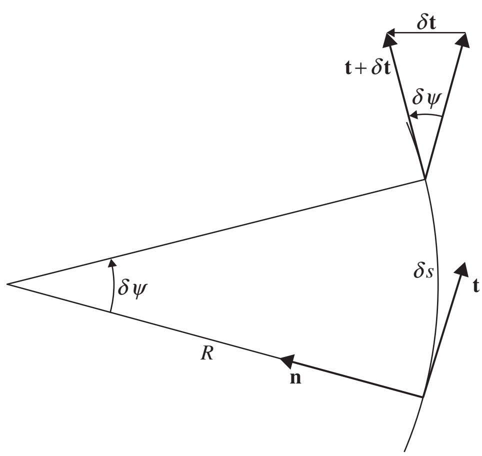

FIGURE 3.1 Rate of change of the unit tangent vector **t** following the motion.

toward the left following the motion, and for $R < 0$, the air parcels turn toward the right following the motion.

Noting that in the limit $\delta s \rightarrow 0$, $\delta \mathbf{t}$ is directed parallel to $\mathbf{n}$, the preceding relationship yields $D\mathbf{t}/Ds = \mathbf{n}/R$. Thus,

$$\frac{D\mathbf{t}}{Dt} = \frac{D\mathbf{t}}{Ds}\frac{Ds}{Dt} = \frac{\mathbf{n}}{R}V$$

and

$$\frac{D\mathbf{V}}{Dt} = \mathbf{t}\frac{DV}{Dt} + \mathbf{n}\frac{V^2}{R} \tag{3.8}$$

Therefore, the acceleration following the motion is the sum of the rate of change of speed of the air parcel and its centripetal acceleration due to the curvature of the trajectory. Because the Coriolis force always acts normal to the direction of motion, its natural coordinate form is simply

$$-f\,\mathbf{k} \times \mathbf{V} = -f\,V\mathbf{n}$$

whereas the pressure gradient force can be expressed as

$$-\nabla_p \Phi = -\left(\mathbf{t}\frac{\partial \Phi}{\partial s} + \mathbf{n}\frac{\partial \Phi}{\partial n}\right)$$

The horizontal momentum equation may thus be expanded into the following component equations in the natural coordinate system:

$$\frac{DV}{Dt} = -\frac{\partial \Phi}{\partial s} \tag{3.9}$$

$$\frac{V^2}{R} + f\,V = -\frac{\partial \Phi}{\partial n} \tag{3.10}$$

Equations (3.9) and (3.10) express the force balances parallel to and normal to the direction of flow, respectively. For motion parallel to the geopotential height contours, $\partial \Phi/\partial s = 0$, and the speed is constant following the motion. If, in addition, the geopotential gradient normal to the direction of motion is constant along a trajectory, (3.10) implies that the radius of curvature of the trajectory is also constant. In that case the flow can be classified into several simple categories depending on the relative contributions of the three terms in (3.10) to the net force balance.

3.2.2 Geostrophic Flow

Flow in a straight line ($R \rightarrow \pm\infty$) parallel to height contours is referred to as *geostrophic motion*. In geostrophic motion the horizontal components of the Coriolis force and pressure gradient force are in exact balance so that $V = V_g$,

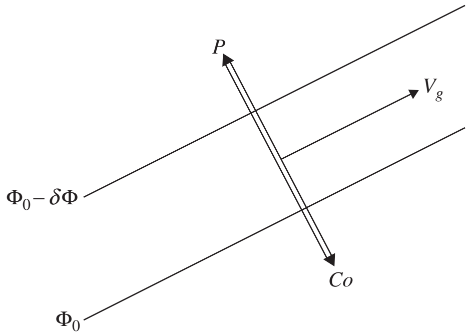

FIGURE 3.2 Balance of forces for geostrophic equilibrium. The pressure gradient force is designated by P and the Coriolis force by Co.

where the geostrophic wind V_g is defined by[2]

$$f\,V_g = -\partial\Phi/\partial n \tag{3.11}$$

This balance is indicated schematically in Figure 3.2. The actual wind can be in exact geostrophic motion only if the height contours are parallel to latitude circles. As discussed in Section 2.4.1, the geostrophic wind is generally a good approximation to the actual wind in extratropical synoptic-scale disturbances. However, in some of the special cases treated later, this is not true.

3.2.3 Inertial Flow

If the geopotential field is uniform on an isobaric surface so that the horizontal pressure gradient vanishes, (3.10) reduces to a balance between Coriolis force and centrifugal force:

$$V^2/R + f\,V = 0 \tag{3.12}$$

Equation (3.12) may be solved for the radius of curvature

$$R = -V/f$$

Since from (3.9), the speed must be constant in this case, the radius of curvature is also constant (neglecting the latitudinal dependence of f). Thus, the air parcels follow circular paths in an anticyclonic sense.[3] The period of this

[2]Note that although the actual speed V must always be positive in the natural coordinates, V_g, which is proportional to the height gradient normal to the direction of flow, may be negative, as in the "anomalous" low shown later in Figure 3.5c.

[3]Anticyclonic flow is a clockwise rotation in the Northern Hemisphere and counterclockwise in the Southern Hemisphere. Cyclonic flow has the opposite sense of rotation in each hemisphere.

oscillation is

$$P = \left| \frac{2\pi R}{V} \right| = \frac{2\pi}{|f|} = \frac{\frac{1}{2}\text{ day}}{|\sin \phi|} \tag{3.13}$$

P is equivalent to the time that is required for a Foucault pendulum to turn through an angle of 180°. Thus, it is often referred to as one-half *pendulum day*.

Because both the Coriolis force and the centrifugal force due to the relative motion are caused by inertia of the fluid, this type of motion is traditionally referred to as an *inertial oscillation*, and the circle of radius $|R|$ is called the inertia circle. It is important to realize that the "inertial flow" governed by (3.12) is not the same as inertial motion in an absolute reference frame. The flow governed by (3.12) is just the constant angular momentum oscillation referred to in Section 1.3.4. In this flow the force of gravity, acting orthogonal to the plane of motion, keeps the oscillation on a horizontal surface. In true inertial motion, all forces vanish and the motion maintains a uniform absolute velocity.

In the atmosphere, motions are nearly always generated and maintained by pressure gradient forces; the conditions of uniform pressure required for pure inertial flow rarely exist. In the oceans, however, currents are often generated by transient winds blowing across the surface, rather than by internal pressure gradients. As a result, significant amounts of energy occur in currents that oscillate with near inertial periods. An example recorded by a current meter near the island of Barbados is shown in Figure 3.3.

3.2.4 Cyclostrophic Flow

If the horizontal scale of a disturbance is small enough, the Coriolis force may be neglected in (3.10) compared to the pressure gradient force and the centrifugal force. The force balance normal to the direction of flow is then

$$\frac{V^2}{R} = -\frac{\partial \Phi}{\partial n}$$

If this equation is solved for V, we obtain the speed of the *cyclostrophic wind*

$$V = \left(-R \frac{\partial \Phi}{\partial n} \right)^{1/2} \tag{3.14}$$

As indicated in Figure 3.4, cyclostrophic flow may be either cyclonic or anticyclonic. In both cases the pressure gradient force is directed toward the center of curvature and the centrifugal force away from the center of curvature.

The cyclostrophic balance approximation is valid provided that the ratio of the centrifugal force to the Coriolis force is large. This ratio $V/(fR)$ is equivalent to the Rossby number discussed in Section 2.4.2. As an example of cyclostrophic scale motion, we consider a typical tornado. Suppose that the tangential velocity is 30 m s^{-1} at a distance of 300 m from the center of the vortex.

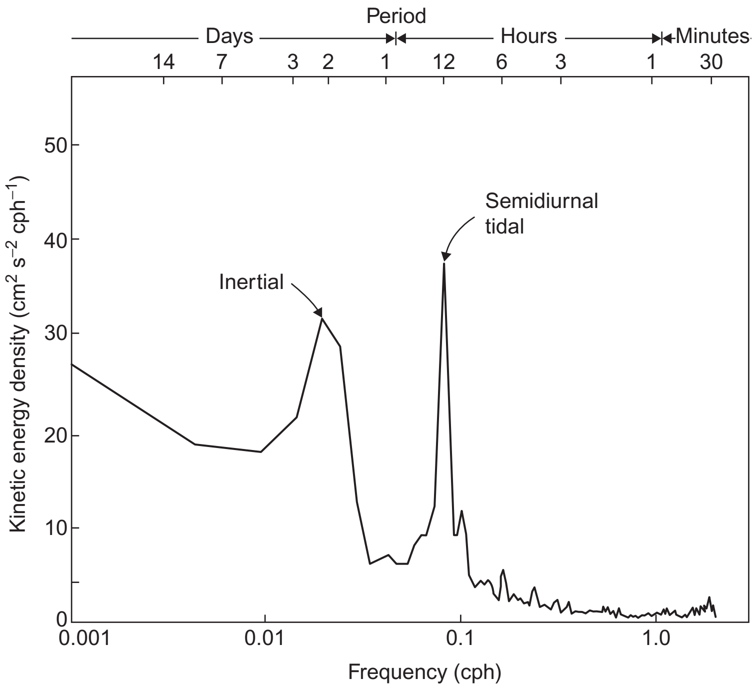

FIGURE 3.3 Power spectrum of kinetic energy at 30-m depth in the ocean near Barbados (13°N). Ordinate shows kinetic energy density per unit frequency interval (cph^{-1} designates cycles per hour). This type of plot indicates the manner in which the total kinetic energy is partitioned among oscillations of different periods. Note the strong peak at 53 h, which is the period of an inertial oscillation at 13° latitude. (*After Warsh et al., 1971. Copyright © American Meteorological Society. Reprinted with permission.*)

Assuming that $f = 10^{-4}$ s^{-1}, the Rossby number is just $\text{Ro} = V/|fR| \approx 10^3$, which implies that the Coriolis force can be neglected in computing the balance of forces for a tornado. However, the majority of tornadoes in the Northern Hemisphere are observed to rotate in a cyclonic (counterclockwise) sense. This is due to the fact that they are embedded in environments that favor cyclonic rotation (see Section 9.6.1). Smaller-scale vortices, however, such as dust devils and water spouts, do not have a preferred direction of rotation. According to data collected by Sinclair (1965), they are observed to be anticyclonic as often as cyclonic.

3.2.5 The Gradient Wind Approximation

Horizontal frictionless flow that is parallel to the height contours so that the tangential acceleration vanishes ($DV/Dt = 0$) is called *gradient flow*. Gradient flow is a three-way balance among the Coriolis force, the centrifugal force, and the horizontal pressure gradient force. Like geostrophic flow, pure gradient flow

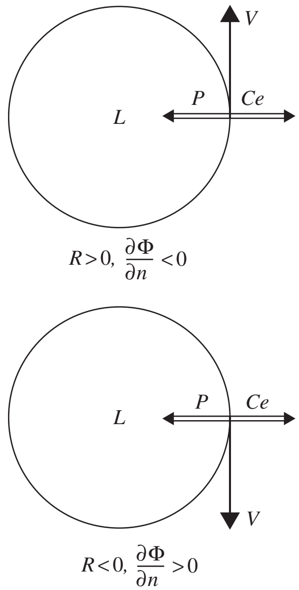

FIGURE 3.4 Force balance in cyclostrophic flow: *P* designates the pressure gradient; *Ce* designates the centrifugal force.

can exist only under very special circumstances. It is always possible, however, to define a gradient wind, which at any point is just the wind component parallel to the height contours that satisfies (3.10). For this reason, (3.10) is commonly referred to as the gradient wind equation. Because (3.10) takes into account the centrifugal force due to the curvature of parcel trajectories, the gradient wind is often a better approximation to the actual wind than the geostrophic wind.

The gradient wind speed is obtained by solving (3.10) for V to yield

$$\begin{aligned} V &= -\frac{fR}{2} \pm \left(\frac{f^2R^2}{4} - R\frac{\partial\Phi}{\partial n}\right)^{1/2} \\ &= -\frac{fR}{2} \pm \left(\frac{f^2R^2}{4} + fRV_g\right)^{1/2} \end{aligned} \tag{3.15}$$

where in the lower expression (3.11) is used to express $\partial\Phi/\partial n$ in terms of the geostrophic wind. Not all the mathematically possible roots of (3.15) correspond to physically possible solutions, since it is required that V be real and nonnegative. In Table 3.1 the various roots of (3.15) are classified according to the signs of R and $\partial\Phi/\partial n$ in order to isolate the physically meaningful solutions.

The force balances for the four permitted solutions are illustrated in Figure 3.5. Equation (3.15) shows that in cases of both regular and anomalous highs the pressure gradient is limited by the requirement that the quantity under

TABLE 3.1 Classification of Roots of the Gradient Wind Equation in the Northern Hemisphere

Sign $\partial\Phi/\partial n$	$R > 0$	$R < 0$
Positive ($V_g < 0$)	Positive root[a]: unphysical	Positive root: antibaric flow (anomalous low)
	Negative root: unphysical	Negative root: unphysical
Negative ($V_g > 0$)	Positive root: cyclonic flow (regular low)	Positive root: ($V > -fR/2$): anticyclonic flow (anomalous high)
	Negative root: unphysical	Negative root: ($V < -fR/2$): anticyclonic flow (regular high)

[a] *The terms "positive root" and "negative root" in columns 2 and 3 refer to the sign taken in the final term in Eq. (3.15).*

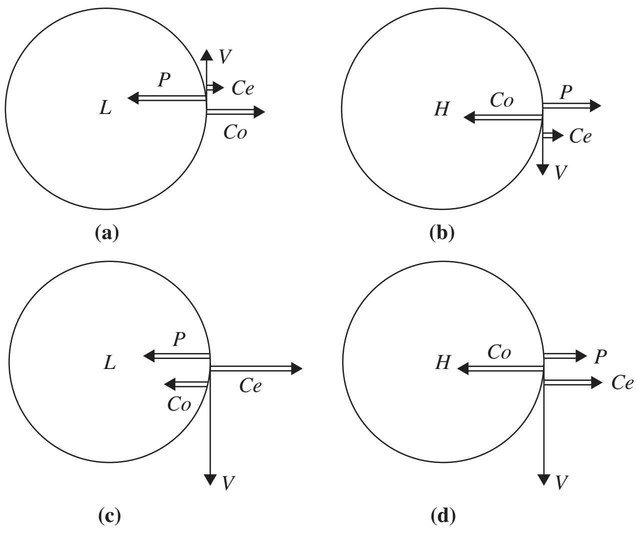

FIGURE 3.5 Force balances in the Northern Hemisphere for the four types of gradient flow: (a) regular low, (b) regular high, (c) anomalous low, and (d) anomalous high.

the radical be nonnegative—that is,

$$\left|f V_g\right| = \left|\frac{\partial\Phi}{\partial n}\right| < \frac{|R|f^2}{4} \tag{3.16}$$

Thus, the pressure gradient in a high must approach zero as $|R| \to 0$. It is for this reason that the pressure field near the center of a high is always flat and the wind gentle compared to the region near the center of a low.

The absolute angular momentum about the axis of rotation for the circularly symmetric motions shown in Figure 3.5 is given by $VR + fR^2/2$. From (3.15) it is verified readily that regular gradient wind balances have positive absolute angular momentum in the Northern Hemisphere, whereas anomalous cases have negative absolute angular momentum. Because the only source of negative absolute angular momentum is the Southern Hemisphere, the anomalous cases are unlikely to occur, except perhaps close to the equator.

In all cases except the anomalous low (Figure 3.5c) the horizontal components of the Coriolis and pressure gradient forces are oppositely directed. Such flow is called *baric*. The anomalous low is antibaric; the geostrophic wind V_g defined in (3.11) is negative for an anomalous low and is clearly not a useful approximation to the actual speed.[4] Furthermore, as shown in Figure 3.5, gradient flow is cyclonic only when the centrifugal force and the horizontal component of the Coriolis force have the same sense ($Rf > 0$); it is anticyclonic when these forces have the opposite sense ($Rf < 0$). Since the direction of anticyclonic and cyclonic flow is reversed in the Southern Hemisphere, the requirement that $Rf > 0$ for cyclonic flow holds regardless of the hemisphere considered.

The definition of the geostrophic wind (3.11) can be used to rewrite the force balance normal to the direction of flow (3.10) in the form

$$V^2/R + fV - fV_g = 0$$

Dividing through by fV shows that the ratio of the geostrophic wind to the gradient wind is

$$\frac{V_g}{V} = 1 + \frac{V}{fR} \tag{3.17}$$

For normal cyclonic flow ($fR > 0$), V_g is larger than V, whereas for anticyclonic flow ($fR < 0$), V_g is smaller than V. Therefore, the geostrophic wind is an overestimate of the balanced wind in a region of cyclonic curvature and an underestimate in a region of anticyclonic curvature. For midlatitude synoptic systems, the difference between gradient and geostrophic wind speeds generally does not exceed 10 to 20%. [Note that the magnitude of $V/(fR)$ is just the Rossby number.] For tropical disturbances, the Rossby number is in the range of 1 to 10, and the gradient wind formula must be applied rather than the geostrophic wind. Equation (3.17) also shows that the antibaric anomalous low, which has $V_g < 0$, can exist only when $V/(fR) < -1$. Thus, antibaric flow is associated with small-scale intense vortices such as tornadoes.

---

[4] Remember that in the natural coordinate system the speed V is positive definite.

3.3 TRAJECTORIES AND STREAMLINES

In the natural coordinate system used in the previous section to discuss balanced flow, $s(x, y, t)$ was defined as the distance along the curve in the horizontal plane traced out by the path of an air parcel. The path followed by a particular air parcel over a finite period of time is called the *trajectory* of the parcel. Thus, the radius of curvature R of the path s referred to in the gradient wind equation is the radius of curvature for a parcel trajectory. In practice, R is often estimated by using the radius of curvature of a geopotential height contour, as this can be estimated easily from a synoptic chart. However, the height contours are actually *streamlines* of the gradient wind (i.e., lines that are everywhere parallel to the instantaneous wind velocity).

It is important to distinguish clearly between streamlines, which give a "snapshot" of the velocity field at any instant, and trajectories, which trace the motion of individual fluid parcels over a finite time interval. In Cartesian coordinates, horizontal trajectories are determined by the integration of

$$\frac{Ds}{Dt} = V(x, y, t) \tag{3.18}$$

over a finite time span for each parcel to be followed, whereas streamlines are determined by the integration of

$$\frac{dy}{dx} = \frac{v(x, y, t_0)}{u(x, y, t_0)} \tag{3.19}$$

with respect to x at time t_0. (Note that since a streamline is parallel to the velocity field, its slope in the horizontal plane is just the ratio of the horizontal velocity components.) Only for *steady-state* motion fields (i.e., fields in which the local rate of change of velocity vanishes) do the streamlines and trajectories coincide. However, synoptic disturbances are not steady-state motions. They generally move at speeds of the same order as the winds that circulate about them. To gain an appreciation for the possible errors involved in using the curvature of the streamlines instead of the curvature of the trajectories in the gradient wind equation, it is necessary to investigate the relationship between the curvature of the trajectories and the curvature of the streamlines for a moving pressure system.

We let $\beta(x, y, t)$ designate the angular direction of the wind at each point on an isobaric surface, and R_t and R_s designate the radii of curvature of the trajectories and streamlines, respectively. Then, from Figure 3.6, $\delta s = R\,\delta\beta$ so that in the limit $\delta s \to 0$

$$\frac{D\beta}{Ds} = \frac{1}{R_t} \quad \text{and} \quad \frac{\partial \beta}{\partial s} = \frac{1}{R_s} \tag{3.20}$$

where $D\beta/Ds$ means the rate of change of wind direction along a trajectory (positive for counterclockwise turning) and $\partial\beta/\partial s$ is the rate of change of wind

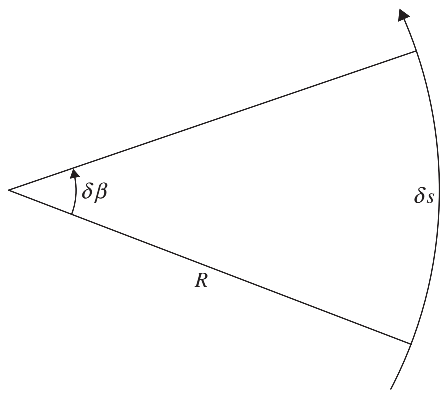

FIGURE 3.6 Relationship between the change in angular direction of the wind $\delta\beta$ and the radius of curvature R.

direction along a streamline at any instant. Thus, the rate of change of wind direction following the motion is

$$\frac{D\beta}{Dt} = \frac{D\beta}{Ds}\frac{Ds}{Dt} = \frac{V}{R_t} \tag{3.21}$$

or, after expanding the total derivative,

$$\frac{D\beta}{Dt} = \frac{\partial\beta}{\partial t} + V\frac{\partial\beta}{\partial s} = \frac{\partial\beta}{\partial t} + \frac{V}{R_s} \tag{3.22}$$

Combining (3.21) and (3.22), we obtain a formula for the local turning of the wind:

$$\frac{\partial\beta}{\partial t} = V\left(\frac{1}{R_t} - \frac{1}{R_s}\right) \tag{3.23}$$

Equation (3.23) indicates that the trajectories and streamlines will coincide only when the local rate of change of the wind direction vanishes.

In general, midlatitude synoptic systems move eastward as a result of advection by upper-level westerly winds. In such cases there is a local turning of the wind due to the motion of the system even if the shape of the height contour pattern remains constant as the system moves. The relationship between R_t and R_s in such a situation can be determined easily for an idealized circular pattern of height contours moving at a constant velocity $\mathbf{C}$. In this case the local turning of the wind is entirely due to the motion of the streamline pattern so that

$$\frac{\partial\beta}{\partial t} = -\mathbf{C}\cdot\nabla\beta = -C\frac{\partial\beta}{\partial s}\cos\gamma = -\frac{C}{R_s}\cos\gamma$$

where γ is the angle between the streamlines (height contours) and the direction of motion of the system. Substituting the preceding equation into (3.23) and solving for R_t with the aid of (3.20), we obtain the desired relationship between the curvature of the streamlines and the curvature of the trajectories:

$$R_t = R_s\left(1 - \frac{C\cos\gamma}{V}\right)^{-1} \tag{3.24}$$

Equation (3.24) can be used to compute the curvature of the trajectory anywhere on a moving pattern of streamlines. In Figure 3.7 the curvatures of the trajectories for parcels initially located due north, east, south, and west of the center of a cyclonic system are shown both for the case of a wind speed greater than the speed of movement of the height contours and for the case of a wind speed less than the speed of movement of the height contours. In these examples the plotted trajectories are based on a geostrophic balance so that the height

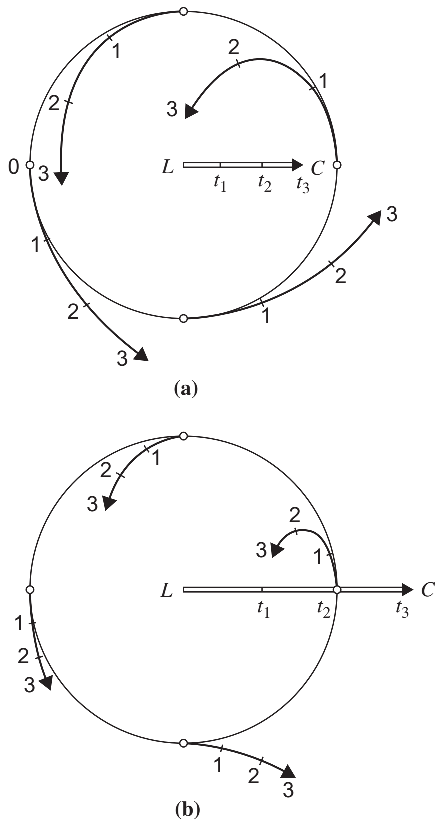

FIGURE 3.7 Trajectories for moving circular cyclonic circulation systems in the Northern Hemisphere with (a) $V = 2C$ and (b) $2V = C$. Numbers indicate positions at successive times. L designates a pressure minimum.

contours are equivalent to streamlines. It is also assumed for simplicity that the wind speed does not depend on the distance from the center of the system.

In the case shown in Figure 3.7b, there is a region south of the low center where the curvature of the trajectories is opposite that of the streamlines. Because synoptic-scale pressure systems usually move at speeds comparable to the wind speed, the gradient wind speed computed on the basis of the curvature of the height contours is often no better an approximation to the actual wind speed than the geostrophic wind. In fact, the actual gradient wind speed will vary along a height contour with the variation of the trajectory curvature.

3.4 THE THERMAL WIND

The geostrophic wind must have vertical shear in the presence of a horizontal temperature gradient, as can be shown easily from simple physical considerations based on hydrostatic equilibrium. Since the geostrophic wind (3.4) is proportional to the geopotential gradient on an isobaric surface, a geostrophic wind directed along the positive y axis that increases in magnitude with height requires that the slope of the isobaric surfaces with respect to the x axis also must increase with height, as shown in Figure 3.8. According to the hypsometric equation (1.30), the thickness δz corresponding to a (positive) pressure interval δp is

$$\delta z \approx g^{-1} RT \delta \ln p \tag{3.25}$$

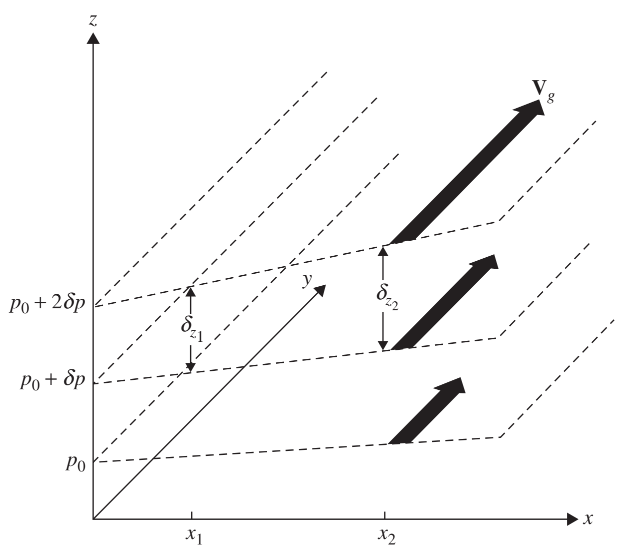

FIGURE 3.8 Relationship between vertical shear of the geostrophic wind and horizontal thickness gradients. (Note that $\delta p < 0$.)

Thus, the thickness of the layer between two isobaric surfaces is proportional to the mean temperature in the layer, T. In Figure 3.8 the mean temperature T_1 of the column denoted δz_1 must be less than the mean temperature T_2 for the column denoted δz_2. Thus, an increase with height of a positive x directed pressure gradient must be associated with a positive x directed temperature gradient. The air in a vertical column at x_2, because it is warmer (less dense), must occupy a greater depth for a given pressure drop than the air at x_1.

Equations for the rate of change with height of the geostrophic wind components are derived most easily using the isobaric coordinate system. In isobaric coordinates the geostrophic wind (3.4) has components given by

$$v_g = \frac{1}{f}\frac{\partial \Phi}{\partial x} \quad \text{and} \quad u_g = -\frac{1}{f}\frac{\partial \Phi}{\partial y} \tag{3.26}$$

where the derivatives are evaluated with pressure held constant. Also, with the aid of the ideal gas law, we can write the hydrostatic equation as

$$\frac{\partial \Phi}{\partial p} = -\alpha = -\frac{RT}{p} \tag{3.27}$$

Differentiating (3.26) with respect to pressure, and applying (3.27), we obtain

$$p\frac{\partial v_g}{\partial p} \equiv \frac{\partial v_g}{\partial \ln p} = -\frac{R}{f}\left(\frac{\partial T}{\partial x}\right)_p \tag{3.28}$$

$$p\frac{\partial u_g}{\partial p} \equiv \frac{\partial u_g}{\partial \ln p} = \frac{R}{f}\left(\frac{\partial T}{\partial y}\right)_p \tag{3.29}$$

or in vectorial form

$$\frac{\partial \mathbf{V}_g}{\partial \ln p} = -\frac{R}{f}\mathbf{k} \times \nabla_p T \tag{3.30}$$

Equation (3.30) is often referred to as the *thermal wind* equation. However, it is actually a relationship for the vertical wind *shear* (i.e., the rate of change of the geostrophic wind with respect to $\ln p$). Strictly speaking, the term *thermal wind* refers to the vector difference between geostrophic winds at two levels. Designating the thermal wind vector by $\mathbf{V}_T$, we may integrate (3.30) from pressure level p_0 to level p_1 $(p_1 < p_0)$ to get

$$\mathbf{V}_T \equiv \mathbf{V}_g(p_1) - \mathbf{V}_g(p_0) = -\frac{R}{f}\int_{p_0}^{p_1} \left(\mathbf{k} \times \nabla_p T\right) d\ln p \tag{3.31}$$

Letting $\langle T \rangle$ denote the mean temperature in the layer between pressure p_0 and p_1, the x and y components of the thermal wind are thus given by

$$u_T = -\frac{R}{f}\left(\frac{\partial \langle T \rangle}{\partial y}\right)_p \ln\left(\frac{p_0}{p_1}\right); \quad v_T = \frac{R}{f}\left(\frac{\partial \langle T \rangle}{\partial x}\right)_p \ln\left(\frac{p_0}{p_1}\right) \tag{3.32}$$

Alternatively, we may express the thermal wind for a given layer in terms of the horizontal gradient of the geopotential difference between the top and the bottom of the layer:

$$u_T = -\frac{1}{f}\frac{\partial}{\partial y}(\Phi_1 - \Phi_0); \quad v_T = \frac{1}{f}\frac{\partial}{\partial x}(\Phi_1 - \Phi_0) \tag{3.33}$$

The equivalence of (3.32) and (3.33) can be verified readily by integrating the hydrostatic equation (3.27) vertically from p_0 to p_1 after replacing T by the mean $\langle T \rangle$. The result is the hypsometric equation (1.29):

$$\Phi_1 - \Phi_0 \equiv gZ_T = R\langle T \rangle \ln\left(\frac{p_0}{p_1}\right) \tag{3.34}$$

The quantity Z_T is the *thickness* of the layer between p_0 and p_1 measured in units of geopotential meters. From (3.34) we see that the thickness is proportional to the mean temperature in the layer. Hence, lines of equal Z_T (isolines of thickness) are equivalent to the isotherms of mean temperature in the layer. It can also be used to estimate the mean horizontal temperature advection in a layer, as shown in Figure 3.9. It is clear from the vector form of the thermal

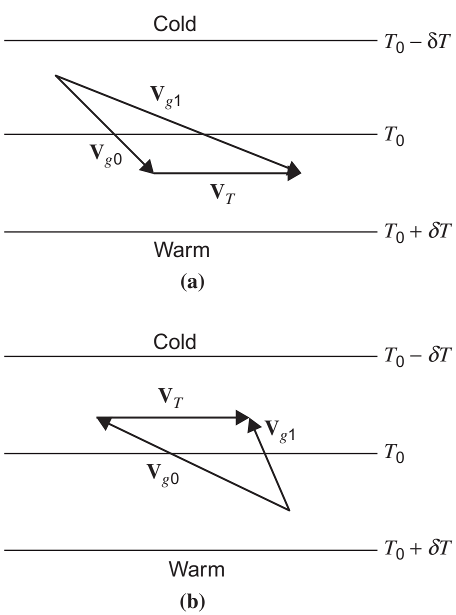

FIGURE 3.9 Relationship between turning of geostrophic wind and temperature advection: (a) backing of the wind with height and (b) veering of the wind with height.

wind relation

$$\mathbf{V}_T = \frac{1}{f}\mathbf{k} \times \nabla(\Phi_1 - \Phi_0) = \frac{g}{f}\mathbf{k} \times \nabla Z_T = \frac{R}{f}\mathbf{k} \times \nabla\langle T\rangle \ln\left(\frac{p_0}{p_1}\right) \tag{3.35}$$

that the thermal wind blows parallel to the isotherms (lines of constant thickness) with the warm air to the right facing downstream in the Northern Hemisphere. Thus, as is illustrated in Figure 3.9a, a geostrophic wind that turns counterclockwise with height (backs) is associated with cold-air advection. Conversely, as shown in Figure 3.9b, clockwise turning (veering) of the geostrophic wind with height implies warm advection by the geostrophic wind in the layer.

It is therefore possible to obtain a reasonable estimate of the horizontal temperature advection and its vertical dependence at a given location solely from data on the vertical profile of the wind given by a single sounding. Alternatively, the geostrophic wind at any level can be estimated from the mean temperature field, provided that the geostrophic velocity is known at a single level. Thus, for example, if the geostrophic wind at 850 hPa is known and the mean horizontal temperature gradient in the layer 850 to 500 hPa is also known, the thermal wind equation can be applied to obtain the geostrophic wind at 500 hPa.

3.4.1 Barotropic and Baroclinic Atmospheres

A *barotropic* atmosphere is one in which the density depends only on the pressure, $\rho = \rho(p)$, so that isobaric surfaces are also surfaces of constant density. For an ideal gas, the isobaric surfaces will also be isothermal if the atmosphere is barotropic. Thus, $\nabla_p T = 0$ in a barotropic atmosphere, and the thermal wind equation (3.30) becomes $\partial \mathbf{V}_g / \partial \ln p = 0$, which states that the geostrophic wind is independent of height in a barotropic atmosphere. Thus, barotropy provides a very strong constraint on the motions in a rotating fluid; the large-scale motion can depend only on horizontal position and time, not on height.

An atmosphere in which density depends on both the temperature and the pressure, $\rho = \rho(p, T)$, is referred to as a *baroclinic* atmosphere. In a baroclinic atmosphere the geostrophic wind generally has vertical shear, and this shear is related to the horizontal temperature gradient by the thermal wind equation (3.30). Obviously, the baroclinic atmosphere is of primary importance in dynamic meteorology. However, as shown in later chapters, much can be learned by study of the simpler barotropic atmosphere.

3.5 VERTICAL MOTION

As mentioned previously, for synoptic-scale motions the vertical velocity component is typically of the order of a few centimeters per second. Routine meteorological soundings, however, only give the wind speed to an accuracy of about a meter per second. Thus, in general the vertical velocity is not measured directly but must be inferred from the fields that are measured directly.

Two methods for inferring the vertical motion field are the kinematic method, based on the equation of continuity, and the adiabatic method, based on the thermodynamic energy equation. Both methods are usually applied using the isobaric coordinate system so that $\omega(p)$ is inferred rather than $w(z)$. These two measures of vertical motion can be related to each other with the aid of the hydrostatic approximation.

Expanding Dp/Dt in the (x, y, z) coordinate system yields

$$\omega \equiv \frac{Dp}{Dt} = \frac{\partial p}{\partial t} + \mathbf{V} \cdot \nabla p + w \left(\frac{\partial p}{\partial z} \right) \tag{3.36}$$

Now, for synoptic-scale motions, the horizontal velocity is geostrophic to a first approximation. Therefore, we can write $\mathbf{V} = \mathbf{V}_g + \mathbf{V}_a$, where $\mathbf{V}_a$ is the *ageostrophic* wind and $|\mathbf{V}_a| \ll |\mathbf{V}_g|$. However, $\mathbf{V}_g = (\rho f)^{-1}\mathbf{k} \times \nabla p$, so that $\mathbf{V}_g \cdot \nabla p = 0$. Using this result plus the hydrostatic approximation, (3.36) may be rewritten as

$$\omega = \frac{\partial p}{\partial t} + \mathbf{V}_a \cdot \nabla p - g\rho w \tag{3.37}$$

Comparing the magnitudes of the three terms on the right in (3.37), we find that for synoptic-scale motions

$$\begin{gathered} \partial p/\partial t \sim 10 \text{ hPa d}^{-1} \\ \mathbf{V}_a \cdot \nabla p \sim \left(1 \text{ m s}^{-1}\right)\left(1 \text{ Pa km}^{-1}\right) \sim 1 \text{ hPa d}^{-1} \\ g\rho w \sim 100 \text{ hPa d}^{-1} \end{gathered}$$

Thus, it is quite a good approximation to let

$$\omega = -\rho g w \tag{3.38}$$

3.5.1 The Kinematic Method

One method of deducing the vertical velocity is based on integrating the continuity equation in the vertical. Integration of (3.5) with respect to pressure from a reference level p_s to any level p yields

$$\begin{aligned} \omega(p) &= \omega(p_s) - \int_{p_s}^{p} \left(\frac{\partial u}{\partial x} + \frac{\partial v}{\partial y} \right)_p dp \\ &= \omega(p_s) + (p_s - p) \left(\frac{\partial \langle u \rangle}{\partial x} + \frac{\partial \langle v \rangle}{\partial y} \right)_p \end{aligned} \tag{3.39}$$

Here the angle brackets denote a pressure-weighted vertical average:

$$\langle\ \rangle \equiv (p - p_s)^{-1} \int_{p_s}^{p} ()dp$$

With the aid of (3.38), the averaged form of (3.39) can be rewritten as

$$w(z) = \frac{\rho\,(z_s)\,w\,(z_s)}{\rho(z)} - \frac{p_s - p}{\rho(z)g}\left(\frac{\partial\,\langle u\rangle}{\partial x} + \frac{\partial\,\langle v\rangle}{\partial y}\right) \tag{3.40}$$

where z and z_s are the heights of pressure levels p and p_s, respectively.

Application of (3.40) to infer the vertical velocity field requires knowledge of the horizontal divergence. To determine the horizontal divergence, the partial derivatives $\partial u/\partial x$ and $\partial v/\partial y$ are generally estimated from the fields of u and v by using *finite difference* approximations (see Section 13.2.1). For example, to determine the divergence of the horizontal velocity at the point x_0, y_0 in Figure 3.10, we write

$$\frac{\partial u}{\partial x} + \frac{\partial v}{\partial y} \approx \frac{u\,(x_0 + d) - u\,(x_0 - d)}{2d} + \frac{v\,(y_0 + d) - v\,(y_0 - d)}{2d} \tag{3.41}$$

However, for synoptic-scale motions in midlatitudes, the horizontal velocity is nearly in geostrophic equilibrium. Except for the small effect due to the variation of the Coriolis parameter (see Problem 3.19), the geostrophic wind is nondivergent; that is, $\partial u/\partial x$ and $\partial v/\partial y$ are nearly equal in magnitude but opposite in sign. Thus, the horizontal divergence is due primarily to the small departures of the wind from geostrophic balance (i.e., the ageostrophic wind). A 10% error in evaluating one of the wind components in (3.41) can easily cause the estimated divergence to be in error by 100%. For this reason, the continuity equation method is not recommended for estimating the vertical motion field from observed horizontal winds.

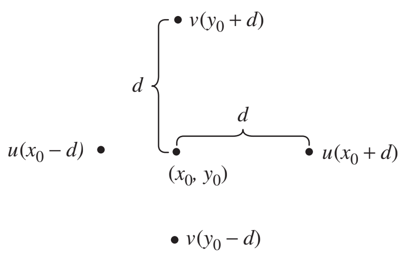

FIGURE 3.10 Grid for estimation of the horizontal divergence.

3.5.2 The Adiabatic Method

A second method for inferring vertical velocities, which is not so sensitive to errors in the measured horizontal velocities, is based on the thermodynamic energy equation. If the diabatic heating J is small compared to the other terms in the heat balance, (3.6) yields

$$\omega = S_p^{-1}\left(\frac{\partial T}{\partial t} + u\frac{\partial T}{\partial x} + v\frac{\partial T}{\partial y}\right) \tag{3.42}$$

Because temperature advection can usually be estimated quite accurately in midlatitudes by using geostrophic winds, the adiabatic method can be applied when only geopotential and temperature data are available. A disadvantage of the adiabatic method is that the local rate of change of temperature is required. Unless observations are taken at close intervals in time, it may be difficult to accurately estimate $\partial T/\partial t$ over a wide area. This method is also rather inaccurate in situations where strong diabatic heating is present, such as storms in which heavy rainfall occurs over a large area. Chapter 6 presents an alternative method for estimating ω, based on the so-called *omega equation*, that does not suffer from these difficulties.

3.6 SURFACE PRESSURE TENDENCY

The development of a negative surface *pressure tendency* is a classic warning of an approaching cyclonic weather disturbance. A simple expression that relates the surface pressure tendency to the wind field, and thus in theory might be used as the basis for short-range forecasts, can be obtained by taking the limit $p \to 0$ in (3.39) to get

$$\omega\left(p_s\right) = -\int_0^{p_s} (\nabla \cdot \mathbf{V})\, dp \tag{3.43}$$

followed by substituting from (3.37) to yield

$$\frac{\partial p_s}{\partial t} \approx -\int_0^{p_s} (\nabla \cdot \mathbf{V})\, dp \tag{3.44}$$

Here we have assumed that the surface is horizontal so that $w_s = 0$, and have neglected advection by the ageostrophic surface velocity in accord with the scaling arguments in Section 3.5.1.

According to (3.44), the surface pressure tendency at a given point is determined by the total convergence of mass into the vertical column of atmosphere above that point. This result is a direct consequence of the hydrostatic assumption, which implies that the pressure at a point is determined solely by the weight of the column of air above that point. Temperature changes in the air column will affect the heights of upper-level pressure surfaces, but not the surface pressure.

Although, as stated earlier, the tendency equation might appear to have potential as a forecasting aid, its utility is severely limited due to the fact that, as discussed in Section 3.5.1, $\nabla \cdot \mathbf{V}$ is difficult to compute accurately from observations because it depends on the ageostrophic wind field. In addition, there is a strong tendency for vertical compensation. Thus, when there is convergence in the lower troposphere, there is divergence aloft, and vice versa. The net integrated convergence or divergence is then a small residual in the vertical integral of a poorly determined quantity.

Nevertheless, (3.44) does have qualitative value as an aid in understanding the origin of surface pressure changes and the relationship of such changes to the horizontal divergence. This can be illustrated by considering (as one possible example) the development of a thermal cyclone. We suppose that a heat source generates a local warm anomaly in the midtroposphere (Figure 3.11a). Then, according to the hypsometric equation (3.34), the heights of the upper-level pressure surfaces are raised above the warm anomaly, resulting in a horizontal pressure gradient force at the upper levels, which drives a divergent upper-level wind. By (3.44) this upper-level divergence will initially cause the surface pressure to decrease, thus generating a surface low below the warm anomaly (Figure 3.11b). The horizontal pressure gradient associated with the surface low then drives a low-level convergence and vertical circulation, which tends to compensate the upper-level divergence. The degree of compensation between upper divergence and lower convergence will determine whether the surface pressure continues to fall, remains steady, or rises.

The thermally driven circulation of the preceding example is by no means the only type of circulation possible (e.g., cold-core cyclones are important synoptic-scale features). However, it does provide insight into how dynamical processes at upper levels are communicated to the surface and how the

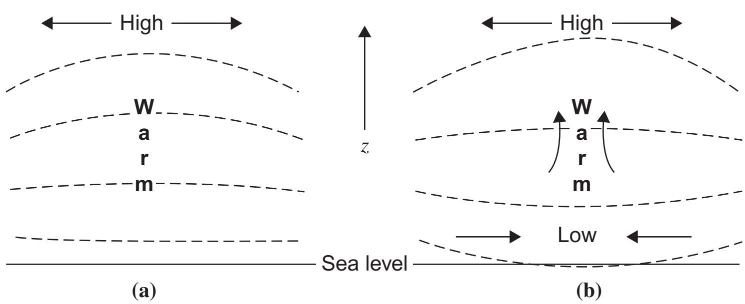

FIGURE 3.11 Adjustment of surface pressure to a midtropospheric heat source. *Dashed lines* indicate isobars. (a) Initial height increase at upper-level pressure surface. (b) Surface response to upper-level divergence.

surface and upper troposphere are dynamically connected through the divergent circulation. This subject is considered in detail in Chapter 6.

Equation (3.44) is a lower boundary condition that determines the evolution of pressure at constant height. If the isobaric coordinate system of dynamical equations (3.2), (3.5), (3.6), and (3.27) is used as the set of governing equations, the lower boundary condition should be expressed in terms of the evolution of geopotential (or geopotential height) at constant pressure. Such an expression can be obtained simply by expanding $D\Phi/Dt$ in isobaric coordinates

$$\frac{\partial \Phi}{\partial t} = -\mathbf{V}_a \cdot \nabla \Phi - \omega \frac{\partial \Phi}{\partial p}$$

and substituting from (3.27) and (3.43) to get

$$\frac{\partial \Phi_s}{\partial t} \approx -\frac{RT_s}{p_s} \int_0^{p_s} (\nabla \cdot \mathbf{V})\, dp \tag{3.45}$$

where we have again neglected advection by the ageostrophic wind.

In practice, the boundary condition (3.45) is difficult to use because it should be applied at pressure p_s, which is itself changing in time and space. In simple models it is usual to assume that p_s is constant (usually 1000 hPa) and to let $\omega = 0$ at p_s. For modern forecast models, an alternative coordinate system is generally employed in which the lower boundary is always a coordinate surface. This approach is described in Section 10.3.1.

PROBLEMS

3.1. An aircraft flying a heading of 60° (i.e., 60° to the east of north) at air speed 200 m s^{-1} moves relative to the ground due east (90°) at 225 m s^{-1}. If the plane is flying at constant pressure, what is its rate of change in altitude (in meters per kilometer horizontal distance) assuming a steady pressure field, geostrophic winds, and $f = 10^{-4}\,\mathrm{s}^{-1}$?

3.2. The actual wind is directed 30° to the right of the geostrophic wind. If the geostrophic wind is 20 m s^{-1}, what is the rate of change of wind speed? Let $f = 10^{-4}\,\mathrm{s}^{-1}$.

3.3. A tornado rotates with constant angular velocity ω. Show that the surface pressure at the center of the tornado is given by

$$p = p_0 \exp\left(\frac{-\omega^2 r_0^2}{2RT}\right)$$

where p_0 is the surface pressure at a distance r_0 from the center and T is the temperature (assumed constant). If the temperature is 288 K and pressure and wind speed at 100 m from the center are 1000 hPa and 100 m s^{-1}, respectively, what is the central pressure?

3.4. Calculate the geostrophic wind speed (m s^{-1}) on an isobaric surface for a geopotential height gradient of 100 m per 1000 km, and compare with all possible gradient wind speeds for the same geopotential height gradient and a radius of curvature of ± 500 km. Let $f = 10^{-4}$ s^{-1}.

3.5. Determine the maximum possible ratio of the normal anticyclonic gradient wind speed to the geostrophic wind speed for the same pressure gradient.

3.6. Show that the geostrophic balance in isothermal coordinates may be written

$$f\mathbf{V}_g = \mathbf{k} \times \nabla_T (RT \ln p + \Phi)$$

3.7. Determine the radii of curvature for the trajectories of air parcels located 500 km to the east, north, south, and west of the center of a circular low-pressure system, respectively. The system is moving eastward at 15 m s^{-1}. Assume geostrophic flow with a uniform tangential wind speed of 15 m s^{-1}.

3.8. Determine the normal gradient wind speeds for the four air parcels of Problem 3.7. Using the radii of curvature computed in the previous problem, compare these speeds with the geostrophic speed. (Let $f = 10^{-4}$ s^{-1}.) Use the gradient wind speeds calculated here to recompute the radii of curvature for the four air parcels referred to in Problem 3.7. Use these new estimates of the radii of curvature to recompute the gradient wind speeds for the four air parcels. What fractional error is made in the radii of curvature by using the geostrophic wind approximation in this case? [Note that further iterations could be carried out but would converge rapidly.]

3.9. Show that as the pressure gradient approaches zero, the gradient wind reduces to the geostrophic wind for a normal anticyclone and to inertial flow (Section 3.2.3) for an anomalous anticyclone.

3.10. The mean temperature in the layer between 750 and 500 hPa decreases eastward by 3°C per 100 km. If the 750-hPa geostrophic wind is from the southeast at 20 m s^{-1}, what is the geostrophic wind speed and direction at 500 hPa? Let $f = 10^{-4}$ s^{-1}.

3.11. What is the mean temperature advection in the 750- to 500-hPa layer in Problem 3.10?

3.12. Suppose that a vertical column of the atmosphere at 43°N is initially isothermal from 900 to 500 hPa. The geostrophic wind is 10 m s^{-1} from the south at 900 hPa, 10 m s^{-1} from the west at 700 hPa, and 20 m s^{-1} from the west at 500 hPa. Calculate the mean horizontal temperature gradients in the two layers 900 to 700 hPa and 700 to 500 hPa. Compute the rate of advective temperature change in each layer. How long would this advection pattern have to persist in order to establish a dry adiabatic lapse rate between 600 and 800 hPa? (Assume that the lapse rate is constant between 900 and 500 hPa and that the 800- to 600-hPa layer thickness is 2.25 km.)

3.13. An airplane pilot crossing the ocean at 45°N latitude has both a pressure altimeter and a radar altimeter, the latter measuring his absolute height above the sea. Flying at an air speed of 100 m s^{-1}, he maintains altitude by referring to his pressure altimeter set for a sea-level pressure of 1013 hPa. He holds an indicated 6000-m altitude. At the beginning of a 1-h period he notes that his radar altimeter reads 5700 m, and at the end of the hour he notes that it reads 5950 m. In what direction and approximately how far has he drifted from his heading?

3.14. Work out a gradient wind classification scheme equivalent to Table 3.1 for the Southern Hemisphere (f¡0) case.

3.15. In the geostrophic momentum approximation (Hoskins, 1975) the gradient wind formula for steady circular flow (3.17) is replaced by the approximation

$$VV_g R^{-1} + fV = fV_g$$

Compare the speeds V computed using this approximation with those obtained in Problem 3.8 using the gradient wind formula.

3.16. How large can the ratio $V_g/(fR)$ be before the geostrophic momentum approximation differs from the gradient wind approximation by 10% for cyclonic flow?

3.17. The planet Venus rotates about its axis so slowly that to a reasonable approximation the Coriolis parameter may be set equal to zero. For steady, frictionless motion parallel to latitude circles, the momentum equation (2.20) then reduces to a type of cyclostrophic balance:

$$\frac{u^2 \tan\phi}{a} = -\frac{1}{\rho}\frac{\partial p}{\partial y}$$

By transforming this expression to isobaric coordinates, show that the thermal wind equation in this case can be expressed in the form

$$\omega_r^2\,(p_1) - \omega_r^2\,(p_0) = \frac{-R\ln(p_0/p_1)}{(a\sin\phi\cos\phi)}\frac{\partial\langle T\rangle}{\partial y}$$

where R is the gas constant, a is the radius of the planet, and $\omega_r \equiv u/(a\cos\phi)$ is the relative angular velocity. How must $\langle T\rangle$ (the vertically averaged temperature) vary with respect to latitude in order for ω_r to be a function only of pressure? If the zonal velocity at about 60 km above the equator ($p_1 = 2.9 \times 10^5$ Pa) is 100 m s^{-1} and the zonal velocity vanishes at the surface of the planet ($p_0 = 9.5 \times 10^6$ Pa), what is the vertically averaged temperature difference between the equator and the pole, assuming that ω_r depends only on pressure? The planetary radius is $a = 6100$ km, and the gas constant is $R = 187$ J kg^{-1} K^{-1}.

3.18. Suppose that during the passage of a cyclonic storm the radius of curvature of the isobars is observed to be 800 km at a station where the wind is veering (turning clockwise) at a rate of 10° per hour. What is the radius of curvature of the trajectory for an air parcel that is passing over the station? (The wind speed is 20 m s^{-1}.)

3.19. Show that the divergence of the geostrophic wind in isobaric coordinates on the spherical earth is given by

$$\nabla \cdot \mathbf{V}_g = -\frac{1}{fa}\frac{\partial\Phi}{\partial x}\left(\frac{\cos\phi}{\sin\phi}\right) = -v_g\left(\frac{\cot\phi}{a}\right)$$

(Use the spherical coordinate expression for the divergence operator given in Appendix C.)

3.20. The following wind data were received from 50 km to the east, north, west, and south of a station, respectively: 90°, 10 m s^{-1}; 120°, 4 m s^{-1}; 90°, 8 m s^{-1}; and 60°, 4 m s^{-1}. Calculate the approximate horizontal divergence at the station.

3.21. Suppose that the wind speeds given in Problem 3.20 are each in error by ±10%. What would be the percentage error in the calculated horizontal divergence in the worst case?

3.22. The divergence of the horizontal wind at various pressure levels above a given station is shown in the following table. Compute the vertical velocity at each level assuming an isothermal atmosphere with temperature 260 K and letting $w = 0$ at 1000 hPa.

Pressure (hPa)	$\nabla \cdot \mathbf{V}(\times 10^{-5}\ \mathrm{s}^{-1})$
1000	+0.9
850	+0.6
700	+0.3
500	0.0
300	−0.6
100	−1.0

3.23. Suppose that the lapse rate at the 850-hPa level is 4 K km^{-1}. If the temperature at a given location is decreasing at a rate of 2 K h^{-1}, the wind is westerly at 10 m s^{-1}, and the temperature decreases toward the west at a rate of 5 K/100 km, compute the vertical velocity at the 850-hPa level using the adiabatic method.

MATLAB Exercises

M3.1. For the situations considered in Problems M2.1 and M2.2, make further modifications in the MATLAB scripts to compute the vertical profiles of density and of the static stability parameter S_p defined in (3.7). Plot these in the interval from $z = 0$ to $z = 15$ km. You will need to approximate the vertical derivative in S_p using a finite difference approximation (see Section 13.2.1).

M3.2. The objective of this exercise is to gain an appreciation for the difference between trajectories and streamlines in synoptic-scale flows. An idealized representation of a midlatitude synoptic disturbance in an atmosphere with no zonal mean flow is given by the simple sinusoidal pattern of geopotential,

$$\Phi(x, y, t) = \Phi_0 + \Phi' \sin[k(x - ct)] \cos\ ly$$

where $\Phi_0(p)$ is the standard atmosphere geopotential dependent only on pressure, Φ' is the magnitude of the geopotential wave disturbance, c is the phase speed of zonal propagation of the wave pattern, and k and l are the wave numbers in the x and y directions, respectively. If it is assumed that the flow is in geostrophic balance, then the geopotential is proportional to the stream function. Let the zonal and meridional wave numbers be equal

$(k = l)$ and define a perturbation wind amplitude $U' \equiv \Phi' k / f_0$, where f_0 is a constant Coriolis parameter. Trajectories are then given by the paths in (x, y) space obtained by solving the coupled set of ordinary differential equations:

$$\frac{Dx}{Dt} = u = -f_0^{-1}\frac{\partial \Phi}{\partial y} = +U' \sin\left[k\left(x - ct\right)\right] \sin ly$$
$$\frac{Dy}{Dt} = v = +f_0^{-1}\frac{\partial \Phi}{\partial x} = +U' \cos\left[k\left(x - ct\right)\right] \cos ly$$

[Note that U' (taken to be a positive constant) denotes the amplitude of both the x and y components of the disturbance wind.] The MATLAB script **trajectory_1.m** provides an accurate numerical solution to these equations for the special case in which the zonal mean wind vanishes. Three separate trajectories are plotted in the code. Run this script letting $U' = 10$ m s^{-1} for cases with $c = 5$, 10, and 15 m s^{-1}. Describe the behavior of the three trajectories for each of these cases. Why do the trajectories have their observed dependence on the phase speed c at which the geopotential height pattern propagates?

M3.3. The MATLAB script **trajectory_2.m** generalizes the case of Problem M3.2 by adding a mean zonal flow. In this case the geopotential distribution is specified to be $\Phi(x, y, t) = \Phi_0 - f_0 \bar{U} l^{-1} \sin ly + \Phi' \sin\left[k\left(x - ct\right)\right] \cos ly$.

- **(a)** Solve for the latitudinal dependence of the mean zonal wind for this case.
- **(b)** Run the script with the initial x position specified as $x = -2250$ km and $U' = 15$ m s^{-1}. Do two runs, letting $\bar{U} = 10$ m s^{-1}, $c = 5$ m s^{-1} and $\bar{U} = 5$ m s^{-1}, $c = 10$ m s^{-1}, respectively. Determine the zonal distance that the ridge originally centered at $x = -2250$ km has propagated in each case. Use this information to briefly explain the characteristics (i.e., the shapes and lengths) of the 4-day trajectories for each of these cases.
- **(c)** Which combination of initial position, $\bar{U}$ and c, will produce a straight-line trajectory?

M3.4. The MATLAB script **trajectory_3.m** can be used to examine the dispersion of a cluster of N parcels initially placed in a circle of small radius for a geopotential distribution representing the combination of a zonal mean jet plus a propagating wave with NE to SW tilt of trough and ridge lines. The user must input the mean zonal wind amplitude, $\bar{U}$, the disturbance horizontal wind, U', the propagation speed of the waves, c, and the initial y position of the center of the cluster.

- **(a)** Run the model for three cases specifying $y = 0$, $U' = 15$ m s^{-1}, and $\bar{U} = 10, 12$, and 15 m s^{-1}, respectively. Compute 20-day trajectories for all parcel clusters. Give an explanation for the differences in the dispersion of the parcel cluster for these three cases.
- **(b)** For the situation with $c = 10$ m s^{-1}, $U' = 15$ m s^{-1}, and $\bar{U} = 12$ m s^{-1}, run three additional cases with the initial y specified to be 250, 500, and 750 km.

Describe how the results differ from the case with $y = 0$ km and $\bar{U} = 12$ m s^{-1}, and give an explanation for the differences in these runs.

Chapter 4

Circulation, Vorticity, and Potential Vorticity

In classical mechanics the principle of conservation of angular momentum is often invoked in the analysis of motions that involve rotation. This principle provides a powerful constraint on the behavior of rotating objects. Analogous conservation laws also apply to the rotational field of a fluid. However, it should be obvious that in a continuous medium, such as the atmosphere, the definition of "rotation" is subtler than that for rotation of a solid object.

Circulation and vorticity are the two primary measures of rotation in a fluid. Circulation, which is a scalar integral quantity, is a *macroscopic* measure of rotation for a finite area of the fluid. Vorticity, however, is a vector field that gives a *microscopic* measure of the rotation at any point in the fluid. Potential vorticity extends the concept of vorticity to include thermodynamic constraints on the motion, yielding a powerful framework for interpreting atmospheric dynamics.

4.1 THE CIRCULATION THEOREM

The *circulation*, C, about a closed contour in a fluid is defined as the line integral evaluated along the contour of the component of the velocity vector that is locally tangent to the contour:

$$C \equiv \oint \mathbf{U} \cdot d\mathbf{l} = \oint |\mathbf{U}| \cos\ \alpha\ dl$$

where $\mathbf{l}(s)$ is a position vector extending from the origin to the point $s(x, y, z)$ on the contour C, and $d\mathbf{l}$ represents the limit of $\delta\mathbf{l} = \mathbf{l}(s + \delta s) - \mathbf{l}(s)$ as $\delta s \to 0$. Hence, as indicated in Figure 4.1, $d\mathbf{l}$ is a displacement vector locally tangent to the contour. By convention the circulation is taken to be positive if $C > 0$ for counterclockwise integration around the contour.

That circulation is a measure of rotation is demonstrated readily by considering a circular ring of fluid of radius R in solid-body rotation at angular velocity $\boldsymbol{\Omega}$ about the z axis. In this case, $\mathbf{U} = \boldsymbol{\Omega} \times \mathbf{R}$, where $\mathbf{R}$ is the distance from the axis of rotation to the ring of fluid. Thus, the circulation about the ring is

An Introduction to Dynamic Meteorology. DOI: 10.1016/B978-0-12-384866-6.00004-0

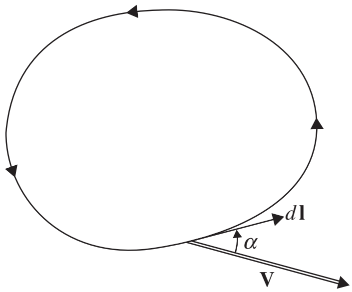

FIGURE 4.1 Circulation about a closed contour.

given by

$$C \equiv \oint \mathbf{U} \cdot d\mathbf{l} = \int_0^{2\pi} \Omega R^2 d\lambda = 2\Omega\pi R^2$$

In this case the circulation is just 2π times the angular momentum of the fluid ring about the axis of rotation. Alternatively, note that $C/(\pi R^2) = 2\Omega$, so that the circulation divided by the area enclosed by the loop is just twice the angular speed of rotation of the ring. Unlike angular momentum or angular velocity, circulation can be computed without reference to an axis of rotation; it can thus be used to characterize fluid rotation in situations where "angular velocity" is not easily defined.

The circulation theorem is obtained by taking the line integral of Newton's second law for a closed chain of fluid particles. In the absolute coordinate system, the result (neglecting viscous forces) is

$$\oint \frac{D_a \mathbf{U}_a}{Dt} \cdot d\mathbf{l} = -\oint \frac{\nabla p \cdot d\mathbf{l}}{\rho} - \oint \nabla \Phi \cdot d\mathbf{l} \tag{4.1}$$

where the gravitational force is represented as the gradient of geopotential Φ^*, defined in terms of true gravity, so that $\nabla\Phi^* = -\mathbf{g}^* = g^*\mathbf{k}$. The integrand on the left side can be rewritten as[1]

$$\frac{D_a \mathbf{U}_a}{Dt} \cdot d\mathbf{l} = \frac{D}{Dt}(\mathbf{U}_a \cdot d\mathbf{l}) - \mathbf{U}_a \cdot \frac{D_a}{Dt}(d\mathbf{l})$$

or after observing that since $\mathbf{l}$ is a position vector, $D_a\mathbf{l}/Dt \equiv \mathbf{U}_a$,

$$\frac{D_a \mathbf{U}_a}{Dt} \cdot d\mathbf{l} = \frac{D}{Dt}(\mathbf{U}_a \cdot d\mathbf{l}) - \mathbf{U}_a \cdot d\mathbf{U}_a \tag{4.2}$$

[1] Note that for a scalar, $D_a/Dt = D/Dt$ (i.e., the rate of change following the motion does not depend on the reference system). For a vector, however, this is not the case, as was shown in Section 2.1.1.

Substituting (4.2) into (4.1) and using the fact that the line integral about a closed loop of a perfect differential is zero, so that

$$\oint \nabla\Phi \cdot d\mathbf{l} = \oint d\Phi = 0$$

and noting that

$$\oint \mathbf{U}_a \cdot d\mathbf{U}_a = \frac{1}{2}\oint d(\mathbf{U}_a \cdot \mathbf{U}_a) = 0$$

we obtain the circulation theorem:

$$\frac{DC_a}{Dt} = \frac{D}{Dt}\oint \mathbf{U}_a \cdot d\mathbf{l} = -\oint \rho^{-1} dp \tag{4.3}$$

The term that is on the right side in (4.3) is called the solenoidal term, where $dp = \nabla p \cdot d\mathbf{l}$ is the pressure increment along an increment of arc length. For a barotropic fluid, the density is a function only of pressure, and the solenoidal term is zero. Thus, in a barotropic fluid the absolute circulation is conserved following the motion. This result, called *Kelvin's circulation theorem*, is a fluid analog of angular momentum conservation in solid-body mechanics.

For meteorological analysis, it is more convenient to work with the relative circulation C rather than the absolute circulation; a portion of the absolute circulation, C_e, is due to the rotation of Earth about its axis. To compute C_e, we apply Stokes's theorem to the vector $\mathbf{U}_e$, where $\mathbf{U}_e = \boldsymbol{\Omega} \times \mathbf{r}$ is the velocity of Earth at position $\mathbf{r}$:

$$C_e = \oint \mathbf{U}_e \cdot d\mathbf{l} = \int_A\int (\nabla \times \mathbf{U}_e) \cdot \mathbf{n}\, dA$$

where A is the area enclosed by the contour and the unit normal $\mathbf{n}$ is defined by the counterclockwise sense of the line integration using the "right rule." Thus, for the contour of Figure 4.1, $\mathbf{n}$ would be directed out of the page. If the line integral is computed in the horizontal plane, $\mathbf{n}$ is directed along the local vertical (Figure 4.2). Now, by a vector identity (see Appendix C),

$$\nabla \times \mathbf{U}_e = \nabla \times (\boldsymbol{\Omega} \times \mathbf{r}) = \nabla \times (\boldsymbol{\Omega} \times \mathbf{R}) = \boldsymbol{\Omega}\nabla \cdot \mathbf{R} = 2\boldsymbol{\Omega}$$

so that $(\nabla \times \mathbf{U}_e) \cdot \mathbf{n} = 2\Omega \sin\phi \equiv f$ is just the Coriolis parameter. Hence, the circulation in the horizontal plane due to the rotation of Earth is

$$C_e = 2\Omega\langle\sin\phi\rangle\, A = 2\Omega A_e$$

where $\langle\sin\phi\rangle$ denotes an average over the area element A, and A_e is the projection of A in the equatorial plane, as illustrated in Figure 4.2. Thus, the relative circulation may be expressed as

$$C = C_a - C_e = C_a - 2\Omega A_e \tag{4.4}$$

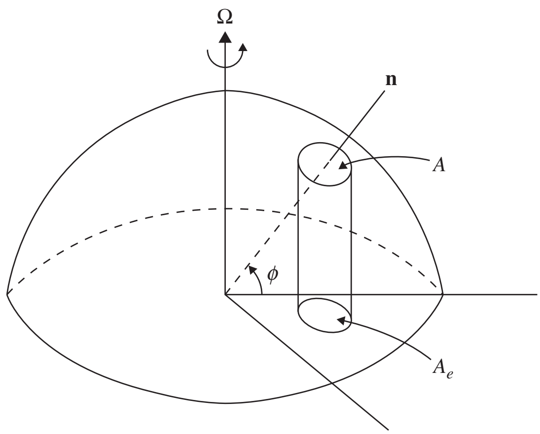

FIGURE 4.2 Area A_e subtended on the equatorial plane by horizontal area A centered at latitude ϕ.

Differentiating (4.4) following the motion and substituting from (4.3), we obtain the *Bjerknes circulation theorem*:

$$\frac{DC}{Dt} = -\oint \frac{dp}{\rho} - 2\Omega \frac{DA_e}{Dt} \tag{4.5}$$

For a barotropic fluid, (4.5) can be integrated following the motion from an initial state (designated by subscript 1) to a final state (designated by subscript 2), yielding the circulation change

$$C_2 - C_1 = -2\Omega\,(A_2 \sin\phi_2 - A_1 \sin\phi_1) \tag{4.6}$$

Equation (4.6) indicates that in a barotropic fluid the relative circulation for a closed chain of fluid particles will be changed if either the horizontal area enclosed by the loop changes or the latitude changes. Furthermore, a negative absolute circulation in the Northern Hemisphere can develop only if a closed chain of fluid particles is advected across the equator from the Southern Hemisphere. The anomalous gradient wind balances discussed in Section 3.2.5 are examples of systems with negative absolute circulations (see Problem 4.6).

Examples

Suppose that the air within a circular region of radius 100 km centered at the equator is initially motionless with respect to Earth. If this circular air mass were moved to the North Pole along an isobaric surface preserving its area, the circulation about the circumference would be

$$C = -2\Omega\pi r^2 \sin(\pi/2) - \sin(0)$$

Thus, the mean tangential velocity at the radius $r = 100$ km would be

$$V = C/(2\pi r) = -\Omega r \approx -7 \text{ m s}^{-1}$$

The negative sign here indicates that the air has acquired anticyclonic relative circulation.

In a baroclinic fluid, circulation may be generated by the pressure-density solenoid term in (4.3). This process can be illustrated effectively by considering the development of a sea breeze circulation, as shown in Figure 4.3. For the situation depicted, the mean temperature in the air over the ocean is colder than the mean temperature over the adjoining land. Thus, if the pressure is uniform at ground level, the isobaric surfaces above the ground will slope downward toward the ocean, while the isopycnic surfaces (surfaces of constant density) will slope downward toward the land.

To compute the acceleration as a result of the intersection of the pressure-density surfaces, we apply the circulation theorem by integrating around a circuit in a vertical plane perpendicular to the coastline. Substituting the ideal gas law into (4.3), we obtain

$$\frac{DC_a}{Dt} = -\oint RTd\ln p$$

For the circuit shown in Figure 4.3, there is a contribution to the line integral only for the vertical segments of the loop, since the horizontal segments are taken at constant pressure. The resulting rate of increase in the circulation is

$$\frac{DC_a}{Dt} = R\ln\left(\frac{p_0}{p_1}\right)(\overline{T}_2 - \overline{T}_1) > 0$$

Letting $\langle v\rangle$ be the mean tangential velocity along the circuit, we find that

$$\frac{D\langle v\rangle}{Dt} = \frac{R\ln(p_0/p_1)}{2(h+L)}(\overline{T}_2 - \overline{T}_1) \tag{4.7}$$

If we let $p_0 = 1000$ hPa, $p_1 = 900$ hPa, $\overline{T}_2 - \overline{T}_1 = 10^\circ$ C, $L = 20$ km, and $h = 1$ km, (4.7) yields an acceleration of about 7×10^{-3} m s^{-2}. In the absence of frictional retarding forces, this would produce a wind speed of 25 m s^{-1} in about 1 h. In reality, as the wind speed increases, the frictional force reduces the acceleration rate, and temperature advection reduces the land–sea temperature contrast so that a balance is obtained between the generation of kinetic energy by the pressure-density solenoids and frictional dissipation.

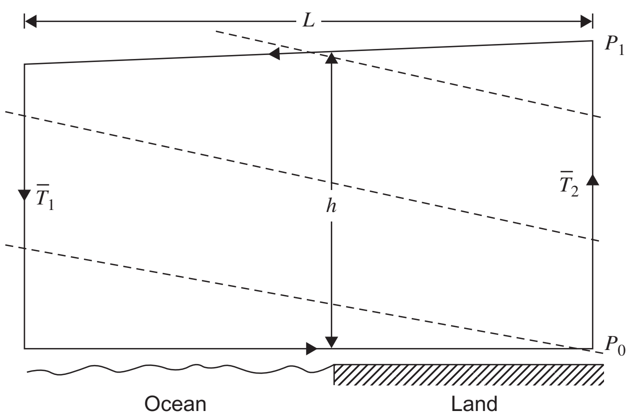

FIGURE 4.3 Application of the circulation theorem to the sea breeze problem. The closed *heavy solid line* is the loop about which the circulation is to be evaluated. *Dashed lines* indicate surfaces of constant density.

4.2 VORTICITY

Vorticity, the microscopic measure of rotation in a fluid, is a vector field defined as the curl of velocity. The absolute vorticity $\boldsymbol{\omega}_a$ is the curl of the absolute velocity, whereas the relative vorticity $\boldsymbol{\omega}$ is the curl of the relative velocity:

$$\boldsymbol{\omega}_a \equiv \nabla \times \mathbf{U}_a, \qquad \boldsymbol{\omega} \equiv \nabla \times \mathbf{U}$$

so that in Cartesian coordinates,

$$\boldsymbol{\omega} = \left(\frac{\partial w}{\partial y} - \frac{\partial v}{\partial z}, \frac{\partial u}{\partial z} - \frac{\partial w}{\partial x}, \frac{\partial v}{\partial x} - \frac{\partial u}{\partial y} \right)$$

A scale analysis of the scalar components of the vorticity vector for synoptic-scale motions reveals that the dominant contributions to the horizontal components, $\frac{\partial u}{\partial z}$ and $\frac{\partial v}{\partial z}$,[2] scale like $\frac{U}{H}$, whereas the vertical components, $\frac{\partial u}{\partial y}$ and $\frac{\partial v}{\partial x}$, scale like $\frac{U}{L}$. Therefore, the vertical component of vorticity is of size $\frac{H}{L}$ relative to the horizontal component, or about $10\,\text{km}/1000\,\text{km} = 0.01$. We see that the vorticity vector points mainly in the horizontal direction, and this is true even if we include the planetary contribution, which has size $\frac{fH}{U} = \text{Ro}^{-1}\frac{H}{L} \sim 0.1$, where Ro is the Rossby number. For a westerly jet stream with winds increasing upward in the troposphere, the vorticity vector points mostly toward the north.

As a result of this analysis, it may seem strange, but in fact for large-scale dynamic meteorology we are in general concerned only with the vertical components of absolute and relative vorticity, which are designated by η and ζ, respectively:

$$\eta \equiv \mathbf{k} \cdot (\nabla \times \mathbf{U}_a), \qquad \zeta \equiv \mathbf{k} \cdot (\nabla \times \mathbf{U})$$

In the remainder of this book, η and ζ are referred to as absolute and relative vorticities, respectively, without adding the explicit modifier "vertical component of." We defer a full explanation for why we focus on the relatively small vertical component of vorticity until after we have discussed potential vorticity, but the essential point is that, on synoptic and larger scales, the vertical component of vorticity is tightly coupled to the vertical gradient of potential temperature, which is very large compared to the horizontal gradient.

Regions of positive ζ are associated with cyclonic storms in the Northern Hemisphere; regions of negative ζ are associated with cyclonic storms in the Southern Hemisphere. In both cases ζ has the same sign as f, the local value of the planetary rotation, so that we may uniformly define cyclonic by $f\zeta > 0$. Thus, the distribution of relative vorticity is an excellent diagnostic for weather analysis.

---

[2]Terms involving w are negligible by comparison for synoptic-scale weather systems.

The difference between absolute and relative vorticity is *planetary vorticity*, which is just the local vertical component of the vorticity of Earth due to its rotation; $\mathbf{k} \cdot \nabla \times \mathbf{U}_e = 2\Omega \sin\phi \equiv f$. Thus, $\eta = \zeta + f$ or, in Cartesian coordinates,

$$\zeta = \frac{\partial v}{\partial x} - \frac{\partial u}{\partial y}, \qquad \eta = \frac{\partial v}{\partial x} - \frac{\partial u}{\partial y} + f$$

The relationship between relative vorticity and relative circulation C discussed in the previous section can be clearly seen by considering an alternative approach in which the vertical component of vorticity is defined as the circulation about a closed contour in the horizontal plane divided by the area enclosed, in the limit where the area approaches zero:

$$\zeta \equiv \lim_{A \to 0} \left(\oint \mathbf{V} \cdot d\mathbf{l} \right) A^{-1} \tag{4.8}$$

This latter definition makes explicit the relationship between circulation and vorticity discussed in the introduction to this chapter. The equivalence of these two definitions of ζ is demonstrated by considering the circulation about a rectangular element of area $\delta x \delta y$ in the (x, y) plane, as shown in Figure 4.4. Evaluating $\mathbf{V} \cdot d\mathbf{l}$ for each side of the rectangle in the figure yields the circulation

$$\begin{aligned}\delta C &= u\delta x + \left(v + \frac{\partial v}{\partial x}\delta x \right) \delta y - \left(u + \frac{\partial u}{\partial y}\delta y \right) \delta x - v\delta y \\ &= \left(\frac{\partial v}{\partial x} - \frac{\partial u}{\partial y} \right) \delta x \delta y\end{aligned}$$

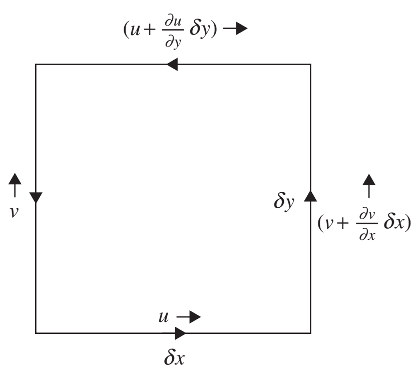

FIGURE 4.4 Relationship between circulation and vorticity for an area element in the horizontal plane.

Dividing through by the area $\delta A = \delta x \delta y$ gives

$$\frac{\delta C}{\delta A} = \left(\frac{\partial v}{\partial x} - \frac{\partial u}{\partial y}\right) \equiv \zeta$$

In more general terms the relationship between vorticity and circulation is given simply by Stokes's theorem applied to the velocity vector:

$$\oint \mathbf{U} \cdot d\mathbf{l} = \iint_A (\nabla \times \mathbf{U}) \cdot \mathbf{n} dA$$

Here A is the area enclosed by the contour and $\mathbf{n}$ is a unit normal to the area element dA (positive in the right sense). Thus, Stokes's theorem states that the circulation about any closed loop is equal to the integral of the normal component of vorticity over the area enclosed by the contour. Hence, for a finite area, circulation divided by area gives the *average* normal component of vorticity in the region. As a consequence, the vorticity of a fluid in solid-body rotation is just twice the angular velocity of rotation. Vorticity may thus be regarded as a measure of the local angular velocity of the fluid.

4.2.1 Vorticity in Natural Coordinates

Physical interpretation of vorticity is facilitated by considering the vertical component of vorticity in the natural coordinate system (see Section 3.2.1). If we compute the circulation about the infinitesimal contour shown in Figure 4.5, we obtain[3]

$$\delta C = V\left[\delta s + d(\delta s)\right] - \left(V + \frac{\partial V}{\partial n}\delta n\right)\delta s$$

However, from this figure, $d(\delta s) = \delta\beta\delta n$, where $\delta\beta$ is the angular change in the wind direction in the distance δs. Hence,

$$\delta C = \left(-\frac{\partial V}{\partial n} + V\frac{\delta\beta}{\delta s}\right)\delta n\, \delta s$$

or, in the limit $\delta n, \delta s \to 0$

$$\zeta = \lim_{\delta n, \delta s \to 0} \frac{\delta C}{(\delta n\, \delta s)} = -\frac{\partial V}{\partial n} + \frac{V}{R_s} \tag{4.9}$$

[3]Recall that n is a coordinate in the horizontal plane perpendicular to the local flow direction with positive values to the left of an observer facing downstream.

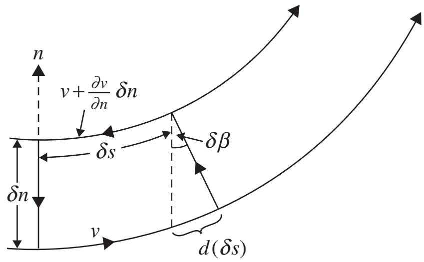

FIGURE 4.5 Circulation for an infinitesimal loop in the natural coordinate system.

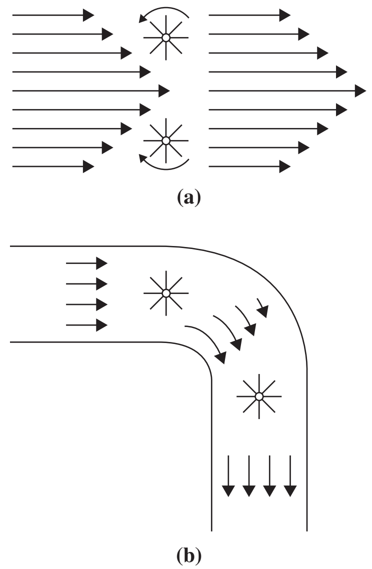

FIGURE 4.6 Two types of two-dimensional flow: (a) linear shear flow with vorticity and (b) curved flow with zero vorticity.

where R_s is the radius of curvature of the streamlines [Eq. (3.20)]. It is now apparent that the net vertical vorticity component is the result of the sum of two parts: (1) the rate of change of wind speed normal to the direction of flow $-\partial V/\partial n$, called the *shear* vorticity; and (2) the turning of the wind along a streamline V/R_s, called the *curvature* vorticity. Thus, even straight-line motion may have vorticity if the speed changes normal to the flow axis. For example, in the jet stream shown schematically in Figure 4.6a, there will be cyclonic relative vorticity north of the velocity maximum and anticyclonic relative vorticity to the south (Northern Hemisphere conditions), as is recognized easily when the turning of a small paddle wheel placed in the flow is considered. The lower of the two paddle wheels in Figure 4.6a will turn in a clockwise direction (anticyclonically) because the wind force on the blades north of its axis of rotation is stronger than the force on the blades to the south of the axis. The upper wheel will, of course, experience a counterclockwise (cyclonic) turning. Thus, the poleward and equatorward sides of a westerly jet stream are referred to as the cyclonic and anticyclonic shear sides, respectively.

Conversely, curved flow may have zero vorticity provided that the shear vorticity is equal and opposite to the curvature vorticity. This is the case in the example shown in Figure 4.6b, where a frictionless fluid with zero relative vorticity upstream flows around a bend in a canal. The fluid along the inner boundary on the curve flows faster in just the right proportion so that the paddle wheel does not turn.

4.3 THE VORTICITY EQUATION

The previous section discussed kinematic properties of vorticity. This section addresses vorticity dynamics using the equations of motion to determine contributions to the time rate of change of vorticity.

4.3.1 Cartesian Coordinate Form

For motions of synoptic scale, the vorticity equation can be derived using the approximate horizontal momentum equations (2.24) and (2.25). We differentiate the zonal component equation with respect to y and the meridional component equation with respect to x:

$$\frac{\partial}{\partial y}\left(\frac{\partial u}{\partial t}+u\frac{\partial u}{\partial x}+v\frac{\partial u}{\partial y}+w\frac{\partial u}{\partial z}-fv=-\frac{1}{\rho}\frac{\partial p}{\partial x}\right) \tag{4.10}$$

$$\frac{\partial}{\partial x}\left(\frac{\partial v}{\partial t}+u\frac{\partial v}{\partial x}+v\frac{\partial v}{\partial y}+w\frac{\partial v}{\partial z}+fu=-\frac{1}{\rho}\frac{\partial p}{\partial y}\right) \tag{4.11}$$

Subtracting (4.10) from (4.11) and recalling that $\zeta=\partial v/\partial x-\partial u/\partial y$, we obtain the vorticity equation

$$\begin{aligned}&\frac{\partial \zeta}{\partial t}+u\frac{\partial \zeta}{\partial x}+v\frac{\partial \zeta}{\partial y}+w\frac{\partial \zeta}{\partial z}+(\zeta+f)\left(\frac{\partial u}{\partial x}+\frac{\partial v}{\partial y}\right)\\&+\left(\frac{\partial w}{\partial x}\frac{\partial v}{\partial z}-\frac{\partial w}{\partial y}\frac{\partial u}{\partial z}\right)+v\frac{df}{dy}=\frac{1}{\rho^2}\left(\frac{\partial \rho}{\partial x}\frac{\partial p}{\partial y}-\frac{\partial \rho}{\partial y}\frac{\partial p}{\partial x}\right)\end{aligned} \tag{4.12}$$

Using the fact that the Coriolis parameter depends only on y so that $Df/Dt = v(df/dy)$, (4.12) may be rewritten in the form

$$\frac{D}{Dt}(\zeta + f) = -(\zeta + f)\left(\frac{\partial u}{\partial x} + \frac{\partial v}{\partial y}\right) - \left(\frac{\partial w}{\partial x}\frac{\partial v}{\partial z} - \frac{\partial w}{\partial y}\frac{\partial u}{\partial z}\right) + \frac{1}{\rho^2}\left(\frac{\partial \rho}{\partial x}\frac{\partial p}{\partial y} - \frac{\partial \rho}{\partial y}\frac{\partial p}{\partial x}\right) \tag{4.13}$$

Equation (4.13) states that the rate of change of the absolute vorticity following the motion is given by the sum of the three terms on the right, called the divergence (or vortex stretching) term, the tilting or twisting term, and the solenoidal term, respectively.

The concentration or dilution of vorticity by the divergence field—the first term on the right in (4.13)—is the fluid analog of the change in angular velocity resulting from a change in the moment of inertia of a solid body when angular momentum is conserved. If the horizontal flow is divergent, the area enclosed by a chain of fluid parcels will increase with time, and if circulation is to be conserved, the average absolute vorticity of the enclosed fluid must decrease (i.e., the vorticity will be diluted). If, however, the flow is convergent, the area enclosed by a chain of fluid parcels will decrease with time and the vorticity will be concentrated. This mechanism for changing vorticity following the motion is very important in synoptic-scale disturbances.

The second term on the right in (4.13) represents vertical vorticity generated by the tilting of horizontally oriented components of vorticity into the vertical by a nonuniform vertical motion field. This mechanism is illustrated in Figure 4.7,

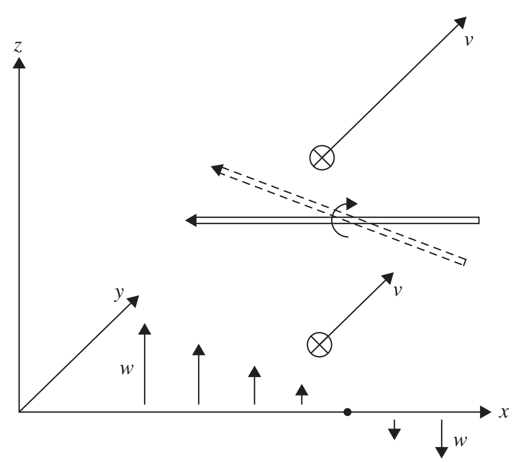

FIGURE 4.7 Vorticity generation by the tilting of a horizontal vorticity vector (*double arrow*).

which shows a region where the y component of velocity is increasing with height so that there is a component of shear vorticity oriented in the negative x direction as indicated by the double arrow. If at the same time there is a vertical motion field in which w decreases with increasing x, advection by the vertical motion will tend to tilt the vorticity vector initially oriented parallel to x so that it has a component in the vertical. Thus, if $\partial v/\partial z > 0$ and $\partial w/\partial x < 0$, there will be a generation of positive vertical vorticity.

Finally, the third term on the right in (4.13) is just the microscopic equivalent of the solenoidal term in the circulation theorem (4.5). To show this equivalence, we may apply Stokes's theorem to the solenoidal term to get

$$-\oint \alpha dp \equiv -\oint \alpha \nabla p \cdot d\mathbf{l} = -\iint_A \nabla \times (\alpha \nabla p) \cdot \mathbf{k} dA$$

where A is the horizontal area bounded by the curve $\mathbf{l}$. Applying the vector identity $\nabla \times (\alpha \nabla p) \equiv \nabla\alpha \times \nabla p$, the equation becomes

$$-\oint \alpha dp = -\iint_A (\nabla\alpha \times \nabla p) \cdot \mathbf{k} dA$$

However, the solenoidal term in the vorticity equation can be written

$$-\left(\frac{\partial\alpha}{\partial x}\frac{\partial p}{\partial y} - \frac{\partial\alpha}{\partial y}\frac{\partial p}{\partial x}\right) = -(\nabla\alpha \times \nabla p) \cdot \mathbf{k}$$

Thus, the solenoidal term in the vorticity equation is just the limit of the solenoidal term in the circulation theorem divided by the area when the area goes to zero.

4.3.2 The Vorticity Equation in Isobaric Coordinates

A somewhat simpler form of the vorticity equation arises when the motion is referred to the isobaric coordinate system. This equation can be derived in vector form by operating on the momentum equation (3.2) with the vector operator $\mathbf{k} \cdot \nabla\times$, where ∇ now indicates the horizontal gradient on a surface of constant pressure. However, to facilitate this process it is desirable to first use the vector identity

$$(\mathbf{V} \cdot \nabla)\mathbf{V} = \nabla\left(\frac{\mathbf{V} \cdot \mathbf{V}}{2}\right) + \zeta\, \mathbf{k} \times \mathbf{V} \tag{4.14}$$

where $\zeta = \mathbf{k} \cdot (\nabla \times \mathbf{V})$, to rewrite (3.2) as

$$\frac{\partial \mathbf{V}}{\partial t} = -\nabla\left(\frac{\mathbf{V} \cdot \mathbf{V}}{2} + \Phi\right) - (\zeta + f)\mathbf{k} \times \mathbf{V} - \omega\frac{\partial \mathbf{V}}{\partial p} \tag{4.15}$$

We now apply the operator $\mathbf{k} \cdot \nabla \times$ to (4.15). Using the facts that for any scalar A, $\nabla \times \nabla A = 0$ and for any vectors $\mathbf{a}$, $\mathbf{b}$,

$$\nabla \times (\mathbf{a} \times \mathbf{b}) = (\nabla \cdot \mathbf{b})\,\mathbf{a} - (\mathbf{a} \cdot \nabla)\,\mathbf{b} - (\nabla \cdot \mathbf{a})\,\mathbf{b} + (\mathbf{b} \cdot \nabla)\,\mathbf{a} \tag{4.16}$$

we can eliminate the first term on the right and simplify the second term so that the resulting vorticity equation becomes

$$\frac{\partial \zeta}{\partial t} = -\mathbf{V} \cdot \nabla\,(\zeta + f) - \omega \frac{\partial \zeta}{\partial p} - (\zeta + f)\,\nabla \cdot \mathbf{V} + \mathbf{k} \cdot \left(\frac{\partial \mathbf{V}}{\partial p} \times \nabla \omega \right) \tag{4.17}$$

Comparing (4.13) and (4.17), we see that in the isobaric system there is no vorticity generation by pressure-density solenoids. This difference arises because in the isobaric system, horizontal partial derivatives are computed with p held constant so that the vertical component of vorticity is $\zeta = (\partial v/\partial x - \partial u/\partial y)_p$, whereas in height coordinates it is $\zeta = (\partial v/\partial x - \partial u/\partial y)_z$. In practice the difference is generally unimportant because, as shown in the next section, the solenoidal term is usually sufficiently small so that it can be neglected for synoptic-scale motions.

4.3.3 Scale Analysis of the Vorticity Equation

In Section 2.4 the equations of motion were simplified for synoptic-scale motions by evaluating the order of magnitude of various terms. The same technique can be applied to the vorticity equation. Characteristic scales for the field variables based on typical observed magnitudes for synoptic-scale motions are chosen as follows:

$U \sim 10$ m s^{-1}	horizontal scale
$W \sim 1$ cm s^{-1}	vertical scale
$L \sim 10^6$ m	length scale
$H \sim 10^4$ m	depth scale
$\delta p \sim 10$ hPa	horizontal pressure scale
$\rho \sim 1$ kg m^{-3}	mean density
$\delta\rho/\rho \sim 10^{-2}$	fractional density fluctuation
$L/U \sim 10^5$ s	time scale
$f_0 \sim 10^{-4}$ s^{-1}	Coriolis parameter
$\beta \sim 10^{-11}$ m^{-1} s^{-1}	"beta" parameter

Again we have chosen an advective time scale because the vorticity pattern, like the pressure pattern, tends to move at a speed comparable to the horizontal wind speed. Using these scales to evaluate the magnitude of the terms in (4.12), we first note that

$$\zeta = \frac{\partial v}{\partial x} - \frac{\partial u}{\partial y} \lesssim \frac{U}{L} \sim 10^{-5}\text{s}^{-1}$$

where the inequality in this expression means less than or equal to in order of magnitude. Thus,

$$\zeta / f_0 \lesssim U / (f_0 L) \equiv \text{Ro} \sim 10^{-1}$$

For midlatitude synoptic-scale systems, the relative vorticity is often small (order Rossby number) compared to the planetary vorticity. For such systems, ζ may be neglected compared to f in the divergence term in the vorticity equation

$$(\zeta + f)\left(\frac{\partial u}{\partial x} + \frac{\partial v}{\partial y}\right) \approx f\left(\frac{\partial u}{\partial x} + \frac{\partial v}{\partial y}\right)$$

This approximation does not apply near the center of intense cyclonic storms. In such systems $|\zeta / f| \sim 1$, and the relative vorticity should be retained.

The magnitudes of the various terms in (4.12) can now be estimated as

$$\begin{aligned}
\frac{\partial \zeta}{\partial t}, u\frac{\partial \zeta}{\partial x}, v\frac{\partial \zeta}{\partial y} &\sim \frac{U^2}{L^2} \sim 10^{-10}\ \text{s}^{-2} \\
w\frac{\partial \zeta}{\partial z} &\sim \frac{WU}{HL} \sim 10^{-11}\ \text{s}^{-2} \\
v\frac{df}{dy} &\sim U\beta \sim 10^{-10}\ \text{s}^{-2} \\
f\left(\frac{\partial u}{\partial x} + \frac{\partial v}{\partial y}\right) &\lesssim \frac{f_0 U}{L} \sim 10^{-9}\ \text{s}^{-2} \\
\left(\frac{\partial w}{\partial x}\frac{\partial v}{\partial z} - \frac{\partial w}{\partial y}\frac{\partial u}{\partial z}\right) &\lesssim \frac{WU}{HL} \sim 10^{-11}\ \text{s}^{-2} \\
\frac{1}{\rho^2}\left(\frac{\partial \rho}{\partial x}\frac{\partial p}{\partial y} - \frac{\partial \rho}{\partial y}\frac{\partial p}{\partial x}\right) &\lesssim \frac{\delta\rho\delta p}{\rho^2 L^2} \sim 10^{-11}\ \text{s}^{-2}
\end{aligned}$$

The inequality is used in the last three terms because in each case it is possible that the two parts of the expression might partially cancel so that the actual magnitude would be less than indicated. In fact, this must be the case for the divergence term (the fourth in the list) because if $\partial u/\partial x$ and $\partial v/\partial y$ were not nearly equal and opposite, the divergence term would be an order of magnitude greater than any other term and the equation could not be satisfied. Therefore, scale analysis of the vorticity equation indicates that synoptic-scale motions must be quasi-nondivergent. The divergence term will be small enough to be balanced by the vorticity advection terms only if

$$\left|\left(\frac{\partial u}{\partial x}+\frac{\partial v}{\partial y}\right)\right| \lesssim 10^{-6}\ \mathrm{s}^{-1}$$

so that the horizontal divergence must be small compared to the vorticity in synoptic-scale systems. From the aforementioned scalings and the definition of the Rossby number, we see that

$$\left|\left(\frac{\partial u}{\partial x}+\frac{\partial v}{\partial y}\right)\Big/ f_0\right| \lesssim \mathrm{Ro}^2$$

and

$$\left|\left(\frac{\partial u}{\partial x}+\frac{\partial v}{\partial y}\right)\Big/ \zeta\right| \lesssim \mathrm{Ro}$$

Thus, the ratio of the horizontal divergence to the relative vorticity is the same magnitude as the ratio of relative vorticity to planetary vorticity.

Retaining only the terms of order $10^{-10}\ \mathrm{s}^{-2}$ in the vorticity equation yields the approximate form valid for synoptic-scale motions,

$$\frac{D_h(\zeta+f)}{Dt} = -f\left(\frac{\partial u}{\partial x}+\frac{\partial v}{\partial y}\right) \tag{4.18}$$

where

$$\frac{D_h}{Dt} \equiv \frac{\partial}{\partial t}+u\frac{\partial}{\partial x}+v\frac{\partial}{\partial y}$$

As mentioned earlier, (4.18) is not accurate in intense cyclonic storms. For these the relative vorticity should be retained in the divergence term:

$$\frac{D_h(\zeta+f)}{Dt} = -(\zeta+f)\left(\frac{\partial u}{\partial x}+\frac{\partial v}{\partial y}\right) \tag{4.19}$$

Equation (4.18) states that the change of absolute vorticity following the horizontal motion on the synoptic scale is given approximately by the concentration or dilution of planetary vorticity caused by the convergence or divergence of the horizontal flow, respectively. In (4.19), however, it is the concentration or dilution of absolute vorticity that leads to changes in absolute vorticity following the motion.

The form of the vorticity equation given in (4.19) also indicates why cyclonic disturbances can be much more intense than anticyclones. For a fixed amplitude of convergence, relative vorticity will increase, and the factor $(\zeta+f)$ becomes larger, which leads to even higher rates of increase in the relative vorticity. For a fixed rate of divergence, however, relative vorticity will decrease, but when $\zeta \to -f$, the divergence term on the right approaches zero and the relative vorticity cannot become more negative no matter how strong the divergence. (This difference in the potential intensity of cyclones and anticyclones was discussed in Section 3.2.5 in connection with the gradient wind approximation.)

The approximate forms given in (4.18) and (4.19) do not remain valid, however, in the vicinity of atmospheric fronts. The horizontal scale of variation in frontal zones is only $\sim$100 km, and the vertical velocity scale is $\sim$10 cm s^{-1}. For these scales, vertical advection, tilting, and solenoidal terms all may become as large as the divergence term.

4.4 POTENTIAL VORTICITY

We return now to circulation to show that Kelvin's theorem applies to baroclinic dynamics for certain integration contours, which has very deep implications for dynamic meteorology. Rather than arbitrary closed contours, we now restrict the possibilities to those that fall on isentropic surfaces, for which potential temperature is constant. We prove that for these contours, the solenoidal term is exactly zero.

With the aid of the ideal gas law (1.25), the definition of potential temperature (2.44) can be expressed as a relationship between pressure and density for a surface of constant θ:

$$\rho = p^{c_v/c_p}(R\theta)^{-1}(p_s)^{R/c_p}$$

Hence, on an isentropic surface, density is a function of pressure alone, and the solenoidal term in the circulation theorem (4.3) vanishes;

$$\oint \frac{dp}{\rho} \propto \oint dp^{(1-c_v/c_p)} = 0$$

For adiabatic and frictionless flow, then, the circulation computed for a closed chain of fluid parcels on a constant θ surface reduces to the same form as in a barotropic fluid; that is, it *satisfies Kelvin's circulation theorem* even though the fluid is baroclinic!

From Stokes's theorem, we may replace the circulation in favor of the component of vorticity normal to the surface

$$C_a = \oint \mathbf{U}_a \cdot d\mathbf{l} = \iint_A \omega_a \cdot \mathbf{n}\, dA \tag{4.20}$$

where $\mathbf{n}$ is a unit vector normal to the surface. Now we replace $\mathbf{n}$ and dA in favor of conserved quantities. Consider an infinitesimal cylinder (Figure 4.8) that is bounded above and below by constant potential temperature surfaces; for adiabatic flow, both the potential temperature and the mass of air in this cylinder, dm, are conserved. A leading-order Taylor approximation across the cylinder gives $d\theta \approx |\nabla\theta| dh$, where dh is the "height" of the cylinder. The mass

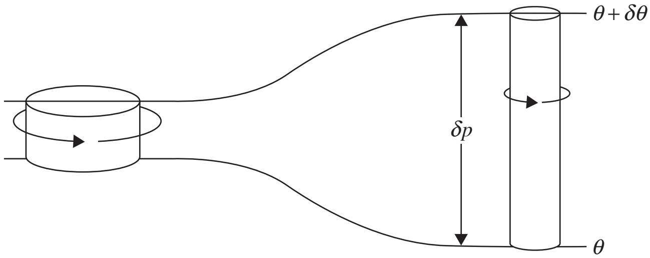

FIGURE 4.8 A cylindrical column of air moving adiabatically, conserving potential vorticity.

of air in the cylinder is given by $dm = \rho dAdh$ so that

$$dA = \frac{dm}{\rho}\frac{|\nabla\theta|}{d\theta} \tag{4.21}$$

Taking the infinitesimal cylinder to be sufficiently small so that the vorticity normal to the surface is nearly constant,

$$\frac{DC_a}{Dt} \approx \frac{D}{Dt}\left[\boldsymbol{\omega}_a \cdot \mathbf{n}\, dA\right] = 0 \tag{4.22}$$

where

$$\mathbf{n} = \frac{\nabla\theta}{|\nabla\theta|} \tag{4.23}$$

Using (4.21) and (4.23) in (4.22), and noting that both dm and $d\theta$ are conserved following the motion, gives

$$\frac{D}{Dt}\left[\frac{\boldsymbol{\omega}_a \cdot \nabla\theta}{\rho}\right] = 0 \tag{4.24}$$

This celebrated equation, the **Ertel potential vorticity theorem**, is one of the most important theoretical results in dynamic meteorology. It says that the potential vorticity, or PV,

$$\Pi = \frac{\boldsymbol{\omega}_a \cdot \nabla\theta}{\rho} \tag{4.25}$$

is conserved following the motion.

What makes this result so profound is that it links all of the basic physical conservation laws into a single expression. Although it may appear, as one studies a fluid, that the momentum field fluctuates independently of the thermodynamic fields, the potential vorticity places a powerful constraint on those fluctuations: They must evolve in a way that preserves the PV following the motion. Take, for example, the situation where the absolute vorticity vector has no horizontal components so that the PV is given by

$$\frac{1}{\rho}\left(\frac{\partial v}{\partial x} - \frac{\partial u}{\partial y} + f\right)\frac{\partial \theta}{\partial z} \tag{4.26}$$

In this case we see that the PV is the product of the absolute vorticity and the static stability so that if one increases, the other must decrease. This is illustrated in Figure 4.8: As the air parcel moves to the right, the static stability decreases, and as a result the vorticity must increase to conserve PV; the connections to angular momentum conservation and to vortex stretching are particularly clear.

The vertical contribution to the PV in (4.25) scales like $\frac{U\theta^*}{\rho HL} + \frac{f\theta^*}{H}$, where θ^* and ρ^* are typical potential temperature and density scale values; the second term represents the contribution from planetary rotation. The horizontal contribution—that is, from expanding (4.25)—scales like $\frac{U\theta^*}{\rho^* HL}$ (neglecting the small contribution from w), so that the ratio of vertical to horizontal contributions is

$$1 + \mathrm{Ro}^{-1} \tag{4.27}$$

On synoptic and larger scales, where the Rossby number is small (roughly 0.1), this analysis shows that the dominant contribution to the PV comes from the vertical direction. This serves to *explain why we focus on the vertical component of vorticity in dynamic meteorology*: Although the vorticity vector lies primarily in the horizontal direction, the gradient of potential temperature is mainly in the vertical and this promotes the importance of vertical vorticity. A leading-order approximation to the PV is

$$\Pi \approx \frac{f}{\rho}\frac{\partial \theta}{\partial z} \tag{4.28}$$

Picking typical values for the troposphere, we get an estimate of characteristic PV values of

$$\begin{aligned}\Pi_{trop} &\cong \left(\frac{10^{-4}\mathrm{s}^{-1}}{1\mathrm{kg\ m}^{-3}}\right)\left(5\ \mathrm{K\ km}^{-1}\right) \\ &= 0.5 \times 10^{-6}\ \mathrm{K\ m^2\ s^{-1}\ kg^{-1}} \equiv 0.5\,\mathrm{PVU}\end{aligned} \tag{4.29}$$

The definition "PVU" is a commonly adopted scaling of "PV Units" (1 PVU = 10^{-6} K m^2 s^{-1} kg^{-1}). In the lower stratosphere, where $\frac{\partial \theta}{\partial z}$ is an order of magnitude larger, characteristic values of PV are larger as well.

Because there is an abrupt jump in PV values at the troposphere PV provides a useful dynamical definition for that interface. In fact, for adiabatic and frictionless conditions, when both PV and potential temperature are conserved, maps of potential temperature on the "dynamical" tropopause (defined as a PV surface) provide a particularly useful summary of extratropical weather systems,

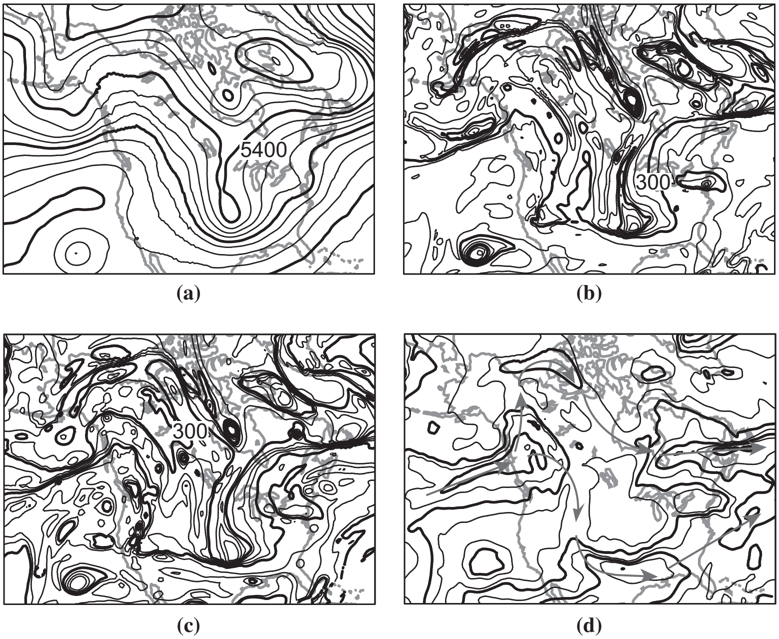

FIGURE 4.9 Comparison of 500-hPa geopotential height (a) and tropopause maps of pressure (b) potential temperature (c) and wind speed (d) on January 12, 2012. Geopotential height is shown every 60 m, potential temperature every 5 K, pressure every 50 hPa, and wind speed every 10 m s^{-1}. Every fourth contour is shown *bold* except every second contour for wind speed. *Gray arrows* in (d) illustrate the path of the main branches of jet streams.

because the potential temperature contours are simply advected by the wind on the tropopause. Moreover, compared to the alternative of PV contours on potential temperature surfaces, a single map suffices to describe the state of the tropopause.

An example comparing the structure of the dynamical tropopause with a conventional map of 500-hPa geopotential height is shown in Figure 4.9. Familiar features on the 500 hPa chart include a long-wave pattern with a ridge over western North America and a trough over the center of the continent, and short-wave troughs near New York and approaching the Pacific coastline near the Alaska panhandle. In addition to the wave-like features, cyclonic vortices are located southwest of California, over Hudson Bay, and near Baffin Island.

Tropopause pressure (Figure 4.9b) reveals that troughs are regions where the tropopause is depressed to lower altitudes; in fact, the tropopause is below 500 hPa in several of the troughs and vortices. Therefore, troughs are associated with large values of stratospheric potential vorticity that have been locally lowered to elevations normally considered tropospheric. In ridges and subtropical latitudes, the tropopause is elevated, with pressure values of 200 to 250 hPa, and therefore the PV is anomalously low compared to the surroundings.

Tropopause potential temperature (Figure 4.9c) shows that most of the troughs apparent in the 500-hPa chart are in fact vortical near their core. We may infer this by the appearance of closed potential temperature contours, since, if potential temperature and potential vorticity are conserved, air is trapped within closed tropopause potential temperature contours. For this reason, these features are sometimes called material eddies, since the only means of moving the disturbance is to displace the material comprising it. This stands in contrasts to waves, which may propagate information without net transport of the medium. In addition to the disturbances, notice the long ribbons where the horizontal gradient of tropopause potential temperature is concentrated into fronts, separated by zones that are mixed and filled with small-scale noise. Along some of these fronts—for example, the base of the trough in the central United States—the pressure field reveals that the tropopause is essentially vertical.

Finally, since jet streams are located near the tropopause, this perspective is much more useful than isobaric surfaces, which require several maps to depict jet streams located at different elevations. We see that a midlatitude jet reaches the west coast of Canada before splitting into northern and southern branches; the southern branch also has a subtropical connection that is apparent near the southern edge of the domain (Figure 4.9d).

For completeness, we note that a form of the Ertel potential vorticity equation may be derived that includes a source of momentum, $\mathcal{F}$, such as frictional dissipation, and a source of entropy, $\mathcal{H}$, such as latent heating. The result is

$$\frac{D\Pi}{Dt} = \frac{\boldsymbol{\omega}_a}{\rho} \cdot \nabla \mathcal{H} + \frac{\nabla \theta}{\rho} \cdot \left(\nabla \times \frac{\mathcal{F}}{\rho} \right) \tag{4.30}$$

where Π is the Ertel PV defined by (4.25). The first right-side term is positive, where the vorticity vector points in the direction of a local maximum in the entropy source. This often occurs near extratropical cyclones, where clouds and precipitation are found in the lower and midtroposphere (Figure 4.10a).

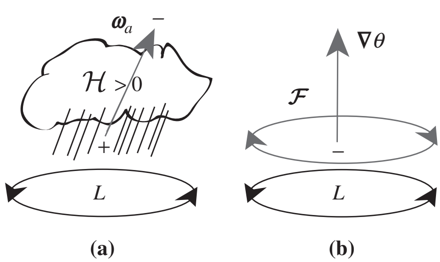

FIGURE 4.10 Cartoon illustrating the role of sources of (a) entropy and (b) momentum on changing the potential vorticity. (a) Depicts a precipitating cloud above a surface cyclone, where the vorticity vector, $\boldsymbol{\omega}$, points upward and to the right. Latent heating reaches a maximum in the cloud, which produces a positive (negative) PV tendency below (above) the cloud. (b) Depicts the role of surface friction (*gray arrow* opposite surface circulation). The curl of surface friction points in the opposite direction of the vorticity vector, producing a negative PV tendency.

In this case, near the surface the vertical component of vorticity points upward toward a maximum in latent heat release where condensation takes place; above the maximum in heating, potential vorticity decreases because the vorticity vector and gradient in heating point in opposite directions. The second right-side term is positive where the curl of the frictional force points in the same direction as the gradient in entropy. Again, appealing to extratropical cyclones, assuming that surface friction acts opposite to the motion, the curl of friction is a vector that points in the opposite direction from the gradient in entropy, which produces a negative tendency to the Ertel PV (Figure 4.10b).

4.5 SHALLOW WATER EQUATIONS

In a homogeneous incompressible fluid, potential vorticity conservation takes a somewhat simpler form. To see this, we first derive the shallow water equations, which provide a very useful simplification that we will use later to isolate essential aspects of atmospheric dynamics. Beyond constant density, the shallow approximation implies that the depth of the fluid is small compared to the the horizontal scale of the features of interest. As a result of this small aspect ratio, we may use the hydrostatic approximation

$$\frac{\partial p}{\partial z} = \rho_0 g \tag{4.31}$$

where ρ_0 is a constant density. Integrating the hydrostatic equation over the depth of the fluid, $h(x, y)$, gives

$$p(z) = \rho_0 g(h - z) + p(h) \tag{4.32}$$

where $p(h)$ is the pressure at the top of the layer of shallow water due to the layer above, which we take to be a constant. Using (4.32) to replace pressure in the momentum equation gives

$$\frac{D_h \mathbf{V}}{Dt} = -g\boldsymbol{\nabla}_h h \, - f\mathbf{k} \times \mathbf{V} \tag{4.33}$$

We assume that $\mathbf{V}$ is initially a function of (x, y) only, and since h is a function of (x, y), (4.33) indicates that $\mathbf{V}$ will remain two-dimensional for all time.

Mass conservation for a constant density fluid has the simple form

$$\boldsymbol{\nabla} \cdot (u, v, w) = 0 \tag{4.34}$$

Incompressibility also simplifies the first law of thermodynamics, since the fluid can no longer do work. Therefore, if no heat is added, the temperature is constant following the motion (see 2.41). Water pressure is a function of density and temperature, $p = f(T, \rho)$, but following the motion incompressibility implies

$dp = \frac{\partial f}{\partial T}dT + \frac{\partial f}{\partial \rho}d\rho = 0$, so that

$$\frac{Dp}{Dt} = 0 \tag{4.35}$$

Applying this fact to (4.32) yields

$$\frac{D_h h}{Dt} = w(h) \tag{4.36}$$

where $w = \frac{Dz}{Dt}$ is the vertical motion, which *is* a function of (x, y, z). Integrating (4.34) over depth h gives $w(h) = -h\nabla_h \cdot \mathbf{V}$, which may be used to eliminate w from (4.36)

$$\frac{D_h h}{Dt} = -h\nabla_h \cdot \mathbf{V} \tag{4.37}$$

The shallow water equations consist of (4.33) and (4.37), which describe the evolution of three unknowns (u, v, h). Following a derivation similar to that in Section 4.3.1, the shallow water vorticity equation may be derived from (4.33) and yields

$$\frac{D_h}{Dt}(\zeta + f) = -(\zeta + f)\left(\frac{\partial u}{\partial x} + \frac{\partial v}{\partial y}\right) \tag{4.38}$$

In the shallow water system, absolute vorticity increases following the motion through vortex stretching.

Shallow water potential vorticity conservation is obtained by replacing divergence on the right side of (4.38) using (4.37) to give

$$\frac{D_h}{Dt}\left[\frac{\zeta + f}{h}\right] = 0 \tag{4.39}$$

Thus, the shallow water potential vorticity,$(\zeta + f)/h$, is given by the absolute vorticity divided by the fluid depth. Following the motion, if the absolute vorticity increases, then the depth of the fluid must as well. One may think of the inverse depth as an analog of static stability in shallow water by noting that the layer top and bottom surfaces are isentropic surfaces. When the layer depth, h, becomes smaller, the isentropes are closer together.

Since the potential vorticity depends on x and y, only (4.39) provides a dramatic simplification to the Ertel PV, which is very useful for gaining insight into large-scale dynamics. For example, consider westerly flow impinging on an infinitely long topographic barrier as shown in Figure 4.11. We suppose that flow upstream of the mountain barrier is uniform with $\zeta = 0$. Each fluid column of depth h is confined between constant entropy surfaces θ_0 and $\theta_0 + \delta\theta$ and remains between those surfaces as it crosses the barrier. Air that previously crossed the barrier leaves the upper surface higher near the mountain both upstream and downstream, for reasons that will be explored in Chapter 5.

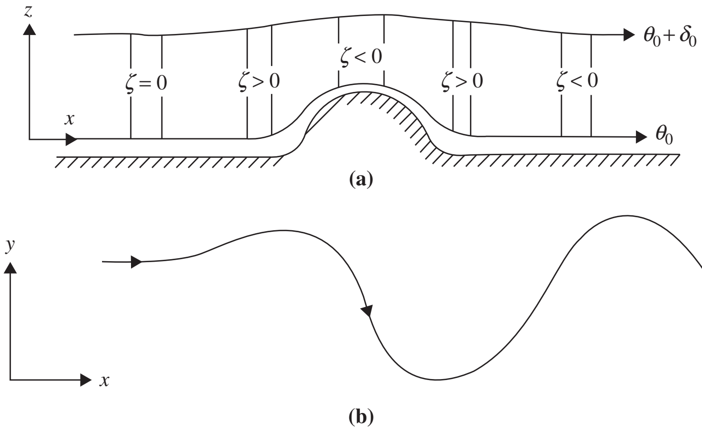

FIGURE 4.11 Schematic view of westerly flow over a topographic barrier: (a) the depth of a fluid column as a function of x and (b) the trajectory of a parcel in the $(x,\ y)$ plane.

As fluid columns approach the topographic barrier, they stretch vertically, which causes ζ to increase in order to conserve potential vorticity, $(\zeta+f)/h$. Positive cyclonic vorticity is associated with cyclonic curvature in the flow, which causes a poleward drift so that f also increases; this in turn reduces the change in ζ required for potential vorticity conservation. As the column begins to cross the barrier, its vertical extent decreases, and the relative vorticity must then become negative. Thus, the air column will acquire anticyclonic vorticity and move southward.

When the air column has passed over the barrier and returned to its original depth, it will be south of its original latitude so that f will be smaller and the relative vorticity must be positive. Thus, the trajectory must have cyclonic curvature and the column will be deflected poleward. When the parcel returns again to its original latitude, it will still have a poleward velocity component and will continue poleward gradually, acquiring anticyclonic curvature until its direction is again reversed. The parcel will then move downstream, conserving potential vorticity by following a wave-like trajectory in the horizontal plane. Therefore, steady westerly flow over a large-scale ridge will result in an anticyclonic flow over the mountain, a cyclonic flow pattern to the east of the barrier, followed by a wavetrain downstream.

The situation for easterly flow impinging on a mountain barrier is quite different (Figure 4.12). Upstream stretching leads to a cyclonic turning of the flow, which results in an equatorward component of motion. As the column moves westward and equatorward over the barrier, its depth contracts and its absolute vorticity must then decrease so that potential vorticity can be conserved. This reduction in absolute vorticity arises both from development of anticyclonic relative vorticity and from a decrease in f due to the equatorward motion. The anticyclonic relative vorticity gradually turns the column so that when it reaches

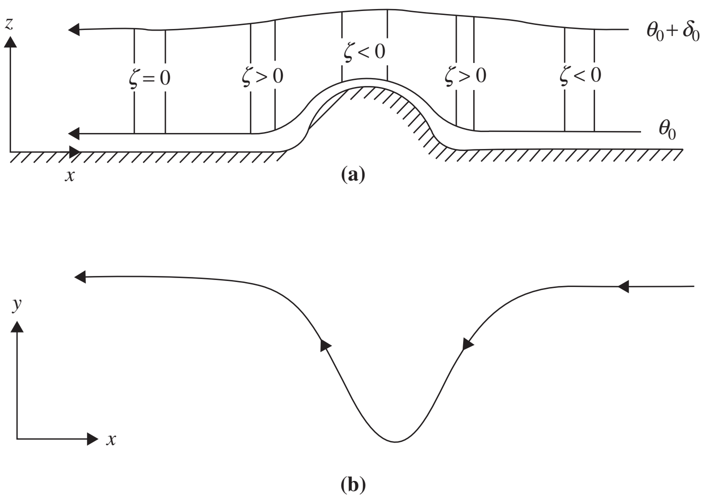

FIGURE 4.12 As in Figure 4.11, but for easterly flow.

the top of the barrier, it is headed westward. As it continues westward down the barrier, conserving potential vorticity, the process is simply reversed, with the result that some distance downstream from the mountain barrier, the air column is again moving westward at its original latitude.

Thus, the dependence of the Coriolis parameter on latitude creates a dramatic difference between westerly and easterly flow over large-scale topographic barriers. In the case of a westerly wind, the barrier generates a wave-like disturbance in the streamlines that extends far downstream. However, in the case of an easterly wind, the disturbance in the streamlines damps out away from the barrier.

4.5.1 Barotropic Potential Vorticity

Further simplification of potential vorticity is possible beyond the shallow water equations by making the barotropic assumption. Recall that a barotropic fluid is defined as one for which pressure depends only on density. For shallow water, (4.32) implies that in this case h and z are constant, so that $w = 0$ and the fluid is horizontally nondivergent

$$\frac{\partial u}{\partial x} + \frac{\partial v}{\partial y} = 0 \tag{4.40}$$

Potential vorticity conservation simplifies to

$$\frac{D_h}{Dt}(\zeta + f) = 0 \tag{4.41}$$

which states that absolute vorticity is conserved following the motion. Equation (4.41) is called the barotropic vorticity equation and has been widely used in theoretical studies of large-scale dynamical meteorology.

For nondivergent horizontal motion, the flow field can be represented by a *streamfunction* $\psi\,(x, y)$ defined so that the velocity components are given as $u = -\partial\psi/\partial y,\ v = +\partial\psi/\partial x$. The vorticity is then given by

$$\zeta = \partial v/\partial x - \partial u/\partial y = \partial^2\psi/\partial x^2 + \partial^2\psi/\partial y^2 \equiv \nabla_h^2\psi$$

Thus, the velocity field and the vorticity can both be represented in terms of the variation of the single scalar field $\psi\,(x, y)$, and (4.41) can be written as a prognostic equation for vorticity in the form

$$\frac{\partial}{\partial t}\nabla^2\psi = -\mathbf{V}_\psi \cdot \nabla\left(\nabla^2\psi + f\right) \tag{4.42}$$

where $\mathbf{V}_\psi \equiv \mathbf{k} \times \nabla\psi$ is a nondivergent horizontal wind. Equation (4.42) states that the local tendency of relative vorticity is given by the advection of absolute vorticity. This equation can be solved numerically to predict the evolution of the streamfunction and thus of the vorticity and wind fields. Because the flow in the midtroposphere is often nearly nondivergent on the synoptic scale, (4.42) provides a surprisingly good model for short-term forecasts of the synoptic-scale 500-hPa flow field.

Conservation of absolute vorticity following the motion provides a strong constraint on the flow, as can be shown by a simple example that again illustrates an asymmetry between westerly and easterly flow. Suppose that at a certain point (x_0, y_0) the flow is in the zonal direction and the relative vorticity vanishes so that $\eta(x_0, y_0) = f_0$. Then, if absolute vorticity is conserved, the motion at any point along a parcel trajectory that passes through (x_0, y_0) must satisfy $\zeta + f = f_0$. Because f increases toward the north, trajectories that curve northward in the downstream direction must have $\zeta = f_0 - f < 0$, whereas trajectories that curve southward must have $\zeta = f_0 - f > 0$. However, as indicated in Figure 4.13, if the flow is westerly, northward curvature downstream implies $\zeta > 0$, whereas southward curvature implies $\zeta < 0$. Thus, westerly zonal flow must remain purely zonal if absolute vorticity is to be conserved following the motion. The easterly flow case, also shown in Figure 4.13, is just the opposite. Northward and southward curvatures are associated with negative and positive

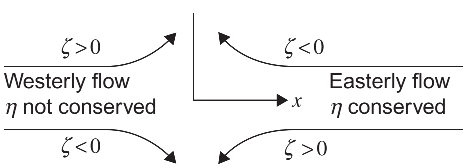

FIGURE 4.13 Absolute vorticity conservation for curved flow trajectories.

relative vorticities, respectively. Hence, an easterly current can curve either to the north or to the south and still conserve absolute vorticity.

4.6 ERTEL POTENTIAL VORTICITY IN ISENTROPIC COORDINATES

We consider here a more detailed treatment of the Ertel potential vorticity in isentropic coordinates, including nonconservative effects due to sources of momentum and entropy. We begin with a description of the basic conservation laws in isentropic coordinates.

4.6.1 Equations of Motion in Isentropic Coordinates

If the atmosphere is stably stratified so that potential temperature θ is a monotonically increasing function of height, θ may be used as an independent vertical coordinate. The vertical "velocity" in this coordinate system is just $\dot{\theta} \equiv D\theta/Dt$. Thus, adiabatic motions are two-dimensional when viewed in an isentropic coordinate frame. An infinitesimal control volume in isentropic coordinates with cross-sectional area δA and vertical extent $\delta\theta$ has a mass

$$\delta M = \rho\delta A\delta z = \delta A\left(-\frac{\delta p}{g}\right) = \frac{\delta A}{g}\left(-\frac{\partial p}{\partial\theta}\right)\delta\theta = \sigma\delta A\delta\theta \tag{4.43}$$

Here the "density" in $(x,\ y,\ \theta)$ space is defined as

$$\sigma \equiv -g^{-1}\partial p/\partial\theta \tag{4.44}$$

The horizontal momentum equation in isentropic coordinates may be obtained by transforming the isobaric form (4.15) to yield

$$\frac{\partial \mathbf{V}}{\partial t} + \nabla_\theta\left(\frac{\mathbf{V}\cdot\mathbf{V}}{2} + \Psi\right) + (\zeta_\theta + f)\,\mathbf{k}\times\mathbf{V} = -\dot{\theta}\frac{\partial \mathbf{V}}{\partial\theta} + \mathbf{F}_r \tag{4.45}$$

where ∇_θ is the gradient on an isentropic surface, $\zeta_\theta \equiv \mathbf{k}\cdot\nabla_\theta\times\mathbf{V}$ is the isentropic relative vorticity, and $\Psi \equiv c_pT + \Phi$ is the Montgomery streamfunction (see Problem 2.11 in Chapter 2). We have included a frictional term $\mathbf{F}_r$ on the right side, along with the diabatic vertical advection term. The continuity equation can be derived with the aid of (4.43) in a manner analogous to that used for the isobaric system in Section 3.1.2. The result is

$$\frac{\partial\sigma}{\partial t} + \nabla_\theta\cdot(\sigma\mathbf{V}) = -\frac{\partial}{\partial\theta}\left(\sigma\dot{\theta}\right) \tag{4.46}$$

The Ψ and σ fields are linked through the pressure field by the hydrostatic equation, which in the isentropic system takes the form

$$\frac{\partial\Psi}{\partial\theta} = \Pi(p) \equiv c_p\left(\frac{p}{p_s}\right)^{R/c_p} = c_p\frac{T}{\theta} \tag{4.47}$$

where Π is called the *Exner function*. Equations (4.44) through (4.47) form a closed set for prediction of $\mathbf{V}$, σ, Ψ, and p, provided that $\dot{\theta}$ and $\mathbf{F}_r$ are known.

4.6.2 The Potential Vorticity Equation

If we take $\mathbf{k}\cdot\nabla_\theta\times$(4.45) and rearrange the resulting terms, we obtain this isentropic vorticity equation:

$$\frac{\widetilde{D}}{Dt}(\zeta_\theta+f)+(\zeta_\theta+f)\,\nabla_\theta\cdot\mathbf{V}=\mathbf{k}\cdot\nabla_\theta\times\left(\mathbf{F}_r-\dot{\theta}\frac{\partial\mathbf{V}}{\partial\theta}\right) \tag{4.48}$$

where

$$\frac{\widetilde{D}}{Dt}=\frac{\partial}{\partial t}+\mathbf{V}\cdot\nabla_\theta$$

is the total derivative following the horizontal motion on an isentropic surface.

Noting that $\sigma^{-2}\partial\sigma/\partial t=-\partial\sigma^{-1}/\partial t$, we can rewrite (4.46) in the form

$$\frac{\widetilde{D}}{Dt}\left(\sigma^{-1}\right)-\left(\sigma^{-1}\right)\nabla_\theta\cdot\mathbf{V}=\sigma^{-2}\frac{\partial}{\partial\theta}\left(\sigma\dot{\theta}\right) \tag{4.49}$$

Multiplying each term in (4.48) by σ^{-1} and in (4.49) by $(\zeta_\theta+f)$ and adding, we obtain the desired conservation law:

$$\frac{\widetilde{D}\Pi}{Dt}=\frac{\partial\Pi}{\partial t}+\mathbf{V}\cdot\nabla_\theta\Pi=\frac{\Pi}{\sigma}\frac{\partial}{\partial\theta}\left(\sigma\dot{\theta}\right)+\sigma^{-1}\mathbf{k}\cdot\nabla_\theta\times\left(\mathbf{F}_r-\dot{\theta}\frac{\partial\mathbf{V}}{\partial\theta}\right) \tag{4.50}$$

where $\Pi\equiv(\zeta_\theta+f)/\sigma$ is the Ertel potential vorticity. If the diabatic and frictional terms on the right side of (4.50) can be evaluated, it is possible to determine the evolution of Π following the *horizontal* motion on an isentropic surface. When the diabatic and frictional terms are small, potential vorticity is approximately conserved following the motion on isentropic surfaces.

Weather disturbances that have sharp gradients in dynamical fields, such as jets and fronts, are associated with large anomalies in the Ertel potential vorticity. In the upper troposphere such anomalies tend to be advected rapidly under nearly adiabatic conditions. Thus, the potential vorticity anomaly patterns are conserved materially on isentropic surfaces. This material conservation property makes potential vorticity anomalies particularly useful in identifying and tracing the evolution of meteorological disturbances.

4.6.3 Integral Constraints on Isentropic Vorticity

The isentropic vorticity equation (4.48) can be written in the form

$$\frac{\partial\zeta_\theta}{\partial t}=-\nabla_\theta\cdot\left[\left(\zeta_\theta+f\right)\mathbf{V}\right]+\mathbf{k}\cdot\nabla_\theta\times\left(\mathbf{F}_r-\dot{\theta}\frac{\partial\mathbf{V}}{\partial\theta}\right) \tag{4.51}$$

Using the fact that any vector $\mathbf{A}$ satisfies the relationship

$$\mathbf{k} \cdot (\nabla_\theta \times \mathbf{A}) = \nabla_\theta \cdot (\mathbf{A} \times \mathbf{k})$$

we can rewrite (4.51) in the form

$$\frac{\partial \zeta_\theta}{\partial t} = -\nabla_\theta \cdot \left[(\zeta_\theta + f)\mathbf{V} - \left(\mathbf{F}_r - \dot{\theta} \frac{\partial \mathbf{V}}{\partial \theta} \right) \times \mathbf{k} \right] \tag{4.52}$$

Equation (4.52) expresses the remarkable fact that isentropic vorticity can only be changed by the divergence or convergence of the horizontal flux vector in brackets on the right side. The vorticity cannot be changed by vertical transfer across the isentropes. Furthermore, integration of (4.52) over the area of an isentropic surface and application of the divergence theorem (Appendix C.2) show that for an isentrope that does not intersect the surface of Earth, the global average of ζ_θ is constant. Furthermore, integration of ζ_θ over the sphere shows that the global average ζ_θ is exactly zero. Vorticity on such an isentrope is neither created nor destroyed; it is merely concentrated or diluted by horizontal fluxes along the isentropes.

SUGGESTED REFERENCES

Acheson, *Elementary Fluid Dynamics*, provides a good introduction to vorticity at a graduate level.

Hoskins et al. provide an advanced discussion of Ertel potential vorticity and its uses in diagnosis and prediction of synoptic-scale disturbances.

Pedlosky, *Geophysical Fluid Dynamics*, provides a thorough treatment of circulation, vorticity, and potential vorticity in Chapter 2.

Vallis, *Atmospheric and Oceanic Fluid Dynamics*, discusses vorticity and potential vorticity in Chapter 4.

Williams and Elder, *Fluid Physics for Oceanographers and Physicists*, provides an introduction to vorticity dynamics at an elementary level. This book also provides a good general introduction to fluid dynamics.

PROBLEMS

4.1. What is the circulation about a square of 1000 km on a side for an easterly (i.e., westward flowing) wind that decreases in magnitude toward the north at a rate of 10 m s^{-1} per 500 km? What is the mean relative vorticity in the square?

4.2. A cylindrical column of air at 30°N with radius 100 km expands to twice its original radius. If the air is initially at rest, what is the mean tangential velocity at the perimeter after expansion?

4.3. An air parcel at 30°N moves northward, conserving absolute vorticity. If its initial relative vorticity is 5×10^{-5} s^{-1}, what is its relative vorticity upon reaching 90°N?

4.4. An air column at 60°N with $\zeta = 0$ initially stretches from the surface to a fixed tropopause at 10 km height. If the air column moves until it is over a mountain barrier 2.5 km high at 45°N, what is its absolute vorticity and relative vorticity as it passes the mountain top, assuming that the flow satisfies the barotropic potential vorticity equation?

4.5. Find the average vorticity within a cylindrical annulus of inner radius 200 km and outer radius 400 km if the tangential velocity distribution is given by $V = A/r$, where $A = 10^6\ \mathrm{m^2\ s^{-1}}$ and r is in meters. What is the average vorticity within the inner circle of radius 200 km?

4.6. Show that the anomalous gradient wind cases discussed in Section 3.2.5 have negative absolute circulation in the Northern Hemisphere and thus have negative average absolute vorticity.

4.7. Compute the rate of change of circulation about a square in the (x, y) plane with corners at $(0, 0)$, $(0, L)$, (L, L), and $(L, 0)$ if temperature increases eastward at a rate of 1°C per 200 km and presure increases northward at a rate of 1 hPa per 200 km. Let $L = 1000$ km and the pressure at the point $(0, 0)$ be 1000 hPa.

4.8. Verify the identity (4.14) by expanding the vectors in Cartesian components.

4.9. Derive a formula for the dependence of depth on radius for an incompressible fluid in solid-body rotation in a cylindrical tank with a flat bottom and free surface at the upper boundary. Let H be the depth at the center of the tank, Ω be the angular velocity of rotation of the tank, and a be the radius of the tank.

4.10. By how much does the relative vorticity change for a column of fluid in a rotating cylinder if the column is moved from the center of the tank to a distance 50 cm from the center? The tank is rotating at the rate of 20 revolutions per minute, the depth of the fluid at the center is 10 cm, and the fluid is initially in solid-body rotation.

4.11. A cyclonic vortex is in cyclostrophic balance with a tangential velocity profile given by the expression $V = V_0(r/r_0)^n$, where V_0 is the tangential velocity component at the distance r_0 from the vortex center. Compute the circulation about a streamline at radius r, the vorticity at radius r, and the pressure at radius r. (Let p_0 be the pressure at r_0 and assume that density is a constant.)

4.12. A westerly zonal flow at 45° is forced to rise adiabatically over a north–south-oriented mountain barrier. Before striking the mountain, the westerly wind increases linearly toward the south at a rate of 10 m s^{-1} per 1000 km. The crest of the mountain range is at 800 hPa and the tropopause, located at 300 hPa, remains undisturbed. What is the initial relative vorticity of the air? What is its relative vorticity when it reaches the crest if it is deflected 5° latitude toward the south during the forced ascent? If the current assumes a uniform speed of 20 m s^{-1} during its ascent to the crest, what is the radius of curvature of the streamlines at the crest?

4.13. A cylindrical vessel of radius a and constant depth H rotating at an angular velocity Ω about its vertical axis of symmetry is filled with a homogeneous, incompressible fluid that is initially at rest with respect to the vessel. A volume of fluid V is then withdrawn through a point sink at the center of the cylinder, thus creating a vortex. Neglecting friction, derive an expression for the resulting relative azimuthal velocity as a function of radius (i.e., the velocity in a coordinate system rotating with the tank). Assume that the motion is independent of depth and that $V \ll \pi a^2 H$. Also compute the relative vorticity and the relative circulation.

4.14. **(a)** How far must a zonal ring of air initially at rest with respect to Earth's surface at 60° latitude and 100-km height be displaced latitudinally to acquire an easterly (east to west) component of 10 m s^{-1} with respect to Earth's surface?
(b) To what height must it be displaced vertically in order to acquire the same velocity? Assume a frictionless atmosphere.

4.15. The horizontal motion within a cylindrical annulus with permeable walls of inner radius 10 cm, outer radius 20 cm, and 10-cm depth is independent of height and azimuth and is represented by the expressions $u = 7 - 0.2r$, $v = 40 + 2r$, where u and v are the radial and tangential velocity components in cm s^{-1}, positive outward and counterclockwise, respectively, and r is distance from the center of the annulus in centimeters. Assuming an incompressible fluid, find
(a) Circulation about the annular ring
(b) Average vorticity within the annular ring
(c) Average divergence within the annular ring
(d) Average vertical velocity at the top of the annulus if it is zero at the base

4.16. Prove that, as stated in Eq. (4.52), the globally averaged isentropic vorticity on an isentropic surface that does not intersect the ground must be zero. Show that the same result holds for the isobaric vorticity on an isobaric surface.

MATLAB Exercises

M4.1. Equation 4.41 showed that for nondivergent horizontal motion, the flow field can be represented by a *streamfunction* $\psi(x, y)$, and the vorticity is then given by $\zeta = \partial^2\psi/\partial x^2 + \partial^2\psi/\partial y^2 \equiv \nabla^2\psi$. Thus, if the vorticity is represented by a single sinusoidal wave distribution in both x and y, the streamfunction has the same spatial distribution as the vorticity and the opposite sign, as can be verified easily from the fact that the second derivative of a sine is proportional to minus the same sine function. An example is shown in the MATLAB script **vorticity_1.m**. However, when the vorticity pattern is localized in space, the space scales of the streamfunction and vorticity are much different. This latter situation is illustrated in the MATLAB script **vorticity_demo.m**, which shows the streamfunction corresponding to a point source of vorticity at $(\mathrm{x, y}) = (0, 0)$. For this problem you must modify the code in **vorticity_1.m** by specifying $\zeta(x, y) = \exp\left[-b\left(x^2 + y^2\right)\right]$ where b is a constant. Run the model for several values of b from $b = 1 \times 10^{-4}$ km^{-2} to 4×10^{-7} km^{-2}. Show in a table or line plot the dependence of the ratio of the horizontal scales on which vorticity and the streamfunction decay to one-half of their maximum values as a function of the parameter b. Note that for geostrophic motions (with constant Coriolis parameter), the streamfunction defined here is proportional to geopotential height. What can you conclude from this exercise about the information content of a 500-hPa height map versus that of a map of the 500-hPa vorticity field?

M4.2. The MATLAB scripts **geowinds_1.m** (to be used when the mapping toolbox is available) and **geowinds_2.m** (to be used if no mapping toolbox is available) contain contour plots showing the observed 500-hPa height and horizontal wind fields for November 10, 1998, in the North American sector. Also shown is a color plot of the magnitude of the 500-hPa wind with height contours superposed. Using centered difference formulas (see Section 13.2.1), compute the geostrophic wind components, the magnitude of the geostrophic wind, the relative vorticity, the vorticity of the geostrophic wind, and the vorticity minus the vorticity of the geostrophic wind. Following the models of Figures 4.1 and 4.2, superpose these fields on the maps of the 500-hPa height field. Explain the distribution and the sign of regions with large differences between vorticity and geostrophic vorticity in terms of the force balances that were studied in Chapter 3.

Chapter 5

Atmospheric Oscillations

Linear Perturbation Theory

If one is interested in producing an accurate forecast of the circulation at some future time, a detailed numerical model based on the primitive equations and including processes such as latent heating, radiative transfer, and boundary layer drag should produce the best results. However, the inherent complexity of such a model generally precludes any simple interpretation of the physical processes that produce the predicted circulation. If we wish to gain physical insight into the fundamental nature of atmospheric motions, it is helpful to employ simplified models in which certain processes are omitted and compare the results with those of more complete models. It is difficult to gain an appreciation for the processes that produce the wave-like character observed in many meteorological disturbances through the study of numerical integrations alone. Therefore, analytical treatment of idealized representations of the atmosphere are valuable and are the main topic of this chapter.

First, we discuss the *perturbation method*, a simple technique that is useful for qualitative analysis of atmospheric waves. We then use this method to examine several types of waves in the atmosphere. In Chapters 6 and 7, the perturbation method is used to develop the quasi-geostrophic equations and to study the development of *synoptic-wave* disturbances, respectively.

5.1 THE PERTURBATION METHOD

In the perturbation method, all field variables are divided into two parts: a *basic state* portion, which is usually assumed to be independent of time and longitude, and a perturbation portion, which is the local deviation of the field from the basic state. Thus, for example, if $\overline{u}$ designates a time and longitude-averaged zonal velocity, and u' is the deviation from that average, then the complete zonal velocity field is $u(x, t) = \overline{u} + u'(x, t)$. In that case, for example, the inertial acceleration $u\partial u/\partial x$ can be written

$$u\frac{\partial u}{\partial x} = \left(\overline{u} + u'\right)\frac{\partial}{\partial x}\left(\overline{u} + u'\right) = \overline{u}\frac{\partial u'}{\partial x} + u'\frac{\partial u'}{\partial x}$$

An Introduction to Dynamic Meteorology. DOI: 10.1016/B978-0-12-384866-6.00005-2

The basic assumptions of perturbation theory are that the basic state variables must themselves satisfy the governing equations when the perturbations are set to zero, and the perturbation fields must be small enough so that all terms in the governing equations that involve products of the perturbations can be neglected. Terms that depend linearly on perturbation fields drop by half when the perturbation amplitude is cut in half, but terms that are quadratic in the perturbation field become smaller by a factor of four. Therefore, the nonlinear terms become smaller faster than the linear terms and can be neglected in the small-amplitude limit. If $|u'/\overline{u}| \ll 1$, then

$$\left|\overline{u}\partial u'/\partial x\right| \gg \left|u'\partial u'/\partial x\right|$$

If terms that are products of the perturbation variables are neglected, the nonlinear governing equations are reduced to linear differential equations in the perturbation variables in which the basic state variables are specified coefficients. These equations can then be solved by standard methods to determine the character and structure of the perturbations in terms of the known basic state. For equations with constant coefficients, the solutions are sinusoidal or exponential in character. Solution of perturbation equations then determines such characteristics as the propagation speed, vertical structure, and conditions for growth or decay of the waves. The perturbation technique is especially useful in studying the stability of a given basic state flow with respect to small superposed perturbations. This application is the subject of Chapter 7.

5.2 PROPERTIES OF WAVES

Wave motions are oscillations in field variables (e.g., velocity and pressure) that propagate in space and time. In this chapter we are concerned with linear sinusoidal wave motions. Many of the mechanical properties of such waves are also features of a familiar system, the linear harmonic oscillator. An important property of the harmonic oscillator is that the period, or time required to execute a single oscillation, is independent of the amplitude of the oscillation. For most natural vibratory systems, this condition holds only for oscillations of sufficiently small amplitude. The classical example of such a system is the simple pendulum (Figure 5.1) consisting of a mass M suspended by a massless string of length l, free to perform small oscillations about the equilibrium position $\theta = 0$. The component of the gravity force parallel to the direction of motion is $-Mg\sin\theta$. Thus, the equation of motion for the mass M is

$$Ml\frac{d^2\theta}{dt^2} = -Mg\sin\theta$$

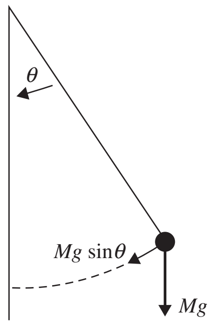

FIGURE 5.1 A simple pendulum.

Now for small displacements, $\sin\theta \approx \theta$ so that the governing equation becomes

$$\frac{d^2\theta}{dt^2} + \nu^2\theta = 0 \tag{5.1}$$

where $\nu^2 \equiv g/l$. The harmonic oscillator equation (5.1) has the general solution

$$\theta = \theta_1 \cos \nu t + \theta_2 \sin \nu t = \theta_0 \cos(\nu t - \alpha)$$

where θ_1, θ_2, θ_0, and α are constants determined by the initial conditions (see Problem 5.1) and ν is the frequency of oscillation. The complete solution can thus be expressed in terms of an amplitude θ_0 and a phase $\phi(t) = \nu t - \alpha$. The phase varies linearly in time by a factor of 2π radians per wave period.

Propagating waves can also be characterized by their amplitudes and phases. In a propagating wave, however, phase depends not only on time but on one or more space variables as well. Thus, for a one-dimensional wave propagating in the x direction, $\phi(x, t) = kx - \nu t - \alpha$. Here the *wave number*, k, is defined as 2π divided by the wavelength. For propagating waves the phase is constant for an observer moving at the *phase speed* $c \equiv \nu/k$. This may be verified by observing that if phase is to remain constant following the motion,

$$\frac{D\phi}{Dt} = \frac{D}{Dt}(kx - \nu t - \alpha) = k\frac{Dx}{Dt} - \nu = 0$$

Thus, $Dx/Dt = c = \nu/k$ for phase to be constant. For $\nu > 0$ and $k > 0$ we have $c > 0$. In that case, if $\alpha = 0$, $\phi = k(x - ct)$, so x must increase with increasing t for ϕ to remain constant. Phase then propagates in the positive direction, as illustrated for a sinusoidal wave in Figure 5.2.

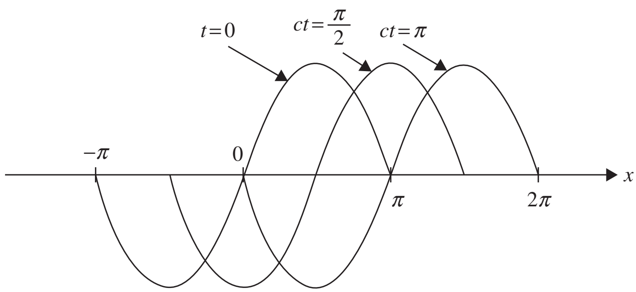

FIGURE 5.2 A sinusoidal wave traveling in the positive x direction at speed c. (Wave number is assumed to be unity.)

5.2.1 Fourier Series

The representation of a perturbation as a simple sinusoidal wave might seem an oversimplification, since disturbances in the atmosphere are never purely sinusoidal. It can be shown, however, that any reasonably well-behaved function of longitude can be represented in terms of a zonal mean plus a *Fourier* series of sinusoidal components:

$$f(x) = \sum_{s=1}^{\infty} (A_s \sin k_s x + B_s \cos k_s x) \tag{5.2}$$

where $k_s = 2\pi s/L$ is the *zonal* wave number (units m^{-1}), L is the distance around a latitude circle, and s, the *planetary* wave number, is an integer designating the number of waves around a latitude circle. The coefficients A_s are calculated by multiplying both sides of (5.2) by $\sin(2\pi nx/L)$, where n is an integer, and integrating around a latitude circle. Applying the orthogonality relationships

$$\int_0^L \sin\frac{2\pi sx}{L} \sin\frac{2\pi nx}{L} dx = \begin{Bmatrix} 0, & s \neq n \\ L/2, & s = n \end{Bmatrix}$$

we obtain

$$A_s = \frac{2}{L}\int_0^L f(x) \sin\frac{2\pi sx}{L} dx$$

In a similar fashion, multiplying both sides in (5.2) by $\cos(2\pi nx/L)$ and integrating gives

$$B_s = \frac{2}{L}\int_0^L f(x) \cos\frac{2\pi sx}{L} dx$$

A_s and B_s are called the *Fourier coefficients*, and

$$f_s(x) = A_s \sin k_s x + B_s \cos k_s x \tag{5.3}$$

is called the sth *Fourier component* or sth harmonic of the function $f(x)$. If the Fourier coefficients are computed for, say, the longitudinal dependence of the (observed) geopotential perturbation, the largest-amplitude Fourier components will be those for which s is close to the observed number of troughs or ridges around a latitude circle. When only qualitative information is desired, it is usually sufficient to limit the analysis to a single typical Fourier component and assume that the behavior of the actual field will be similar to that of the component. The expression for a Fourier component may be written more compactly using complex exponential notation. According to the Euler formula,

$$\exp(i\phi) = \cos\phi + i\sin\phi$$

where $i \equiv (-1)^{1/2}$ is the imaginary unit. Thus, we can write

$$\begin{aligned} f_s(x) &= \mathrm{Re}[C_s \exp(ik_s x)] \\ &= \mathrm{Re}[C_s \cos k_s x + iC_s \sin k_s x] \end{aligned} \tag{5.4}$$

where Re[ ] denotes "real part of" and C_s is a complex coefficient. Comparing (5.3) and (5.4), we see that the two representations of $f_s(x)$ are identical, provided that

$$B_s = \mathrm{Re}[C_s] \quad \text{and} \quad A_s = -\mathrm{Im}[C_s]$$

where Im[ ] stands for "imaginary part of." This exponential notation will generally be used for applications of the perturbation theory that follows and also in Chapter 7.

5.2.2 Dispersion and Group Velocity

A fundamental property of linear oscillators is that the frequency of oscillation ν depends only on the physical characteristics of the oscillator, not on the motion itself. For propagating waves, however, ν generally depends on the wave number of the perturbation as well as the physical properties of the medium. Thus, because $c = \nu/k$, the phase speed also depends on the wave number except in the special case where $\nu \propto k$. For waves in which the phase speed varies with k, the various sinusoidal components of a disturbance originating at a given location are at a later time found in different places—that is, they are dispersed. Such waves are referred to as *dispersive*, and the formula that relates ν and k is called a *dispersion relationship*. Some types of waves, such as acoustic waves, have phase speeds that are independent of the wave number. In such *nondispersive* waves a spatially localized disturbance consisting of a number of Fourier wave components (a *wave group*) will preserve its shape as it propagates in space at the phase speed of the wave.

For dispersive waves, however, the shape of a wave group will not remain constant as the group propagates. Because the individual Fourier components of a wave group may either reinforce or cancel each other, depending on the relative phases of the components, the energy of the group will be concentrated in limited regions as illustrated in Figure 5.3. Furthermore, the group generally broadens in the course of time—that is, the energy is *dispersed*.

When waves are dispersive, the speed of the wave group is generally different from the average phase speed of the individual Fourier components. Hence, as shown in Figure 5.4, individual wave components may move either more rapidly or more slowly than the wave group as the group propagates along. Surface waves in deep water (such as a ship wake) are characterized by dispersion in which individual wave crests move twice as fast as the wave group. In synoptic-scale atmospheric disturbances, however, the group velocity exceeds the phase velocity. The resulting downstream development of new disturbances will be discussed later.

An expression for *group velocity*, which is the velocity at which the observable disturbance (and thus the energy) propagates, can be derived as follows: We consider the superposition of two horizontally propagating waves

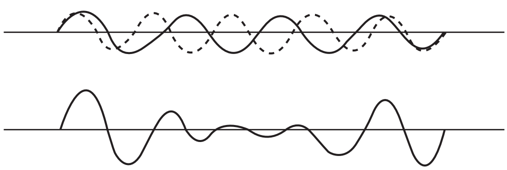

FIGURE 5.3 Wave groups formed from two sinusoidal components of slightly different wavelengths. For nondispersive waves, the pattern in the lower part of the diagram propagates without change of shape. For dispersive waves, the shape of the pattern changes in time.

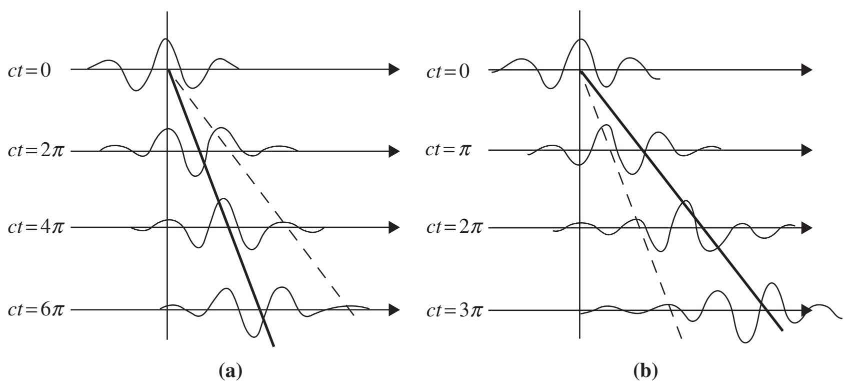

FIGURE 5.4 Schematic showing propagation of wave groups: (a) group velocity less than phase speed and (b) group velocity greater than phase speed. *Heavy lines* show group velocity, and *light lines* show phase speed.

of equal amplitude but slightly different wavelengths, with wave numbers and frequencies differing by $2\delta k$ and $2\delta \nu$, respectively. The total disturbance is thus

$$\Psi\,(x,t) = \exp\{i\,[(k+\delta k)\,x - (\nu+\delta\nu)\,t]\} + \exp\{i\,[(k-\delta k)\,x - (\nu-\delta\nu)\,t]\}$$

where for brevity the Re[ ] notation in (5.4) is omitted and it is understood that only the real part of the right side has physical meaning. Rearranging terms and applying the Euler formula gives

$$\begin{aligned}\Psi &= \left[e^{i(\delta kx - \delta\nu t)} + e^{-i(\delta kx - \delta\nu t)}\right] e^{i(kx-\nu t)} \\ &= 2\cos\left(\delta kx - \delta\nu t\right) e^{i(kx-\nu t)}\end{aligned} \tag{5.5}$$

The disturbance (5.5) is the product of a high-frequency *carrier wave* of wavelength $2\pi/k$ whose phase speed, ν/k, is the average for the two Fourier components, and a low-frequency *envelope* of wavelength $2\pi/\delta k$ that travels at the speed $\delta\nu/\delta k$. Thus, in the limit as $\delta k \to 0$, the horizontal velocity of the envelope, or *group velocity*, is just

$$c_{gx} = \partial\nu/\partial k$$

The wave energy thus propagates at the group velocity. This result applies generally to arbitrary wave envelopes provided that the wavelength of the wave group, $2\pi/\delta k$, is large compared to the wavelength of the dominant component, $2\pi/k$.

5.2.3 Wave Properties in Two and Three Dimensions

Developing a complete understanding of wave properties in two and three dimensions is sufficiently important to the remainder of this chapter and aspects of later chapters that we devote this section to a vector-oriented description of wave properties. We discuss two dimensions for ease of presentation, but the notation is sufficiently general that properties for three dimensions should be clear.

A two-dimensional plane wave in a scalar field, f, may be expressed as

$$f(x,y,t) = \mathrm{Re}\left\{A\,e^{i(kx+ly-\nu t)}\right\} = \mathrm{Re}\left\{A\,e^{i\phi}\right\} \tag{5.6}$$

Independent variables (x, y) and t represent space and time, respectively. k and l are the x and y wave numbers (m^{-1}), and ν is the frequency (s^{-1}). The wave is determined by *amplitude*, A (units of f), and *phase angle*, ϕ. Note that ϕ is a linear function of the independent variables, and it proves useful to consider the space and time properties of ϕ separately.

At any instant in time, $\phi = kx + ly + C$, C constant, so ϕ is uniform along lines of constant $kx + ly$. This implies $d\phi = \frac{\partial\phi}{\partial x}\delta x + \frac{\partial\phi}{\partial y}\delta y = 0$ for ϕ constant.

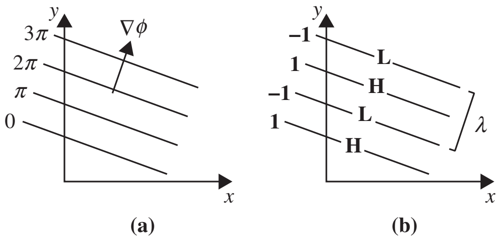

FIGURE 5.5 Two-dimensional plane wave at a fixed time: (a) phase angle, ϕ, and (b) phase, $e^{i\phi}$. Wavelength is denoted λ. Note that if $\nu > 0$, the wave travels in the direction of the wave vector, $\nabla\phi$.

Therefore, the slope of these lines is $\frac{\delta y}{\delta x}\Big|_{\phi} = -k/l$. Constant values of

$$e^{i\phi} = e^{i(\phi+2\pi n)} \tag{5.7}$$

where n is an integer, define lines of constant *phase*, such as lows and highs (Figure 5.5). The *wave vector* is defined by

$$\mathbf{K} = \nabla\phi \tag{5.8}$$

$\mathcal{K} = |\mathbf{K}|$ is the *total wave number*, and therefore $\lambda = \frac{2\pi}{\mathcal{K}}$ is the *wavelength*—that is, the distance between lines of constant phase.

At any fixed point in space, $\phi = C - \nu t$, C constant, so ϕ is a linear function of time. Therefore, frequency is defined as

$$\nu = -\frac{\partial\phi}{\partial t} \tag{5.9}$$

which is the rate at which lines of constant phase pass a fixed point in space. The wave *period* is $\frac{2\pi}{|\nu|}$, which is the length of time between points of constant phase (units: seconds). The wave *phase speed* (m s^{-1}) is determined by how fast lines of constant phase move along the wave vector

$$c = \frac{\nu}{\mathcal{K}} = -\frac{1}{|\nabla\phi|}\frac{\partial\phi}{\partial t} \tag{5.10}$$

This definition represents a generalization of phase speed from the one-dimensional example given in the previous section. In particular, for two and three dimensions, the phase speed is *not* the same as $c_x = \frac{\nu}{k}$ and $c_y = \frac{\nu}{l}$, which define the rate at which phase lines travel along the x and y coordinate axes, respectively. Furthermore, c, c_x, and c_y do not satisfy rules of vector addition, so $c^2 \neq c_x^2 + c_y^2$.

Note that, in general, ϕ and A may be complex numbers. If ϕ has an imaginary part, $\phi = \phi_r + i\phi_i$, then $e^{i\phi} = e^{i(\phi_r + i\phi_i)} = e^{i\phi_r}e^{-\phi_i} \equiv A^* e^{i\phi_r}$. ϕ_r is the wave phase angle as interpreted in the preceding, and $A^* = Ae^{-\phi_i}$ is a modified amplitude that depends on time and/or space. For example, if the frequency, ν, contributes the imaginary part, then the wave has *time-dependent* amplitude that grows or decays with time. Such waves are referred to as *unstable* to distinguish them from the *neutral* waves with fixed A. In Chapter 7 we seek waves that grow in time, and therefore will study conditions that contribute to imaginary frequency.

We return now to group velocity, which provides the speed and direction in which an observer must travel in order to follow waves of a certain wavelength and frequency. Rather than a pure plane wave, which exists over all space, we take the phase angle, ϕ in (5.6), to be a slowly varying function of space and time due to variable ν and $\mathbf{K}$. Equations (5.8) and (5.9) define the wave vector and frequency respectively, even when these quantities vary in space and time. Together, (5.8) and (5.9) imply

$$\frac{\partial \mathbf{K}}{\partial t} + \nabla \nu = 0 \tag{5.11}$$

Frequency is defined by a dispersion relationship, so that ν is a function of $\mathbf{K}$. As such, $\nabla \nu$ may be evaluated using the chain rule

$$\nabla \nu = (\nabla_k \nu \cdot \nabla)\mathbf{K} \tag{5.12}$$

where $\nabla_k \nu = \left(\frac{\partial \nu}{\partial k}, \frac{\partial \nu}{\partial l}\right)$ is the group velocity, $\mathbf{C}_g$. Therefore, (5.11) can be written as

$$\frac{\partial \mathbf{K}}{\partial t} + (\mathbf{C}_g \cdot \nabla)\mathbf{K} = 0 \tag{5.13}$$

Consequently, in a frame of reference moving with the group velocity, the wave vector is conserved; that is, we follow a group of waves with fixed wavelength and frequency.

5.2.4 A Wave Solution Strategy

Approximations to the full equations governing atmospheric dynamics will be solved for wave motions many times. Even though aspects of each individual case are different, a guide to the general approach to solving these problems is as follows:

1. **Choose a basic state** The basic state is a simplified representation of the atmosphere. Typically we wish to eliminate all complications except those essential to the motions of interest. For example, in this chapter we will often make use of basic states that are at rest and in hydrostatic balance. The basic state is like a musical instrument, and we wish to know what tones naturally emerge.
2. **Linearize the governing equations** Given a basic state, the governing equations can be linearized using the perturbation method of Section 5.1

3. **Assume wave solutions of the form in equation (5.6)** If the coefficients of the linearized equations do not depend on an independent variable, then the functions that depend on the independent variable may be represented as waves, $e^{i\phi}$, as in equation (5.6), provided that the independent variable is periodic. If, for example, the domain of interest is not periodic in the y direction, or the basic state varies in y, then we cannot assume wave solutions in that direction. Instead, a general functional form must be assumed in that direction, such as $F(y)e^{i(kx-\nu t)}$, which typically leads to an ordinary differential equation that must be solved for the structure function $F(y)$.
4. **Solve for the dispersion and polarization relationships** Substituting the wave form into the linearized governing equations typically results in a simpler closed set of algebraic equations or, in cases having nonconstant coefficients, with a set of ordinary differential equations. Normally the wave number is taken as the independent variable, and the frequency is determined as a function of the wave number; this gives the dispersion relationship. The wave amplitude is unconstrained, but the relationships between variables, the polarization relations, must be determined. Variables are *in phase* if they share the same form and sign (e.g., sin(x)) and *out of phase* if they have the same form and opposite sign (e.g., sin(x) and −sin(x)). If the variables are 90° out of phase, they are *in quadrature* (e.g., sin(x) and cos(x)).

5.3 SIMPLE WAVE TYPES

Waves in fluids result from the action of restoring forces on fluid parcels that have been displaced from their equilibrium positions. The restoring forces may be due to compressibility, gravity, rotation, or electromagnetic effects. This section considers the two simplest examples of linear waves in fluids: acoustic waves and shallow water gravity waves.

5.3.1 Acoustic or Sound Waves

Sound waves, or acoustic waves, are *longitudinal waves*. That is, they are waves in which the particle oscillations are parallel to the direction of propagation. Sound is propagated by the alternating adiabatic compression and expansion of the medium. As an example, Figure 5.6 shows a schematic section along a tube that has a diaphragm at its left end. If the diaphragm is set into vibration, the air adjacent to it will be alternately compressed and expanded as the diaphragm moves inward and outward. The resulting oscillating pressure gradient force will be balanced by an oscillating acceleration of the air in the adjoining region, which will cause an oscillating pressure oscillation further into the tube, and so on. The result of this continual adiabatic increase and decrease of pressure through alternating compression and rarefaction is, as shown in Figure 5.6, a sinusoidal pattern of pressure and velocity perturbations that propagates to the right down the tube. Individual air parcels do not, however, have a net rightward

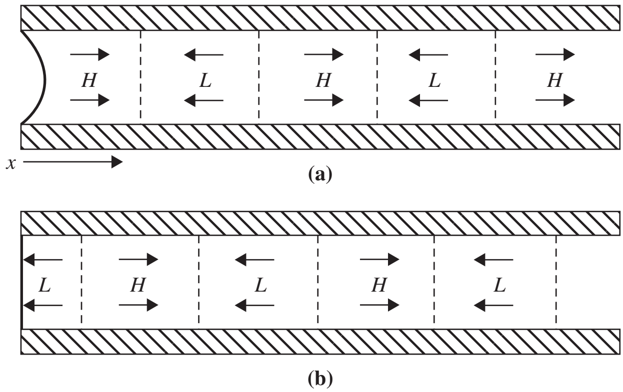

FIGURE 5.6 Schematic diagram illustrating the propagation of a sound wave in a tube with a flexible diaphragm at the left end. Labels H and L designate centers of high- and low-perturbation pressure. *Arrows* show velocity perturbations. The situation one-quarter period (b) later than in (a) for propagation in the positive x direction.

motion; they only oscillate back and forth, while the pressure pattern moves rightward at the speed of sound.

To introduce the perturbation method, we consider the problem illustrated by Figure 5.6—that is, one-dimensional sound waves propagating in a straight pipe parallel to the x axis. To exclude the possibility of *transverse* oscillations (i.e., oscillations in which the particle motion is at right angles to the direction of phase propagation), we assume at the outset that $v = w = 0$. In addition, we eliminate all dependence on y and z by assuming that $u = u(x,t)$. With these restrictions, the momentum equation, continuity equation, and thermodynamic energy equation for adiabatic motion are, respectively,

$$\frac{Du}{Dt} + \frac{1}{\rho}\frac{\partial p}{\partial x} = 0 \tag{5.14}$$

$$\frac{D\rho}{Dt} + \rho\frac{\partial u}{\partial x} = 0 \tag{5.15}$$

$$\frac{D\ln\theta}{Dt} = 0 \tag{5.16}$$

where for this case $D/Dt = \partial/\partial t + u\partial/\partial x$. Recalling from (2.44) and the ideal gas law that potential temperature may be expressed as

$$\theta = (p/\rho R)\,(p_s/p)^{R/c_p}$$

where $p_s = 1000$ hPa, we may eliminate θ in (5.16) to give

$$\frac{1}{\gamma}\frac{D\ln p}{Dt} - \frac{D\ln\rho}{Dt} = 0 \tag{5.17}$$

where $\gamma = c_p/c_v$. Eliminating ρ between (5.15) and (5.17) gives

$$\frac{1}{\gamma}\frac{D\ln p}{Dt} + \frac{\partial u}{\partial x} = 0 \tag{5.18}$$

The dependent variables are now divided into constant basic state portions (denoted by overbars) and perturbation portions (denoted by primes):

$$\begin{aligned} u(x,t) &= \overline{u} + u'(x,t) \\ p(x,t) &= \overline{p} + p'(x,t) \\ \rho(x,t) &= \overline{\rho} + \rho'(x,t) \end{aligned} \tag{5.19}$$

Substituting (5.19) into (5.14) and (5.18) we obtain

$$\frac{\partial}{\partial t}\left(\overline{u}+u'\right) + \left(\overline{u}+u'\right)\frac{\partial}{\partial x}\left(\overline{u}+u'\right) + \frac{1}{(\overline{\rho}+\rho')}\frac{\partial}{\partial x}\left(\overline{p}+p'\right) = 0$$

$$\frac{\partial}{\partial t}\left(\overline{p}+p'\right) + \left(\overline{u}+u'\right)\frac{\partial}{\partial x}\left(\overline{p}+p'\right) + \gamma\left(\overline{p}+p'\right)\frac{\partial}{\partial x}\left(\overline{u}+u'\right) = 0$$

We next observe that provided $\left|\rho'/\overline{\rho}\right| \ll 1$, we can use the binomial expansion to approximate the density term as

$$\frac{1}{(\overline{\rho}+\rho')} = \frac{1}{\overline{\rho}}\left(1+\frac{\rho'}{\overline{\rho}}\right)^{-1} \approx \frac{1}{\overline{\rho}}\left(1-\frac{\rho'}{\overline{\rho}}\right)$$

Neglecting products of the perturbation quantities and noting that the basic state fields are constants, we obtain the linear perturbation equations[1]

$$\left(\frac{\partial}{\partial t} + \overline{u}\frac{\partial}{\partial x}\right)u' + \frac{1}{\overline{\rho}}\frac{\partial p'}{\partial x} = 0 \tag{5.20}$$

$$\left(\frac{\partial}{\partial t} + \overline{u}\frac{\partial}{\partial x}\right)p' + \gamma\overline{p}\frac{\partial u'}{\partial x} = 0 \tag{5.21}$$

Eliminating u' by operating on (5.21) with $(\partial/\partial t + \overline{u}\partial/\partial x)$ and substituting from (5.20), we get[2]

$$\left(\frac{\partial}{\partial t} + \overline{u}\frac{\partial}{\partial x}\right)^2 p' - \frac{\gamma\overline{p}}{\overline{\rho}}\frac{\partial^2 p'}{\partial x^2} = 0 \tag{5.22}$$

---

[1] It is not necessary that the perturbation velocity be small compared to the mean velocity for linearization to be valid. It is only required that quadratic terms in the perturbation variables be small compared to the dominant linear terms in (5.20) and (5.21).

[2] Note that the squared differential operator in the first term expands in the usual way as

$$\left(\frac{\partial}{\partial t} + \overline{u}\frac{\partial}{\partial x}\right)^2 = \frac{\partial^2}{\partial t^2} + 2\overline{u}\frac{\partial^2}{\partial t\partial x} + \overline{u}^2\frac{\partial^2}{\partial x^2}$$

which is a form of the standard *wave equation* familiar from electromagnetic theory. A simple solution representing a plane sinusoidal wave propagating in x is

$$p' = A \exp\left[ik\left(x - ct\right)\right] \tag{5.23}$$

where for brevity we omit the Re{ } notation, but it is to be understood that only the real part of (5.23) has physical significance. Substituting the assumed solution (5.23) into (5.22), we find that the phase speed c must satisfy

$$\left(-ikc + ik\overline{u}\right)^2 - \left(\gamma\overline{p}/\overline{\rho}\right)\left(ik\right)^2 = 0$$

where we have canceled out the factor $A \exp\left[ik\left(x - ct\right)\right]$, which is common to both terms. Solving for c gives

$$c = \overline{u} \pm \left(\gamma\overline{p}/\overline{\rho}\right)^{1/2} = \overline{u} \pm \left(\gamma R\overline{T}\right)^{1/2} \tag{5.24}$$

Therefore, (5.23) is a solution of (5.22), provided that the phase speed satisfies (5.24). According to (5.24), the speed of wave propagation relative to the zonal current is $c - \overline{u} = \pm c_s$, where $c_s \equiv \left(\gamma R\overline{T}\right)^{1/2}$ is called the *adiabatic speed of sound*.

The mean zonal velocity here plays only a role of *Doppler shifting* the sound wave so that the frequency relative to the ground corresponding to a given wave number k is

$$\nu = kc = k\left(\overline{u} \pm c_s\right)$$

Thus, in the presence of a wind, the frequency as heard by a fixed observer depends on the location of the observer relative to the source. If $\overline{u} > 0$, the frequency of a stationary source will appear to be higher for an observer to the east (downstream) of the source ($c = \overline{u} + c_s$) than for an observer to the west (upstream) of the source $c = \overline{u} - c_s$.

5.3.2 Shallow Water Waves

The second example of pure wave motion concerns the horizontally propagating oscillations known as shallow water waves. This analysis provides a clear introduction to the primary wave motions in the extratropical latitudes: Rossby waves and gravity waves.

We linearize the shallow water equations (derived in Section 4.5) for a resting basic state having water depth $\overline{h}$ and fixed ambient rotation given by a constant Coriolis parameter f. The linearized momentum (4.33) and mass continuity (4.37) equations are

$$\frac{\partial u'}{\partial t} = -g\frac{\partial h'}{\partial x} + fv'$$
$$\frac{\partial v'}{\partial t} = -g\frac{\partial h'}{\partial y} - fu' \tag{5.25}$$
$$\frac{\partial h'}{\partial t} = -\bar{h}\left(\frac{\partial u'}{\partial x} + \frac{\partial v'}{\partial y}\right)$$

Primes denote perturbation values—that is, departures from the state of rest. (5.25) represent a set of three coupled first-order partial differential equations in the unknowns, u', v', h'. One approach to solving these equations is to form and solve a single third-order partial differential equation. This is accomplished by taking $\partial/\partial t$ of the third equation in (5.25), which gives

$$\frac{\partial^2 h'}{\partial t^2} = -\bar{h}\left(\frac{\partial^2 u'}{\partial t \partial x} + \frac{\partial^2 v'}{\partial t \partial y}\right) \tag{5.26}$$

The terms on the right side of (5.26) may be replaced using the first two equations of (5.25):

$$\frac{\partial^2 h'}{\partial t^2} = \bar{h}\left(g\nabla_h^2 h' - f\zeta'\right) \tag{5.27}$$

Again take $\partial/\partial t$, which gives the third-order equation

$$\frac{\partial^3 h'}{\partial t^3} + \left(f^2 - g\bar{h}\nabla_h^2\right)\frac{\partial h'}{\partial t} = 0 \tag{5.28}$$

where $\partial\zeta'/\partial t$ is replaced using the linearized version of (4.38) (noting that f is taken constant here):

$$\frac{\partial \zeta'}{\partial t} = -f\left(\frac{\partial u'}{\partial x} + \frac{\partial v'}{\partial y}\right) \tag{5.29}$$

Assuming that the lateral boundaries are periodic and, since the coefficients f and $g\bar{h}$ are constant, we may assume wave solutions of the form

$$h' = \mathrm{Re}\left\{Ae^{i(kx+ly-\nu t)}\right\} \tag{5.30}$$

Using (5.30) in (5.28) gives a cubic polynomial for the frequency

$$\nu^3 - \nu\left[f^2 + g\bar{h}\left(k^2 + l^2\right)\right] = 0 \tag{5.31}$$

This is the dispersion relationship for shallow water waves. Clearly $\nu = 0$ is a solution, and if $\nu \neq 0$, then

$$\nu^2 = f^2 + g\bar{h}\left(k^2 + l^2\right) \tag{5.32}$$

For readers familiar with linear algebra, we note an alternative solution method. Taking solutions of the form (5.30) for h', u', and v', and substituting directly into (5.25), converts the set of partial differential equations to algebraic equations that may be written as

$$\mathbf{Ax} = 0 \tag{5.33}$$

where $\mathbf{x}$ is the column vector of the unknowns $[u'v'h']^{\mathrm{T}}$, and

$$\mathbf{A} = \begin{bmatrix} -i\nu & -f & ikg \\ f & -i\nu & ilg \\ \bar{h}k & -\bar{h}l & -\nu \end{bmatrix} \tag{5.34}$$

A nontrivial solution to (5.33) is obtained only if $\mathbf{A}$ is not invertible. This is enforced by setting the determinant of $\mathbf{A}$ to zero, which gives (5.31).

Turning now to the structure of the waves, consider first the case where $\nu = 0$. Appealing to (5.25), we see that since the waves are stationary, the left sides are zero. Clearly, these waves depend on rotation, since when $f = 0$, the wave amplitude, A, must also be zero. For non zero f, (5.25) implies

$$\begin{aligned} v' &= \frac{g}{f}\frac{\partial h}{\partial x} \\ u' &= -\frac{g}{f}\frac{\partial h}{\partial y} \end{aligned} \tag{5.35}$$

The stationary waves are in a state of geostrophic balance and are an example of **Rossby waves** in the limit of constant Coriolis parameter. The case of propagating Rossby waves, with nonconstant Coriolis parameter, will be explored in Section 5.7.

Solutions for $\nu \neq 0$ are called **inertia–gravity waves**, since particle oscillations depend on both gravitational and inertial forces. The inertial aspect will be discussed in Section 5.7 so that we may focus here on the gravitational aspect. In the limiting case $f = 0$, we have simply **gravity waves**, and from (5.32) the wave speed becomes

$$c = \sqrt{g\bar{h}} \tag{5.36}$$

Since the waves all move at the same speed, they are nondispersive. For a fluid $\bar{h} = 4$ km deep, the shallow water gravity wave speed is approximately 200 m s^{-1}. Thus, long waves on the ocean surface travel very rapidly. It should be emphasized again that this theory applies only to waves of wavelength

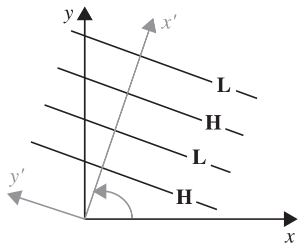

FIGURE 5.7 Coordinate rotation to align the y axis with wave fronts so that $l = 0$.

much greater than $\bar{h}$. Such long waves may be produced by very large-scale disturbances such as earthquakes.[3]

In order to further expose wave structure and the physics of motion, we rotate coordinates such that the y direction is oriented along the phase lines (Figure 5.7). Since this yields the same interpretation as $l = 0$, we omit the prime notation on x and y. In this case, the general expressions for flow normal to and along phase lines, u' and v', respectively, are

$$\begin{aligned} u' &= \frac{\nu k g}{\nu^2 - f^2} h' \\ v' &= \frac{-ikgf}{\nu^2 - f^2} h' \end{aligned} \tag{5.37}$$

From (4.34) and the third equation in (5.25),

$$\frac{\partial w'}{\partial z} = -\frac{\partial u'}{\partial x} = \frac{1}{\bar{h}} \frac{\partial h'}{\partial t} \tag{5.38}$$

Integrating in z gives the w' field

$$w'(z) = \frac{1}{\bar{h}} \frac{\partial h'}{\partial t} \int_0^z dz' = \frac{-ikcz}{\bar{h}} h' \tag{5.39}$$

Taking the real part of w' gives

$$\mathrm{Re}\{w'\} = -\frac{kcz}{\bar{h}} \mathrm{Re}\{ih'\} = \frac{kczA}{\bar{h}} \sin(\phi) \tag{5.40}$$

This shows that w' is in *quadrature* with h', so that w' will lead (lag) h' by 90° if the waves move to the right (left).

Setting $\nu = c = 0$ in (5.37) and (5.39) recovers the geostrophic flow of stationary Rossby waves: $u' = 0$ (no flow normal to phase lines), $v' = -ikg/f$,

[3]Long waves excited by underwater earthquakes or volcanic eruptions are called *tsunamis*.

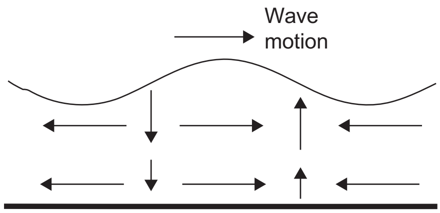

FIGURE 5.8 Depiction of shallow water gravity wave height and velocity fields for the case where the coordinates have been rotated as shown in Figure 5.7.

and $w = 0$. For the inertia gravity waves ($\nu \neq 0$), notice that the flow along phase lines is zero in the absence of ambient rotation. In that case, the physics of wave propagation is particularly clear. From (5.32) we see that $\nu^2 - f^2$ is strictly positive, and in the rotated coordinates, $u' = c/\overline{h}$. This shows that the u' field is either *in phase*, or *out of phase*, with the h' field depending on the sign of c. Waves that move to the right ($c > 0$) are shown in Figure 5.8. Convergence and divergence of the u field raise and lower the height of the fluid, respectively, moving the wave to the right in Figure 5.8. As expected from mass conservation, the w field exhibits rising motion near convergence, which increases linearly with height from zero at the bottom boundary. Changing the sign of c has no effect on h', but reverses the u and w fields so that the wave moves to the left.

Finally, consider the vorticity and potential vorticity (PV) of the waves in the rotated coordinates. Since there is no variation in the y direction, the relative vorticity is simply

$$\zeta' = \frac{\partial v'}{\partial x} = \frac{k^2 g f}{\nu^2 - f^2} h' \tag{5.41}$$

A linearized version of the shallow water potential vorticity equation (4.39) is obtained from (5.29) and the third equation in (5.25), which yields

$$\frac{\partial}{\partial t}\left[\zeta' - \frac{f}{\overline{h}} h'\right] = 0 \tag{5.42}$$

Linearization has removed all advection terms from the PV conservation equation, so that (5.42) states that the linearized PV

$$Q' = \zeta' - \frac{f}{\overline{h}} h' \tag{5.43}$$

is conserved *locally*, at every point in space. This is an extremely powerful constraint on the linear dynamics, which we will exploit in Section 5.6 when solving initial-vale problems for (5.25).

For shallow water Rossby waves, vorticity in the rotated coordinates becomes

$$\zeta'_{RW} = -\frac{k^2 g}{f} h' \tag{5.44}$$

which is out of phase with the height field and larger for shorter waves. Rossby wave PV is given by ζ reduced by $\frac{f}{\bar{h}}h'$, which has the same sign as ζ except for unrealistically long waves.

For shallow water inertia–gravity waves, vorticity in the rotated coordinates becomes

$$\zeta'_{GW} = \frac{f}{\bar{h}}\, h' \tag{5.45}$$

which is in phase with the height field, and nonzero provided there exists ambient rotation. From (5.45) and (5.43), it is clear that inertia–gravity wave PV is identically zero.

A summary of the essential differences between Rossby and inertia–gravity waves for rotating shallow water follows:

- Rossby waves are stationary for f constant, whereas inertia–gravity waves move very fast.
- Inertia–gravity waves have small relative vorticity but are strongly divergent, whereas Rossby waves have geostrophic winds with zero divergence and large relative vorticity.
- Inertia–gravity waves have zero potential vorticity, whereas Rossby waves generally have nonzero potential vorticity.

These properties generalize to waves in a stratified atmosphere, considered in the next two sections. They provide a useful framework for eliminating inertia–gravity waves from the full nonlinear equations, yielding the quasi-geostrophic equations, which we use to understand the dynamics of extratropical weather systems in Chapters 6 and 7.

5.4 INTERNAL GRAVITY (BUOYANCY) WAVES

The nature of gravity wave propagation in the stratified atmosphere is considered now in the absence of ambient rotation. Atmospheric gravity waves can only exist when the atmosphere is stably stratified so that a fluid parcel displaced vertically will undergo buoyancy oscillations (see Section 2.7.3). Because the buoyancy force is the restoring force responsible for gravity waves, the term *buoyancy wave* is actually more appropriate as a name for these waves. However, in this text we will generally use the traditional name *gravity wave*.

In a fluid, such as the ocean, which is bounded both above and below, gravity waves propagate primarily in the horizontal plane, since vertically traveling waves are reflected from the boundaries to form standing waves. However, in a fluid that has no upper boundary, such as the atmosphere, gravity waves may propagate vertically as well as horizontally. In vertically propagating waves the phase is a function of height. Such waves are referred to as *internal* waves. Although internal gravity waves are not generally of great importance for synoptic-scale weather forecasting (and indeed are nonexistent in the filtered quasi-geostrophic models), they can be important in mesoscale motions. For example, they are responsible for the occurrence of mountain *lee waves*. They also are believed to be an important mechanism for transporting energy and momentum into the middle atmosphere, and are often associated with the formation of clear air turbulence (CAT).

5.4.1 Pure Internal Gravity Waves

For simplicity we neglect the Coriolis force and limit our discussion to two-dimensional internal gravity waves propagating in the x, z plane. An expression for the frequency of such waves can be obtained by modifying the parcel theory developed in Section 2.7.3.

Internal gravity waves are transverse waves in which the parcel oscillations are parallel to the phase lines as indicated in Figure 5.9. A parcel displaced a distance δs along a line tilted at an angle α to the vertical as shown in Figure 5.8 will undergo a vertical displacement $\delta z = \delta s \cos\alpha$. For such a parcel the *vertical* buoyancy force per unit mass is just $-N^2\delta z$, as was shown in (2.52). Thus, the component of the buoyancy force parallel to the tilted path along which the parcel oscillates is just

$$-N^2\delta z\cos\alpha = -N^2\left(\delta s\cos\alpha\right)\cos\alpha = -\left(N\cos\alpha\right)^2\delta s$$

The momentum equation for the parcel oscillation is then

$$\frac{d^2\left(\delta s\right)}{dt^2} = -\left(N\cos\alpha\right)^2\delta s \tag{5.46}$$

which has the general solution $\delta s = \exp\left[\pm i\left(N\cos\alpha\right)t\right]$. Thus, the parcels execute a simple harmonic oscillation at the frequency $\nu = N\cos\alpha$. This frequency depends only on the static stability (measured by the buoyancy frequency N) and the angle of the phase lines to the vertical.

The preceding heuristic derivation can be verified by considering the linearized equations for two-dimensional internal gravity waves. For simplicity, we

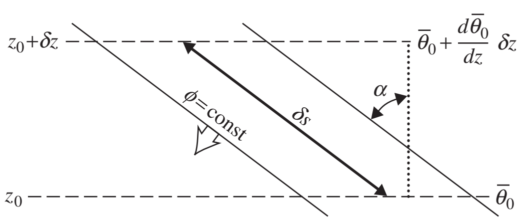

FIGURE 5.9 Parcel oscillation path (*heavy arrow*) for pure gravity waves with phase lines tilted at an angle α to the vertical.

employ the Boussinesq approximation of Section 2.8, in which density is treated as a constant except where it is coupled with gravity in the buoyancy term of the vertical momentum equation. Thus, in this approximation the atmosphere is considered to be incompressible, and local density variations are assumed to be small perturbations of the constant basic state density field. Because the vertical variation of the basic state density is neglected except where coupled with gravity, the Boussinesq approximation is only valid for motions in which the vertical scale is less than the atmospheric scale height $H(\approx 8\,\text{km})$.

Neglecting the effects of rotation, the basic equations for two-dimensional motion of an incompressible atmosphere may be written as

$$\frac{\partial u}{\partial t}+u\frac{\partial u}{\partial x}+w\frac{\partial u}{\partial z}+\frac{1}{\rho}\frac{\partial p}{\partial x}=0 \tag{5.47}$$

$$\frac{\partial w}{\partial t}+u\frac{\partial w}{\partial x}+w\frac{\partial w}{\partial z}+\frac{1}{\rho}\frac{\partial p}{\partial z}+g=0 \tag{5.48}$$

$$\frac{\partial u}{\partial x}+\frac{\partial w}{\partial z}=0 \tag{5.49}$$

$$\frac{\partial \theta}{\partial t}+u\frac{\partial \theta}{\partial x}+w\frac{\partial \theta}{\partial z}=0 \tag{5.50}$$

where the potential temperature θ is related to pressure and density by

$$\theta=\frac{p}{\rho R}\left(\frac{p_s}{p}\right)^{\kappa}$$

which, after taking logarithms on both sides, yields

$$\ln\theta=\gamma^{-1}\ln p-\ln\rho+\text{constant} \tag{5.51}$$

We now linearize (5.47) through (5.51) by letting

$$\begin{aligned} &\rho=\rho_0+\rho' && u=\overline{u}+u' \\ &p=\overline{p}\,(z)+p' && w=w' \\ &\theta=\overline{\theta}\,(z)+\theta' && \end{aligned} \tag{5.52}$$

where the basic state zonal flow $\overline{u}$ and the density ρ_0 are both assumed to be constant. The basic state pressure field must satisfy the hydrostatic equation

$$d\overline{p}/dz=-\rho_0 g \tag{5.53}$$

while the basic state potential temperature must satisfy (5.51) so that

$$\ln\overline{\theta}=\gamma^{-1}\ln\overline{p}-\ln\rho_0+\text{constant} \tag{5.54}$$

The linearized equations are obtained by substituting from (5.52) into (5.47) through (5.51) and neglecting all terms that are products of the perturbation variables. Thus, for example, the last two terms in (5.48) are approximated as

$$\begin{aligned}\frac{1}{\rho}\frac{\partial p}{\partial z}+g&=\frac{1}{\rho_0+\rho'}\left(\frac{d\overline{p}}{dz}+\frac{\partial p'}{\partial z}\right)+g\\&\approx\frac{1}{\rho_0}\frac{d\overline{p}}{dz}\left(1-\frac{\rho'}{\rho_0}\right)+\frac{1}{\rho_0}\frac{\partial p'}{\partial z}+g=\frac{1}{\rho_0}\frac{\partial p'}{\partial z}+\frac{\rho'}{\rho_0}g\end{aligned}\tag{5.55}$$

where (5.53) has been used to eliminate $\overline{p}$. The perturbation form of (5.51) is obtained by noting that

$$\begin{aligned}\ln\left[\overline{\theta}\left(1+\frac{\theta'}{\overline{\theta}}\right)\right]&=\gamma^{-1}\ln\left[\overline{p}\left(1+\frac{p'}{\overline{p}}\right)\right]\\&\quad-\ln\left[\rho_0\left(1+\frac{\rho'}{\rho_0}\right)\right]+\text{const.}\end{aligned}\tag{5.56}$$

Now, recalling that $\ln(ab)=\ln(a)+\ln(b)$ and that $\ln(1+\varepsilon)\approx\varepsilon$ for any $\varepsilon\ll 1$, we find with the aid of (5.54) that (5.56) may be approximated by

$$\frac{\theta'}{\overline{\theta}}\approx\frac{1}{\gamma}\frac{p'}{\overline{p}}-\frac{\rho'}{\rho_0}$$

Solving for ρ' yields

$$\rho'\approx-\rho_0\frac{\theta'}{\overline{\theta}}+\frac{p'}{c_s^2}\tag{5.57}$$

where $c_s^2\equiv\overline{p}\gamma/\rho_0$ is the square of the speed of sound. For buoyancy wave motions $\left|\rho_0\theta'/\overline{\theta}\right|\gg\left|p'/c_s^2\right|$; that is, density fluctuations due to pressure changes are small compared with those due to temperature changes. Therefore, to a first approximation,

$$\theta'/\overline{\theta}=-\rho'/\rho_0\tag{5.58}$$

Using (5.55) and (5.58), the linearized version of the equation set (5.47) through (5.50), we can write as

$$\left(\frac{\partial}{\partial t}+\overline{u}\frac{\partial}{\partial x}\right)u'+\frac{1}{\rho_0}\frac{\partial p'}{\partial x}=0\tag{5.59}$$

$$\left(\frac{\partial}{\partial t}+\overline{u}\frac{\partial}{\partial x}\right)w'+\frac{1}{\rho_0}\frac{\partial p'}{\partial z}-\frac{\theta'}{\overline{\theta}}g=0\tag{5.60}$$

$$\frac{\partial u'}{\partial x}+\frac{\partial w'}{\partial z}=0\tag{5.61}$$

$$\left(\frac{\partial}{\partial t}+\overline{u}\frac{\partial}{\partial x}\right)\theta'+w'\frac{d\overline{\theta}}{dz}=0\tag{5.62}$$

Subtracting $\partial(5.59)/\partial z$ from $\partial(5.60)/\partial x$, we can eliminate p' to obtain

$$\left(\frac{\partial}{\partial t}+\bar{u}\frac{\partial}{\partial x}\right)\left(\frac{\partial w'}{\partial x}-\frac{\partial u'}{\partial z}\right)-\frac{g}{\bar{\theta}}\frac{\partial \theta'}{\partial x}=0 \tag{5.63}$$

which is just the y component of the vorticity equation. With the aid of (5.61) and (5.62), u' and θ' can be eliminated from (5.63) to yield a single equation for w':

$$\left(\frac{\partial}{\partial t}+\bar{u}\frac{\partial}{\partial x}\right)^2\left(\frac{\partial^2 w'}{\partial x^2}+\frac{\partial^2 w'}{\partial z^2}\right)+N^2\frac{\partial^2 w'}{\partial x^2}=0 \tag{5.64}$$

where $N^2 \equiv g\,d\ln\bar{\theta}/dz$ is the square of the buoyancy frequency, which is assumed to be constant.[4]

Equation (5.64) has harmonic wave solutions of the form

$$w' = \mathrm{Re}\left[\hat{w}\exp(i\phi)\right] = w_r\cos\phi - w_i\sin\phi \tag{5.65}$$

where $\hat{w} = w_r + iw_i$ is a complex amplitude with real part w_r and imaginary part w_i, and $\phi = kx + mz - \nu t$ is the phase, which is assumed to depend linearly on z as well as on x and t. Here the horizontal wave number k is real because the solution is always sinusoidal in x. The vertical wave number $m = m_r + im_i$ may, however, be complex, in which case m_r describes sinusoidal variation in z and m_i describes exponential decay or growth in z, depending on whether m_i is positive or negative. When m is real, the total wave number may be regarded as a vector $\boldsymbol{\kappa} \equiv (k, m)$, directed perpendicular to lines of constant phase, and in the direction of phase increase, whose components, $k = 2\pi/L_x$ and $m = 2\pi/L_z$, are inversely proportional to the horizontal and vertical wavelengths, respectively. Substitution of the assumed solution into (5.64) yields the dispersion relationship

$$(\nu - \bar{u}k)^2\left(k^2+m^2\right) - N^2k^2 = 0$$

so that

$$\hat{\nu} \equiv \nu - \bar{u}k = \pm Nk\Big/\left(k^2+m^2\right)^{1/2} = \pm Nk/\left|\boldsymbol{\kappa}\right| \tag{5.66}$$

where $\hat{\nu}$, the *intrinsic frequency*, is the frequency relative to the mean wind. Here, the plus sign is to be taken for eastward phase propagation and the minus sign for westward phase propagation, relative to the mean wind.

[4]Strictly speaking, N^2 cannot be exactly constant if ρ_0 is constant. However, for shallow disturbances the variation of N^2 with height is unimportant.

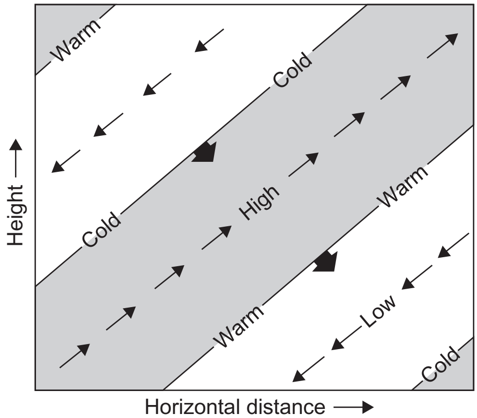

FIGURE 5.10 Idealized cross-section showing phases of pressure, temperature, and velocity perturbations for an internal gravity wave. *Thin arrows* indicate the perturbation velocity field; *blunt solid arrows*, the phase velocity. *Shading* shows regions of upward motion.

If we let $k > 0$ and $m < 0$, then lines of constant phase tilt eastward with increasing height as shown in Figure 5.10 (i.e., for $\phi = kx + mz$ to remain constant as x increases, z must also increase when $k > 0$ and $m < 0$). The choice of the positive root in (5.66) then corresponds to eastward and downward phase propagation relative to the mean flow, with horizontal and vertical phase speeds (relative to the mean flow) given by $c_x = \hat{\nu}/k$ and $c_z = \hat{\nu}/m$, respectively.[5] The components of the group velocity, $c_{gx}$and c_{gz}, however, are given by

$$c_{gx} = \frac{\partial \nu}{\partial k} = \overline{u} \pm \frac{Nm^2}{\left(k^2 + m^2\right)^{3/2}} \tag{5.67}$$

$$c_{gz} = \frac{\partial \nu}{\partial m} = \pm \frac{(-Nkm)}{\left(k^2 + m^2\right)^{3/2}} \tag{5.68}$$

where the upper or lower signs are chosen in the same way as in (5.66). Thus, the vertical component of group velocity has a sign opposite to that of the vertical phase speed relative to the mean flow (downward phase propagation implies upward energy propagation). Furthermore, it is easily shown from (5.45) that the group velocity vector is parallel to lines of constant phase. Internal gravity waves thus have the remarkable property that group velocity is perpendicular

[5]Note that phase speed is not a vector. The phase speed in the direction perpendicular to constant phase lines (i.e., the blunt arrows in Figure 5.10) is given by $\nu/(k^2 + m^2)^{1/2}$, which is not equal to $\left(c_x^2 + c_z^2\right)^{1/2}$.

to the direction of phase propagation. Because energy propagates at the group velocity, this implies that energy propagates parallel to the wave crests and troughs, rather than perpendicular to them as in acoustic waves or shallow water gravity waves. In the atmosphere, internal gravity waves generated in the troposphere by cumulus convection, by flow over topography, and by other processes may propagate upward many scale heights into the middle atmosphere, even though individual fluid parcel oscillations may be confined to vertical distances much less than a kilometer.

Referring again to Figure 5.10, it is evident that the angle of the phase lines to the local vertical is given by

$$\cos\alpha = L_z/(L_x^2 + L_z^2)^{1/2} = \pm k/(k^2 + m^2)^{1/2} = \pm k/|\boldsymbol{\kappa}|$$

Thus, $\hat{\nu} = \pm N\cos\alpha$ (i.e., gravity wave frequencies must be less than the buoyancy frequency) in agreement with the heuristic parcel oscillation model (5.46). The tilt of phase lines for internal gravity waves depends only on the ratio of the intrinsic wave frequency to the buoyancy frequency and is independent of wavelength.

5.5 LINEAR WAVES OF A ROTATING STRATIFIED ATMOSPHERE

Rotation is now considered by extending the analysis of linear waves in a stratified atmosphere. As in the shallow water analysis of Section 5.3.2, rotation permits the existence of stationary Rossby waves. Gravity waves with horizontal scales greater than a few hundred kilometers and periods greater than a few hours are hydrostatic, but they are influenced by the Coriolis effect and are characterized by parcel oscillations that are elliptical rather than straight lines as in the pure gravity wave case. This *elliptical polarization* can be understood qualitatively by observing that the Coriolis effect resists horizontal parcel displacements in a rotating fluid, but in a manner somewhat different from that in which the buoyancy force resists vertical parcel displacements in a statically stable atmosphere. In the latter case the resistive force is opposite to the direction of parcel displacement, whereas in the former it is at right angles to the horizontal parcel velocity.

5.5.1 Pure Inertial Oscillations

Section 3.2.3 showed that a parcel put into horizontal motion in a resting atmosphere with a constant Coriolis parameter executes a circular trajectory in an anticyclonic sense. A generalization of this type of inertial motion to the case with a geostrophic mean zonal flow can be derived using a parcel argument similar to that used for the buoyancy oscillation in Section 2.7.3.

If the basic state flow is assumed to be a zonally directed geostrophic wind u_g, and it is assumed that the parcel displacement does not perturb the pressure field, the approximate equations of motion become

$$\frac{Du}{Dt} = fv = f\frac{Dy}{Dt} \tag{5.69}$$

$$\frac{Dv}{Dt} = f\left(u_g - u\right) \tag{5.70}$$

We consider a parcel that is moving with the geostrophic basic state motion at a position $y = y_0$. If the parcel is displaced across stream by a distance δy, we can obtain its new zonal velocity from the integrated form of (5.49):

$$u\left(y_0 + \delta y\right) = u_g\left(y_0\right) + f\delta y \tag{5.71}$$

The geostrophic wind at $y_0 + \delta y$ can be approximated as

$$u_g\left(y_0 + \delta y\right) = u_g\left(y_0\right) + \frac{\partial u_g}{\partial y}\delta y \tag{5.72}$$

Using (5.71) and (5.72) to evaluate (5.50) at $y_0 + \delta y$ yields

$$\frac{Dv}{Dt} = \frac{D^2\delta y}{Dt^2} = -f\left(f - \frac{\partial u_g}{\partial y}\right)\delta y = -f\frac{\partial M}{\partial y}\delta y \tag{5.73}$$

where we have defined the *absolute momentum*, $M \equiv fy - u_g$.

This equation is mathematically of the same form as (2.52), the equation for the motion of a vertically displaced particle in a stratified atmosphere. Depending on the sign of the coefficient on the right side in (5.73), the parcel will either be forced to return to its original position or will accelerate further from that position. This coefficient thus determines the condition for *inertial instability*:

$$f\frac{\partial M}{\partial y} = f\left(f - \frac{\partial u_g}{\partial y}\right)\begin{cases} > 0 & \text{stable} \\ = 0 & \text{neutral} \\ < 0 & \text{unstable}\end{cases} \tag{5.74}$$

Viewed in an inertial reference frame, instability results from an imbalance between the pressure gradient and inertial forces for a parcel displaced radially in an axisymmetric vortex. In the Northern Hemisphere, where f is positive, the flow is inertially stable provided that the absolute vorticity of the basic flow, $\partial M/\partial y$, is positive. In the Southern Hemisphere, however, inertial stability requires that the absolute vorticity be negative. Observations show that for extratropical synoptic-scale systems the flow is always inertially stable, although near neutrality often occurs on the anticyclonic shear side of upper-level jet streaks. The occurrence of inertial instability over a large area would immediately trigger inertially unstable motions, which would mix the fluid laterally just as convection mixes it vertically, and reduce the shear until the absolute vorticity times f was again positive. (This explains why anticyclonic shears cannot become arbitrarily large.)

5.5.2 Rossby and Inertia–Gravity Waves

When the flow is both inertially and gravitationally stable, parcel displacements are resisted by both rotation and buoyancy. The resulting oscillations are called *inertia–gravity waves*. The dispersion relation for such waves can be analyzed using a variant of the parcel method applied in Section 5.4 We consider parcel oscillations along a slantwise path in the (y, z) plane as shown in Figure 5.11. For a vertical displacement δz, the buoyancy force component parallel to the slope of the parcel oscillation is $-N^2 \delta z \cos\alpha$, and for a meridional displacement δy the Coriolis (inertial) force component parallel to the slope of the parcel path is $-f^2\, \delta y \sin\alpha$, where we have assumed that the geostrophic basic flow is constant in latitude. Thus, the harmonic oscillator equation for the parcel (5.46) is modified to the form

$$\frac{D^2 \delta s}{Dt^2} = -(f \sin\alpha)^2\, \delta s - (N \cos\alpha)^2\, \delta s \tag{5.75}$$

where δs is again the perturbation parcel displacement.

The frequency now satisfies the dispersion relationship

$$\nu^2 = N^2 \cos^2\alpha + f^2 \sin^2\alpha \tag{5.76}$$

Since in general $N^2 > f^2$, (5.76) indicates that inertia–gravity wave frequencies must lie in the range $f \leq |\nu| \leq N$. The frequency approaches N as the trajectory slope approaches the vertical, and approaches f as the trajectory slope approaches the horizontal. For typical midlatitude tropospheric conditions, inertia–gravity wave periods are in the approximate range of 12 min to 15 h. Rotational effects become important, however, only when the second term

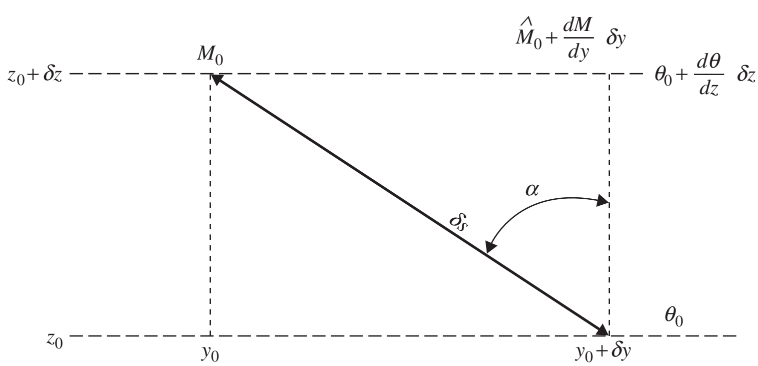

FIGURE 5.11 Parcel oscillation path in the meridional plane for an inertia–gravity wave. (See text for definition of symbols.)

on the right in (5.76) is similar in magnitude to the first term. This requires that $\tan^2 \alpha \sim N^2/f^2 = 10^4$, in which case it is clear from (5.76) that $\nu \ll N$. Thus, only low-frequency gravity waves are modified significantly by Earth's rotation, and these have very small parcel trajectory slopes.

The heuristic parcel derivation can again be verified using the linearized dynamical equations. In this case, however, it is necessary to include rotation. The small parcel trajectory slopes of the relatively long period waves that are altered significantly by rotation imply that the horizontal scales are much greater than the vertical scales for these waves. Therefore, we may assume that the motions are in hydrostatic balance. If in addition we assume a motionless basic state, the linearized equations (5.59) through (5.62) are replaced by the set

$$\frac{\partial u'}{\partial t} - fv' + \frac{1}{\rho_0}\frac{\partial p'}{\partial x} = 0 \tag{5.77}$$

$$\frac{\partial v'}{\partial t} + fu' + \frac{1}{\rho_0}\frac{\partial p'}{\partial y} = 0 \tag{5.78}$$

$$\frac{1}{\rho_0}\frac{\partial p'}{\partial z} - \frac{\theta'}{\overline{\theta}}g = 0 \tag{5.79}$$

$$\frac{\partial u'}{\partial x} + \frac{\partial v'}{\partial y} + \frac{\partial w'}{\partial z} = 0 \tag{5.80}$$

$$\frac{\partial \theta'}{\partial t} + w'\frac{d\overline{\theta}}{dz} = 0 \tag{5.81}$$

The hydrostatic relationship in (5.79) may be used to eliminate θ' in (5.81) to yield

$$\frac{\partial}{\partial t}\left(\frac{1}{\rho_0}\frac{\partial p'}{\partial z}\right) + N^2 w' = 0 \tag{5.82}$$

Letting

$$\begin{aligned}
u' &= \mathrm{Re}\left[\hat{u}\exp i\,(kx + ly + mz - \nu t)\right] \\
v' &= \mathrm{Re}\left[\hat{v}\exp i\,(kx + ly + mz - \nu t)\right] \\
w' &= \mathrm{Re}\left[\hat{w}\exp i\,(kx + ly + mz - \nu t)\right] \\
p'/\rho_0 &= \mathrm{Re}\left[\hat{p}\exp i\,(kx + ly + mz - \nu t)\right]
\end{aligned}$$

and substituting into (5.77), (5.78), and (5.82), we obtain

$$\hat{u} = \left(\nu^2 - f^2\right)^{-1} (\nu k + ilf)\,\hat{p} \tag{5.83}$$

$$\hat{v} = \left(\nu^2 - f^2\right)^{-1} (\nu l - ikf)\,\hat{p} \tag{5.84}$$

$$\hat{w} = -\left(\nu m/N^2\right)\hat{p} \tag{5.85}$$

which with the aid of (5.80) yields the dispersion relation

$$m^2\nu^3 - \left[N^2(k^2 + l^2) + f^2 m^2\right]\nu = 0 \tag{5.86}$$

As in the shallow water dispersion relationship (5.31), there exists a zero root corresponding to stationary Rossby waves. Time independence implies geostrophic flow from (5.77) and (5.78), and from (5.81) that $w' = 0$.

For $\nu \neq 0$, we have the classic dispersion relationship for hydrostatic inertia–gravity waves,

$$\nu^2 = f^2 + N^2\left(k^2 + l^2\right)m^{-2} \tag{5.87}$$

Because hydrostatic waves must have $(k^2 + l^2)/m^2 \ll 1$, (5.87) indicates that for vertical propagation to be possible (m real) the frequency must satisfy the inequality $|f| < |\nu| \ll N$. Equation (5.87) is just the limit of (5.76) when we let

$$\sin^2\alpha \rightarrow 1, \cos^2\alpha = \left(k^2 + l^2\right)/m^2$$

which is consistent with the hydrostatic approximation. Note also that (5.87) may be approximated exactly by the shallow water dispersion relationship (5.32) if one uses the "equivalent depth" of $\overline{h} = \frac{N^2}{gm^2}$ for the water depth.

If axes are chosen to make $l = 0$ (Figure 5.7), it may be shown (see Problem 5.14) that the ratio of the vertical to the horizontal components of group velocity is given by

$$\left|c_{gz}/c_{gx}\right| = |k/m| = \left(\nu^2 - f^2\right)^{1/2}/N \tag{5.88}$$

Thus, for fixed υ, inertia–gravity waves propagate more closely to the horizontal than pure internal gravity waves. However, as in the latter case the group velocity vector is again parallel to lines of constant phase.

Eliminating $\hat{p}$ between (5.83) and (5.84) for the case $l = 0$ yields the relationship $\hat{v} = -if\hat{u}/\nu$, from which it is easily verified that if $\hat{u}$ is real, the perturbation horizontal motions satisfy the relations

$$u' = \hat{u}\cos(kx + mz - \nu t), \quad v' = \hat{u}(f/\nu)\sin(kx + mz - \nu t) \tag{5.89}$$

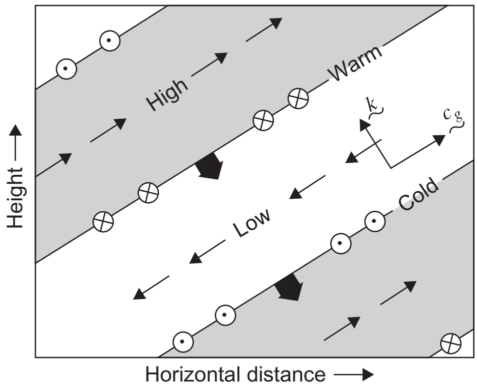

FIGURE 5.12 Vertical section in a plane containing the wave vector $\boldsymbol{k}$ showing the phase relationships among velocity, geopotential, and temperature fluctuations in an upward propagating inertia–gravity wave with $m < 0$, $\nu > 0$, and $f > 0$ (Northern Hemisphere). *Thin sloping lines* denote the surfaces of constant phase (perpendicular to the wave vector), and *thick arrows* show the direction of phase propagation. *Thin arrows* show the perturbation zonal and vertical velocity fields. Meridional wind perturbations are shown by *arrows* pointed into the page (northward) and out of the page (southward). Note that the perturbation wind vector turns clockwise (anticyclonically) with height. (*After Andrews et al., 1987.*)

so that the horizontal velocity vector rotates anticyclonically (that is, clockwise in the Northern Hemisphere) with time. As a result, parcels follow elliptical trajectories in a plane orthogonal to the wave number vector. Equations (5.89) also show that the horizontal velocity vector turns anticyclonically with height for waves with upward energy propagation (e.g., waves with $m < 0$ and $\nu < 0$). These characteristics are illustrated by the vertical cross-section shown in Figure 5.12. The anticyclonic turning of the horizontal wind with height and time is a primary method for identifying inertia–gravity oscillations in meteorological data.

A linearized vorticity equation is derived from $\partial/\partial x$ (5.78) $-\partial/\partial y$ (5.77), which gives

$$\frac{\partial \zeta'}{\partial t} = -f\left(\frac{\partial u'}{\partial x} + \frac{\partial v'}{\partial y}\right) = f\frac{\partial w'}{\partial z} \tag{5.90}$$

From (5.81) $\partial w'/\partial z$ may be eliminated from (5.90) to give the linearized potential vorticity equation

$$\frac{\partial \Pi'}{\partial t} = 0 \tag{5.91}$$

This states that the linearized PV

$$\Pi' = \zeta' + f\frac{\partial}{\partial z}\left(\frac{\theta'}{d\bar{\theta}/dz}\right) \tag{5.92}$$

is conserved at every point in space, as was the case for linear shallow water waves. Polarization relationships (5.83) and (5.84) for the $l = 0$ case can be used to show that for Rossby waves

$$\zeta' = -\frac{k^2}{f}\hat{p} \tag{5.93}$$

and for inertia–gravity waves

$$\zeta' = \frac{fm^2}{N^2}\hat{p} \tag{5.94}$$

This result may be used to show (see Problem 5.16) that if the buoyancy frequency, N, is constant, inertia-gravity waves have zero linearized potential vorticity (5.92). Therefore, as in linearized shallow water, the linearized potential vorticity equation (5.91) effectively filters gravity waves from the dynamics. We will exploit this fact in the next section, where we show that geostrophic balance emerges in the long-time limit for arbitrary initial states. This result also motivates the derivation of the quasi-geostrophic equations in Chapter 6, which essentially generalizes (5.91) to include nonlinear advection of linearized PV (5.92).

5.6 ADJUSTMENT TO GEOSTROPHIC BALANCE

This section investigates the process by which geostrophic balance is achieved from an unbalanced initial condition—that is, the *adjustment* process. For simplicity we utilize the linearized shallow water equations of Section 5.3.2; similar considerations apply to a continuously stratified atmosphere. The problem addressed here is the solution of the full linearized equations (5.25) in the limit of large time, starting from an arbitrary initial condition.

The key to solving this problem comes from (5.42), the linearized shallow water potential vorticity equation,

$$\frac{\partial Q'}{\partial t} = 0 \tag{5.95}$$

where Q' designates the perturbation potential vorticity. This implies the conservation relationship

$$Q'(x, y, t) = \zeta'/f - h'/\overline{h} = \text{Const.} \tag{5.96}$$

Thus, if we know the distribution of Q' at the initial time, we know Q' for all time

$$Q'(x, y, t) = Q'(x, y, 0)$$

and the final adjusted state can be determined without solving the time-dependent problem. Note that, in general, u', v', and h' evolve in time, but only in such a way that Q' is constant at every point in space.

This problem was first solved by Rossby in the 1930s and is often referred to as the Rossby adjustment problem. As a simplified, albeit somewhat unrealistic, example of the adjustment process, we consider an idealized shallow water system on a rotating plane with initial conditions

$$u', v' = 0; \quad h' = -h_0 \operatorname{sgn}(x) \tag{5.97}$$

where $\operatorname{sgn}(x) = 1$ for $x > 0$ and $\operatorname{sgn}(x) = -1$ for $x < 0$. This corresponds to an initial step function in h' at $x = 0$, with the fluid motionless. Thus, from (5.96)

$$\left(\zeta'/f\right) - \left(h'/\bar{h}\right) = \left(h_0/\bar{h}\right) \operatorname{sgn}(x) \tag{5.98}$$

Using (5.98) to eliminate ζ' in (5.27) yields

$$\frac{\partial^2 h'}{\partial t^2} - c^2\left(\frac{\partial^2 h'}{\partial x^2} + \frac{\partial^2 h'}{\partial y^2}\right) + f^2 h' = -f^2 h_0 \operatorname{sgn}(x) \tag{5.99}$$

where $c^2 = g\bar{h}$.

Because initially h' is independent of y, it will remain so for all time. Thus, in the final steady state (5.99) becomes

$$-c^2 \frac{d^2 h'}{dx^2} + f^2 h' = -f^2 h_0 \operatorname{sgn}(x) \tag{5.100}$$

which has the solution

$$\frac{h'}{h_0} = \begin{Bmatrix} -1 + \exp\left(-x/\lambda_R\right) & \text{for } x > 0 \\ +1 - \exp\left(+x/\lambda_R\right) & \text{for } x < 0 \end{Bmatrix} \tag{5.101}$$

where $\lambda_R \equiv f_0^{-1}\sqrt{g\bar{h}}$ is the Rossby *radius of deformation*. Hence, the radius of deformation may be interpreted as the horizontal length scale over which the height field adjusts during the approach to geostrophic equilibrium. For $|x| \gg \lambda_R$ the original h' remains unchanged. Substituting from (5.101) into (5.25) shows that the steady velocity field is geostrophic and nondivergent:

$$u' = 0, \quad \text{and} \quad v' = \frac{g}{f}\frac{\partial h'}{\partial x} = -\frac{g h_0}{f \lambda_R} \exp\left(-|x|/\lambda_R\right) \tag{5.102}$$

The steady-state solution (5.102) is shown in Figure 5.13.

Note that (5.102) could not be derived merely by setting $\partial/\partial t = 0$ in (5.25). That would yield geostrophic balance, and *any* distribution of h' would satisfy

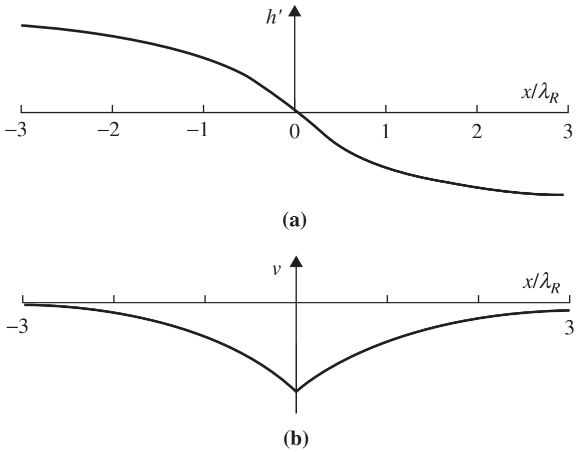

FIGURE 5.13 The geostrophic equilibrium solution corresponding to adjustment from the initial state defined in (5.97). (a) Final surface elevation profiles and (b) the geostrophic velocity profile in the final state. (*After Gill, 1982.*)

the equations:

$$fu' = -g\frac{\partial h'}{\partial y}, \quad fv' = g\frac{\partial h'}{\partial x}, \quad \frac{\partial u'}{\partial x} + \frac{\partial v'}{\partial y} = 0$$

Only by combining (5.25) to obtain the potential vorticity equation, and requiring the flow to satisfy potential vorticity conservation at all intermediate times, can the degeneracy of the geostrophic final state be eliminated. In other words, although any height field can satisfy the steady-state versions of (5.25), there is only one field that is consistent with a given initial state; this field can be found readily because it can be computed from the distribution of potential vorticity, which is conserved.

Although the final state can be computed without solving the time-dependent equation, if the evolution of the adjustment process is required, it is necessary to solve (5.99) subject to the initial conditions (5.97), which is beyond the scope of this discussion. We can, however, compute the amount of energy that is dispersed by gravity waves during the adjustment process. This only requires computing the energy change between initial and final states.

The potential energy per unit horizontal area is given by

$$\int_0^{h'} \rho gz dz = \rho g h'^2/2$$

Thus, the potential energy released per unit length in y during adjustment is

$$\int_{-\infty}^{+\infty} \frac{\rho g h_0^2}{2} dx - \int_{-\infty}^{+\infty} \frac{\rho g h'^2}{2} dx$$
$$= 2 \int_{0}^{+\infty} \frac{\rho g h_0^2}{2} \left[1 - \left(1 - e^{-x/\lambda_R} \right)^2 \right] dx \tag{5.103}$$
$$= \frac{3}{2} \rho g h_0^2 \lambda_R$$

In the nonrotating case ($\lambda_R \to \infty$) all potential energy available initially is released (converted to kinetic energy) so that there is an infinite energy release. (Energy is radiated away in the form of gravity waves, leaving a flat free surface extending to $|x| \to \infty$ as $t \to \infty$.)

In the rotating case only the finite amount given in (5.103) is converted to kinetic energy, and only a portion of this kinetic energy is radiated away. The rest remains in the steady geostrophic circulation. The kinetic energy in the steady-state per unit length is

$$2 \int_{0}^{+\infty} \rho \bar{h} \frac{v'^2}{2} dx = \rho \bar{h} \left(\frac{g h_0}{f \lambda_R} \right)^2 \int_{0}^{+\infty} e^{-2x/\lambda_R} dx = \frac{1}{2} \rho g h_0^2 \lambda_R \tag{5.104}$$

Thus, in the rotating case a finite amount of potential energy is released, but only one-third of the potential energy released goes into the steady geostrophic flow. The remaining two-thirds is radiated away in the form of inertia–gravity waves. This simple analysis illustrates the following points

- It is difficult to extract the potential energy of a rotating fluid. Although there is an infinite reservoir of potential energy in this example (because h' is finite as $|x| \to \infty$), only a finite amount is converted before geostrophic balance is achieved.
- Conservation of potential vorticity allows one to determine the steady-state geostrophically adjusted velocity and height fields without carrying out a time integration.
- The length scale for the steady solution is the Rossby radius λ_R.

5.7 ROSSBY WAVES

The wave type that is of most importance for large-scale meteorological processes is the *Rossby wave*, or *planetary wave*. In an inviscid barotropic fluid of constant depth (where the divergence of the horizontal velocity must vanish), the Rossby wave is an absolute vorticity-conserving motion that owes its existence to the variation of the Coriolis parameter with latitude. More generally, in a baroclinic atmosphere, the Rossby wave is a potential vorticity-conserving motion that owes its existence to the gradient of potential vorticity.

The variation of the Coriolis parameter with latitude can be approximated by expanding the latitudinal dependence of f in a Taylor series about a reference latitude ϕ_0 and retaining only the first two terms to yield

$$f = f_0 + \beta y \tag{5.105}$$

where $\beta \equiv (df/dy)_{\phi_0} = 2\Omega \cos\phi_0/a$ and $y = 0$ at ϕ_0. This approximation is usually referred to as the *midlatitude β-plane* approximation. Rossby wave propagation can be understood in a qualitative fashion by considering a closed chain of fluid parcels initially aligned along a circle of latitude. Recall that the absolute vorticity η is given by $\eta = \zeta + f$, where ζ is the relative vorticity and f is the Coriolis parameter. Assume that $\zeta = 0$ at time t_0. Now suppose that at t_1, δy is the meridional displacement of a fluid parcel from the original latitude. Then at t_1 we have

$$(\zeta + f)_{t_1} = f_{t_0}$$

or

$$\zeta_{t_1} = f_{t_0} - f_{t_1} = -\beta \delta y \tag{5.106}$$

where $\beta \equiv df/dy$ is the planetary vorticity gradient at the original latitude.

From (5.106) it is evident that if the chain of parcels is subject to a sinusoidal meridional displacement under absolute vorticity conservation, the resulting perturbation vorticity will be positive for a southward displacement and negative for a northward displacement.

This perturbation vorticity field will induce a meridional velocity field, which advects the chain of fluid parcels southward west of the vorticity maximum and northward west of the vorticity minimum, as indicated in Figure 5.14.

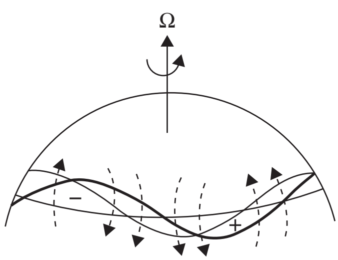

FIGURE 5.14 Perturbation vorticity field and induced velocity field (*dashed arrows*) for a meridionally displaced chain of fluid parcels. The *heavy wavy line* shows original perturbation position; the *light line* shows westward displacement of the pattern due to advection by the induced velocity.

Thus, the fluid parcels oscillate back and forth about their equilibrium latitude, and the pattern of vorticity maxima and minima propagates to the west. This westward propagating vorticity field constitutes a Rossby wave. Just as a positive vertical gradient of potential temperature resists vertical fluid displacements and provides the restoring force for gravity waves, the meridional gradient of absolute vorticity resists meridional displacements and provides the restoring mechanism for Rossby waves.

The speed of westward propagation, c, can be computed for this simple example by letting $\delta y = a \sin[k(x - ct)]$, where a is the maximum northward displacement. Then $v = D(\delta y)/Dt = -kca \cos[k(x - ct)]$, and

$$\zeta = \partial v/\partial x = k^2 ca \sin[k(x - ct)]$$

Substitution for δy and ζ in (5.106) then yields

$$k^2 ca \sin[k(x - ct)] = -\beta a \sin[k(x - ct)]$$

or

$$c = -\beta/k^2 \tag{5.107}$$

Thus, the phase speed is westward relative to the mean flow and is inversely proportional to the square of the zonal wave number.

5.7.1 Free Barotropic Rossby Waves

The dispersion relationship for barotropic Rossby waves may be derived formally by finding wave-type solutions of the linearized barotropic vorticity equation. The barotropic vorticity equation (4.41) states that the vertical component of absolute vorticity is conserved following the horizontal motion. For a midlatitude β-plane this equation has the form

$$\left(\frac{\partial}{\partial t} + u\frac{\partial}{\partial x} + v\frac{\partial}{\partial y}\right)\zeta + \beta v = 0 \tag{5.108}$$

We now assume that the motion consists of a constant basic state zonal velocity plus a small horizontal perturbation:

$$u = \overline{u} + u', \quad v = v', \quad \zeta = \partial v'/\partial x - \partial u'/\partial y = \zeta'$$

We define a perturbation streamfunction ψ' according to

$$u' = -\partial\psi'/\partial y, \quad v' = \partial\psi'/\partial x$$

from which $\zeta' = \nabla^2\psi'$. The perturbation form of (5.108) is then

$$\left(\frac{\partial}{\partial t} + \overline{u}\frac{\partial}{\partial x}\right)\nabla^2\psi' + \beta\frac{\partial\psi'}{\partial x} = 0 \tag{5.109}$$

where as usual we have neglected terms involving the products of perturbation quantities. We seek a solution of the form

$$\psi' = \mathrm{Re}\left[\Psi \exp(i\phi)\right]$$

where $\phi = kx + ly - \nu t$. Here k and l are wave numbers in the zonal and meridional directions, respectively. Substituting for ψ' in (5.109) gives

$$(-\nu + k\overline{u})\left(-k^2 - l^2\right) + k\beta = 0$$

which may immediately be solved for ν:

$$\nu = \overline{u}k - \beta k/K^2 \tag{5.110}$$

where $K^2 \equiv k^2 + l^2$ is the total horizontal wave number squared.

Recalling that $c = \nu/k$, we find that the zonal phase speed relative to the mean wind is

$$c - \overline{u} = -\beta/K^2 \tag{5.111}$$

which reduces to (5.109) when the mean wind vanishes and $l \to 0$. Thus, the Rossby wave zonal phase propagation is always *westward* relative to the mean zonal flow. Furthermore, the Rossby wave phase speed depends inversely on the square of the horizontal wave number. Therefore, Rossby waves are dispersive waves whose phase speeds increase rapidly with increasing wavelength.

For a typical midlatitude synoptic-scale disturbance, with similar meridional and zonal scales ($l \approx k$) and zonal wavelength of order 6000 km, the Rossby wave speed relative to the zonal flow calculated from (5.111) is approximately -8 m s^{-1}. Because the mean zonal wind is generally westerly and greater than 8 m s^{-1}, synoptic-scale Rossby waves usually move eastward, but at a phase speed relative to the ground that is somewhat less than the mean zonal wind speed. For longer wavelengths the westward Rossby wave phase speed may be large enough to balance the eastward advection by the mean zonal wind so that the resulting disturbance is stationary relative to Earth's surface. From (5.111) it is clear that the free Rossby wave solution becomes stationary when

$$K^2 = \beta/\overline{u} \equiv K_s^2 \tag{5.112}$$

The significance of this condition is discussed in the next subsection.

Unlike the phase speed, which is always westward relative to the mean flow, the zonal group velocity for a Rossby wave may be either eastward or westward relative to the mean flow, depending on the ratio of the zonal and meridional wave numbers (see Problem 5.20). Stationary Rossby modes (i.e., modes with $c = 0$) have zonal group velocities that are eastward relative to the ground. Synoptic-scale Rossby waves also tend to have zonal group velocities that are eastward relative to the ground. For synoptic waves, advection by the mean zonal wind is generally larger than the Rossby phase speed so that the phase speed is also eastward relative to the ground, but is slower than the zonal group velocity. As shown earlier in Figure 5.4b, this implies that new disturbances tend to develop downstream of existing disturbances, which is an important consideration for forecasting.

It is possible to carry out a less restrictive analysis of free planetary waves using the perturbation form of the full primitive equations. In that case the structure of the free modes depends critically on the boundary conditions at the surface and the upper boundary. The results of such an analysis are mathematically complicated, but qualitatively yield waves with horizontal dispersion properties similar to those in the shallow water model. It turns out that the free oscillations allowed in a hydrostatic gravitationally stable atmosphere consist of eastward- and westward-moving gravity waves that are slightly modified by Earth's rotation and westward-moving Rossby waves that are slightly modified by gravitational stability. These free oscillations are the normal modes of oscillation of the atmosphere. As such, they are continually excited by the various forces acting on the atmosphere. Planetary scale-free oscillations, although they can be detected by careful observational studies, generally have rather weak amplitudes. Presumably this is because the forcing is quite weak at the large phase speeds characteristic of most such waves. An exception is the 16-day period zonal wave number 1 normal mode, which can be quite strong in the winter stratosphere.

5.7.2 Forced Topographic Rossby Waves

Although free propagating Rossby modes are only rather weakly excited in the atmosphere, forced stationary Rossby modes are of primary importance for understanding the planetary-scale circulation pattern. Such modes may be forced by longitudinally dependent diabatic heating patterns or by flow over topography. Of particular importance for the Northern Hemisphere extratropical circulation are stationary Rossby modes forced by flow over the Rockies and the Himalayas. It is just the topographic Rossby wave that was described qualitatively in the discussion of streamline deflections in potential vorticity-conserving flows crossing mountain ranges in Section 4.3.

As the simplest possible dynamical model of topographic Rossby waves, we use a modified version of the the shallow potential vorticity equation (4.39). We assume that the upper boundary is at a fixed height H, and the lower boundary is at the variable height $h_T(x, y)$ where $|h_T| \ll H$. We also approximate ζ by the geostrophic value, ζ_g, and assume that $|\zeta_g| \ll f_0$. We can then approximate (4.39) by

$$H\left(\frac{\partial}{\partial t} + \mathbf{V}\cdot\mathbf{\nabla}\right)(\zeta_g + f) = -f_0\frac{Dh_T}{Dt} \tag{5.113}$$

Linearizing and applying the midlatitude β-plane approximation yields

$$\left(\frac{\partial}{\partial t} + \bar{u}\frac{\partial}{\partial x}\right)\zeta_g' + \beta v_g' = -\frac{f_0}{H}\bar{u}\frac{\partial h_T}{\partial x} \tag{5.114}$$

We now examine solutions of (5.114) for the special case of a sinusoidal lower boundary. We specify the topography to have the form

$$h_T(x, y) = \mathrm{Re}\,[h_0 \exp(ikx)] \cos ly \tag{5.115}$$

and represent the geostrophic wind and vorticity by the perturbation streamfunction

$$\psi(x, y) = \mathrm{Re}\,[\psi_0 \exp(ikx)] \cos ly \tag{5.116}$$

Then (5.114) has a steady-state solution with complex amplitude given by

$$\psi_0 = f_0 h_0 / \left[H\left(K^2 - K_s^2\right)\right] \tag{5.117}$$

The streamfunction is either exactly in phase (ridges over the mountains) or exactly out of phase (troughs over the mountains), with the topography depending on the sign of $K^2 - K_s^2$. For long waves ($K < K_s$) the topographic vorticity source in (5.114) is balanced primarily by the meridional advection of planetary vorticity (the β effect). For short waves ($K > K_s$) the source is balanced primarily by the zonal advection of relative vorticity.

The topographic wave solution (5.117) has the unrealistic characteristic that when the wave number exactly equals the critical wave number K_s, the amplitude goes to infinity. From (5.112) it is clear that this singularity occurs at the zonal wind speed for which the free Rossby mode becomes stationary. Thus, it may be thought of as a resonant response of the barotropic system.

Charney and Eliassen (1949) used the topographic Rossby wave model to explain the winter mean longitudinal distribution of 500-hPa heights in Northern Hemisphere midlatitudes. They removed the resonant singularity by including boundary layer drag in the form of Ekman pumping, which for the barotropic vorticity equation is simply a linear damping of the relative vorticity (see Section 8.3.4). The vorticity equation thus takes the form

$$\left(\frac{\partial}{\partial t} + \bar{u}\frac{\partial}{\partial x}\right)\zeta_g' + \beta v_g' + r\zeta_g' = -\frac{f_0}{H}\bar{u}\frac{\partial h_T}{\partial x} \tag{5.118}$$

where $r \equiv \tau_e^{-1}$ is the inverse of the spin-down time defined in (8.37).

For steady flow, (5.118) has a solution with complex amplitude

$$\psi_0 = f_0 h_0 / \left[H\left(K^2 - K_s^2 - i\varepsilon\right)\right] \tag{5.119}$$

where $\varepsilon \equiv rK^2\,(k\bar{u})^{-1}$. Thus, boundary layer drag shifts the response's phase and removes the singularity at resonance. However, the amplitude is still a maximum for $K = K_s$ and the trough in the streamfunction occurs one-quarter cycle east of the mountain crest, in approximate agreement with observations.

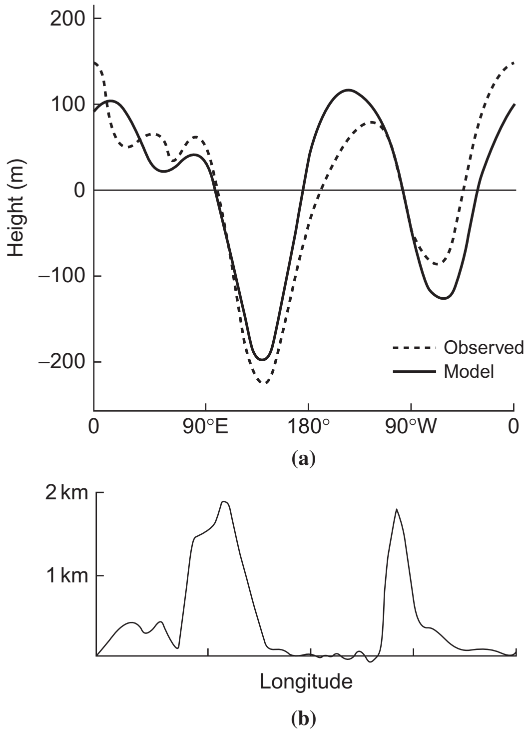

FIGURE 5.15 (a) Longitudinal variation of the disturbance in geopotential height ($\equiv f_0\Psi/g$) in the Charney–Eliassen model for the parameters given in the text (*solid line*) compared with the observed 500-hPa height perturbations at 45°N in January (*dashed line*). (b) Smoothed profile of topography at 45°N used in the computation. (*After Held, 1983.*)

By use of a Fourier expansion, (5.118) can be solved for realistic distributions of topography. The results for an x-dependence of h_T given by a smoothed version of Earth's topography at 45°N, a meridional wave number corresponding to a latitudinal half-wavelength of 35°, $\tau_e = 5$ days, $\bar{u} = 17$ m s^{-1}, $f_0 = 10^{-4}$ s^{-1}, and $H = 8$ km are shown in Figure 5.15. Despite its simplicity, the Charney–Eliassen model does a remarkable job of reproducing the observed 500-hPa stationary wave pattern in Northern Hemisphere midlatitudes.

SUGGESTED REFERENCES

Chapman and Lindzen, *Atmospheric Tides*: *Thermal and Gravitational*, is the classic reference on both observational and theoretical aspects of tides, a class of atmospheric motions for which the linear perturbations method has proved to be particularly successful.

Gill, *Atmosphere-Ocean Dynamics*, has a very complete treatment of gravity, inertia–gravity, and Rossby waves, with particular emphasis on observed oscillations in the oceans.

Hildebrand, *Advanced Calculus for Applications*, is one of many standard textbooks that discuss the mathematical techniques used in this chapter, including the representation of functions in Fourier series and the general properties of the wave equation.

Nappo, *An Introduction to Atmospheric Gravity Waves*, is an excellent introduction to the theory and observation of gravity waves in the atmosphere.

Scorer, *Natural Aerodynamics*, contains an excellent qualitative discussion on many aspects of waves generated by barriers such as lee waves.

PROBLEMS

5.1. Show that the Fourier component $F(x) = \mathrm{Re}\,[C \exp(imx)]$ can be written as

$$F(x) = |C| \cos m (x + x_0)$$

where $x_0 = m^{-1} \sin^{-1}(C_i/|C|)$ and C_i stands for the imaginary part of C.

5.2. In the study of atmospheric wave motions, it is often necessary to consider the possibility of amplifying or decaying waves. In such a case we might assume that a solution has the form

$$\psi = A \cos(kx - \nu t - kx_0) \exp(\alpha t)$$

where A is the initial amplitude, α the amplification factor, and x_0 the initial phase. Show that this expression can be written more concisely as

$$\psi = \mathrm{Re}\left[Be^{ik(x-ct)}\right]$$

where both B and c are complex constants. Determine the real and imaginary parts of B and c in terms of A, α, k, ν, and x_0.

5.3. Several of the wave types discussed in this chapter are governed by equations that are generalizations of the wave equation

$$\frac{\partial^2 \psi}{\partial t^2} = c^2 \frac{\partial^2 \psi}{\partial x^2}$$

This equation can be shown to have solutions corresponding to waves of arbitrary profile moving at the speed c in both positive and negative x directions. We consider an arbitrary initial profile of the field ψ; $\psi = f(x)$ at $t = 0$. If the profile is translated in the positive x direction at speed c without change of shape, then $\psi = f(x')$, where x' is a coordinate moving at speed c so that $x = x' + ct$. Thus, in terms of the fixed coordinate x we can write $\psi = f(x - ct)$, corresponding to a profile that moves in the positive x direction at speed c without change of shape. Verify that $\psi = f(x - ct)$ is a solution for any arbitrary continuous profile $f(x - ct)$. [*Hint*: Let $x - ct = x'$ and differentiate f using the chain rule.]

5.4. Assuming that the pressure perturbation for a one-dimensional acoustic wave is given by (5.23), find the corresponding solutions of the zonal wind and density perturbations. Express the amplitude and phase for u' and ρ' in terms of the amplitude and phase of p'.

5.5. Show that for isothermal motion ($DT/Dt = 0$) the acoustic wave speed is given by $(gH)^{1/2}$, where $H = RT/g$ is the scale height.

5.6. In Section 5.3.1 the linearized equations for acoustic waves were developed for the special situation of one-dimensional propagation in a horizontal tube. Although this situation does not appear to be directly applicable to the atmosphere, there is a special atmospheric mode, the *Lamb wave*, which is a horizontally propagating acoustic mode with no vertical velocity perturbation ($w' = 0$). Such oscillations have been observed following violent explosions such as volcanic eruptions and atmospheric nuclear tests. Using (5.20) and (5.21), plus the linearized forms of the hydrostatic equation, and the continuity equation (5.15), derive the height dependence of the perturbation fields for the Lamb mode in an isothermal basic state atmosphere, assuming that the pressure perturbation at the lower boundary ($z = 0$) has the form (5.23). Determine the vertically integrated kinetic energy density per unit horizontal area for this mode.

5.7. If the surface height perturbation in a shallow water gravity wave is given by

$$h' = \mathrm{Re}\left[Ae^{ik(x-ct)}\right]$$

find the corresponding velocity perturbation $u'(x, t)$. Sketch the phase relationship between h' and u' for an eastward propagating wave.

5.8. Assuming that the vertical velocity perturbation for a two-dimensional internal gravity wave is given by (5.65), obtain the corresponding solution for the u', p', and θ' fields. Use these results to verify the approximation

$$\left|\rho_0\theta'/\overline{\theta}\right| \gg \left|p'/c_s^2\right|$$

which was used in (5.58).

5.9. For the situation in the preceding problem, express the vertical flux of horizontal momentum, $\rho_0\overline{u'w'}$, in terms of the amplitude A of the vertical velocity perturbation. Hence, show that the momentum flux is positive for waves in which phase speed propagates eastward and downward.

5.10. Show that if (5.60) is replaced by the hydrostatic equation (i.e., the terms in w' are neglected), the resulting frequency equation for internal gravity waves is just the asymptotic limit of (5.66) for waves in which $|k| \ll |m|$.

5.11. **(a)** Show that the intrinsic group velocity vector in two-dimensional internal gravity waves is parallel to lines of constant phase.

(b) Show that in the long-wave limit ($|k| \ll |m|$) the magnitude of the zonal component of the group velocity equals the magnitude of the zonal phase speed so that energy propagates one wavelength per wave period.

5.12. Determine the perturbation horizontal and vertical velocity fields for stationary gravity waves forced by flow over sinusoidally varying topography given the following conditions: The height of the ground is $h = h_0 \cos kx$, where $h_0 = 50$ m is a constant; $N = 2 \times 10^{-2}\ \mathrm{s}^{-1}$; $\overline{u} = 5\ \mathrm{m\,s}^{-1}$; and $k = 3 \times 10^{-3}\ \mathrm{m}^{-1}$. *Hint*: For small-amplitude topography ($h_0 k \ll 1$) we can approximate the lower boundary condition by

$$w' = Dh/Dt = \overline{u}\partial h/\partial x \quad \text{at z} = 0$$

5.13. Verify the group velocity relationship for inertia–gravity waves that are given in (5.88).

5.14. Show that when $\overline{u} = 0$ the wave number vector $\boldsymbol{\kappa}$ for an internal inertia–gravity wave is perpendicular to the group velocity vector.

5.15. Derive an expression for the group velocity of a barotropic Rossby wave with dispersion relation (5.110). Show that for stationary waves the group velocity always has an eastward zonal component relative to Earth. Hence, Rossby wave energy propagation must be downstream of topographic sources.

5.16. Prove that the internal gravity waves of Section 5.5.2 have zero linearized potential vorticity in the case of constant buoyancy frequency, N.

MATLAB Exercises

M5.1. **(a)** The MATLAB script **phase_demo.m** shows that the Fourier series $F(x) = A\sin(kx) + B\cos(kx)$ is equivalent to the form $F(x) = \mathrm{Re}\, C\exp(ikx)$ where A and B are real coefficients and C is a complex coefficient. Modify the MATLAB script to confirm that the expression $F(x) = |C|\cos k(x + x_0) = |C|\cos(kx + \alpha)$ represents the same Fourier series where $kx_0 \equiv \alpha = \sin^{-1}(C_i/|C|)$, C_i stands for the imaginary part of C, α is the "phase" defined in the MATLAB script. Plot your results as the third subplot in the script.

(b) By running the script for several input phase angles (e.g., 0, 30, 60, and 90°), determine the relationship between α and the location of the maximum of $F(x)$.

M5.2. In this problem you will examine the formation of a "wave envelope" for a combination of dispersive waves. The example is that of a deep water wave in which the group velocity is half of the phase velocity. The MATLAB script **grp_vel_3.m** has code to show the wave height field at four different times for a group composed of various numbers of waves with differing wave numbers and frequencies. Study the code and determine the period and wavelength of the carrier wave. Then run the script several times, varying the number of wave modes from 4 to 32. Determine the half-width of the envelope at time $t = 0$ (top line on the graph) as a function of the number of modes in the group. The half-width is here defined as two times the distance from the point of maximum amplitude ($x = 0$) to the point along the envelope where the amplitude is half the maximum. You can estimate this from the graph using the **ginput** command to determine the distance. Use MATLAB to plot a curve of the half-width versus number of wave modes.

M5.3. The script **geost_adjust_1.m** together with the function **yprim_adj_1.m** illustrates one-dimensional geostrophic adjustment of the velocity field in a barotropic model for a sinusoidally varying initial height field. The equations are a simplification of (5.25) in the text for the case of no y dependence. Initially $u' = v' = 0,\ \phi' \equiv gh' = 9.8\cos(kx)$. The final balanced wind in this case will have only a meridional component. Run the program **geost_adjust_1.m** for the cases of latitude 30 and 60°, choosing a time value of at least 10 days. For each of these cases choose values of wavelength of 2000, 4000, 6000, and 8000 km (a total of eight runs). Construct a table showing the initial and final values of the fields u', v', ϕ' and the ratio of the final energy to the initial energy. You can read the values from the MATLAB graphs by using the **ginput** command or, for greater accuracy, add lines in the MATLAB code to print out the values needed. Modify the MATLAB script to determine the partition of final state energy per unit mass between the kinetic energy ($v'^2/2$) and the potential energy $\phi'^2/(2gH)$. Compute the ratio of final kinetic energy to potential energy for each of your eight cases and show this in a table.

M5.4. The script **geost_adjust_2.m** together with the function **yprim_adj_2.m** extends Problem M5.3 by using Fourier expansion to examine the geostrophic adjustment for an isolated initial height disturbance of the form $h_0(x) = -h_m/\left[1 + (x/L)^2\right]$. The version given here uses 64 Fourier modes and employs a fast Fourier transform algorithm (FFT). (There are 128 modes in the FFT, but only one-half of them provide real information.) In this case you may run the model for only 5 days of integration time (it requires a lot of computation compared to the previous case). Choose an initial zonal scale of the disturbance of 500 km and run the model for latitudes (in degrees) of 15, 30, 45, 60, 75, and 90 (six runs). Study the animations for each case. Note that the zonal flow is entirely in a gravity wave mode that propagates away from the initial disturbance. The meridional flow has a propagating gravity wave component, but also a geostrophic part (cyclonic flow). Use the **ginput** command to estimate the zonal scale of the final geostrophic flow (v component) by measuring the distance from the negative velocity maximum just west of the center to the positive maximum just east of the center. Plot a curve showing the zonal scale as a function of latitude. Compare this scale with the Rossby radius of deformation defined in the text. (Note that $gH = 400\ \mathrm{m^2\ s^{-2}}$ in this example.)

M5.5. This problem examines the variation of phase velocity for Rossby waves as the zonal wavelength is varied. Run the MATLAB program **rossby_1.m** with zonal wavelengths specified as 5000, 10,000 and 20,000 km. For each of these cases try different values of the mean zonal wind until you find the mean wind for which the Rossby wave is approximately stationary.

M5.6. The MATLAB script **rossby_2.m** shows an animation of the Rossby waves generated by a vorticity disturbance initially localized in the center of the domain, with mean wind zero. Run the script and note that the waves excited have westward phase speeds, but that disturbances develop on the eastward side of the original disturbance. By following the development of these disturbances, make a crude estimate of the characteristic wavelength and the group velocity for the disturbances appearing to the east of the original disturbance at time $t = 7.5$ days. (Wavelength can be estimated by using **ginput** to measure the distance between adjacent troughs.) Compare your estimate with the group velocity formula derived from (5.108). Can you think of a reason why your estimate for group velocity may differ from that given in the formula?

M5.7. The MATLAB script **rossby_3.m** gives the surface height and meridional velocity disturbances for topographic Rossby waves generated by flow over an isolated ridge. The program uses a Fourier series approach to the solution. Ekman damping with a 2-day damping time is included to minimize the effect of waves propagating into the mountain from upstream (but this cannot be entirely avoided). Run this program for input zonal mean winds from 10 to

100 m/s at 10-m/s intervals. For each run use **ginput** to estimate the scale of the leeside trough by measuring the zonal distance between the minimum and maximum in the meridional velocity. (This should be equal approximately to one-half the wavelength of the dominant disturbance.) Compare your results in each case with the zonal wavelength for resonance given by solving (5.112) to determine the resonant $L_x = 2\pi/k$, where $K^2 = k^2 + l^2$ and $l = \pi/8 \times 10^6$ in units of 1/m. (Do not expect exact agreement because the actual disturbance corresponds to the sum over many separate zonal wavelengths.)

Chapter 6

Quasi-geostrophic Analysis

A primary goal of dynamic meteorology is to interpret the observed structure of large-scale atmospheric motions in terms of the physical laws governing the motions. These laws, which express the conservation of momentum, mass, and energy, completely determine the relationships among the pressure, temperature, and velocity fields. As we saw in Chapter 2, these governing laws are quite complicated even when the hydrostatic approximation (which is valid for all large-scale meteorological systems) is applied. For extratropical synoptic-scale motions, however, the horizontal velocities are approximately geostrophic (see Section 2.4). Such motions, which are usually referred to as *quasi-geostrophic*, are often simpler to analyze than are tropical disturbances or planetary-scale disturbances. They are also the major systems of interest in traditional short-range weather forecasting, and are thus a reasonable starting point for dynamical analysis.

In addition to the observation that extratropical weather systems are nearly geostrophic and hydrostatic, we found in the linear wave analyses of Chapter 5 that the properties of Rossby waves resemble these weather systems, whereas those of inertia–gravity waves do not. Specifically, Rossby waves have relatively slow phase speeds and nonzero potential vorticity, whereas the inertia–gravity waves are fast moving and have little or no potential vorticity. We will exploit these properties here in order to filter the full equations to a simpler set, the quasi-geostrophic (QG) equations. Before developing this system of equations, it is useful to briefly summarize the observed structure of midlatitude synoptic systems and the mean circulations in which they are embedded. We then develop the QG equations using potential vorticity and potential temperature, which provides one framework ("*PV Thinking*") for understanding. A second framework for dynamics ("*w Thinking*") is based on the diagnosis of vertical motion through an *"omega equation,"* and will also be thoroughly explored.

6.1 THE OBSERVED STRUCTURE OF EXTRATROPICAL CIRCULATIONS

Atmospheric circulation systems depicted on a synoptic chart rarely resemble the simple circular vortices discussed in Chapter 3. Rather, they are generally

An Introduction to Dynamic Meteorology. DOI: 10.1016/B978-0-12-384866-6.00006-4

highly asymmetric in form, with the strongest winds and largest temperature gradients concentrated along narrow bands called *fronts*. Also, such systems generally are highly baroclinic; the amplitudes and phases of the geopotential and velocity perturbations both change substantially with height. Part of this complexity is due to the fact that these synoptic systems are not superposed on a uniform mean flow, but are embedded in a slowly varying planetary scale flow that is itself highly baroclinic. Furthermore, this planetary scale flow is influenced by *orography* (i.e., by large-scale terrain variations) and continent-ocean heating contrasts so that it is highly longitude dependent. Therefore, while viewing synoptic systems as disturbances superposed on a zonal flow that varies only with latitude and height is a useful first approximation in theoretical analyses (see, e.g., Chapter 7), more complete descriptions require the observed zonal asymmetry.

Zonally averaged cross-sections do provide some useful information on the gross structure of the planetary scale circulation in which synoptic-scale eddies are embedded. Figure 6.1 shows meridional cross-sections of the longitudinally averaged zonal wind and temperature for the solstice seasons of (a) December, January, and February (DJF) and (b) June, July, and August (JJA). These sections extend from approximately sea level (1000 hPa) to about 32 km altitude (10 hPa). Thus, the troposphere and lower stratosphere are shown. This chapter is concerned with the structure of the wind and temperature fields in the troposphere, and the stratosphere is discussed in Chapter 12.

The average pole to equator temperature gradient in the Northern Hemisphere troposphere is much larger in winter than in summer. In the Southern Hemisphere the difference between summer and winter temperature distributions is smaller, due mainly to the large thermal inertia of the oceans, together with the greater fraction of the surface that is covered by oceans in the Southern Hemisphere. Since the mean zonal wind and temperature fields satisfy the thermal wind relationship to a high degree of accuracy, the seasonal cycle in zonal wind speeds is similar to that of the meridional temperature gradient. In the Northern Hemisphere the maximum zonal wind speed in the winter is twice as large as in the summer, whereas in the Southern Hemisphere the difference between winter and summer zonal wind maxima is much smaller. Furthermore, in both seasons the core of maximum zonal wind speed (called the mean jet stream axis) is located just below the *tropopause* (the boundary between the troposphere and stratosphere) at the latitude where the thermal wind integrated through the troposphere is a maximum. In both hemispheres, this is about 30° latitude during winter, but moves poleward to about 45° during summer.

The zonally averaged meridional cross-sections of Figure 6.1 are not representative of the mean wind structure at all longitudes, which can be seen in the distribution of the time-averaged zonal wind component for DJF on the 200-hPa surface in the Northern Hemisphere (Figure 6.2). It is clear that at some longitudes there are very large deviations of the time-mean zonal flow from its longitudinally averaged distribution. In particular, there are strong zonal wind

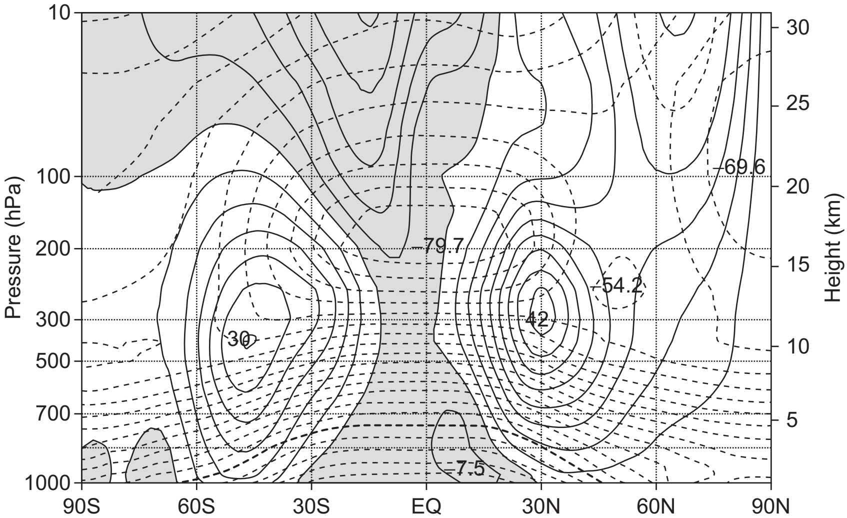

(a)

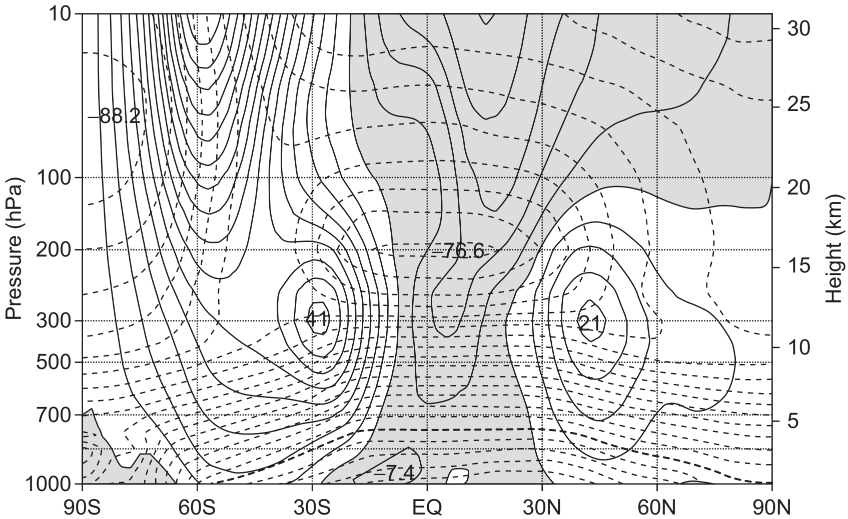

(b)

FIGURE 6.1 Meridional cross-sections of longitudinally and time-averaged zonal wind (*solid contours*, interval of 5 m s^{-1}) and temperature (*dashed contours*, interval of 5 K) for December–February (a) and June–August (b). Easterly winds are *shaded* and 0°C isotherm is *darkened*. Wind maxima shown in m s^{-1}, temperature minima shown in °C. (*Based on NCEP/NCAR reanalyses; after Wallace, 2003*.)

maxima (jets) near 30°N just east of the Asian and North American continents and north of the Arabian peninsula; distinct minima occur in the eastern Pacific and eastern Atlantic. Synoptic-scale disturbances tend to develop preferentially in the regions of maximum time-mean zonal winds associated with the western

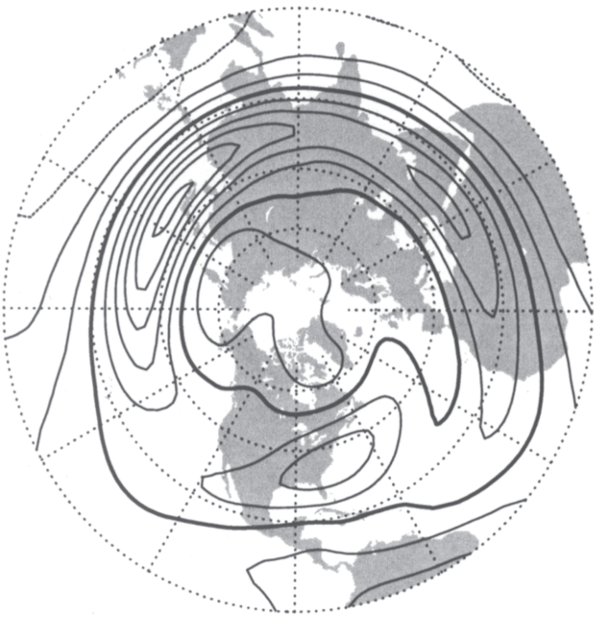

FIGURE 6.2 Mean zonal wind at the 200-hPa level for December through February, averaged for years 1958–1997. Contour interval 10 m s^{-1} (heavy contour, 20 m s^{-1}). (*Based on NCEP/NCAR reanalyses; after Wallace, 2003*.)

Pacific and western Atlantic jets and to propagate downstream along *storm tracks* that approximately follow the jet axes.

The large departure of the northern winter climatological jet stream from zonal symmetry can also be readily inferred from examination of Figure 6.3, which shows the mean 500-hPa geopotential contours for January and July in the Northern Hemisphere. Striking departures from zonal symmetry are apparent, which are linked to the distributions of continents and oceans. The most prominent asymmetries are the troughs in January to the east of the American and Asian continents. Referring to Figure 6.2, we see that the intense jet at 35°N and 140°E is a result of the semipermanent trough in that region. Thus, it is apparent that the mean flow in which synoptic systems are embedded should really be regarded as a longitude-dependent time-averaged flow. In northern summer, 500-hPa geopotential height increases much more over high latitudes as compared to the tropics due to warming in the polar region. As a result, the pole–equator temperature contrast is smaller than in winter, and the height contrast and jet stream are weaker and located at higher latitude.

In addition to its longitudinal dependence, the planetary scale flow also varies from day to day due to its interactions with transient synoptic-scale disturbances. In fact, observations show that the transient planetary scale flow amplitude is comparable to that of the time-mean. As a result, monthly mean

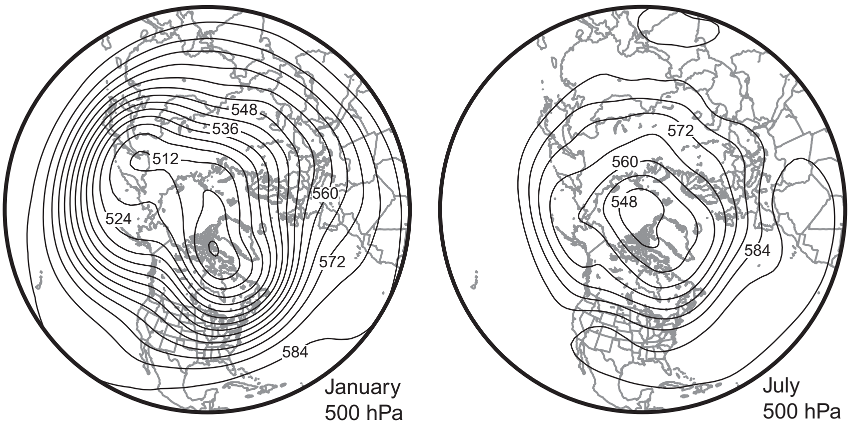

FIGURE 6.3 Mean 500-hPa geopotential height contours in January (*left*) and July (*right*) in the Northern Hemisphere (30-year average). Geopotential height contours are shown every 60 meters. (*Adapted from NOAA/ESRL http://www.esrl.noaa.gov/psd/.*)

charts tend to smooth out the actual structure of the instantaneous jet stream since the position and intensity of the jet vary. Thus, at any time the planetary scale flow in the region of the jet stream has much greater baroclinicity than indicated on time-averaged charts. This point is illustrated schematically in Figure 6.4, which shows a latitude–height cross-section through an observed jet stream over North America. Figure 6.4a shows the zonal wind and potential temperature, whereas Figure 6.4b shows the potential temperature and Ertel potential vorticity. The 2-PVU contour of potential vorticity approximately marks the tropopause. As illustrated in Figure 6.4a, the axis of the jet stream tends to be located above a narrow sloping zone of strong potential temperature gradients called the *polar-frontal* zone. This is the zone that in general separates the cold air of polar origin from warm tropical air. The occurrence of an intense jet core above this zone of large-magnitude potential temperature gradients is, of course, not mere coincidence but rather a consequence of thermal wind balance.

The potential temperature contours in Figure 6.4 illustrate the strong static stability in the stratosphere. They also illustrate the fact that isentropes (constant θ surfaces) cross the tropopause in the vicinity of the jet so that air can move between the troposphere and the stratosphere without diabatic heating or cooling. The strong gradient of Ertel potential vorticity at the tropopause, however, provides a strong resistance to cross-tropopause flow along the isentropes. Note, however, that in the frontal region the potential vorticity surfaces are displaced substantially downward so that the frontal zone is characterized by a strong positive anomaly in potential vorticity associated with the strong relative vorticity on the poleward side of the jet and the strong static stability on the cold air side of the frontal zone.

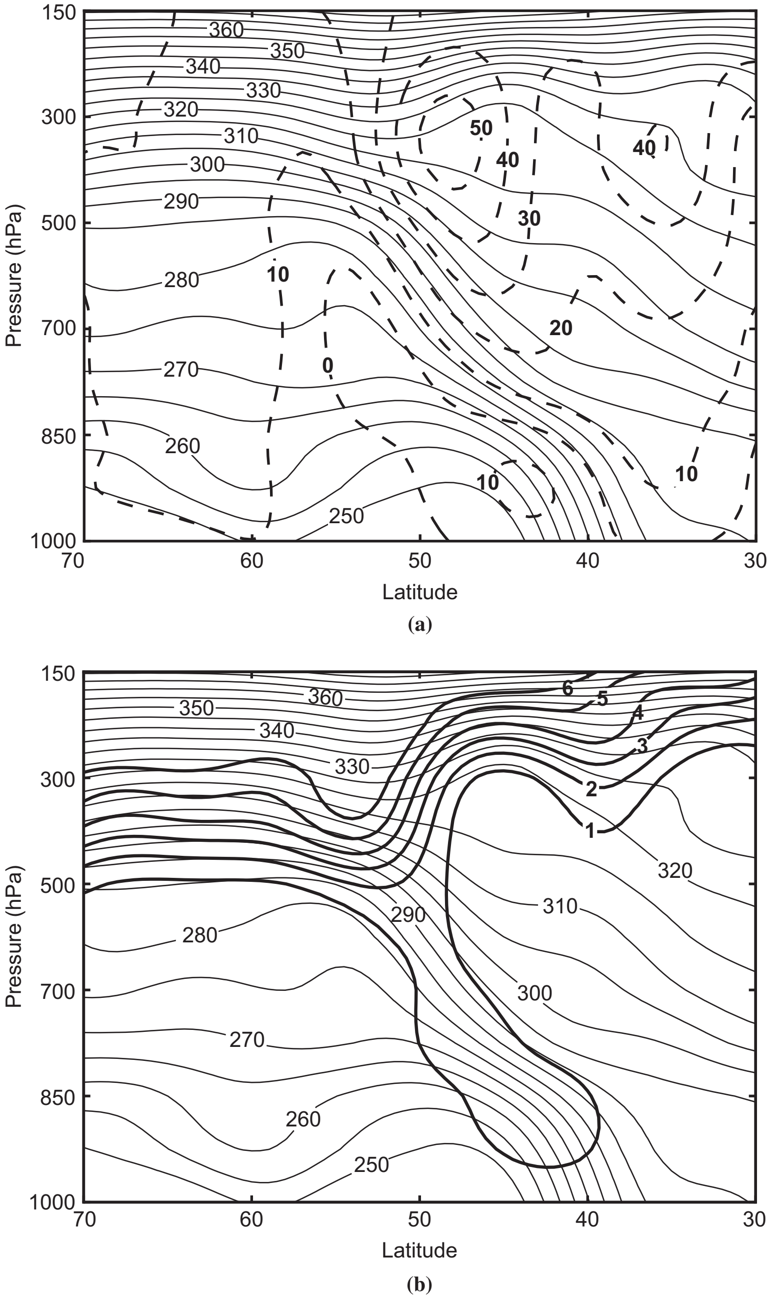

FIGURE 6.4 Latitude–height cross-sections through a cold front at 80W longitude on 2000 UTC January 14, 1999. (a) Potential temperature contours (*thin solid lines*, K) and zonal wind isotachs (*dashed lines*, m s^{-1}). (b) *Thin solid contours* as in (a), *heavy dashed contours*, Ertel potential vorticity labeled in PVU(1-PVU $= 10^{-6}$ K kg^{-1} m^2 s^{-1}).

It is a common observation in fluid dynamics that jets in which strong velocity shears occur may be unstable with respect to small perturbations. Any small disturbance introduced into an unstable jet will tend to amplify, drawing energy from the jet as it grows. For synoptic-scale systems in midlatitudes, the primary instability is called *baroclinic instability* because it depends on the meridional temperature gradient or, equivalently, from thermal-wind balance, on vertical wind shear. Athough horizontal temperature gradients maximize near frontal zones, baroclinic instability is not identical to frontal instability, as most baroclinic instability models describe only geostrophically scaled motions, whereas disturbances in the vicinity of strong frontal zones must be highly ageostrophic. As shown in Chapter 7, baroclinic disturbances may themselves act to intensify pre-existing temperature gradients and thus generate frontal zones.

Disturbances in the midlatitude storm tracks take the form of baroclinic waves and smaller-scale vortices. A statistical analysis of the meridional wind reveals that the baroclinic waves have a dominant wavelength of about 4000 km, and travel eastward at approximately 10 to 15 m s^{-1}(Figure 6.5). The vertical structure of the waves indicates a westward tilt with height in the geopotential height field and, consistent with hydrostatic balance, an eastward tilt with height in the temperature field (Figure 6.6). Vertical motion peaks in the middle troposphere, with rising motion between the trough and ridge and sinking motion west of the trough. It is these organized patterns of vertical motion that are largely responsible for clouds and precipitation in middle latitudes, and understanding the dynamical source for these circulations is a major subject of this chapter. Key aspects of an idealized developing baroclinic system are captured in the schematic vertical cross-section illustrated in Figure 6.7. Throughout the troposphere the trough and ridge axes tilt westward (or upstream) with height,[1] whereas the axes of warmest and coldest air are observed to have the opposite tilt. As will be shown later, the westward tilt of the troughs and ridges is necessary in order that the mean flow transfers potential energy to the developing wave. In the mature stage (not shown in Figure 6.7) the troughs at 500 and 1000 hPa are nearly in phase and, as a consequence, thermal advection and energy conversion are quite weak.

This statistical description of baroclinic waves is manifest in individual realizations of weather disturbances in the form of extratropical cyclones. The stages in the development of a typical extratropical cyclone are shown schematically in Figure 6.8. In the stage of rapid development there is a cooperative interaction between the upper-level and surface flows; strong cold advection is seen to occur west of the trough at the surface, with weaker warm advection to the east. This pattern of thermal advection is a direct consequence of the fact that the trough at 500 hPa lags (lies to the west of) the surface trough so that the mean geostrophic wind in the 1000- to 500-hPa layer is directed across the

---

[1] As Figure 6.6 reveals, in reality, the phase tilts tend to be concentrated below the 700-hPa level.

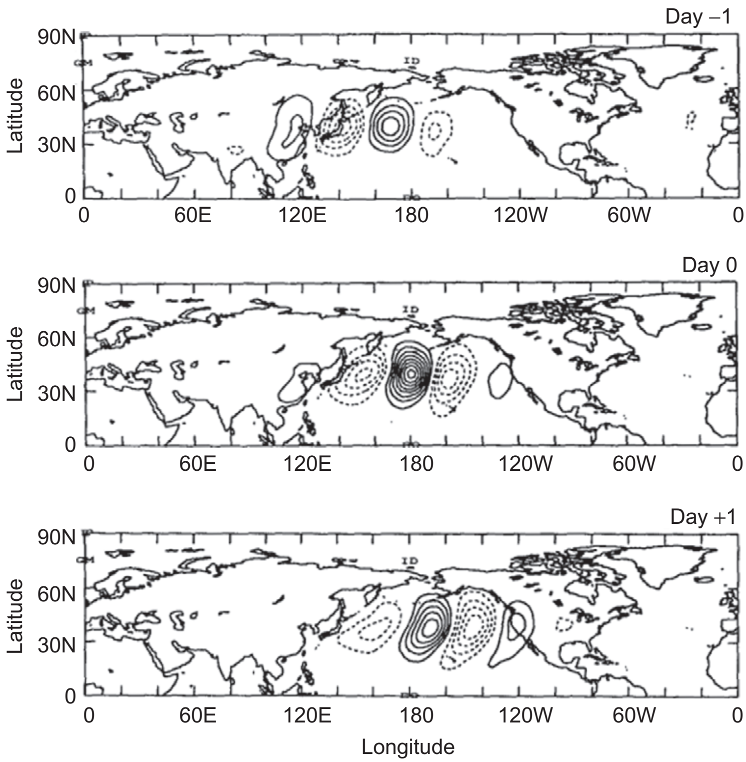

FIGURE 6.5 Linear regression of the meridional wind relative to the base point at 40°N, 180°W. Contours are shown every 2 m s^{-1} with negative values *dashed*. The top, middle, and bottom panels show lags of -1, 0, and $+1$ days, respectively, relative to the base point, which reveals the motion of the baroclinic waves across the North Pacific ocean. (*After Chang, 1993. Copyright © American Meteorological Society. Reprinted with permission.*)

1000- to 500-hPa thickness lines toward larger thickness west of the surface trough and toward smaller thickness east of the surface trough.

6.2 DERIVATION OF THE QUASI-GEOSTROPHIC EQUATIONS

The main goal of this chapter is to show how the observed structure of midlatitude synoptic systems can be interpreted in terms of the constraints imposed on synoptic-scale motions by the dynamical equations. Specifically, we show that for motions that are nearly hydrostatic and geostrophic, the three-dimensional flow field is determined approximately by the pressure field. Given the small magnitude of vertical motion on these scales, this is a remarkable result. Here we use height, z, as the vertical coordinate, and make the Boussinesq approximation

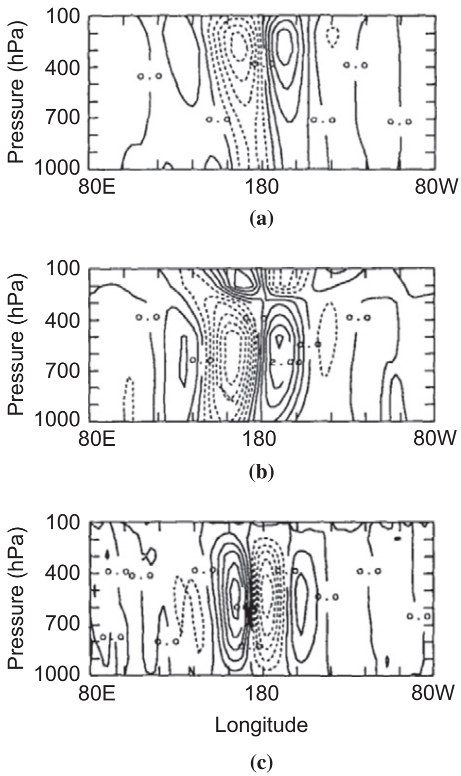

FIGURE 6.6 Linear regression is shown on the longitude–height plane of (a) geopotential height (b) temperature, and (c) vertical motion (ω) relative to the meridional wind at the base point located at 300 hPa, 40°N, and 180°W. Contours are shown every 20 m for geopotential height, 0.5 K for temperature, and 0.02 Pa s^{-1} for vertical motion, with negative values *dashed*. (*After Chang, 1993. Copyright © American Meteorological Society. Reprinted with permission.*) The vertical structure of baroclinic waves is revealed: westward tilt with height for geopotential height anomalies, eastward tilt with height for temperature, and rising motion eastward of the geopotential height trough axis.

so that density is treated as a constant everywhere except for the buoyancy force. This approach has the advantage of simplicity and clarity compared to using pressure as a vertical coordinate, which involves a left-handed coordinate system and reverses the sign of vertical motion (negative is rising). Nevertheless, most weather and climate data are contained in pressure coordinates, so in Section 6.7 we present the isobaric-coordinate form of the equations. For completeness, the isobaric equations also allow for a linear variation of the Coriolis parameter (β-plane approximation), whereas the rest of this chapter employs the f-plane approximation (constant value); this simplifies the analysis and is a good approximation in midlatitudes, since ambient potential vorticity gradients near jet streams are much larger than those of f.

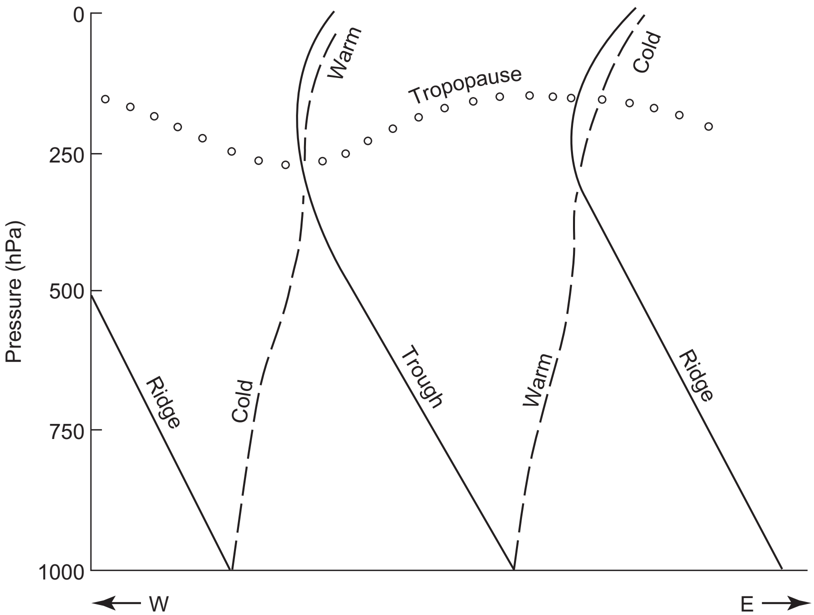

FIGURE 6.7 West–east cross-section through a developing baroclinic wave. *Solid lines* are trough and ridge axes; *dashed lines* are axes of temperature extrema; the chain of *open circles* denotes the tropopause.

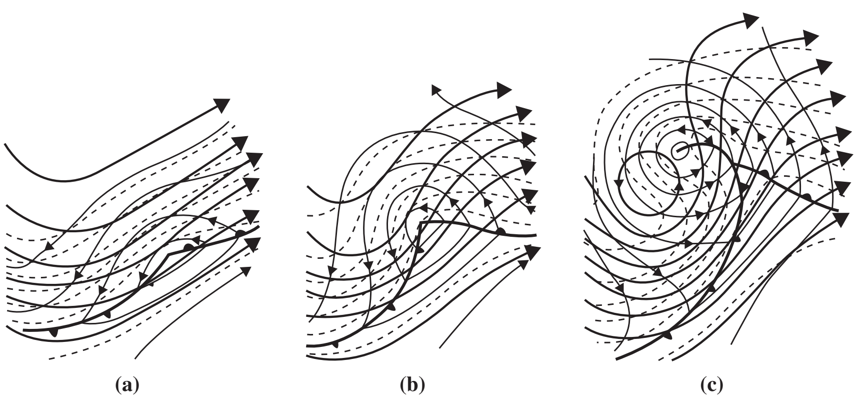

FIGURE 6.8 Schematic 500-hPa contours (*heavy solid lines*), 1000-hPa contours (*thin lines*), and 1000–500-hPa thickness (*dashed lines*) for a developing extratropical cyclone at three stages of development: (a) incipient development stage, (b) rapid development stage, and (c) occlusion stage. (*After Palmén and Newton, 1969.*)

6.2.1 Preliminaries

The geostrophic wind, $\mathbf{V}_g = (u_g, v_g)$ is given by

$$\mathbf{V}_g = \frac{1}{\rho_0 f}\mathbf{k} \times \nabla_h p = \frac{1}{\rho_0 f}\left(-\frac{\partial p}{\partial y}, \frac{\partial p}{\partial x}\right) \tag{6.1}$$

where ρ_0 and f are constants as a result of the Boussinesq and f-plane approximations, respectively. Recall that ∇_h is the horizontal gradient operator $(\frac{\partial}{\partial x}, \frac{\partial}{\partial y})$. The geostrophic relative vorticity, ζ_g, measures the rotational component of the geostrophic wind about the vertical axis,

$$\zeta_g = \frac{\partial v_g}{\partial x} - \frac{\partial u_g}{\partial y} = \frac{1}{\rho_0 f}\nabla_h^2 p \tag{6.2}$$

where the second relationship derives from (6.1); the geostrophic relative vorticity is determined completely by the pressure field.

We will assume that the wind in all but one of the advection terms of the equations may be approximated by the geostrophic wind. The basis for this assumption derives from the following scaling arguments. The Eulerian time tendency and horizontal advection scale like

$$\frac{\partial}{\partial t} + u\frac{\partial}{\partial x} + v\frac{\partial}{\partial y} \sim \frac{U}{L} \tag{6.3}$$

and, for $w \sim Ro\frac{H}{L}U$, vertical advection scales like

$$w\frac{\partial}{\partial z} \sim \frac{U}{L}Ro \tag{6.4}$$

where Ro is the Rossby number, U/fL, discussed in Section 2.4.2. Vertical advection may be neglected for small Rossby number, provided the vertical gradient of the advected quantity is not on the order of Ro^{-1} or larger. Moreover, since the Lagrangian tendency of horizontal momentum scales with the Rossby number, the ageostrophic wind does as well—see (2.24) and (2.25); as a result, the ageostrophic wind is small compared to the geostrophic wind. Therefore, for a small Rossby number, to good approximation we can we make the replacement

$$\frac{D}{Dt} \rightarrow \frac{D}{Dt_g} = \frac{\partial}{\partial t} + \mathbf{V}_g \cdot \nabla_h = \frac{\partial}{\partial t} + u_g\frac{\partial}{\partial x} + v_g\frac{\partial}{\partial y} \tag{6.5}$$

which is simply the material derivative following the geostrophic wind.

In addition to a nearly geostrophic horizontal wind ("quasi-geostrophic"), we assume that the vertical distribution of pressure is nearly hydrostatic ("quasi-hydrostatic"). Recall that although we do not have a prognostic (forecast) equation for w, this does not mean that w is zero, but rather that it must be deduced diagnostically from the other variables. As was done in Section 2.4.3, we assume a *reference atmosphere* (denoted here by overbars) that is at rest and in exact hydrostatic balance:

$$\frac{\partial \overline{p}}{\partial z} = -\overline{\rho} g$$

Perturbations from the reference state are also in hydrostatic balance,

$$\frac{\partial p}{\partial z} = \frac{\rho_0}{\overline{\theta}} \theta g \tag{6.6}$$

where p and θ are the disturbance pressure and potential temperature, respectively, ρ_0 is a constant density (a result of the Boussinesq approximation), and $\overline{\theta}$ is a function of z only. The full value of potential temperature will be denoted by θ_{tot}.

Together, the assumptions of geostrophic and hydrostatic balance produce the thermal wind relation (see Section 3.4):

$$\mathbf{V}_{\text{T}} = \frac{\partial \mathbf{V}_g}{\partial z} = \frac{g}{f\overline{\theta}} \mathbf{k} \times \nabla_h \theta \tag{6.7}$$

We notice that the disturbance potential temperature plays the same role as pressure does for the geostrophic wind: Wind flows along the contours with greatest magnitude near the largest gradients.

From equation (2.54), in the absence of strong diabatic heating, and for a small Rossby number, the first law of thermodynamics can be expressed as

$$\boxed{\frac{D\theta}{Dt_g} = -w\frac{d\overline{\theta}}{dz}} \tag{6.8}$$

which is the **quasi-geostrophic thermodynamic energy equation**. Equation (6.8) says that the perturbation potential temperature following the geostrophic motion changes due to vertical advection of the reference potential temperature. Note that the appearance of vertical advection in (6.8) reflects the large static stability of the reference atmosphere (on the order of $1/Ro$). To simplify the subsequent discussion, we take the static stability to be constant, which is a reasonable leading-order approximation for the troposphere. This implies that the buoyancy frequency (see Section 2.7.3),

$$N = \left[\frac{g}{\overline{\theta}} \frac{d\overline{\theta}}{dz} \right]^{1/2} \tag{6.9}$$

is also constant.

Finally, since many results that follow assume a familiarity with the gradient and Laplacian operations on scalar fields, we provide a brief review of these terms and their interpretation. Given a two-dimensional scalar function, ϕ, the gradient of ϕ, $\nabla_h \phi$, is a *vector* quantity that is directed toward larger values and

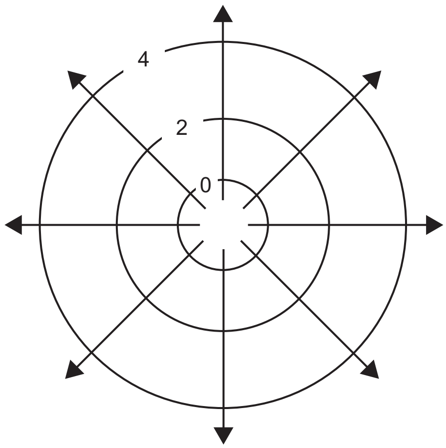

FIGURE 6.9 Illustration of the gradient operator for a scalar function, ϕ. The gradient of ϕ, a vector field, is illustrated by *arrows* that are directed toward larger values and orthogonal to *lines* of constant ϕ. The Laplacian is given by the divergence of the gradient, which is a local maximum near the local minimum in ϕ.

orthogonal to lines of constant ϕ (Figure 6.9). The Laplacian is given by the divergence of the gradient of ϕ, $\nabla_h^2\phi = \nabla_h \cdot (\nabla_h \phi)$, which is a *scalar* quantity. Since the gradient points toward larger values, the Laplacian is positive and a local maximum near local minima in ϕ; conversely, the Laplacian is negative and a local minimum near local maxima in ϕ.

6.3 POTENTIAL VORTICITY DERIVATION OF THE QG EQUATIONS

Consider now conservation of potential vorticity, which will provide the basis for one perspective of quasi-geostrophic dynamics. In Sections 5.3.2 and 5.5.2, we discovered that fast gravity-wave motions have zero potential vorticity. The dynamics of extratropical weather systems are more closely related to Rossby waves, which are geostrophically balanced and have nonzero PV, so it proves useful to filter the gravity waves from the governing equations. This is accomplished by the linearized PV equation (5.91), but the linear dynamics are deficient in many aspects needed to understand weather systems, including interactions between these systems and the jet stream. These interactions come from advection terms in the PV equation, which are lacking in (5.91) and must be reintroduced. It turns out that this is easily accomplished. First, we use the perturbation method of Section 5.1 to linearize the Ertel PV around the reference atmosphere described in Section 6.2.1, while retaining the nonlinear advection terms. Second, we replace the wind by the geostrophic wind in both the PV and the advection terms by the reasoning leading to (6.5).

For the Boussinesq approximation, the Ertel PV conservation law (4.24) can be expressed as

$$\frac{D\Pi}{Dt} = \frac{D}{Dt}\left[\frac{\boldsymbol{\omega}_a \cdot \nabla\theta_{\text{tot}}}{\rho_o}\right] = 0 \tag{6.10}$$

where

$$\boldsymbol{\omega}_a = (\eta, \xi, \zeta + f) \tag{6.11}$$

is the three-dimensional vorticity vector. Since $\nabla\theta_{\text{tot}} = \left(\frac{\partial\theta}{\partial x}, \frac{\partial\theta}{\partial y}, \frac{\partial\theta}{\partial z} + \frac{d\overline{\theta}}{dz}\right)$, we immediately notice that the x and y contributions to the dot product in (6.10) involve nonlinear terms[2] and must be discarded, leaving

$$\frac{D}{Dt}\left[\frac{1}{\rho_o}(\zeta + f)\frac{\partial\theta_{\text{tot}}}{\partial z}\right] = 0 \tag{6.12}$$

Substituting $\theta_{\text{tot}} = \overline{\theta} + \theta$, and again discarding nonlinear terms gives

$$\frac{D}{Dt}\frac{1}{\rho_o}\left[(\zeta + f)\frac{d\overline{\theta}}{dz} + f\frac{\partial\theta}{\partial z}\right] = 0 \tag{6.13}$$

Factoring the constant $\frac{d\overline{\theta}}{dz}$ yields

$$\frac{D}{Dt}\frac{1}{\rho_o}\frac{d\overline{\theta}}{dz}\left[\zeta + f + f\frac{\partial}{\partial z}\left(\frac{d\overline{\theta}}{dz}^{-1}\theta\right)\right] = 0 \tag{6.14}$$

Although $\frac{d\overline{\theta}}{dz}$ is assumed constant, we introduce it within the vertical derivative since this general form holds even in the case where $\frac{d\overline{\theta}}{dz}$ is a function of z. Finally, approximating the wind geostrophically gives

$$\frac{D}{Dt_g}\frac{1}{\rho_o}\frac{d\overline{\theta}}{dz}\left[\zeta_g + f + f\frac{\partial}{\partial z}\left(\frac{d\overline{\theta}}{dz}^{-1}\theta\right)\right] = 0 \tag{6.15}$$

or

$$\boxed{\frac{D}{Dt_g}\frac{1}{\rho_o}\frac{d\overline{\theta}}{dz}q = 0} \tag{6.16}$$

where

$$\boxed{q = \zeta_g + f + f\frac{\partial}{\partial z}\left(\frac{d\overline{\theta}}{dz}^{-1}\theta\right)} \tag{6.17}$$

is the **quasi-geostrophic potential vorticity** (QG PV).

---

[2] Products of the functions of the dependent variables—in this case, disturbance vorticity and potential temperature.

Equation (6.16) says that the QG PV is conserved following the geostrophic motion, analogous to Ertel PV conservation following the full flow. We note that the leading factor, $\frac{1}{\rho_o}\frac{d\bar{\theta}}{dz}$, is independent of time and merely scales the QG PV by a constant function of z. It is customary to discard this factor; however, in doing so the units change to those of vorticity (s^{-1}). Although, as a result of linearization, the QG PV involves a sum of vorticity and static stability compared to a product for the Ertel PV, the dynamical interpretation following an air parcel is qualitatively similar: Increases in vorticity must be accompanied by decreases in static stability in order to conserve PV.

Taking the vertical derivative of the quasi-geostrophic thermodynamic energy equation (6.8) and using the result to replace the static stability term in (6.15) gives

$$\boxed{\frac{D}{Dt_g}\left(\zeta_g + f\right) = f\frac{\partial w}{\partial z}} \tag{6.18}$$

which is the **quasi-geostrophic vorticity equation**. Following the geostrophic motion, the geostrophic absolute vorticity, $\zeta_g + f$, changes due to stretching of planetary rotation by vertical motion. The fact that the contribution from stretching of relative vorticity is absent indicates that the quasi-geostrophic approximation is only formally valid when the relative vorticity is small compared to f. This is consistent with the small Rossby number approximation, since the ratio of the scaling for vorticity, U/L, to f is $U/(fL)$. Fortunately, it turns out that quasi-geostrophic equations remain qualitatively useful for observed disturbance amplitudes despite this restrictive condition. The vertical motion in the quasi-geostrophic vorticity equation is linked to horizontal motion by the **quasi-geostrophic mass continuity equation**,

$$\boxed{\frac{\partial u_a}{\partial x} + \frac{\partial v_a}{\partial y} + \frac{\partial w}{\partial z} = 0} \tag{6.19}$$

where $\mathbf{V}_a = (u_a, v_a)$ is the ageostrophic wind. This result derives directly from the Boussinesq approximation (see 2.60) and the fact that the geostrophic wind is horizontally nondivergent on the f-plane.

We return now to the question of momentum conservation for the quasi-geostrophic approximation. If we approximate the momentum geostrophically in the momentum equations (e.g., 2.24 and 2.25), steady-state expressions result and there are no dynamics. Therefore, ageostrophic effects must be present in the momentum equation (hence, *quasi*-geostrophy), and this is one reason why we did not begin our analysis with momentum conservation. Approximating the material derivative geostrophically, the momentum equation can be written in general as

$$\frac{D\mathbf{V}_g}{Dt_g} = -\frac{1}{\rho_o}\nabla_h(p_g + p_a) - f\mathbf{k}\times(\mathbf{V}_g + \mathbf{V}_a) \tag{6.20}$$

which allows for ageostrophic effects in both the pressure and wind fields. Forming a vorticity equation as in Chapter 4, by taking $\frac{\partial}{\partial x}$ of the v_g-momentum equation minus $\frac{\partial}{\partial y}$ of the u_g-momentum equation, gives

$$\frac{D\zeta_g}{Dt_g} = -f\left(\frac{\partial u_a}{\partial x} + \frac{\partial v_a}{\partial y}\right) = f\frac{\partial w}{\partial z} \tag{6.21}$$

where the last equality is accomplished by the quasi-geostrophic mass continuity equation. Noting that f is a constant allows it to be added to the material derivative, which recovers the quasi-geostrophic vorticity equation (6.18). This shows that (6.20) is consistent with the previously derived equations, but for reasons described subsequently, there is ambiguity in the individual terms in (6.20).

Ambiguity in the momentum equation involves two effects. First, since the curl of a gradient is zero, we may add an arbitrary field, $\tilde{p}_a$, to p_a in (6.20) and arrive at the same vorticity equation, (6.18). Second, we may add an arbitrary vector field, $\tilde{\mathbf{V}}_a$, to the ageostrophic wind in the momentum equation and arrive at the same vorticity equation, provided that $\nabla_h \cdot \tilde{\mathbf{V}}_a = 0$. Thus, p_a and $\mathbf{V}_a$ are arbitrary fields, but they are related through the **quasi-geostrophic divergence equation**,

$$\nabla_h^2 p_a = \rho_0 f \zeta_a + 2J(u_g, v_g) \tag{6.22}$$

which is obtained from equation (6.20) by taking $\frac{\partial}{\partial x}$ of the u_g-momentum equation plus $\frac{\partial}{\partial y}$ of the v_g-momentum equation. Here, $J(u_g, v_g) = \frac{\partial u_g}{\partial x}\frac{\partial v_g}{\partial y} - \frac{\partial v_g}{\partial x}\frac{\partial u_g}{\partial y}$ is a Jacobian, and $\zeta_a = \frac{\partial v_a}{\partial x} - \frac{\partial u_a}{\partial y}$ is the ageostrophic vertical vorticity. Although (6.22) provides a diagnostic equation relating the ageostrophic pressure and the rotational part of the ageostrophic wind to the geostrophic wind, lacking additional information, one of the ageostrophic quantities must be eliminated in order to close the system. This choice is arbitrary, and therefore so are the terms on the right side of (6.20). The most common choice, $p_a = 0$, puts all ageostrophic effects into $\mathbf{V}_a$, giving the **quasi-geostrophic momentum equation**

$$\boxed{\frac{D\mathbf{V}_g}{Dt_g} = -f\mathbf{k} \times \mathbf{V}_a} \tag{6.23}$$

We emphasize that this arbitrary choice has no effect on the dynamics of vorticity or potential vorticity. The divergent part of the ageostrophic wind is well constrained through the continuity equation and will play an essential role in "w-Thinking." First we explore the "PV Thinking" view of quasi-geostrophic dynamics, which has no role for ageostrophic motion.

Section's Key Points

- The QG equations are defined by a small Rossby number and for a reference atmosphere that has strong stratification.
- The QG PV is a linearization of the Ertel PV consisting of a sum of contributions from the vertical component of vorticity and the disturbance static stability.
- Following the geostrophic motion, geostrophic vorticity changes due to stretching of ambient planetary rotation.
- Neglecting ageostrophic effects on pressure, following the geostrophic motion, geostrophic momentum changes due to Coriolis turning of the ageostrophic wind. The divergent ageostrophic wind links to vertical motion by the mass continuity equation, and the rotational ageostrophic wind is approximated from the geostrophic wind by the QG divergence equation.

6.4 POTENTIAL VORTICITY THINKING

The fact that potential vorticity conservation represents all of the fundamental physical conservation laws in a single equation provides the basis for a very powerful and simple interpretation of the dynamics of weather systems. Before reviewing the two essential elements comprising "PV Thinking," inversion and conservation, we examine the scaling properties of the QG PV.

Using the geostrophic and hydrostatic relationships to replace the vorticity and potential temperature in the QG PV (6.17), and recalling that N is the buoyancy frequency, gives

$$q - f = \frac{1}{\rho_o f}\nabla_h^2 p + \frac{1}{\rho_o}\frac{\partial}{\partial z}\frac{f}{N^2}\frac{\partial p}{\partial z} \tag{6.24}$$

so that the QG PV is determined completely by the pressure field. This remarkable fact will allow us to make forecasts knowing only the pressure at the initial time, and to understand why and how the system evolves. Nondimensionalizing (6.24) using length scales L and H in the horizontal and vertical, respectively, and a geostrophic scaling[3] for the pressure field, $p \sim \rho_o U f L$ gives

$$q - f \sim \frac{U}{L}\left(\hat{\nabla}_h^2 \hat{p} + \frac{1}{B^2}\frac{\partial^2 \hat{p}}{\partial \hat{z}^2}\right) \tag{6.25}$$

where we have assumed that the buoyancy frequency, N, is a constant, hats denote nondimensional variables that are assumed to have values on the order of one, and B is the nondimensional Burger number. In analogy with vorticity, $q - f$ may be thought of as the "relative" QG PV, and we see that the natural scaling for this quantity is the same as for vertical vorticity, U/L. Including the

[3]The nondimensional geostrophic wind is then given in terms of the nondimensional pressure by $\hat{\mathbf{V}}_g = -\hat{k} \times \hat{p}$.

scaling factor from (6.16) gives a scaling for QG PV, $\frac{U}{\rho_o L}\frac{d\bar{\theta}}{dz}$, in the same units as the Ertel PV.

The Burger number is a fundamental measure of the importance of stratification relative to rotation, and can be expressed in at least four useful forms:

$$B = \frac{NH}{fL} = \frac{L_R}{L} = \frac{H}{H_R} = \frac{Ro}{Fr} \tag{6.26}$$

The second equality shows that the Burger number is given by the ratio of the Rossby radius, $L_R = \frac{NH}{f}$, to the scaling length of the motion, L. Disturbances that are large compared to the Rossby radius have a small Burger number, which promotes the importance of vortex stretching. The third equality shows that the Burger number is also given by the ratio of the scaling depth, H, to the Rossby depth, $H_R = \frac{fL}{N}$. Rossby depth measures the vertical influence of disturbances, which increases with disturbance length scale and rotation, and for smaller static stability. Finally, the Burger number is also given by the ratio of the Rossby number, $Ro = \frac{U}{fL}$, to the Froude number, $Fr = \frac{U}{NH}$, both of which are non-dimensional. As we have seen, the Rossby number measures the importance of disturbance vorticity, $\frac{U}{L}$, relative to the ambient vorticity, f, and, in the present context, the Froude number[4] measures the importance of disturbance vertical shear, $\frac{U}{H}$, relative to the buoyancy frequency, N. In deriving the QG equations we have assumed strong ambient rotation ($\zeta \ll f$) and stratification (large $\frac{d\bar{\theta}}{dz}$), so that both Ro and Fr are small (much less than one), which implies a Burger number close to unity and equal importance for the two terms in the QG PV. This in turn implies that the natural disturbance length scales are $L \sim L_R$ and $H \sim H_R$, which provide useful guides in discussing the dynamics of weather features.

Section's Key Points

- The QG PV is determined completely by the pressure field.
- The relative importance of the vorticity and static stability contributions to the QG PV is measured by the Burger number.

6.4.1 PV Inversion, Induced Flow, and Piecewise PV Inversion

PV inversion is a kinematic diagnostic technique involving the recovery of other fields from the PV. For unity B, (6.25) can be written as

$$\hat{q} - Ro^{-1} = \hat{\nabla}^2 \hat{p} \tag{6.27}$$

[4]By the thermal-wind relationship, vertical shear of the geostrophic wind is proportional to the horizontal temperature gradient, so the Froude number measures the slope of the isentropes.

The constant Ro^{-1} is due to the ambient rotation and stratification and, although large, has no dynamical significance since it merely changes the value of the PV everywhere. Therefore, features of interest in the nondimensional QG PV, $\hat{q}$, are determined by the Laplacian of the nondimensional pressure field. Areas of relatively low pressure are associated with large values of QG PV, and areas of high pressure with relatively small QG PV. QG PV inversion involves recovering the pressure from QG PV by solving

$$\hat{p} = \hat{\nabla}^{-2}\hat{q} \tag{6.28}$$

Since $\hat{\nabla}^2$ involves taking derivatives, we expect that $\hat{\nabla}^{-2}$ will involve taking antiderivatives, integrals, to recover the pressure field from the QG PV.

Returning to the full-dimensional form of the QG PV, multiplying (6.24) by f we find

$$f(q-f) = \frac{1}{\rho_o}\nabla_h^2 p + \frac{1}{\rho_o}\frac{\partial}{\partial z}\frac{f^2}{N^2}\frac{\partial p}{\partial z} = \mathsf{L}p \tag{6.29}$$

where

$$\mathsf{L} = \frac{1}{\rho_o}\nabla_h^2 + \frac{1}{\rho_o}\frac{\partial}{\partial z}\frac{f^2}{N^2}\frac{\partial}{\partial z} \tag{6.30}$$

is an operator that is approximately a three-dimensional Laplacian, "stretched" in the z direction relative to x and y by $\frac{f^2}{N^2}$; the nondimensionalized version discussed in (6.28) removes this stretching. The product fq is a useful combination because it is positive (negative) for cyclones (anticyclones) in both Northern and Southern hemispheres, providing a "hemispherically neutral" interpretation for PV Thinking.[5] Since L acts like a Laplacian, $f(q-f)$ will be a maximum where p is a minimum, which for cyclones implies $q > 0$ in the Northern Hemisphere and $q < 0$ in the Southern Hemisphere; the reverse applies to anticyclones.

As for the nondimensional case, symbolically we may define QG PV inversion by the operator that reverses the action of L,

$$p = \mathsf{L}^{-1}(fq) \tag{6.31}$$

which recovers the pressure field from the QG PV field (the constant from $L^{-1}f^2$ is taken to be zero). Given the pressure field, the geostrophic wind and the disturbance potential temperature are recovered from (6.1) and (6.6), respectively. From this point of view, the wind and potential temperature field are "induced," or caused, by the QG PV.

[5]This relation derives from relative vorticity, so that cyclones have the same sign as the local planetary rotation, f.

Boundary conditions must be supplied when inverting the potential vorticity. Assuming periodic conditions in the horizontal, boundary conditions on horizontal boundaries such as the surface include a specification of the pressure (Dirichlet condition), the vertical derivative of pressure (Neumann condition), or a linear combination of the pressure and its vertical derivative (Robin condition); "free-space" solutions apply in the absence of boundary conditions. From the hydrostatic equation (6.6), Neumann conditions involve a specification of the potential temperature field at the boundary. Assuming that the surface potential temperature field is independent of the potential vorticity provides a powerful approach to atmospheric dynamics because both the QG PV and θ are conserved following the motion. Since the conservation law for surface potential temperature (6.8 with $w = 0$) resembles that for QG PV (6.16), surface potential temperature may be thought of as QG PV at the surface. Mathematically, one can make this association precise by replacing the inhomogeneous Neumann boundary condition with a homogeneous one (setting $\theta = 0$ at $z = 0$), provided the QG PV is augmented by a "spike" contribution at $z = 0$ that is directly proportional to surface θ. This "PV-θ" perspective is particularly useful for understanding how PV anomalies in the troposphere, such as those associated with tropopause undulations, interact with surface features, such as surface cyclones.

To illustrate the concepts associated with PV inversion, we consider two canonical disturbances in this chapter. The first disturbance is modeled after a "short-wave" trough, which appears on upper-tropospheric weather maps as an isolated trough of low pressure (low geopotential height on pressure surfaces). This disturbance is associated with a localized blob of cyclonic QG PV, taken here to be in the middle troposphere with Gaussian structure and a maximum value of 2 PVU (Figure 6.10). The flow induced by the PV blob is largest near the "edge" of the disturbance, and decays with distance (Figure 6.10a), which illustrates the important nonlocal aspect of the inversion: The wind is nonzero more than 1000 km from the region having QG PV. This leads to the notion of "action at a distance," where a dynamical process may depend on the flow induced by a remote PV anomaly.

The disturbance in Figure 6.10 is embedded within the simplest possible jet stream, with a zonal wind that is constant in x and y and if the zonal wind increases linearly upward from zero at the ground. Despite its simplicity, it is apparent from Figure 6.10b that this configuration is a rather good model for a short-wave trough in a westerly jet stream. The "stretched"-Laplacian solution is evident in the vertical cross-sections, which reveal that the nonlocal influence extends to the surface, with an area of low pressure due to the QG PV aloft (Figure 6.10c). Finally, in Figure 6.10d we see that the PV blob is associated with a local maximum in cyclonic vorticity, cyclonic wind flow around the PV blob, and a local maximum in static stability, with "warm" air above the PV blob and "cold" air below.

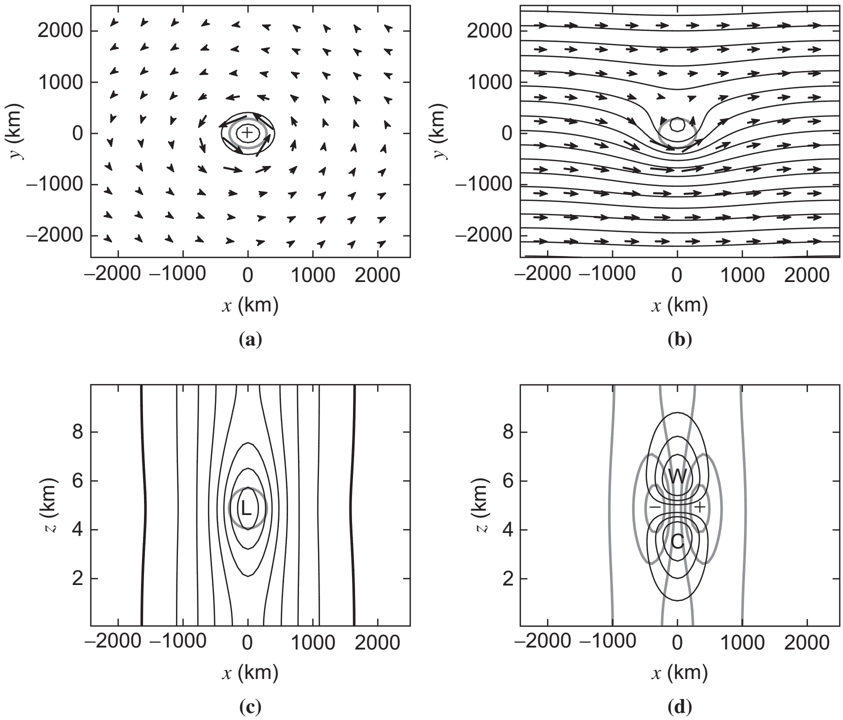

FIGURE 6.10 Inversion of an idealized localized blob of QG PV having a magnitude of 2 PVU embedded in a jet stream consisting of a westerly wind increasing linearly with height. (a) PV contours at altitude of 5 km are shown every 0.5 PVU; wind induced by the PV anomaly is shown by *arrows*, with a maximum wind speed of 22 m s^{-1}; (b) *pressure contours* every 42 hPa (equivalent to 60-m height contours on an isobaric surface) and full wind vectors (wind due to the PV anomaly plus the westerly jet), with a maximum wind speed of 36 m s^{-1}; (c) anomaly pressure every 21 hPa (equivalent to 30-m height contours) with *bold zero contour*; and (d) meridional wind every 6 m s^{-1} and potential-temperature anomalies every 2 K ("W" and "C" imply "warm" and "cold" values). In (a) through (c), the 1-PVU QG PV contour is denoted by the *thick gray line*.

As mentioned previously, surface potential temperature plays the role of PV. Warm (cold) air at the surface is associated with low (high) pressure and, by thermal wind reasoning, cyclonic circulation that decays upward from the surface into the troposphere (Figure 6.11). This may be understood from the hydrostatic equation and the fact that, with zero QG PV, solutions to Laplace problems have extrema on the boundaries. A leading-order approximation to the tropopause is a rigid boundary similar to the surface, in which case cold (warm) air is associated with low (high) pressure and cyclonic (anticyclonic) circulation that decays downward from the tropopause.

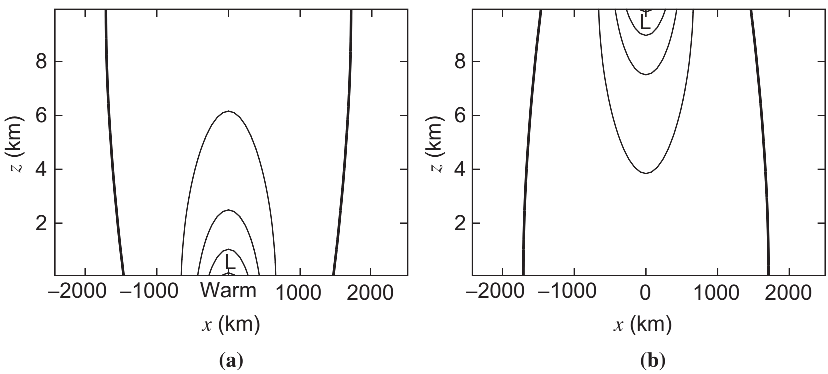

FIGURE 6.11 Pressure contours associated with (a) surface warm anomaly and (b) tropopause cold anomaly. Pressure is contoured every 21 hPa (equivalent to 30-m height contours) with *bold zero contour*. The potential temperature anomalies have an amplitude of 10 K and the same horizontal shape as the PV anomaly in Figure 6.10.

The notion of induced flow is most powerful when considering discrete portions of the atmosphere, and their interaction (i.e., dynamics). Since the QG PV operator, L, is linear, the atmosphere may be broken into components, the sum of which gives the full fields. This "piecewise PV inversion" framework is expressed mathematically as

$$p = \sum_{i=1}^{N} p_i = \sum_{i=1}^{N} \mathsf{L}^{-1}\left(fq_i\right) \tag{6.32}$$

To each PV element, q_i, one associates a pressure field, p_i, from which the wind and temperature may be recovered; adding up the pieces gives the full field for each variable (because geostrophic and hydrostatic balance are also linear operations).

To illustrate the concept of piecewise PV inversion we introduce the second canonical disturbance: a straight localized wind maximum within the westerly jet stream known as a "jet streak" (Figure 6.12). An elliptical dipole is used to model the jet streak, with a cyclonic QG PV anomaly poleward of an anticyclonic QG PV anomaly. The flow induced by this dipole produces a jet of strong wind between them (Figure 6.12a) and, adding in the simple linear westerly jet as in the previous example, we see a spatially localized burst of stronger wind within the broader westerlies (Figure 6.12b). Considering now the flow induced by only the positive and negative ellipses of QG PV, we see that the jet is present between the vortices because the contribution from each ellipse reinforces that from the other in this location. Moreover, the flow from each ellipse extends to the other vortex in a symmetrical fashion (Figure 6.12c, d). The dynamics of this system are simply understood by the component of flow from each ellipse

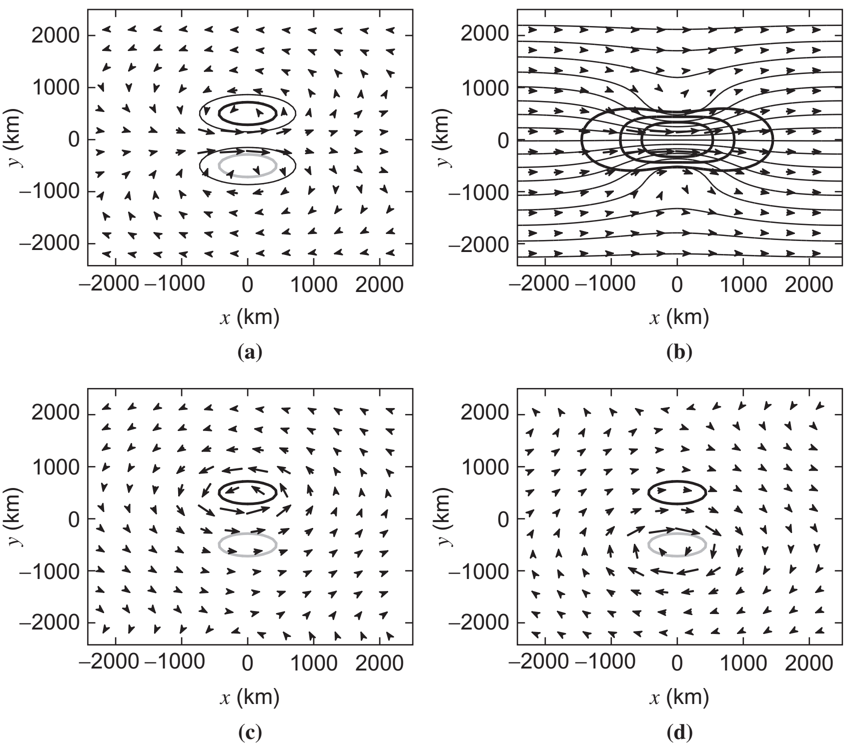

FIGURE 6.12 Idealized model of a "jet streak" as a dipole of QG PV having a magnitude of 2 PVU embedded in a jet stream consisting of a westerly wind increasing linearly with height. (a) PV contours at a height of 5 km are shown every 0.5 PVU; wind induced by the PV anomaly is shown by *arrows*, with a maximum wind speed of 22 m s^{-1}; (b) pressure contours at 5 km every 42 hPa (equivalent to 60-m geopotential height contours on an isobaric surface), full wind vectors (wind due to the PV dipole plus the westerly jet), and isotachs (20, 30, and 40 m s^{-1}) in *thick lines*; (c) wind induced by the positive anomaly; (d) wind induced by the negative PV anomaly. In (c) and (d) the −1- and 1-PVU QG PV contours are denoted by the *thick* gray and black lines, respectively.

advecting the QG PV, which reveals that (1) there is very little dynamics associated with each ellipses' "self" advection; and (2) the dynamics focus around the advection of the QG PV by the opposing ellipse, which advects the ellipses symmetrically downstream (the system moves in a straight line) at a speed much slower than the wind in the jet streak itself.

Section's Key Points

- The pressure field is determined completely by the QG PV through an inversion relationship. Through the geostrophic and hydrostatic relations, the geostrophic wind and potential temperature fields are recovered from the QG PV as well.

- Warm air at the surface is analogous to cyclonic QG PV; cold air at the tropopause is analogous to cyclonic QG PV.
- QG PV inversion is defined by a Laplacian-like operator, so that local maxima in cyclonic QG PV yield local minima in pressure.
- Piecewise QG PV inversion involves breaking the QG PV field into components and associating with each component a pressure field by QG PV inversion; the sum of the pieces is equal to the total pressure field.

6.4.2 PV Conservation and the QG "Height Tendency" Equation

Given the ability to recover the geostrophic wind from the QG PV, QG prediction may now be explored from the PV Thinking perspective. Expanding the QG material derivative in (6.16) gives

$$\frac{\partial q}{\partial t} = -\mathbf{V}_g \cdot \nabla_h q \tag{6.33}$$

which says that the time rate of change of QG PV at a point in space is determined entirely by the advection of the QG PV by the geostrophic wind. This provides the basis for a dynamical forecast model. Given an initial distribution of QG PV, one inverts this field for the pressure using (6.31), which then gives the geostrophic wind. Knowledge of the QG PV and geostrophic wind allows for a prediction of the future configuration of the QG PV from (6.33). At the future time, the QG PV can be inverted for the wind, and the process repeated indefinitely into the future.

To complete the picture, however, we need to specify boundary conditions for (6.33). At Earth's surface, which we approximate as a rigid horizontal surface, there is no vertical motion, and therefore the QG thermodynamic energy equation takes the form

$$\frac{\partial \theta}{\partial t} = -\mathbf{V}_g \cdot \nabla_h \theta \tag{6.34}$$

Notice that this equation is identical to (6.33), where θ plays the role of q. Therefore, in addition to advancing q by (6.33), we also advance θ by (6.34), which provides boundary conditions for the QG PV inversion at the future time. For the upper boundary condition, another rigid horizontal boundary may be used to represent either a crude approximation to the tropopause or a higher level in the stratosphere.

This approach is an extremely powerful approximation to the evolution of extratropical weather systems, where one needs to evaluate the horizontal advection of only a single quantity to predict the future, compared to solving complicated equations for five variables in the full system (u, v, w, p, θ).

Nevertheless, we do not measure QG PV directly, and a forecast of pressure is often more intuitive. We may obtain a pressure forecast equation from (6.33) by noting that $\frac{\partial}{\partial t} f(q - f) = \frac{\partial}{\partial t}(fq) = \mathsf{L}\frac{\partial p}{\partial t}$, so that

$$\mathsf{L}\frac{\partial p}{\partial t} = -\mathbf{V}_g \boldsymbol{\cdot} \nabla_h (fq) \tag{6.35}$$

Here, L is the quasi-Laplacian operator (6.30). Therefore, in order to obtain the pressure tendency, $\frac{\partial p}{\partial t}$, we apply the inversion operator L^{-1} to the QG PV advection term. We expect that near local maxima in QG PV advection, such as downwind of a QG PV maximum, the pressure tendency will be a local minimum (that is, the pressure will fall).

Boundary conditions for the pressure tendency are obtained using the hydrostatic equation (6.6) in (6.34) to yield

$$\frac{\partial}{\partial z}\frac{\partial p}{\partial t} = \frac{\rho_0 g}{\overline{\theta}}\left(-\mathbf{V}_g \boldsymbol{\cdot} \nabla_h \theta\right) \tag{6.36}$$

Warm-air advection at the surface implies that the pressure tendency increases upward from the surface so that, if the tendency is negative (pressure falls), it will be most negative on the boundary.

Replacing q on the right side of (6.35) using (6.17) gives

$$\mathsf{L}\frac{\partial p}{\partial t} = -\mathbf{V}_g \boldsymbol{\cdot} \nabla_h \zeta_g - \mathbf{V}_g \boldsymbol{\cdot} \nabla_h \left(f \frac{\partial}{\partial z} \frac{d\overline{\theta}}{dz}^{-1} \theta \right) \tag{6.37}$$

Using the thermal-wind equation (6.7) on the last term leaves

$$\boxed{\mathsf{L}\frac{\partial p}{\partial t} = -\mathbf{V}_g \boldsymbol{\cdot} \nabla_h (f\zeta_g) + f^2 \frac{\partial}{\partial z}\left[\frac{d\overline{\theta}}{dz}^{-1} \left(-\mathbf{V}_g \boldsymbol{\cdot} \nabla_h \theta\right)\right]} \tag{6.38}$$

which is known as the **quasi-geostrophic pressure tendency equation**, or the **height tendency equation** since, in pressure coordinates, geopotential height plays the role of pressure (see Section 6.7). Recalling the rough rule of thumb that L reverses the sign of the quantity it operates upon, we see that pressure will decrease in time where there is (1) cyclonic geostrophic vorticity advection by the geostrophic wind, and (2) an upward increase in the geostrophic advection of potential temperature. An example of the first situation occurs downwind of upper-level troughs, since cyclonic vorticity is a local maximum in troughs. An example of the second situation occurs where cold air advection in the lower troposphere decreases with height, such as behind a surface cold front. Notice that if the atmosphere is very stable $\left(\text{large } \frac{d\overline{\theta}}{dz}\right)$, the pressure tendency is dominated by vorticity advection *and*, from (6.30), the response is local in the vertical, so that the dynamics become a set of nearly horizontal uncoupled layers.

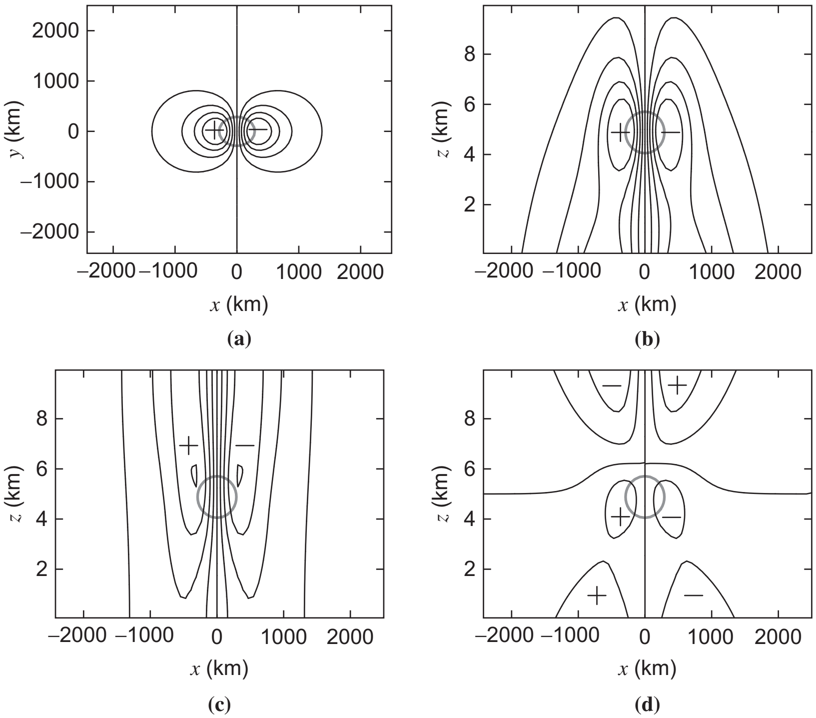

FIGURE 6.13 Pressure tendency associated with the PV blob in vertical shear shown in Figure 6.10. Pressure tendency: (a) plan view at 5-km altitude; (b) cross-section along $y = 0$; (c) cross-section along $y = 0$ of vorticity advection contribution; and (d) cross-section along $y = 0$ of temperature advection contribution. The sum of (c) and (d) equals (b). Pressure tendency *contours* are shown every 5 hPa (day)$^{-1}$, and the 1-PVU QG PV contour by a *thick gray line*.

For the PV blob in westerly shear (refer to Figure 6.10), solution of the pressure tendency equation shows, as expected, that the pressure falls downwind of the PV blob (Figure 6.13a). In the vertical, the pressure falls over a deep layer downwind of the upper-level feature, including at the surface (Figure 6.13b). The response is asymmetric in the vertical direction due to the boundary condition (6.36): Warm air advection to the right of the PV blob implies an upward increase in $\frac{\partial p}{\partial t}$ at the boundaries, so that pressure falls are a local minimum at the surface. From the PV perspective, recall that warm air on the surface acts like cyclonic QG PV, whereas warm air on the tropopause acts like anticyclonic PV; therefore, temperature advection on the surface reinforces the tendency from the PV blob, whereas there is cancellation on the tropopause.

Examining the individual contributions from advection of vorticity and potential temperature, we see that, due to the increase of westerly winds with height, the magnitude of the pressure tendency from vorticity advection is largest above the PV blob and the pressure tendency from potential temperature advection changes sign between the surface and tropopause (Figure 6.13c, d) due in part to the boundary condition effect described previously.

Section's Key Points

- Pressure falls near local maxima of cyclonic QG PV advection.
- Pressure falls near local maxima of cyclonic geostrophic vorticity PV advection.
- Pressure falls near locations having an increase with height of the geostrophic advection of potential temperature (cold-air advection decreasing with height or warm-air advection increasing with height).
- At the surface, geostrophic advection of potential temperature determines the sign of the vertical gradient of the pressure tendency (warm-air advection implies the pressure tendency increases with height).

6.5 VERTICAL MOTION (w) THINKING

Vertical motion plays no role in PV Thinking because advection of potential vorticity is determined entirely by the geostrophic wind. Although temperature and momentum adjustments are implicit in the material conservation of QG PV, it is often helpful for understanding the dynamics of weather systems to consider these changes explicitly. In this framework the QG dynamics are expressed through the thermodynamic energy and vorticity equations

$$\frac{\partial \theta}{\partial t} = -\mathbf{V}_g \cdot \nabla_h \theta - w\frac{d\overline{\theta}}{dz} \tag{6.39}$$

and

$$\frac{\partial}{\partial t}\left(\zeta_g + f\right) = -\mathbf{V}_g \cdot \nabla_h (\zeta + f) + f\frac{\partial w}{\partial z} \tag{6.40}$$

respectively. Vertical motion controls the evolution of both θ and ζ_g. Therefore, we need an equation for w, which will not only mathematically close this framework but will also provide useful information on locations where clouds might form and conditional instability might be released.

To obtain the w equation we eliminate the time derivative between (6.39) and (6.40). First, we use (6.2) and (6.6) to express vorticity and potential temperature in terms of pressure:

$$\frac{\partial \theta}{\partial t} = \frac{\overline{\theta}}{\rho_0 g}\frac{\partial}{\partial z}\frac{\partial p}{\partial t} \quad \frac{\partial \zeta}{\partial t} = \frac{1}{\rho_0 f}\nabla_h^2 \frac{\partial p}{\partial t} \tag{6.41}$$

Time tendencies of pressure can then be eliminated by taking $\frac{g}{f\overline{\theta}}\nabla^2\frac{\partial\theta}{\partial t}$ and $\frac{\partial}{\partial z}\frac{\partial\zeta}{\partial t}$, and subtracting the resulting equations, which gives

$$\nabla_h^2 w + \frac{f^2}{N^2}\frac{\partial^2 w}{\partial z^2} = \frac{g}{\overline{\theta}N^2}\nabla_h^2\left(-\mathbf{V}_g \cdot \nabla_h\theta\right) - \frac{f}{N^2}\frac{\partial}{\partial z}\left(-\mathbf{V}_g \cdot \nabla_h\zeta\right) \tag{6.42}$$

This equation is more commonly known as the "traditional form" of the **quasi-geostrophic vertical motion** equation (or "omega" equation, where omega (ω) is the symbol for vertical motion in pressure coordinates). The left side involves again a quasi-Laplacian operator,

$$\tilde{\mathrm{L}} = \nabla_h^2 + \frac{f^2}{N^2}\frac{\partial^2}{\partial z^2} \tag{6.43}$$

and its interpretation is similar to that for L in QG PV inversion (6.30). Specifically, we see that, for a given forcing, the response in w will be mainly in the horizontal when $\frac{f^2}{N^2}$ is small—that is, for small planetary rotation and large static stability.

From (6.42) we see that upward motion ($w > 0$) is associated with local maxima in warm-air advection and an upward increase in the advection of geostrophic vorticity by the geostrophic wind. In both cases, the term on the right side of (6.42) is negative, which becomes positive when we "flip the sign" for the quasi-Laplacian, $\tilde{\mathrm{L}}$.

A problem with the traditional form of the omega equation is that there exists significant cancellation between the two right-side terms. To expose this cancellation and develop two different forms of the omega equation, we need to expand the right side of (6.42). This involves taking the gradient of vector products, for which vector notation is not well suited. Just as we use vector notation to simplify mathematical manipulations when scalar notation becomes cumbersome, it is often prudent to move to *indicial notation* for situations where vector notation becomes awkward. In many ways, indicial notation is simpler and less ambiguous than vector notation; we introduce only the basic elements needed here.

Indicial notation uses a subscript index to represent the components of a vector. For example, the vector wind $\mathbf{U} = (u, v, w)$ in vector notation may be written as u_i, where $u_1 = u$, $u_2 = v$, and $u_3 = w$ in indicial notation. Similarly, the vector coordinate directions (x, y, z) may be written simply as x_i. The key simplification of indicial notation is that *repeated indices represent sums.* For example, $a_i b_i = a_1 b_1 + a_2 b_2$ in two dimensions. Indices left over after summation, called dummy indices, are free to be changed if done so consistently. The dot product between two vectors can in general be written as

$$c = \mathbf{a} \cdot \mathbf{b} = a_i\, b_j \delta_{ij} = a_i\, b_i = a_j\, b_j \tag{6.44}$$

where δ_{ij} is the Kronecker delta, which takes the value one when $i = j$ and zero otherwise, leaving the familiar sum of products of vector components. Therefore, when expressing dot products it is convenient to match the subscripts of the effected quantities, which obviates the need for δ_{ij}. The gradient operator, ∇ in vector notation, takes the form $e_i \frac{\partial}{\partial x_i}$ for indicial notation, where e_i is a unit vector. This turns out to be useful for our purposes because all of the traditional rules of differential calculus, such as the product and chain rules, apply as usual. Advection combines the gradient operator and dot product, and appears for indicial notation as, for example,

$$U \cdot \nabla \theta = u_i \frac{\partial \theta}{\partial x_i} \tag{6.45}$$

We may now write the traditional form of the omega equation using indicial notation as

$$\tilde{L}w = \frac{g}{\overline{\theta} N^2} \frac{\partial}{\partial x_i} \frac{\partial}{\partial x_i} \left(-v_j \frac{\partial \theta}{\partial x_j} \right) - \frac{f}{N^2} \frac{\partial}{\partial x_3} \left(-v_j \frac{\partial \zeta}{\partial x_j} \right) \tag{6.46}$$

where we have dropped the subscript g on the wind and vorticity, and indices i and j take values 1 and 2 (x and y directions). Taking the innermost derivatives gives

$$\begin{aligned} \tilde{L}w = & \frac{g}{\overline{\theta} N^2} \frac{\partial}{\partial x_i} \left(-\frac{\partial v_j}{\partial x_i} \frac{\partial \theta}{\partial x_j} - v_j \frac{\partial^2 \theta}{\partial x_i \partial x_j} \right) \\ & - \frac{f}{N^2} \left(-\frac{\partial v_j}{\partial x_3} \frac{\partial \zeta}{\partial x_j} - v_j \frac{\partial}{\partial_j} \frac{\partial \zeta}{\partial x_3} \right) \end{aligned} \tag{6.47}$$

From the definition of vorticity, $\zeta_g = \frac{1}{\rho_o f} \frac{\partial^2 p}{\partial x_i^2}$, and the hydrostatic balance, $\frac{1}{\rho_o} \frac{\partial p}{\partial x_3} = \frac{g}{\overline{\theta}} \theta$, we find $\frac{\partial \zeta}{\partial x_3} = \frac{g}{f \overline{\theta}} \frac{\partial^2 \theta}{\partial x_i^2}$. Using this identity in (6.47), and taking the remaining derivative on the first term, gives

$$\begin{aligned} \tilde{L}w = & \frac{g}{\overline{\theta} N^2} \left(-\frac{\partial^2 v_j}{\partial x_i^2} \frac{\partial \theta}{\partial x_j} - 2 \frac{\partial v_j}{\partial x_i} \frac{\partial^2 \theta}{\partial x_i \partial x_j} - v_j \frac{\partial}{\partial x_j} \frac{\partial^2 \theta}{\partial x_i^2} \right) \\ & + \frac{f}{N^2} \left(\frac{\partial v_j}{\partial x_3} \frac{\partial \zeta}{\partial x_j} + v_j \frac{\partial}{\partial x_j} \frac{g}{f \overline{\theta}} \frac{\partial^2 \theta}{\partial x_i^2} \right) \end{aligned} \tag{6.48}$$

Cancellation is now apparent between the last term of each bracketed quantity. Moreover, it may be shown that (see Problem 6.3)

$$\frac{g}{\overline{\theta} N^2} \frac{\partial^2 v_j}{\partial x_i^2} \frac{\partial \theta}{\partial x_j} = \frac{f}{N^2} \frac{\partial v_j}{\partial x_3} \frac{\partial \zeta}{\partial x_j} \tag{6.49}$$

Two other forms of the omega equation are now immediately recovered. Using (6.49) to replace the term involving vorticity in (6.48) gives the compact form

$$\tilde{L}w = -2 \frac{g}{N^2 \overline{\theta}} \frac{\partial}{\partial x_i} \left(\frac{\partial v_j}{\partial x_i} \frac{\partial \theta}{\partial x_j} \right) \tag{6.50}$$

In vector notation this may be written as

$$\boxed{\tilde{L}w = 2\nabla_h \cdot \mathbf{Q}} \tag{6.51}$$

where $\mathbf{Q} \equiv -\frac{g}{N^2\overline{\theta}}\frac{\partial v_j}{\partial x_i}\frac{\partial \theta}{\partial x_j}$ is the "$\mathbf{Q}$-vector." Writing the $\mathbf{Q}$-vector in component form,

$$\begin{aligned}\mathbf{Q} &= -\frac{g}{N^2\overline{\theta}}(Q_1, Q_2)\\ &= -\frac{g}{N^2\overline{\theta}}\left(\frac{\partial u_g}{\partial x}\frac{\partial \theta}{\partial x} + \frac{\partial v_g}{\partial x}\frac{\partial \theta}{\partial y}, \frac{\partial u_g}{\partial y}\frac{\partial \theta}{\partial x} + \frac{\partial v_g}{\partial y}\frac{\partial \theta}{\partial y}\right)\end{aligned} \tag{6.52}$$

we see that vertical motion is associated with products of horizontal wind gradients and horizontal potential temperature gradients. These effects involve changes in horizontal potential temperature gradients, which we shall explore more thoroughly in Chapter 9. Rising air is found in regions where the $\mathbf{Q}$-vector converges, so that the righthand side of (6.51) is negative, and $\tilde{L}$ flips the sign.

The direction and magnitude of the $\mathbf{Q}$-vector at a given point on a weather map can be estimated as follows. First note that the $\mathbf{Q}$-vector can be written as

$$\mathbf{Q} = -\frac{g}{N^2\overline{\theta}}\left(\frac{\partial \mathbf{V}_g}{\partial x}\cdot\nabla_h\theta, \frac{\partial \mathbf{V}_g}{\partial y}\cdot\nabla_h\theta\right) \tag{6.53}$$

By referring the motion to a Cartesian coordinate system in which the x axis is parallel to the local isotherm with cold air on the left, (6.53) can be simplified to give

$$\mathbf{Q} = -\frac{g}{N^2\overline{\theta}}\left|\frac{\partial \theta}{\partial y}\right|\mathbf{k} \times \frac{\partial \mathbf{V}_g}{\partial x} \tag{6.54}$$

where we have used the fact that $\partial u_g/\partial x = -\partial v_g/\partial y$ and $\frac{\partial \theta}{\partial y} < 0$ in the specified coordinates. Thus, the $\mathbf{Q}$-vector can be obtained by evaluating the vectorial change of $\mathbf{V}_g$ along the isotherm (with cold air on the left), rotating this change vector by 90° clockwise, and multiplying the resulting vector by $\frac{g}{N^2\overline{\theta}}|\frac{\partial \theta}{\partial y}|$. An example is shown in Figure 6.14, which shows an idealized pattern of cyclones and anticyclones in a slightly perturbed westerly thermal wind. Near the center of the low, the geostrophic wind change moving eastward along the isotherm is from northerly to southerly. Thus the geostrophic wind change vector points northward, and a 90° clockwise rotation produces a $\mathbf{Q}$-vector parallel to the thermal wind. In the highs, by the same reasoning, the $\mathbf{Q}$-vectors are antiparallel to the thermal wind. The pattern of $\nabla \cdot \mathbf{Q}$ thus yields descent in the region of cold-air advection west of the trough, and ascent in the warm-air advection region east of the trough.

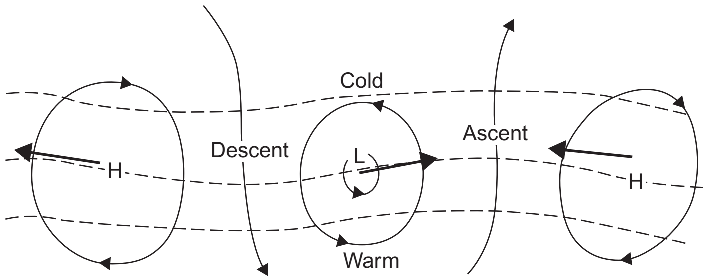

FIGURE 6.14 **Q** vectors (*bold arrows*) for an idealized pattern of isobars (*solid lines*) and isotherms (*dashed lines*) for a family of cyclones and anticyclones. (*After Sanders and Hoskins, 1990.*)

Yet another form of the omega equation is obtained using (6.49) to replace the first term in (6.48) to yield

$$\boxed{\tilde{L}w = 2\frac{f}{N^2}\frac{\partial v_i}{\partial x_3}\frac{\partial \zeta}{\partial x_i} + D} \tag{6.55}$$

where $D = -2\frac{g}{\bar{\theta}N^2}\frac{\partial v_j}{\partial x_i}\frac{\partial^2\theta}{\partial x_i \partial x_j}$ is the "deformation term." Noting that $\partial v_i\, \partial x_3$ is the thermal wind, V_T, then (6.55) becomes, in vector notation, the deformation term is one of two terms in the divergence of the **Q**-vector. In vector notation,

$$\tilde{L}w = -\frac{2}{N^2}\left[-\mathbf{V}_{\mathrm{T}} \cdot \nabla_h(f\zeta_g)\right] + D \tag{6.56}$$

is called the *Sutcliffe form* of the QG omega equation. Neglecting the deformation term, we see that rising air is located near regions of cyclonic vorticity advection by the thermal wind. Although this approximation neglects a potentially important source of vertical motion from the deformation term, advection of vorticity by the thermal wind is easily visualized on upper-level weather maps.

The vertical motion field for the PV blob in westerly shear is shown in Figure 6.15. Notice that **Q**-vectors converge (diverge) in the region of rising (sinking) motion downwind (upwind) of the PV blob. An east–west cross-section through the PV-blob reveals the ageostrophic circulation that links rising and sinking motion by mass continuity. Consider the local time tendency of potential temperature at the level of maximum QG PV. Since disturbance potential temperature is zero at this level, there is no advection of this quantity (see Figure 6.10d), whereas the disturbance advection of the basic-state potential temperature gradient (linear decrease with *y*) implies increasing (decreasing) values to the right (left) of the PV blob. Geostrophic and hydrostatic balance are "disrupted" by this geostrophic advection pattern, but they are "restored" by the ageostrophic circulation. Notice that the vertical motion pattern cools

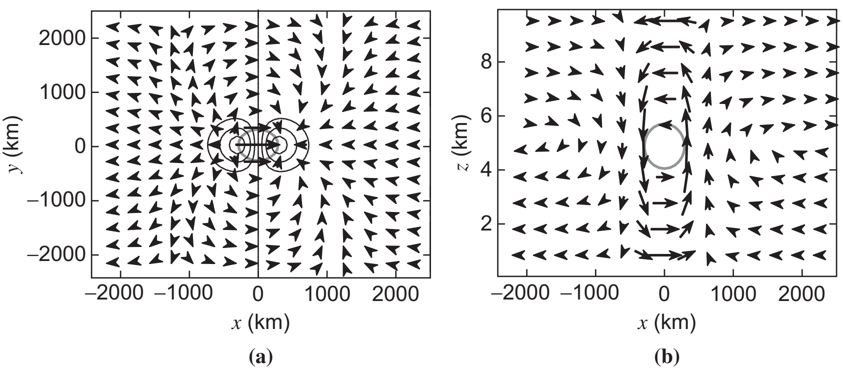

FIGURE 6.15 Vertical motion associated with the PV blob in vertical shear shown in Figure 6.10. (a) Q-vectors and contours of w every 2 cm s^{-1}, with rising air where Q-vectors converge; (b) vertical cross-section along $y = 0$ of the ageostrophic circulation (u_a, w). The 1-PVU QG PV contour is shown by a *thick gray line*.

(warms) the atmosphere in the region of rising (sinking) motion, which opposes the tendency from geostrophic advection discussed previously. Moreover, Coriolis turning of the horizontal ageostrophic wind acts to increase (decrease) the v_g component of the wind above (below) the PV blob, which restores thermal wind balance with the new potential temperature distribution. In the quasi-geostrophic equations, this adjustment "process" is instantaneous, so that the atmosphere is always in quasi-geostrophic and quasi-hydrostatic balance. Linking back to the PV view of dynamics, one can say that the ageostrophic circulations that maintain geostrophic and hydrostatic balance are required if the QG PV is to be conserved following the geostrophic motion.

Note that, in the absence of **Q**-vectors, one may still easily estimate the vertical motion pattern using the Sutcliffe form of the QG omega equation. The thermal wind, dominated by the westerly shear jet, points mostly toward positive x, so that the advection of geostrophic vorticity by the thermal wind is positive (negative) to the right (left) of the PV blob. As a result, one expects rising (sinking) motion to the right (left) of the blob. This technique can be extremely useful for quickly estimating regions of rising and sinking air from weather maps.

For the jet streak example, a four-cell pattern of vertical motion is apparent, with rising motion in the "right entrance" and "left exit" regions of the jet (Figure 6.16). Vertical cross sections through the jet entrance (Figure 6.17, left panel) and exit (Figure 6.17b) regions reveal transverse (across flow) ageostrophic circulations, which increase (decrease) zonal momentum in upper levels. These circulation patterns accelerate (decelerate) the wind into (out of) the jet, as well as increasing (decreasing) the vertical shear of the zonal wind in the jet entrance (exit) regions. Notice that, in the jet entrance region, relatively

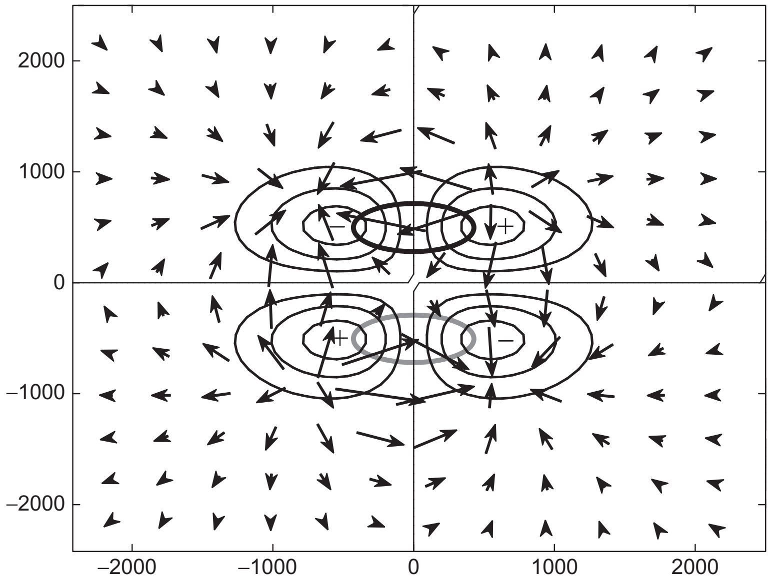

FIGURE 6.16 Vertical motion associated with the jet streak shown in Figure 6.12. *Contours* show vertical motion (w) at 5-km altitude every 1 cm s^{-1}, and *arrows* show the divergent ageostrophic wind. The -1- and 1-PVU QG PV contours are denoted by the *thick gray* and *black lines*, respectively.

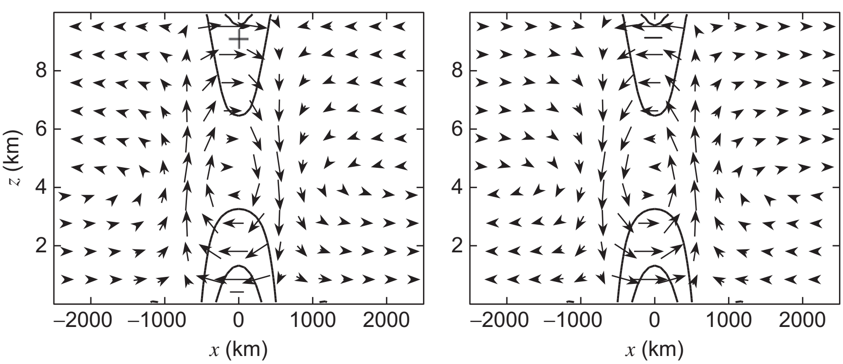

(a) **(b)**

FIGURE 6.17 Vertical cross-section of ageostrophic circulation (u_a, w) near the (a) jet entrance ($x = -700$ km) and (b) jet exit ($x = 700$ km) regions. *Contours* show the acceleration of the geostrophic zonal wind, $\frac{Du}{Dt}$, every 5 m s^{-1} per hour.

warm air rises while relatively cold air sinks, which converts potential energy to kinetic energy of the stronger winds in the jet streak; the reverse process occurs in the jet exit region.

Section's Key Points

- The QG equations have a diagnostic equation for vertical motion.
- Air rises near local maxima in warm-air advection and an upward increase in the advection of geostrophic vorticity by the geostrophic wind.
- Air rises near local maxima of **Q**-vector convergence.
- Air rises near local maxima of cyclonic vorticity advection by the thermal wind.

6.6 IDEALIZED MODEL OF A BAROCLINIC DISTURBANCE

We have developed two dynamically consistent frameworks for interpreting quasi-geostrophic dynamics. Here we apply these frameworks to understand intensifying extratropical cyclones, which is a process referred to as cyclogenesis (see Figures 6.7, 6.8, and accompanying text). Figure 6.18 illustrates the main elements involved in the development process. Nearly all developing cyclones are preceded by an upper-level disturbance that is due to a downward undulation of the tropopause. This downward undulation is associated with a blob of anomalous cyclonic PV, represented by the "+" sign in Figure 6.18. As discussed in connection with Figure 6.10, such a PV blob is associated with low-pressure, cyclonic winds, and warm (cold) air above (below) the blob. At the surface, a developing cyclone appears downshear of the PV blob as a region of relatively warm air at the surface. As discussed in connection with Figure 6.11, anomalously warm air at the surface behaves like cyclonic PV and is associated with low pressure and cyclonic winds that weaken upward. Taken together, these PV anomalies yield pressure fields that tilt westward with height and potential temperature fields that tilt eastward with height. A final important ingredient is the ambient flow, which takes the form of westerly winds that increase upward to a maximum at the tropopause.

From the PV-θ (kinematic) perspective, low pressure develops east of the upper-level PV blob because the induced flow from the blob acts to increase the amplitude of the surface warm anomaly through warm air advection (Figure 6.18b, *heavy dashed line*). Note that this mechanism requires a poleward decrease in the ambient potential temperature field and, by thermal wind, an upward increase in westerly winds as assumed before. Similarly, given a poleward increase of PV at the level of the upper-level PV blob, the amplitude of the anomaly will increase due to equatorward advection of PV by the flow induced from the surface warm anomaly (Figure 6.18b, *thin solid line*).

From a height tendency (dynamic) perspective, we know from Figure 6.13 that pressure falls east of the upper PV blob due to advection of cyclonic QG PV by the ambient westerly shear. Moreover, an upward decrease in the cold-air advection to the west of the developing surface low pressure results in intensification of the upper-level low pressure. One may understand the development of surface high pressure upshear from the PV blob by similar reasoning.

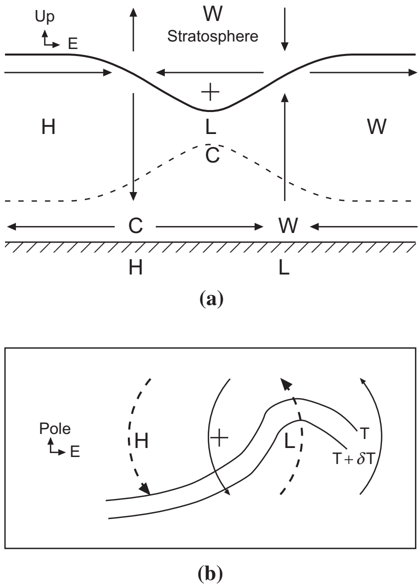

FIGURE 6.18 Schematic of quasi-geostrophic reasoning applied to extratropical cyclone development. (a) East–West vertical section showing the tropopause (*thick solid line*), the surface (*cross-hatched line*), a lower-tropospheric isentropic surface (*dashed line*), and the air circulations required to conserve potential vorticity for the typical case where westerly winds are increasing from the surface to the tropopause. Regions of relatively warm and cold air are given by "W" and "C," respectively, and regions of relatively low and high pressure are given by "L" and "H," respectively. (b) Horizontal plan view showing the surface isotherms (*solid lines*), surface wind associated with the upper-level PV disturbance (*thick dashed lines with arrows*), and surface wind associated with the surface cyclone (*thin solid lines with arrows*). In both (a) and (b), "+" shows the location of the PV disturbance due to the lowered tropopause. (*From Hakim, 2002.*)

From the *w* perspective, low-level vorticity increases east of the upper-level PV blob because of vortex stretching associated with rising air in the troposhpere above this location (Figure 6.18a, *arrows*). From Figure 6.15, we know that PV blobs in westerly shear produce ageostrophic circulations associated with this rising air and convergence near the surface, which increases the vorticity. From the thermodynamic energy equation, rising air tends to cool the column, partially canceling warming due to warm-air advection. By thickness reasoning, the warming over the surface low pressure is associated with an increase in the spacing between pressure surfaces so that, given a fixed upper surface in the lower stratosphere, the increased thickness is realized as a drop in the surface pressure. Again, one may understand the development of surface high pressure upshear from the PV blob by vortex squashing associated with sinking air.

We may now add the contributions of clouds and precipitation to this dry description of cyclogenesis. In the region of rising motion we expect clouds to form due to latent heat release. From the *w* perspective, this added heat helps to intensify the developing cyclone by warming the column. From the PV-θ perspective, we must recognize that latent heating implies that PV is not conserved following air parcels, and from Section 4.4, we note that cyclonic PV is created below the level of maximum heating (see Figure 6.10a). This "new" PV is located above the surface cyclone, and as a result, produces a decrease in pressure and an increase in cyclonic circulation by PV inversion and superposition reasoning.

Finally, we note that the cyclogensis process is accelerated when the ambient static stability is reduced. This may be understood from the PV-θ perspective through an increase in the Rossby depth, which increases flow induced by the upper-level PV blob at the surface. From the w perspective, weaker static stability is also associated with a stronger and deeper ageostrophic circulation. Conversely, the cyclogenesis process is slowed for increasing ambient static stability. This is one reason why the main storm tracks for extratropical cyclones are found over the western margins of the Atlantic and Pacific oceans; the high heat capacity of the upper ocean allows relatively warm water in winter to heat the overlying lower atmosphere, weakening the static stability of the troposphere.

6.7 ISOBARIC FORM OF THE QG EQUATIONS

Gridded weather data and weather maps are typically available in isobaric, rather than constant height, surfaces. The reasons for this are partly historical, but also that density becomes implicit in the governing equations when pressure is used as a vertical coordinate. Nevertheless, using pressure as the vertical coordinate yields a "left-handed" coordinate system, since pressure increases down rather than up, which results in a more cumbersome interpretation of the equations. Upward vertical motion is negative in the isobaric system ($\omega = Dp/Dt$ is the vertical motion). Following is a summary of the QG equations in isobaric coordinates presented without proof. Interpretation of these equations is the same as for the height-coordinate counterparts presented earlier in the chapter, except here additional terms appear due to the inclusion of the β effect (the Coriolis parameter varies linearly with latitude); these are often small in magnitude, but are included here for completeness.

Hydrostatic balance is given by

$$\frac{\partial \Phi}{\partial p} = -\alpha = -RT/p \tag{6.57}$$

The geostrophic wind is defined by

$$\mathbf{V}_g \equiv f_0^{-1}\mathbf{k} \times \nabla_h \Phi \tag{6.58}$$

where Φ is the geopotential, and the β-plane approximation applies to the Coriolis parameter,

$$f = f_0 + \beta y \tag{6.59}$$

where f_0 is a constant, and $\beta \equiv (df/dy)_{\phi_0} = 2\Omega\cos\phi_0/a$ and $y = 0$ at ϕ_0. The QG momentum equation takes the form

$$\frac{D_g\mathbf{V}_g}{Dt} = -f_0\mathbf{k}\times\mathbf{V}_a - \beta y\mathbf{k}\times\mathbf{V}_g \tag{6.60}$$

and the QG mass continuity equation is

$$\frac{\partial u_a}{\partial x} + \frac{\partial v_a}{\partial y} + \frac{\partial \omega}{\partial p} = 0 \tag{6.61}$$

The adiabatic QG thermodynamic energy equation is

$$\left(\frac{\partial}{\partial t} + \mathbf{V}_g\cdot\nabla_h\right)T - \left(\frac{\sigma p}{R}\right)\omega = 0 \tag{6.62}$$

where $\sigma \equiv -RT_0p^{-1}d\ln\theta_0/dp$ measures the static stability of the reference atmosphere. The QG vorticity equation is unchanged aside from the β term,

$$\frac{D_g\zeta_g}{Dt} = -f_0\left(\frac{\partial u_a}{\partial x} + \frac{\partial v_a}{\partial y}\right) - \beta v_g \tag{6.63}$$

The vorticity–temperature-advection form of the QG height tendency equation $(\chi \equiv \partial\Phi/\partial t)$,

$$\left[\nabla^2 + \frac{\partial}{\partial p}\left(\frac{f_0^2}{\sigma}\frac{\partial}{\partial p}\right)\right]\chi = -f_0\mathbf{V}_g\cdot\nabla_h\left(\frac{1}{f_0}\nabla^2\Phi + f\right) - \frac{\partial}{\partial p}\left[-\frac{f_0^2}{\sigma}\mathbf{V}_g\cdot\nabla_h\left(-\frac{\partial\Phi}{\partial p}\right)\right] \tag{6.64}$$

includes advection of the planetary vorticity, as does the QG PV equation,

$$\left(\frac{\partial}{\partial t} + \mathbf{V}_g\cdot\nabla_h\right)q = \frac{D_gq}{Dt} = 0 \tag{6.65}$$

where the QG PV is given by

$$q \equiv \frac{1}{f_0}\nabla^2\Phi + f + \frac{\partial}{\partial p}\left(\frac{f_0}{\sigma}\frac{\partial\Phi}{\partial p}\right) \tag{6.66}$$

The Sutcliffe form of the QG omega (vertical motion) equation includes advection of the planetary vorticity

$$\left(\nabla^2 + \frac{f_0^2}{\sigma}\frac{\partial^2}{\partial p^2}\right)\omega \approx \frac{f_0}{\sigma}\left[\frac{\partial\mathbf{V}_g}{\partial p}\cdot\nabla_h\left(\frac{1}{f_0}\nabla^2\Phi + f\right)\right] \tag{6.67}$$

Finally, the **Q**-vector form of the QG omega (vertical motion) equation is

$$\sigma\nabla^2\omega + f_0^2\frac{\partial^2\omega}{\partial p^2} = -2\nabla\cdot\mathbf{Q} + f_0\beta\frac{\partial v_g}{\partial p} \tag{6.68}$$

where the **Q**-vector is given by

$$\mathbf{Q} \equiv (Q_1, Q_2) = \left(-\frac{R}{p} \frac{\partial \mathbf{V}_g}{\partial x} \cdot \nabla T, -\frac{R}{p} \frac{\partial \mathbf{V}_g}{\partial y} \cdot \nabla T \right) \tag{6.69}$$

SUGGESTED REFERENCES

Blackburn, *Interpretation of Ageostrophic Winds and Implications for Jetstream Maintenance,* discusses the differences between variable f(VF) and constant f(CF) ageostrophic motion.

Bluestein, *Synoptic-Dynamic Meteorology in Midlatitudes, Vol. II,* has a comprehensive treatment of midlatitude synoptic disturbances at the graduate level.

Cunningham and Keyser (2006) provide the theoretical basis for understanding jet streaks from a PV perspective.

Durran and Snellman (1987) illustrate the application of both traditional and **Q**-vector forms of the omega equation in diagnosing the vertical motion of an observed system.

Hakim, Cyclogenesis in *Encyclopedia of Atmospheric Sciences.*

Lackmann, *Midlatitude Synoptic Meteorology: Dynamics, Analysis, and Forecasting*, applies the quasi-geostrophic equations to the problem of weather analysis and forecasting.

Martin, *Mid-Latitude Atmospheric Dynamics: A First Course*, covers similar material as in this chapter, with an emphasis on the development of extratropical cyclones.

Pedlosky, *Geophysical Fluid Dynamics*, *2nd Edition,* presents a detailed formal derivation of the quasi-geostrophic system with applications to both the atmosphere and the oceans.

Vallis, *Atmospheric and Oceanic Fluid Dynamics: Fundamentals and Large-Scale Circulation,* presents a comprehensive treatment of the dynamics of both the atmosphere and ocean, including the quasi-geostrophic equations.

Wallace and Hobbs, *Atmospheric Science: An Introductory Survey,* has an excellent introductory-level description of the observed structure and evolution of midlatitude synoptic-scale disturbances.

PROBLEMS

6.1. Show that for a basic-state having linear shear, $\overline{U} = \lambda z$, λ constant, the basic-state QG PV depends only on z, and that the disturbance QG PV obeys

$$\left(\frac{\partial}{\partial t} + \overline{U}\frac{\partial}{\partial x}\right) q' = 0$$

6.2. Show that the Boussinesq continuity equation,

$$\frac{\partial u}{\partial x} + \frac{\partial v}{\partial y} + \frac{\partial w}{\partial z} = 0$$

can be written as

$$\frac{\partial u_a}{\partial x} + \frac{\partial v_a}{\partial y} + \frac{\partial w}{\partial z} = 0$$

where the subscript a indicates ageostrophic wind.

6.3. Prove identity (6.49).

6.4. In this problem you will derive an equation for the QG streamfunction of the ageostrophic secondary circulation. You should assume constant f and $\frac{d\overline{\theta}}{dz}$, and that the geostrophic flow is two-dimensional (y–z); specifically: $u_g = u_g(z, t)$ only and $v_g = v_g(y, t)$ only.

(a) Starting with geostrophic and hydrostatic balance,

$$\mathbf{V}_g = \frac{1}{\rho_0 f}\mathbf{k} \times \nabla_h p \qquad \frac{\partial p}{\partial z} = \frac{\rho_0 g}{\overline{\theta}}\theta$$

show that the maintenance of thermal wind balance requires

$$\frac{D}{Dt_g}\frac{\partial u_g}{\partial z} = -\frac{g}{\overline{\theta} f}\frac{D}{Dt_g}\frac{\partial \theta}{\partial y}$$

(b) Determine the left side of the result in (a) from the u_g momentum equation.

$$\frac{Du_g}{Dt_g} = f v_a$$

Interpret the result physically.

(c) Determine the right side of the result in (a) from the thermodynamic energy equation. Interpret the result physically.

(d) Now use your results from (b) and (c) in (a), using a streamfunction for the ageostrophic wind: $v_a = \frac{\partial \psi}{\partial z}$ and $w = -\frac{\partial \psi}{\partial y}$. Express your result with all streamfunction terms on the left side of the equation.

(e) Assume that the right side of your result in (d) reaches a local minimum in the midtroposphere. Sketch the ageostrophic circulation streamlines in a y–z cross-section along with arrows showing v_a and w.

6.5. Consider two spherical, cyclonic QG PV anomalies. One anomaly is located at the origin and has unity radius. The second anomaly is located at $(x, y, z) = (2, 0, 0)$ and has radius and amplitude one-half the corresponding values of the other anomaly. Draw an (x, y) sketch estimating the trajectory traced out by these two anomalies assuming that their shape is preserved. Draw a second sketch showing the w field at a level above the anomalies.

6.6. **(a)** Derive the dispersion relationship for 3D QG Rossby waves on the β-plane. Assume plane waves in the absence of mean flow and boundaries. The governing (disturbance PV) equation is modified by an additional term

$$\frac{Dq}{Dt_g} + v\beta = 0$$

(b) Derive the group velocity vector. Explain the result.

6.7. Derive the QG kinetic energy equation

$$\frac{\partial K}{\partial t_g} + \nabla \cdot \vec{S} = \frac{g}{\theta_0} w\theta$$

starting with the QG momentum equation

$$\frac{D\mathbf{V}_g}{Dt_g} = -f\mathbf{k} \times \vec{V}_a$$

6.8. We have considered simple PV distributions associated with points and spheres. Now consider an extremely complicated PV structure, which is completely contained within a cube having sides of length L. Without knowing the detailed structure of the PV, derive a formula relating the circulation on the lateral sides of the cube, and the mean θ on the top and bottom of the cube, to the mean PV in the cube. [*Hint*: First show that the QG PV can be expressed as the divergence of a vector field.]

MATLAB Exercises

M6.1. Examine the impact of disturbance horizontal scale using the idealized QG PV inversion routine **QG_PV_inversion.m**. Use the parallelpiped initial condition ($ipv = 1$) with an amplitude of 2 PVU. Make a plot of how the disturbance minimum pressure changes as a function of the size of the disturbance (controlled by the parameter *iw* in the routine **QG_initial_value.m**). Repeat the exercise using a Dirichlet boundary condition (zero surface pressure; set $idn = -1$) and compare your results to the Neumann case. Repeat the exercise again by moving the boundaries very far apart (set *ZH* to 10 in **grid_setup.m**). Compare the pressure of all three solutions at a fixed distance below the PV anomaly (e.g., 5.5 km below the anomaly). What can you conclude about the sensitivity to boundary conditions for the Neumann and Dirichlet cases?

M6.2. Set the disturbance in the idealized QG PV inversion routine **QG_PV_inversion.m** to a jet streak ($ipv = 5$) with an amplitude of 2 PVU. Compute the wind speed and make a plot of the wind speed and wind vectors (using *quiver*). Make a blocking pattern by changing the sign on the QG PV amplitude variable *pvmag* so that the dipole pattern reverses. Make a plot of wind speed and wind vectors including a constant zonal wind so that the total zonal wind speed between the vortices is zero. Perform piecewise QG PV inversion on the cyclonic and anticyclone vortices in isolation and, including the constant zonal wind, use PV Thinking to explain why the blocking pattern does not move.

M6.3. The code **QG_model.m** is a numerical solver of the quasi-geostrophic equations in $PV - \theta$ form. Initialize the model with a "blob" of PV ($ipv = 4$) in a simple linear-shear jet ($ijet = 1$). Run the model for 96 hours. Use the plotting code **plot_QG_model.m** to create figures for the solution at various times. Diagnose the solution using **QG_diagnostics.m**. From the solutions of the height tendency equation, describe the evolution of the surface pressure field. From the diagnosed vertical motion field, diagnose the vortex stretching term in the vorticity equation, and use the result to describe the evolution of the surface geostrophic vorticity field. Finally, one might expect the PV blob to tilt over in the linear shear. Check to see if this happens, and explain what you find.

M6.4. For the solution in problem M6.3, solve for the rotational ageostrophic wind defined by (6.22) with $p_a = 0$. Since this component of the wind has no divergence, we may express it in terms of a streamfuntion

$$\mathbf{V}_a = \mathbf{k} \times \nabla \psi_a \tag{6.70}$$

Derive an expression for the ageostrophic vorticity from (6.70) that can be used in (6.22). Plot the rotational ageostrophic wind using *quiver* at the level of the blob along with the pressure field. The sum of the geostrophic and the total ageostrophic wind (rotational plus divergent) provides the QG estimate of the gradient wind. How do the results compare with your expectations based on Section 3.2.5?

M6.5. Initialize **QG_model.m** with a blocking configuration (dipole with high PV over low PV) for the PV described in Problem M6.2. Use **QG_diagnostics.m** to determine favored locations for cloud and precipitation. How does the w pattern compare with a jet streak? Add a constant wind to the linear shear using parameter *Unot*, and note that your value should be non-dimensionalized using the scaling parameter, U. Pick a value for *Unot* that makes the block stationary. Next, average the QG PV and boundary potential temperature fields for the last few output times, and use the result as the initial condition for a new experiment with the value of *Unot* that makes the pattern stationary. How does the result differ from the first experiment? Repeat the experiment by adding a small-amplitude random field to the initial condition. What does the result tell you about why blocks are so persistent in the atmosphere?

Chapter 7

Baroclinic Development

Chapter 6 showed that the quasi-geostrophic equations can qualitatively account for the observed relationships among the vorticity, temperature, and vertical velocity fields in midlatitude synoptic-scale systems. The diagnostic approach used in that chapter provided useful insights into the structure of synoptic-scale systems; it also demonstrated the key role of potential vorticity in dynamical analysis. It did not, however, provide quantitative information on the origins, growth rates, and propagation speeds of such disturbances. This chapter shows how the linear perturbation analysis of Chapter 5 can be used to obtain such information from the quasi-geostrophic equations.

The development of synoptic-scale weather disturbances is often referred to as *cyclogenesis*, a term that emphasizes the role of relative vorticity in developing synoptic-scale systems. This chapter analyzes the processes that lead to cyclogenesis. Specifically, we discuss the role of dynamical instability of the mean flow in accounting for the growth of synoptic-scale disturbances. Moreover, even in the absence of such instability, we show that baroclinic disturbances may still amplify over finite periods of time if properly configured. Thus the quasi-geostrophic equations can, indeed, provide a reasonable theoretical basis for understanding the development of synoptic-scale storms, although as discussed in Section 9.2, ageostrophic effects must be included to model the development of fronts and subsynoptic-scale storms.

7.1 HYDRODYNAMIC INSTABILITY

A zonal-mean flow field is said to be hydrodynamically unstable if a small disturbance introduced into the flow grows spontaneously, drawing energy from the mean flow. It is useful to divide fluid instabilities into two types: parcel instability and wave instability. The simplest example of a parcel instability is the convective overturning that occurs when a fluid parcel is displaced vertically in a statically unstable fluid (see Section 2.7.3). Another example is inertial instability, which occurs when a parcel is displaced radially in an axisymmetric vortex with negative absolute vorticity in the Northern Hemisphere or positive absolute vorticity in the Southern Hemisphere. This instability in discussed in Section 5.5.1. A more general type of parcel instability, called *symmetric*

An Introduction to Dynamic Meteorology. DOI: 10.1016/B978-0-12-384866-6.00007-6

instability, may also be significant in weather disturbances; this is discussed in Section 9.3.

Most of the instabilities of importance in meteorology, however, are associated with wave propagation The wave instabilities important for synoptic-scale meteorology generally occur in the form of zonally asymmetric perturbations to a zonally symmetric basic flow field. In general the basic flow is a jet stream that has both horizontal and vertical mean-flow shears. *Barotropic instability* is a wave instability associated with the horizontal shear in a jet-like current. Barotropic instabilities grow by extracting kinetic energy from the mean-flow field. *Baroclinic instability*, however, is associated with vertical shear of the mean flow. Baroclinic instabilities grow by converting potential energy associated with the mean horizontal temperature gradient that must exist to provide thermal wind balance for the vertical shear in the basic state flow. In neither of these instability types does the parcel method provide a satisfactory stability criterion. A more rigorous approach is required in which a linearized version of the governing equations is analyzed to determine the structure and amplification rate for the various wave modes supported by the system.

As indicated in Problem 5.2 of Chapter 5, the traditional approach to instability analysis is to assume that a small perturbation consisting of a single Fourier wave mode of the form $\exp[ik(x - ct)]$ is introduced into the flow, and to determine the conditions for which the phase velocity c has an imaginary part. This technique, which is called the *normal modes* method, is applied in the next section to analyze the stability of a baroclinic current.

An alternative method of instability analysis is the *initial value* approach. This method is motivated by the recognition that in general the perturbations from which storms develop cannot be described as single normal mode disturbances, but may have a complex structure. The initial growth of such disturbances may strongly depend on the potential vorticity distribution in the initial disturbance. On the time scale of a day or two, such growth can be quite different from that of a normal mode of similar scale, although in the absence of nonlinear interactions the fastest-growing normal mode disturbance must eventually dominate.

A strong dependence of cyclogenesis on initial conditions occurs when a large-amplitude upper-level potential vorticity anomaly is advected into a region where there is a preexisting meridional temperature gradient at the surface. In that case, as shown schematically in Figure 7.1, the circulation induced by the upper-level anomaly (which extends downward, as discussed in Section 6.6) leads to temperature advection at the surface; this induces a potential vorticity anomaly near the surface, which in turn reinforces the upper-level anomaly. Under some conditions the surface and upper-level potential vorticity anomalies can become locked in phase so that the induced circulations produce a very rapid amplification of the anomaly pattern. Detailed discussion of the initial value approach to cyclogenesis is beyond the scope of this text. Here we concentrate primarily on the simplest normal mode instability models.

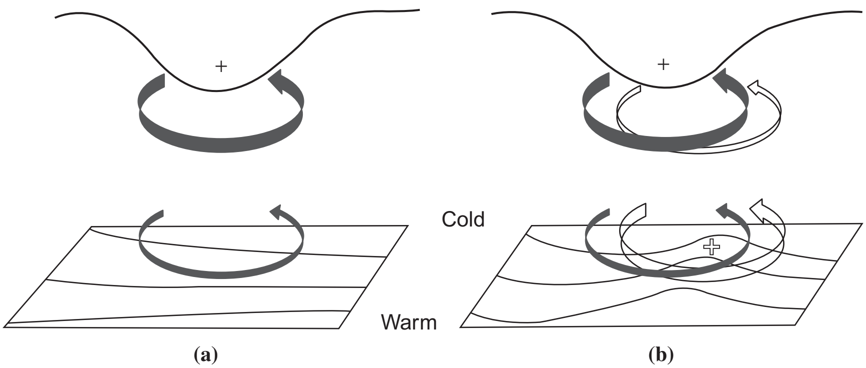

FIGURE 7.1 A schematic picture of cyclogenesis associated with the arrival of an upper-level potential vorticity perturbation over a lower-level baroclinic region. (a) Lower-level cyclonic vorticity induced by the upper-level potential vorticity anomaly. The circulation induced by the potential vorticity anomaly is shown by the *solid arrows*, and potential temperature contours are shown at the lower boundary. The advection of potential temperature by the induced lower-level circulation leads to a warm anomaly slightly east of the upper-level vorticity anomaly. This in turn will induce a cyclonic circulation as shown by the *open arrows* in (b). The induced upper-level circulation will reinforce the original upper-level anomaly and can lead to amplification of the disturbance. (*After Hoskins et al., 1985.*)

7.2 NORMAL MODE BAROCLINIC INSTABILITY: A TWO-LAYER MODEL

Even for a highly idealized mean-flow profile, the mathematical treatment of baroclinic instability in a continuously stratified atmosphere is rather complicated. Before considering such a model, we first focus on the simplest model that can incorporate baroclinic processes. The atmosphere is represented by two discrete layers bounded by surfaces numbered 0, 2, and 4 (generally taken to be the 0-, 500-, and 1000-hPa surfaces, respectively) as shown in Figure 7.2. The quasi-geostrophic vorticity equation for the midlatitude β plane is applied at the 250- and 750-hPa levels, designated by 1 and 3 in Figure 7.2, whereas the thermodynamic energy equation is applied at the 500-hPa level, designated by 2 in Figure 7.2.

Before writing out the specific equations of the two-layer model, it is convenient to define a *geostrophic streamfunction*, $\psi \equiv \Phi/f_0$, for the isobaric form of the quasi-geostrophic equations. Then the geostrophic wind and the geostrophic vorticity can be expressed respectively as

$$\mathbf{V}_\psi = \mathbf{k} \times \nabla_h \psi, \quad \zeta_\mathbf{g} = \nabla_h^2 \psi \tag{7.1}$$

The quasi-geostrophic vorticity equation and the hydrostatic thermodynamic energy equation can then be written in terms of ψ and ω as

$$\frac{\partial}{\partial t}\nabla_h^2 \psi + \mathbf{V}_\psi \cdot \nabla_h \left(\nabla_h^2 \psi\right) + \beta \frac{\partial \psi}{\partial x} = f_0 \frac{\partial \omega}{\partial p} \tag{7.2}$$

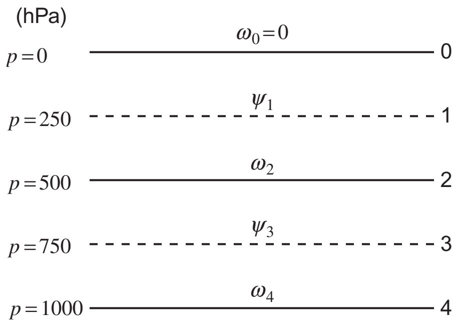

FIGURE 7.2 Arrangement of variables in the vertical for the two-level baroclinic model.

$$\frac{\partial}{\partial t}\left(\frac{\partial \psi}{\partial p}\right) = -\mathbf{V}_\psi \cdot \nabla_h \left(\frac{\partial \psi}{\partial p}\right) - \frac{\sigma}{f_0}\omega \tag{7.3}$$

We now apply the vorticity equation (7.2) at the two levels designated as 1 and 3, which are at the middle of the two layers. To do this we must estimate the divergence term $\partial\omega/\partial p$ at these levels using finite difference approximations to the vertical derivatives:

$$\left(\frac{\partial \omega}{\partial p}\right)_1 \approx \frac{\omega_2 - \omega_0}{\delta p}, \quad \left(\frac{\partial \omega}{\partial p}\right)_3 \approx \frac{\omega_4 - \omega_2}{\delta p} \tag{7.4}$$

where $\delta p = 500$ hPa is the pressure interval between levels 0 to 2 and 2 to 4, and subscript notation is used to designate the vertical level for each dependent variable. The resulting vorticity equations are

$$\frac{\partial}{\partial t}\nabla_h^2\psi_1 + \mathbf{V}_1 \cdot \nabla\left(\nabla_h^2\psi_1\right) + \beta\frac{\partial \psi_1}{\partial x} = \frac{f_0}{\delta p}\omega_2 \tag{7.5}$$

$$\frac{\partial}{\partial t}\nabla_h^2\psi_3 + \mathbf{V}_3 \cdot \nabla_h\left(\nabla_h^2\psi_3\right) + \beta\frac{\partial \psi_3}{\partial x} = -\frac{f_0}{\delta p}\omega_2 \tag{7.6}$$

where we have used the fact that $\omega_0 = 0$, and assumed that $\omega_4 = 0$, which is approximately true for a level-lower boundary surface.

We next write the thermodynamic energy equation (7.3) at level 2. Here we must evaluate $\partial\psi/\partial p$ using the difference formula

$$(\partial\psi/\partial p)_2 \approx (\psi_3 - \psi_1)/\delta p$$

The result is

$$\frac{\partial}{\partial t}(\psi_1 - \psi_3) = -\mathbf{V}_2 \cdot \nabla_h(\psi_1 - \psi_3) + \frac{\sigma\,\delta p}{f_0}\omega_2 \tag{7.7}$$

The first term on the right-hand side in (7.7) is the advection of the 250- to 750-hPa thickness by the wind at 500 hPa. However, ψ_2, the 500-hPa streamfunction, is not a predicted field in this model. Therefore, ψ_2 must be obtained by linearly interpolating between the 250- and 750-hPa levels:

$$\psi_2 = (\psi_1 + \psi_3)/2$$

If this interpolation formula is used, (7.5), (7.6), and (7.7) become a closed set of prediction equations in the variables ψ_1, ψ_3, and ω_2.

7.2.1 Linear Perturbation Analysis

To keep the analysis as simple as possible, we assume that the streamfunctions ψ_1 and ψ_3 consist of basic state parts that depend linearly on y alone, plus perturbations that depend only on x and t. Thus, we let

$$\begin{aligned} \psi_1 &= -U_1 y + \psi_1'(x,t) \\ \psi_3 &= -U_3 y + \psi_3'(x,t) \\ \omega_2 &= \omega_2'(x,t) \end{aligned} \tag{7.8}$$

The zonal velocities at levels 1 and 3 are then constants with the values U_1 and U_3, respectively. Hence, the perturbation field has meridional and vertical velocity components only.

Substituting from (7.8) into (7.5), (7.6), and (7.7) and linearizing yields the perturbation equations

$$\left(\frac{\partial}{\partial t} + U_1 \frac{\partial}{\partial x}\right) \frac{\partial^2 \psi_1'}{\partial x^2} + \beta \frac{\partial \psi_1'}{\partial x} = \frac{f_0}{\delta p}\omega_2' \tag{7.9}$$

$$\left(\frac{\partial}{\partial t} + U_3 \frac{\partial}{\partial x}\right) \frac{\partial^2 \psi_3'}{\partial x^2} + \beta \frac{\partial \psi_3'}{\partial x} = -\frac{f_0}{\delta p}\omega_2' \tag{7.10}$$

$$\left(\frac{\partial}{\partial t} + U_m \frac{\partial}{\partial x}\right) \left(\psi_1' - \psi_3'\right) - U_T \frac{\partial}{\partial x}\left(\psi_1' + \psi_3'\right) = \frac{\sigma\,\delta p}{f_0}\omega_2' \tag{7.11}$$

where we have linearly interpolated to express $\mathbf{V}_2$ in terms of ψ_1 and ψ_3, and have defined

$$U_m \equiv (U_1 + U_3)/2, \qquad U_T \equiv (U_1 - U_3)/2$$

Thus, U_m and U_T are, respectively, the vertically averaged mean zonal wind and the mean thermal wind.

The dynamical properties of this system are more clearly expressed if (7.9), (7.10), and (7.11) are combined to eliminate ω_2'. We first note that (7.9) and

(7.10) can be rewritten as

$$\left[\frac{\partial}{\partial t}+\left(U_m+U_T\right)\frac{\partial}{\partial x}\right]\frac{\partial^2\psi_1'}{\partial x^2}+\beta\frac{\partial\psi_1'}{\partial x}=\frac{f_0}{\delta p}\omega_2' \tag{7.12}$$

$$\left[\frac{\partial}{\partial t}+\left(U_m-U_T\right)\frac{\partial}{\partial x}\right]\frac{\partial^2\psi_3'}{\partial x^2}+\beta\frac{\partial\psi_3'}{\partial x}=-\frac{f_0}{\delta p}\omega_2' \tag{7.13}$$

We now define the barotropic and baroclinic perturbations as

$$\psi_m\equiv\left(\psi_1'+\psi_3'\right)/2;\qquad \psi_T\equiv\left(\psi_1'-\psi_3'\right)/2 \tag{7.14}$$

Adding (7.12) and (7.13) and using the definitions in (7.14) yield

$$\left[\frac{\partial}{\partial t}+U_m\frac{\partial}{\partial x}\right]\frac{\partial^2\psi_m}{\partial x^2}+\beta\frac{\partial\psi_m}{\partial x}+U_T\frac{\partial}{\partial x}\left(\frac{\partial^2\psi_T}{\partial x^2}\right)=0 \tag{7.15}$$

while subtracting (7.13) from (7.12) and combining with (7.11) to eliminate ω_2' yield

$$\begin{aligned}\left[\frac{\partial}{\partial t}+U_m\frac{\partial}{\partial x}\right]\left(\frac{\partial^2\psi_T}{\partial x^2}-2\lambda^2\psi_T\right)+\beta\frac{\partial\psi_T}{\partial x}\\ +U_T\frac{\partial}{\partial x}\left(\frac{\partial^2\psi_m}{\partial x^2}+2\lambda^2\psi_m\right)=0\end{aligned} \tag{7.16}$$

where $\lambda^2\equiv f_0^2/[\sigma(\delta p)^2]$. Equations (7.15) and (7.16) govern the evolution of the barotropic (vertically averaged) and baroclinic (thermal) perturbation vorticities, respectively.

As in Chapter 5, we assume that wave-like solutions exist of the form

$$\psi_m=A\,e^{ik(x-ct)},\qquad \psi_{\mathrm{T}}=B\,e^{ik(x-ct)} \tag{7.17}$$

Substituting these assumed solutions into (7.15) and (7.16) and dividing through by the common exponential factor, we obtain a pair of simultaneous linear algebraic equations for the coefficients A, B:

$$ik\left[\left(c-U_m\right)k^2+\beta\right]A-ik^3U_TB=0 \tag{7.18}$$

$$ik\left[\left(c-U_m\right)\left(k^2+2\lambda^2\right)+\beta\right]B-ikU_T\left(k^2-2\lambda^2\right)A=0 \tag{7.19}$$

Because this set is homogeneous, nontrivial solutions will exist only if the determinant of the coefficients of A and B is zero. Thus, the phase speed c must satisfy the condition

$$\begin{vmatrix}\left(c-U_m\right)k^2+\beta & -k^2U_T\\ -U_T\left(k^2-2\lambda^2\right) & \left(c-U_m\right)\left(k^2+2\lambda^2\right)+\beta\end{vmatrix}=0$$

which gives a quadratic dispersion equation in c:

$$\left(c - U_m\right)^2 k^2\left(k^2 + 2\lambda^2\right) + 2\left(c - U_m\right)\beta\left(k^2 + \lambda^2\right) + \left[\beta^2 + U_T^2 k^2\left(2\lambda^2 - k^2\right)\right] = 0 \tag{7.20}$$

which is analogous to the linear wave dispersion equations developed in Chapter 5. The dispersion relationship in (7.20) yields for the phase speed

$$c = U_m - \frac{\beta\left(k^2 + \lambda^2\right)}{k^2\left(k^2 + 2\lambda^2\right)} \pm \delta^{1/2} \tag{7.21}$$

where

$$\delta \equiv \frac{\beta^2\lambda^4}{k^4\left(k^2 + 2\lambda^2\right)^2} - \frac{U_T^2\left(2\lambda^2 - k^2\right)}{\left(k^2 + 2\lambda^2\right)}$$

We have now shown that (7.17) is a solution for the system (7.15) and (7.16) only if the phase speed satisfies (7.21). Although (7.21) appears to be rather complicated, it is immediately apparent that if $\delta < 0$, the phase speed will have an imaginary part and the perturbations will amplify exponentially. Before discussing the general physical conditions required for exponential growth, it is useful to consider two special cases.

As the first special case we let $U_T = 0$ so that the basic state thermal wind vanishes and the mean flow is barotropic. The phase speeds in this case are

$$c_1 = U_m - \beta k^{-2} \tag{7.22}$$

and

$$c_2 = U_m - \beta\left(k^2 + 2\lambda^2\right)^{-1} \tag{7.23}$$

These are real quantities that correspond to the free (normal mode) oscillations for the two-level model with a barotropic basic state current. The phase speed c_1 is simply the dispersion relationship for a barotropic Rossby wave with no y dependence (see Section 5.7). Substituting from (7.22) for c in (7.18) and (7.19), we see that in this case $B = 0$ so that the perturbation is barotropic in structure. The expression of (7.23), however, may be interpreted as the phase speed for an internal baroclinic Rossby wave. Note that c_2 is a dispersion relationship analogous to the Rossby wave speed for a homogeneous ocean with a free surface, which was given in Problem 7.16. However, in the two-level model, the factor $2\lambda^2$ appears in the denominator in place of the f_0^2/gH for the oceanic case.

In each of these cases there is vertical motion associated with the Rossby wave so that static stability modifies the wave speed. It is left as a problem for the reader to show that if c_2 is substituted into (7.18) and (7.19), the resulting fields of ψ_1 and ψ_3 are 180° out of phase so that the perturbation is baroclinic, although the basic state is barotropic. Furthermore, the ω_2' field is 1/4 cycle out of phase with the 250-hPa geopotential field, with the maximum upward motion occurring west of the 250-hPa trough.

This vertical motion pattern may be understood if we note that $c_2 - U_m < 0$, so that the disturbance pattern moves westward *relative to the mean wind*. Now, viewed in a coordinate system moving with the mean wind, the vorticity changes are due only to the planetary vorticity advection and the convergence terms, while the thickness changes must be caused solely by the adiabatic heating or cooling due to vertical motion. Thus, there must be rising motion west of the 250-hPa trough to produce the thickness changes required by the westward motion of the system.

Comparing (7.22) and (7.23), we see that the phase speed of the baroclinic mode is generally much less than that of the barotropic mode since for average midlatitude tropospheric conditions $\lambda^2 \approx 2 \times 10^{-12}$ m^{-2}, which is approximately equal to k^2 for a zonal wavelength of 4300 km.[1]

As the second special case, we assume that $\beta = 0$. This case corresponds, for example, to a laboratory situation in which the fluid is bounded above and below by rotating horizontal planes so that the gravity and rotation vectors are everywhere parallel. In such a situation

$$c = U_m \pm U_T \left(\frac{k^2 - 2\lambda^2}{k^2 + 2\lambda^2} \right)^{1/2} \tag{7.24}$$

For waves with zonal wave numbers satisfying $k^2 < 2\lambda^2$, (7.24) has an imaginary part. Thus, all waves longer than the critical wavelength $L_c = \sqrt{2}\pi/\lambda$ will amplify. From the definition of λ we can write

$$L_c = \delta p \pi (2\sigma)^{1/2} / f_0$$

For typical tropospheric conditions $(2\sigma)^{1/2} \approx 2 \times 10^{-3}$ N^{-1} m^3 s^{-1}. Thus, with $\delta p = 500$ hPa and $f_0 = 10^{-4}$ s^{-1}, we find that $L_c \approx 3000$ km. It is also clear from this formula that the critical wavelength for baroclinic instability increases with static stability. The role of static stability in stabilizing the shorter waves can be understood qualitatively as follows: For a sinusoidal perturbation, the relative vorticity, and thus the differential vorticity advection, increases with the square of the wave number. However, as shown in Chapter 6, a secondary vertical circulation is required to maintain hydrostatic temperature changes and geostrophic vorticity changes in the presence of differential vorticity advection. Thus, for a geopotential perturbation of fixed amplitude, the

[1]The presence of the free internal Rossby wave should actually be regarded as a weakness of the two-level model. Lindzen et al. (1968) have shown that this mode does not correspond to any free oscillation of the real atmosphere. Rather, it is a spurious mode resulting from the use of the upper boundary condition $\omega = 0$ at $p = 0$, which formally turns out to be equivalent to putting a lid at the top of the atmosphere.

relative strength of the accompanying vertical circulation must increase as the wavelength of the disturbance decreases. Because static stability tends to resist vertical displacements, the shortest wavelengths will thus be stabilized.

It is also of interest that with $\beta = 0$ the critical wavelength for instability does not depend on the magnitude of the basic state thermal wind U_T. The growth rate, however, does depend on U_T. According to (7.17) the time dependence of the disturbance solution has the form exp(–*ikct*). Thus, the exponential growth rate is $\alpha = kc_i$, where c_i designates the imaginary part of the phase speed. In the present case

$$\alpha = kU_T\left(\frac{2\lambda^2 - k^2}{2\lambda^2 + k^2}\right)^{1/2} \tag{7.25}$$

so that the growth rate increases linearly with the mean thermal wind.

Returning to the general case where all terms are retained in (7.21), the stability criterion is understood most easily by computing the *neutral curve*, which connects all values of U_T and k for which $\delta = 0$ so that the flow is *marginally stable*. From (7.21), the condition $\delta = 0$ implies that

$$\frac{\beta^2\lambda^4}{k^4\left(2\lambda^2 + k^2\right)} = U_T^2\left(2\lambda^2 - k^2\right) \tag{7.26}$$

This complicated relationship between U_T and k can best be displayed by solving (7.26) for $k^4/2\lambda^4$, yielding

$$k^4\Big/\left(2\lambda^4\right) = 1 \pm \left[1 - \beta^2\Big/\left(4\lambda^4 U_T^2\right)\right]^{1/2}$$

In Figure 7.3 the nondimensional quantity $k^2/2\lambda^2$, which is proportional to the square of the zonal wave number, is plotted against the nondimensional parameter $2\lambda^2 U_T/\beta$, which is proportional to the thermal wind. As indicated in Figure 7.3, the neutral curve separates the unstable region of the U_T, k plane from the stable region. It is clear that the inclusion of the β effect serves to stabilize the flow, since now unstable roots exist only for $|U_T| > \beta/(2\lambda^2)$. In addition, the minimum value of U_T required for unstable growth depends strongly on k. Thus, the β effect strongly stabilizes the long wave end of the wave spectrum ($k \to 0$). Again, the flow is always stable for waves shorter than the critical wavelength $L_c = \sqrt{2}\pi/\lambda$.

This long-wave stabilization associated with the β effect is caused by the rapid westward propagation of long waves (i.e., Rossby wave propagation), which occurs only when the β effect is included in the model. It can be shown that baroclinically unstable waves always propagate at a speed that lies between maximum and minimum mean zonal wind speeds. Thus, for the two-level model in the usual midlatitude case where $U_1 > U_3 > 0$, the real part of the phase speed satisfies the inequality $U_3 < c_r < U_1$ for unstable waves. In a continuous atmosphere, this would imply that there must be a level where $U = c_r$. Such a

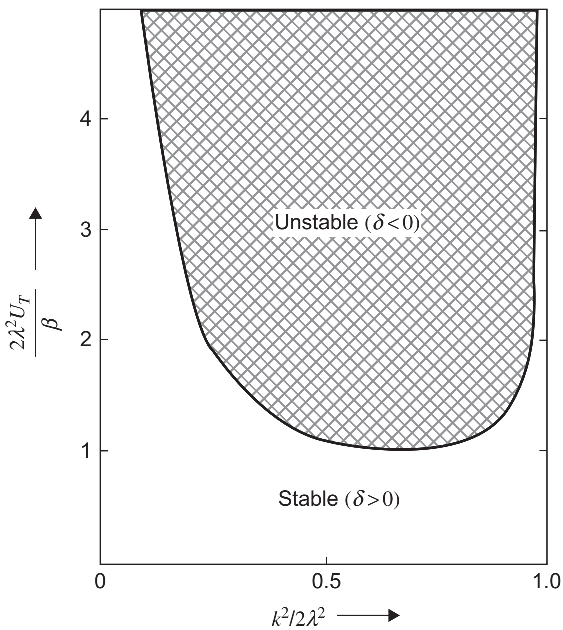

FIGURE 7.3 Neutral stability curve for the two-level baroclinic model.

level is called a *critical level* by theoreticians and a *steering level* by synopticians. For long waves and weak basic state wind shear, the solution given by (7.21) will have $c_r < U_3$, there is no steering level, and unstable growth cannot occur.

Differentiating (7.26) with respect to k and setting $dU_T/dk = 0$, we find that the minimum value of U_T for which unstable waves may exist occurs when $k^2 = \sqrt{2}\lambda^2$. This wave number corresponds to the wave of maximum instability. Wave numbers of observed disturbances should be close to the wave number of maximum instability, because if U_T were gradually raised from zero, the flow would first become unstable for perturbations of wave number $k = 2^{1/4}\lambda$. Those perturbations would then amplify and in the process remove energy from the mean thermal wind, thereby decreasing U_T and stabilizing the flow.

Under normal conditions of static stability the wavelength of maximum instability is about 4000 km, which is close to the average wavelength for midlatitude synoptic systems. Furthermore, the thermal wind required for marginal stability at this wavelength is only about $U_T \approx 4\ \text{m s}^{-1}$, which implies a shear of $8\ \text{m s}^{-1}$ between 250 and 750 hPa. Shears greater than this are certainly common in middle latitudes for the zonally averaged flow. Therefore, the observed behavior of midlatitude synoptic systems is consistent with the hypothesis that such systems can originate from infinitesimal perturbations of a baroclinically unstable basic current. Of course, in the real atmosphere many other factors may influence the development of synoptic systems—for example, due to lateral shear in the jet stream, nonlinear interactions of finite-amplitude perturbations, and the release of latent heat in precipitating systems. However, observational studies, laboratory simulations, and numerical models all suggest that baroclinic instability is a primary mechanism for synoptic-scale wave development in middle latitudes.

7.2.2 Vertical Motion in Baroclinic Waves

Since the two-level model is a special case of the quasi-geostrophic system, the physical mechanisms responsible for forcing vertical motion should be those discussed in Section 6.5. Thus, the forcing of vertical motion can be expressed in terms of the sum of the forcing by thermal advection (evaluated at level 2) plus the differential vorticity advection (evaluated as the difference between the vorticity advection at level 1 and that at level 3). Alternatively, the forcing of vertical motion can be expressed in terms of the divergence of the **Q** vector.

The **Q**-vector form of the omega equation for the two-level model can be derived simply from (6.68). We first estimate the second term on the left-hand side by finite differencing in p. Using (7.4) and again letting $\omega_0 = \omega_4 = 0$, we obtain

$$\frac{\partial^2 \omega}{\partial p^2} \approx \frac{(\partial\omega/\partial p)_3 - (\partial\omega/\partial p)_1}{\delta p} \approx -\frac{2\omega_2}{(\delta p)^2}$$

and observe that temperature in the two-level model is represented as

$$\frac{RT}{p} = -\frac{\partial \Phi}{\partial p} \approx \frac{f_0}{\delta p}\left(\psi_1 - \psi_3\right)$$

Thus, (6.68) becomes

$$\sigma\left(\nabla_h^2 - 2\lambda^2\right)\omega_2 = -2\nabla_h \cdot \mathbf{Q} \tag{7.27}$$

where

$$\mathbf{Q} = \frac{f_0}{\delta p}\left[-\frac{\partial \mathbf{V}_2}{\partial x} \cdot \nabla_h\left(\psi_1 - \psi_3\right), \quad -\frac{\partial \mathbf{V}_2}{\partial y} \cdot \nabla_h\left(\psi_1 - \psi_3\right)\right]$$

In order to examine the forcing of vertical motion in baroclinically unstable waves, we linearize (7.27) by specifying the same basic state and perturbation variables as in (7.8). For this situation, in which the mean zonal wind and the perturbation streamfunctions are independent of y, the **Q** vector has only an x component:

$$Q_1 = \frac{f_0}{\delta p}\left[\frac{\partial^2 \psi_2'}{\partial x^2}\left(U_1 - U_3\right)\right] = \frac{2f_0}{\delta p} U_T \zeta_2'$$

The pattern of the **Q** vector in this case is similar to that of Figure 6.14, with eastward-pointing **Q** centered at the trough and westward-pointing **Q** centered at the ridge. This is consistent with the fact that **Q** represents the change of temperature gradient forced by geostrophic motion alone. In this simple model the temperature gradient is entirely due to the vertical shear of the mean zonal wind [$U_T \propto -\partial T/\partial y$], and the shear of the perturbation meridional velocity tends to advect warm air poleward east of the 500-hPa trough and cold air equatorward west of the 500-hPa trough so that there is a tendency to produce a component of temperature gradient directed eastward at the trough.

The forcing of vertical motion by the **Q** vector in the linearized model is, from (7.27),

$$\left(\frac{\partial^2}{\partial x^2} - 2\lambda^2\right)\omega_2' = -\frac{4f_0}{\sigma \delta p} U_T \frac{\partial \zeta_2'}{\partial x} \tag{7.28}$$

Observing that

$$\left(\frac{\partial^2}{\partial x^2} - 2\lambda^2\right)\omega_2' \propto -\omega_2'$$

we may interpret (7.28) physically by noting that

$$w_2' \propto -\omega_2' \propto -U_T \frac{\partial \zeta_2'}{\partial x} \propto -v_2' \frac{\partial \overline{T}}{\partial y}$$

Thus, sinking motion is forced by negative advection of disturbance vorticity by the basic state thermal wind (or, alternatively, cold advection of the basic state thermal field by the perturbation meridional wind), while rising motion is forced by advection of the opposite sign.

We now have the information required to diagram the structure of a baroclinically unstable disturbance in the two-level model. The lower part of Figure 7.4 shows schematically the phase relationship between the geopotential field and the divergent secondary motion field for the usual midlatitude situation where $U_T > 0$. Linear interpolation has been used between levels so that the trough and ridge axes are straight lines tilted back toward the west with height. In this example the ψ_1 field lags the ψ_3 field by about 65° in phase so that the trough at 250 hPa lies 65° in phase west of the 750-hPa trough. At 500 hPa the perturbation thickness field lags the geopotential field by one-quarter wavelength as shown in the top part of Figure 7.4, and the thickness and vertical motion fields are in phase. Note that the temperature advection by the perturbation meridional wind is in phase with the 500-hPa thickness field so that the advection of the basic state temperature by the perturbation wind acts to intensify the perturbation thickness field. This tendency is also illustrated by the zonally oriented **Q** vectors shown at the 500-hPa level in Figure 7.4.

The pattern of vertical motion forced by the divergence of the **Q** vector, as shown in Figure 7.4, is associated with a divergence–convergence pattern that contributes a positive vorticity tendency nearthe 250-hPa trough and a negative

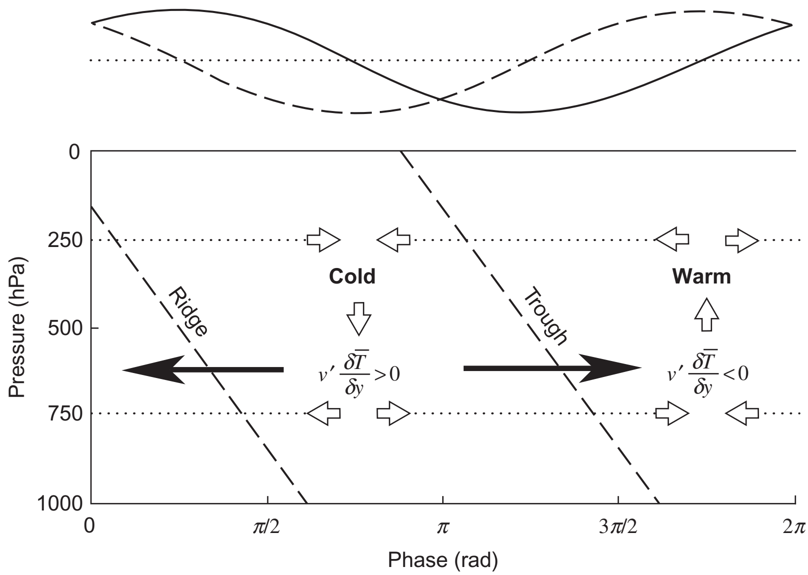

FIGURE 7.4 Structure of an unstable baroclinic wave in the two-level model. (*Top*) Relative phases of the 500-hPa perturbation geopotential (*solid line*) and temperature (*dashed line*). (*Bottom*) Vertical cross-section showing phases of geopotential, meridional temperature advection, ageostrophic circulation (*open arrows*), **Q** vectors (*solid arrows*), and temperature fields for an unstable baroclinic wave in the two-level model.

vorticity tendency near the 750-hPa ridge, with opposite tendencies at the 250-hPa ridge and 750-hPa trough. Since in all cases these vorticity tendencies tend to increase the extreme values of vorticity at the troughs and ridges, this secondary circulation system will act to increase the strength of the disturbance.

The total vorticity change at each level is, of course, determined by the sum of vorticity advection and vortex stretching due to the divergent circulation. The relative contributions of these processes are indicated schematically in Figures 7.5 and 7.6, respectively. As can be seen in Figure 7.5, vorticity advection leads the vorticity field by one-quarter wavelength. Since in this case the basic state wind increases with height, the vorticity advection at 250 hPa is larger than that at 750 hPa. If no other processes influenced the vorticity field, the effect of this differential vorticity advection would be to move the upper-level trough and ridge pattern eastward more rapidly than the lower-level pattern. Thus, the westward tilt of the trough–ridge pattern would quickly be destroyed. The maintenance of this tilt in the presence of differential vorticity advection is due to the concentration of vorticity by vortex stretching associated with the divergent secondary circulation.

Referring to Figure 7.6, we see that concentration of vorticity by the divergence effect lags the vorticity field by about 65° at 250 hPa and leads the vorticity field by about 65° at 750 hPa. As a result, the net vorticity tendencies

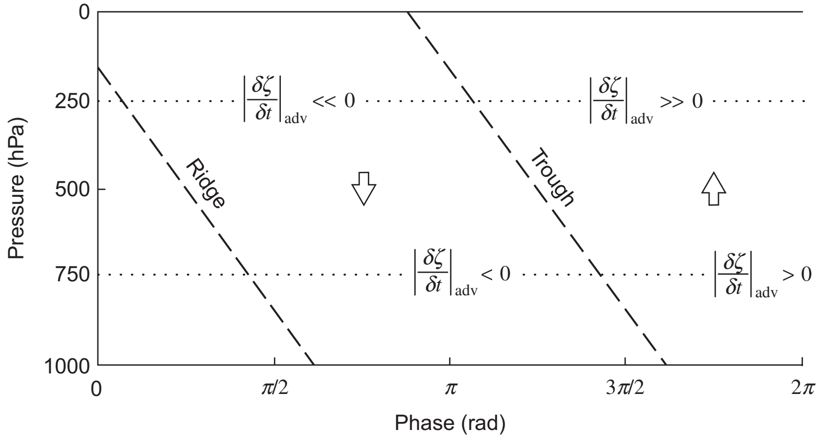

FIGURE 7.5 Vertical cross-section showing the phase of vorticity change due to vorticity advection for an unstable baroclinic wave in the two-level model.

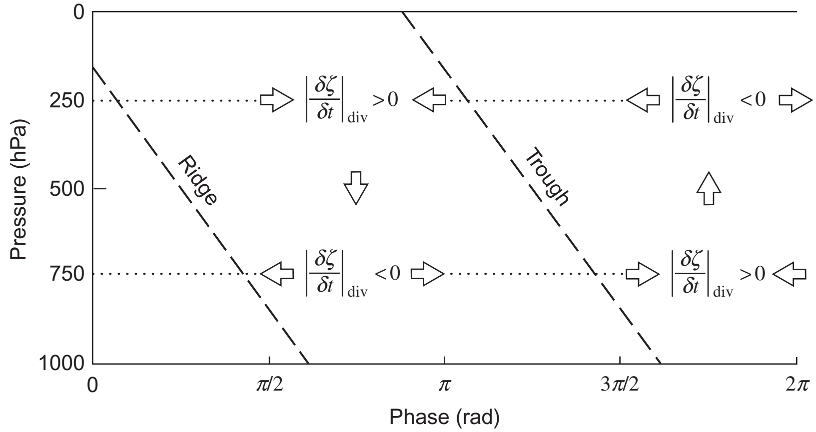

FIGURE 7.6 Vertical cross-section showing the phase of vorticity change due to divergence–convergence for an unstable baroclinic wave in the two-level model.

ahead of the vorticity maxima and minima are less than the advective tendencies at the upper level and greater than the advective tendencies at the lower level:

$$\left|\frac{\partial\zeta_1'}{\partial t}\right| < \left|\frac{\partial\zeta_1'}{\partial t}\right|_{adv}, \quad \left|\frac{\partial\zeta_3'}{\partial t}\right| > \left|\frac{\partial\zeta_3'}{\partial t}\right|_{adv}$$

Furthermore, vorticity concentration by the divergence effect will tend to amplify the vorticity perturbations in the troughs and ridges at both the 250- and 750-hPa levels as required for a growing disturbance.

7.3 THE ENERGETICS OF BAROCLINIC WAVES

The previous section showed that under suitable conditions a vertically sheared geostrophically balanced basic state flow is unstable to small wave-like perturbations with horizontal wavelengths in the range of observed synoptic-scale systems. Such baroclinically unstable perturbations will amplify exponentially by drawing energy from the mean flow. This section considers the energetics of linearized baroclinic disturbances and shows that the potential energy of the mean flow is the energy source for baroclinically unstable perturbations.

7.3.1 Available Potential Energy

Before discussing the energetics of baroclinic waves, it is necessary to consider the energy of the atmosphere from a more general point of view. For all practical purposes, the total energy of the atmosphere is the sum of internal energy, gravitational potential energy, and kinetic energy. However, it is not necessary to consider separately the variations of internal and gravitational potential energy because in a hydrostatic atmosphere these two forms of energy are proportional and may be combined into a single term called the *total potential energy*. The proportionality of internal and gravitational potential energy can be demonstrated by considering these forms of energy for a column of air of unit horizontal cross-section extending from the surface to the top of the atmosphere.

If we let dE_I be the internal energy in a vertical section of the column of height dz, then from the definition of internal energy—see Section (2.6):

$$dE_I = \rho c_v T dz$$

so that the internal energy for the entire column is

$$E_I = c_v \int_0^\infty \rho T dz \tag{7.29}$$

However, the gravitational potential energy for a slab of thickness dz at a height z is just

$$dE_P = \rho g z dz$$

so that the gravitational potential energy in the entire column is

$$E_P = \int_0^\infty \rho g z dz = -\int_{p_0}^0 z dp \tag{7.30}$$

where we have substituted from the hydrostatic equation to obtain the last integral in (7.30). Integrating (7.30) by parts and using the ideal gas law, we obtain

$$E_P = \int_0^\infty p dz = R \int_0^\infty \rho T dz \tag{7.31}$$

Comparing (7.29) and (7.31), we see that $c_v E_P = R E_I$. Thus, the total potential energy may be expressed as

$$E_P + E_I = \left(c_p / c_v\right) E_I = \left(c_p / R\right) E_P \tag{7.32}$$

Therefore, in a hydrostatic atmosphere the total potential energy can be obtained by computing either E_I or E_P alone.

The total potential energy is not a very useful measure of energy in the atmosphere because only a very small fraction of the total potential energy is available for conversion to kinetic energy in storms. To demonstrate qualitatively why most of the total potential energy is unavailable, we consider a simple model atmosphere that initially consists of two equal masses of dry air separated by a vertical partition as shown in Figure 7.7. The two air masses are at uniform potential temperatures θ_1 and θ_2, respectively, with $\theta_1 < \theta_2$. The ground-level pressure on each side of the partition is taken to be 1000 hPa. We wish to compute the maximum kinetic energy that can be realized by an adiabatic rearrangement of mass within the same volume when the partition is removed.

Now for an adiabatic process, total energy is conserved:

$$E_K + E_P + E_I = \text{constant}$$

where E_K denotes the kinetic energy. If the air masses are initially at rest, $E_K = 0$. Thus, if we let primed quantities denote the final state

$$E'_K + E'_P + E'_I = E_P + E_I$$

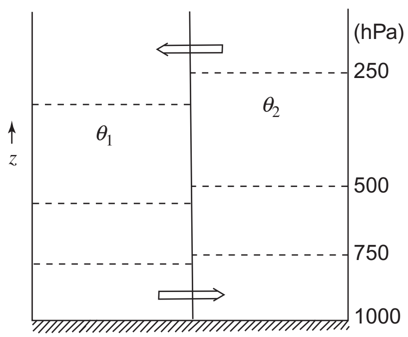

FIGURE 7.7 Two air masses of differing potential temperature separated by a vertical partition. *Dashed lines* indicate isobaric surfaces. *Arrows* show direction of motion when the partition is removed.

so that with the aid of (7.32) the kinetic energy realized by removal of the partition may be expressed as

$$E'_K = \left(c_p/c_v\right)\left(E_I - E'_I\right)$$

Because θ is conserved for an adiabatic process, the two air masses cannot mix. It is clear that E'_I will be a minimum (designated by E''_I) when the masses are rearranged so that the air at potential temperature θ_1 lies entirely beneath the air at potential temperature θ_2, with the 500-hPa surface as the horizontal boundary between the two masses. In that case the total potential energy $(c_p/c_v)E''_I$ is not available for conversion to kinetic energy because no adiabatic process can further reduce E''_I.

The *available potential energy* (APE) can now be defined as the difference between the total potential energy of a closed system and the minimum total potential energy that could result from an adiabatic redistribution of mass. Thus, for the idealized model given earlier, the APE, which is designated by the symbol P, is

$$P = \left(c_p/c_v\right)\left(E_I - E''_I\right) \tag{7.33}$$

which is equivalent to the maximum kinetic energy that can be realized by an adiabatic process.

Lorenz (1960) showed that available potential energy is given approximately by the volume integral over the entire atmosphere of the variance of potential temperature on isobaric surfaces. Thus, letting $\overline{\theta}$ designate the average potential temperature for a given pressure surface and θ' the local deviation from the average, the average available potential energy per unit volume satisfies the proportionality

$$\overline{P} \propto V^{-1} \int \left(\overline{\theta'^2}/\bar{\theta}^2\right) dV$$

where V designates the total volume. For the quasi-geostrophic model, this proportionality is an exact measure of the available potential energy, as shown in the following subsection.

Observations indicate that for the atmosphere as a whole,

$$\overline{P}/\left[\left(c_p/c_v\right)\overline{E}_I\right] \sim 5 \times 10^{-3}, \quad \overline{K}/\overline{P} \sim 10^{-1}$$

Thus, only about 0.5% of the total potential energy of the atmosphere is available, and of the available portion only about 10% is actually converted to kinetic energy. From this point of view the atmosphere is a rather inefficient heat engine.

7.3.2 Energy Equations for the Two-Layer Model

In the two-layer model of Section 7.2, the perturbation temperature field is proportional to $\psi'_1 - \psi'_3$, the 250- to 750-hPa thickness. Thus, in view of the discussion in the previous section, we anticipate that the available potential energy in this case will be proportional to $(\psi_1' - \psi_3')^2$. To show that this in fact must be the case, we derive the energy equations for the system in the following manner: We first multiply (7.9) by $-\psi_1$, (7.10) by $-\psi_3$, and (7.11) by $(\psi_1' - \psi_3')$. We then integrate the resulting equations over one wavelength of the perturbation in the zonal direction.

The resulting zonally averaged[2] terms are denoted by overbars as done previously in Chapter 5:

$$\overline{(\ )} = L^{-1} \int_0^L (\ )\, dx$$

where L is the wavelength of the perturbation. Thus, for the first term in (7.9) we have, after multiplying by $-\psi_1$, averaging and differentiating by parts:

$$-\overline{\psi_1' \frac{\partial}{\partial t}\left(\frac{\partial^2 \psi_1'}{\partial x^2}\right)} = -\frac{\partial}{\partial x}\overline{\left[\psi_1' \frac{\partial}{\partial x}\left(\frac{\partial \psi_1'}{\partial t}\right)\right]} + \overline{\frac{\partial \psi_1'}{\partial x}\frac{\partial}{\partial t}\left(\frac{\partial \psi_1'}{\partial x}\right)}$$

The first term on the right side vanishes because it is the integral of a perfect differential in x over a complete cycle. The second term on the right can be rewritten in the form

$$\frac{1}{2}\frac{\partial}{\partial t}\overline{\left(\frac{\partial \psi_1'}{\partial x}\right)^2}$$

which is just the rate of change of the perturbation kinetic energy per unit mass averaged over a wavelength. Similarly, $-\psi_1'$ times the advection term on the left in (7.9) can be written after integration in x as

$$\begin{aligned} -U_1\overline{\psi_1' \frac{\partial^2}{\partial x^2}\left(\frac{\partial \psi_1'}{\partial x}\right)} &= -U_1\frac{\partial}{\partial x}\overline{\left[\psi_1' \frac{\partial}{\partial x}\left(\frac{\partial \psi_1'}{\partial x}\right)\right]} + U_1\overline{\frac{\partial \psi_1'}{\partial x}\frac{\partial^2 \psi_1'}{\partial x^2}} \\ &= \frac{U_1}{2}\frac{\partial}{\partial x}\overline{\left(\frac{\partial \psi_1'}{\partial x}\right)^2} = 0 \end{aligned}$$

Thus, the advection of kinetic energy vanishes when integrated over a wavelength. Evaluating the various terms in (7.10) and (7.11) in the same manner after multiplying through by $-\psi_3'$ and $(\psi_1' - \psi_3')$, respectively, we obtain the following set of perturbation energy equations:

$$\frac{1}{2}\frac{\partial}{\partial t}\overline{\left(\frac{\partial \psi_1'}{\partial x}\right)^2} = -\frac{f_0}{\delta p}\overline{\omega_2' \psi_1'} \tag{7.34}$$

[2]A zonal average generally designates the average around an entire circle of latitude. However, for a disturbance consisting of a single sinusoidal wave of wave number $k = m/(a\cos\phi)$, where m is an integer, the average over a wavelength is identical to a zonal average.

$$\frac{1}{2}\frac{\partial}{\partial t}\overline{\left(\frac{\partial \psi_3'}{\partial x}\right)^2} = +\frac{f_0}{\delta p}\overline{\omega_2' \psi_3'} \tag{7.35}$$

$$\frac{1}{2}\frac{\partial}{\partial t}\overline{\left(\psi_1' - \psi_3'\right)^2} = U_T\overline{\left(\psi_1' - \psi_3'\right)\frac{\partial}{\partial x}\left(\psi_1' + \psi_3'\right)} + \frac{\sigma \delta p}{f_0}\overline{\omega_2'\left(\psi_1' - \psi_3'\right)} \tag{7.36}$$

where as before $U_T \equiv (U_1 - U_3)/2$.

Defining the perturbation kinetic energy to be the sum of the kinetic energies of the 250- and 750-hPa levels,

$$K' \equiv (1/2)\left[\overline{\left(\partial \psi_1'/\partial x\right)^2} + \overline{\left(\partial \psi_3'/\partial x\right)^2}\right]$$

we find by adding (7.34) and (7.35) that

$$dK'/dt = -\left(f_0/\delta p\right)\overline{\omega_2'\left(\psi_1' - \psi_3'\right)} = -\left(2f_0/\delta p\right)\overline{\omega_2'\psi_T} \tag{7.37}$$

Thus, the rate of change of perturbation kinetic energy is proportional to the correlation between perturbation thickness and vertical motion.

If we now define the perturbation available potential energy as

$$P' \equiv \lambda^2\overline{\left(\psi_1' - \psi_3'\right)^2}/2$$

we obtain from (7.36)

$$\begin{aligned} dP'/dt &= \lambda^2 U_T\overline{\left(\psi_1' - \psi_3'\right)\partial\left(\psi_1' + \psi_3'\right)/\partial x} + \left(f_0/\delta p\right)\overline{\omega_2'\left(\psi_1' - \psi_3'\right)} \\ &= 4\lambda^2 U_T\overline{\psi_T\partial\psi_m/\partial x} + \left(2f_0/\delta p\right)\overline{\omega_2'\psi_T} \end{aligned} \tag{7.38}$$

The last term in (7.38) is just equal and opposite to the kinetic energy source term in (7.37). This term clearly must represent a conversion between potential and kinetic energy. If on average the vertical motion is positive ($\omega_2' < 0$) where the thickness is greater than average ($\psi_1' - \psi_3' > 0$) and vertical motion is negative where thickness is less than average, then

$$\overline{\omega_2'\left(\psi_1' - \psi_3'\right)} = 2\overline{\omega_2'\psi_T} < 0$$

and the perturbation potential energy is being converted to kinetic energy. Physically, this correlation represents an overturning in which cold air aloft is replaced by warm air from below, a situation that clearly tends to lower the center of mass and thus the potential energy of the perturbation. However, the available potential energy and kinetic energy of a disturbance can still grow simultaneously, provided that the potential energy generation due to the first term in (7.38) exceeds the rate of potential energy conversion to kinetic energy.

The potential energy generation term in (7.38) depends on the correlation between the perturbation thickness ψ_T and the meridional velocity at 500 hPa,

$\partial\psi_m/\partial x$. In order to understand the role of this term, it is helpful to consider a particular sinusoidal wave disturbance. Suppose that the barotropic and baroclinic parts of the disturbance can be written, respectively, as

$$\psi_m = A_m \cos k\,(x - ct) \quad \text{and} \quad \psi_T = A_T \cos k\,(x + x_0 - ct) \tag{7.39}$$

where x_0 designates the phase difference. Because ψ_m is proportional to the 500-hPa geopotential and ψ_T is proportional to the 500-hPa temperature (or 250- to 750-hPa thickness), the phase angle kx_0 gives the phase difference between geopotential and temperature fields at 500 hPa. Furthermore, A_m and A_T are measures of the amplitudes of the 500-hPa disturbance geopotential and thickness fields, respectively. Using the expressions in (7.39), we obtain

$$\begin{aligned}
\overline{\psi_T \frac{\partial\psi_m}{\partial x}} &= -\frac{k}{L}\int_0^L A_T A_m \cos k\,(x + x_0 - ct)\sin k\,(x - ct)\,dx \\
&= \frac{kA_T A_m \sin kx_0}{L}\int_0^L [\sin k\,(x - ct)]^2\,dx \\
&= (A_T A_m k \sin kx_0)/2
\end{aligned} \tag{7.40}$$

Substituting from (7.40) into (7.38), we see that for the usual midlatitude case of a westerly thermal wind ($U_T > 0$) the correlation in (7.40) must be positive if the perturbation potential energy is to increase. Thus, kx_0 must satisfy the inequality $0 < kx_0 < \pi$. Furthermore, the correlation will be a positive maximum for $kx_0 = \pi/2$—that is, when the temperature wave lags the geopotential wave by 90° in phase at 500 hPa.

This case was shown schematically earlier in Figure 7.4. Clearly, when the temperature wave lags the geopotential by one-quarter cycle, the northward advection of warm air by the geostrophic wind east of the 500-hPa trough and the southward advection of cold air west of the 500-hPa trough are both maximized. As a result, cold advection is strong below the 250-hPa trough, and warm advection is strong below the 250-hPa ridge. In that case, as discussed previously in Section 6.4.2, the upper-level disturbance will intensify. It should also be noted here that if the temperature wave lags the geopotential wave, the trough and ridge axes will tilt westward with height, which, as mentioned in Section 6.1, is observed to be the case for amplifying midlatitude synoptic systems.

Referring again to Figure 7.4 and recalling the vertical motion pattern implied by the omega equation (7.28), we see that the signs of the two terms on the right in (7.38) cannot be the same. In the westward-tilting perturbation of Figure 7.4, the vertical motion must be downward in the cold air behind the trough at 500 hPa. Hence, the correlation between temperature and vertical velocity must be positive in this situation; that is,

$$\overline{\omega_2'\psi_T} < 0$$

Thus, for quasi-geostrophic perturbations, a westward tilt of the perturbation with height implies both that the horizontal temperature advection will increase the available potential energy of the perturbation and that the vertical circulation will convert perturbation available potential energy to perturbation kinetic energy. Conversely, an eastward tilt of the system with height would change the signs of both terms on the right in (7.38).

Although the signs of the potential energy generation term and the potential energy conversion term in (7.38) are always opposite for a developing baroclinic wave, it is only the potential energy generation rate that determines the growth of the total energy $P' + K'$ of the disturbance. This may be proved by adding (7.37) and (7.38) to obtain

$$d\left(P' + K'\right)/dt = 4\lambda^2 U_T \overline{\psi_T \partial \psi_m / \partial x}$$

Provided the correlation between the meridional velocity and temperature is positive and $U_T > 0$, the total energy of the perturbation will increase. Note that the vertical circulation merely converts disturbance energy between the available potential and kinetic forms without affecting the total energy of the perturbation.

The rate of increase of the total energy of the perturbation depends on the magnitude of the basic state thermal wind U_T. This is, of course, proportional to the zonally averaged meridional temperature gradient. Because the generation of perturbation energy requires systematic poleward transport of warm air and equatorward transport of cold air, it is clear that baroclinically unstable disturbances tend to reduce the meridional temperature gradient and thus the available potential energy of the mean flow. This latter process cannot be described mathematically in terms of the linearized equations. However, from Figure 7.8 we

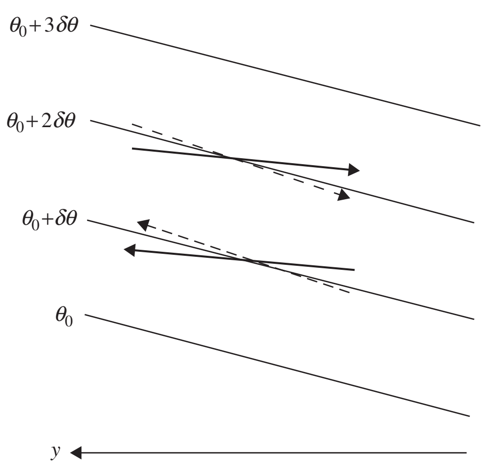

FIGURE 7.8 Slopes of parcel trajectories relative to the zonal-mean potential temperature surfaces for a baroclinically unstable disturbance (*solid arrows*) and for a baroclinically stable disturbance (*dashed arrows*).

can see qualitatively that parcels that move poleward and upward with slopes less than the slope of the zonal-mean potential temperature surface will become warmer than their surroundings, and vice versa for parcels moving downward and equatorward.

For such parcels the correlations between disturbance meridional velocity and temperature and between disturbance vertical velocity and temperature will both be positive as required for baroclinically unstable disturbances. For parcels that have trajectory slopes greater than the mean potential temperature slope, however, both of these correlations will be negative. Such parcels must then convert disturbance kinetic energy to disturbance available potential energy, which is in turn converted to zonal-mean available potential energy. Therefore, in order that perturbations are able to extract potential energy from the mean flow, the perturbation parcel trajectories in the meridional plane must have slopes less than the slopes of the potential temperature surfaces, and a permanent rearrangement of air must take place for there to be a net heat transfer.

Since we have previously seen that poleward-moving air must rise and equatorward-moving air must sink, it is clear that the rate of energy generation can be greater for an atmosphere in which the meridional slope of the potential temperature surfaces is large. We can also see more clearly why baroclinic instability has a short-wave cutoff. As mentioned previously, the intensity of the vertical circulation must increase as the wavelength decreases. Thus, the slopes of the parcel trajectories must increase with decreasing wavelength, and for some critical wavelength the trajectory slopes will become greater than the slopes of the potential temperature surfaces. Unlike convective instability, where the most rapid amplification occurs for the smallest possible scales, baroclinic instability is most effective at an intermediate range of scales.

The energy flow for quasi-geostrophic perturbations is summarized in Figure 7.9 by means of a block diagram. In this type of energy diagram each block represents a reservoir of a particular type of energy, and arrows designate the direction of energy flow. The complete energy cycle cannot be derived in terms of linear perturbation theory but will be discussed qualitatively in Chapter 10.

7.4 BAROCLINIC INSTABILITY OF A CONTINUOUSLY STRATIFIED ATMOSPHERE

In the two previous sections some basic aspects of baroclinic instability were elucidated in the context of a simple two-layer model. The dependence of growth rate on vertical shear and the existence of a short-wave cutoff were clearly demonstrated. The two-layer model, however, does have one severe constraint: It assumes that the altitude dependence of large-scale systems can be adequately represented with only two degrees of freedom in the vertical (i.e., the streamfunctions at the 250- and 750-hPa levels). Although most synoptic-scale systems in midlatitudes are observed to have vertical scales comparable

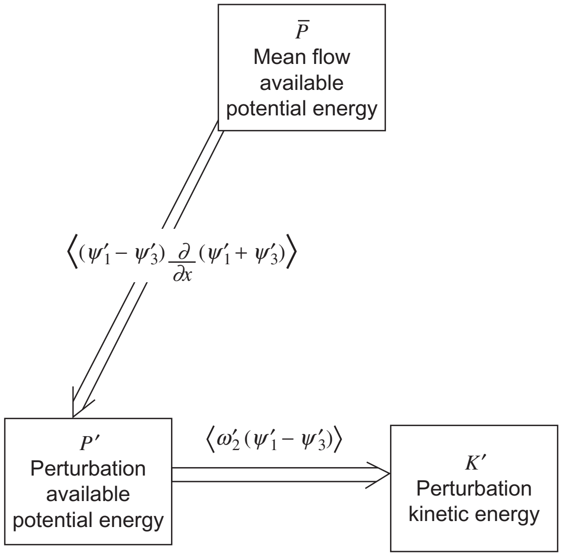

FIGURE 7.9 Energy flow in an amplifying baroclinic wave.

to the depth of the troposphere, observed vertical structures do differ. Disturbances that are concentrated near the ground or near the tropopause can hardly be represented accurately in the two-layer model.

An analysis of the structure of baroclinic modes for realistic mean zonal wind profiles is quite complex, and indeed can only be done by numerical methods. However, without obtaining specific normal mode solutions, it is possible to obtain necessary conditions for baroclinic or barotropic instability from an integral theorem first developed by Rayleigh. This theorem, which is discussed in Section 7.4.2, also shows how baroclinic instability is intimately related to the mean meridional gradient of potential vorticity and the mean meridional temperature gradient at the surface.

If a number of simplifying assumptions are made, it is possible to pose the stability problem for a continuously stratified atmosphere in a fashion that leads to a second-order differential equation for the vertical structure that can be solved by standard methods. This problem was originally studied by the British meteorologist Eady (1949) and, although mathematically similar to the two-layer model, provides additional insights. It is developed in Section 7.4.3.

7.4.1 Log-Pressure Coordinates

Derivation of the Rayleigh theorem and the Eady stability model is facilitated if we transform from the standard isobaric coordinates to a vertical coordinate based on the logarithm of pressure. In the *log-pressure coordinates*, the vertical coordinate is defined as

$$z^* \equiv -H \ln\left(p/p_s\right) \tag{7.41}$$

where p_s is a standard reference pressure (usually taken to be 1000 hPa) and H is a standard scale height, $H \equiv RT_s/g$, with T_s a global average temperature. For the special case of an isothermal atmosphere at temperature T_s, z^* is exactly equal to geometric height, and the density profile is given by the reference density

$$\rho_0\left(z^*\right) = \rho_s \exp\left(-z^*/H\right)$$

where ρ_s is the density at $z^* = 0$.

For an atmosphere with a realistic temperature profile, z^* is only approximately equivalent to the height, but in the troposphere the difference is usually quite small. The vertical velocity in this coordinate system is

$$w^* \equiv Dz^*/dt$$

The horizontal momentum equation in the log-pressure system is the same as that in the isobaric system:

$$D\mathbf{V}/Dt + f\mathbf{k} \times \mathbf{V} = -\boldsymbol{\nabla}_h \Phi \tag{7.42}$$

However, the operator D/Dt is now defined as

$$D/Dt = \partial/\partial t + \mathbf{V} \cdot \boldsymbol{\nabla}_h + w^* \partial/\partial z^*$$

The hydrostatic equation $\partial\Phi/\partial p = -\alpha$ can be transformed to the log-pressure system by multiplying through by p and using the ideal gas law to get

$$\partial\Phi/\partial \ln p = -RT$$

which after dividing through by $-H$ and using (7.41) gives

$$\partial\Phi/\partial z^* = RT/\mathrm{H} \tag{7.43}$$

The log-pressure form of the continuity equation can be obtained by transforming from the isobaric coordinate form (3.5). We first note that

$$w^* \equiv -(H/p)\, Dp/Dt = -H\omega/p$$

so that

$$\frac{\partial\omega}{\partial p} = -\frac{\partial}{\partial p}\left(\frac{pw^*}{H}\right) = \frac{\partial w^*}{\partial z^*} - \frac{w^*}{H} = \frac{1}{\rho_0}\frac{\partial\left(\rho_0 w^*\right)}{\partial z^*}$$

Thus, in log-pressure coordinates the continuity equation becomes simply

$$\frac{\partial u}{\partial x} + \frac{\partial v}{\partial y} + \frac{1}{\rho_0}\frac{\partial\left(\rho_0 w^*\right)}{\partial z^*} = 0 \tag{7.44}$$

It is left as a problem for the reader to show that the first law of thermodynamics (3.6) can be expressed in log-pressure form as

$$\left(\frac{\partial}{\partial t} + \mathbf{V} \cdot \nabla_h\right) \frac{\partial \Phi}{\partial z^*} + w^* N^2 = \frac{\kappa J}{H} \tag{7.45}$$

where

$$N^2 \equiv (R/H) \left(\partial T/\partial z^* + \kappa T/H\right)$$

is the buoyancy frequency squared (see Section 2.7.3) and $\kappa \equiv R/c_p$. Unlike the static stability parameter, S_p, in the isobaric form of the thermodynamic equation (3.6), the parameter N^2 varies only weakly with height in the troposphere; it can be assumed to be constant without serious error. This is a major advantage of the log-pressure formulation.

The quasi-geostrophic potential vorticity equation has the same form as in the isobaric system, but with q defined as

$$q \equiv \nabla_h^2 \psi + f + \frac{1}{\rho_0} \frac{\partial}{\partial z^*} \left(\varepsilon \rho_0 \frac{\partial \psi}{\partial z^*}\right) \tag{7.46}$$

where $\varepsilon \equiv f_0^2/N^2$.

7.4.2 Baroclinic Instability: The Rayleigh Theorem

We now examine the stability problem for a continuously stratified atmosphere on the midlatitude β plane. The linearized form of the quasi-geostrophic potential vorticity equation can be expressed in log-pressure coordinates as

$$\left(\frac{\partial}{\partial t} + \overline{u} \frac{\partial}{\partial x}\right) q' + \frac{\partial \overline{q}}{\partial y} \frac{\partial \psi'}{\partial x} = 0 \tag{7.47}$$

where

$$q' \equiv \nabla_h^2 \psi' + \frac{1}{\rho_0} \frac{\partial}{\partial z^*} \left(\varepsilon \rho_0 \frac{\partial \psi'}{\partial z^*}\right) \tag{7.48}$$

and

$$\frac{\partial \overline{q}}{\partial y} = \beta - \frac{\partial^2 \overline{u}}{\partial y^2} - \frac{1}{\rho_0} \frac{\partial}{\partial z^*} \left(\varepsilon \rho_0 \frac{\partial \overline{u}}{\partial z^*}\right) \tag{7.49}$$

As in the two-layer model, boundary conditions are required at lower- and upper-boundary pressure surfaces. Assuming that the flow is adiabatic and that the vertical motion w^* vanishes at these boundaries, the linearized form of the thermodynamic energy equation (7.45) valid at horizontal boundary surfaces is simply

$$\left(\frac{\partial}{\partial t} + \overline{u} \frac{\partial}{\partial x}\right) \frac{\partial \psi'}{\partial z^*} - \frac{\partial \psi'}{\partial x} \frac{\partial \overline{u}}{\partial z^*} = 0 \tag{7.50}$$

The sidewall boundary conditions are

$$\partial\psi'/\partial x = 0, \quad \text{hence, } \psi' = 0 \quad \text{at} \quad y = \pm L \tag{7.51}$$

We now assume that the perturbation consists of a single zonal Fourier component propagating in the x direction:

$$\psi'(x, y, z, t) = \text{Re}\left\{\Psi\left(y, z\right) \exp\left[ik\left(x - ct\right)\right]\right\} \tag{7.52}$$

where $\Psi(y, z) = \Psi_r + i\Psi_i$ is a complex amplitude, k is the zonal wave number, and $c = c_r + ic_i$ is a complex phase speed. Note that (7.52) can alternatively be expressed as

$$\psi'\left(x, y, z, t\right) = e^{kc_i t}\left[\Psi_r \cos k\left(x - c_r t\right) - \Psi_i \sin k\left(x - c_r t\right)\right]$$

Thus, the relative magnitudes of Ψ_r and Ψ_i determine the phase of the wave for any y, z^*.

Substituting from (7.52) into (7.47) and (7.50) yields

$$(\overline{u} - c)\left[\frac{\partial^2\Psi}{\partial y^2} - k^2\Psi + \frac{1}{\rho_0}\frac{\partial}{\partial z^*}\left(\varepsilon\rho_0\frac{\partial\Psi}{\partial z^*}\right)\right] + \frac{\partial\overline{q}}{\partial y}\Psi = 0 \tag{7.53}$$

and

$$(\overline{u} - c)\,\frac{\partial\Psi}{\partial z^*} - \frac{\partial\overline{u}}{\partial z^*}\Psi = 0 \quad \text{at } z^* = 0 \tag{7.54}$$

If the upper boundary is taken to be a rigid lid at a finite height, as is sometimes done in theoretical studies, the condition (7.54) is appropriate at that boundary as well. Alternatively the upper boundary condition can be specified by requiring Ψ to remain finite as $z^* \to \infty$.

Equation (7.53), together with its boundary conditions, constitutes a linear boundary value problem for $\Psi(y, z^*)$. It is generally not simple to obtain solutions to (7.53) for realistic mean zonal wind profiles. Nevertheless, we can obtain some useful information on stability properties simply by analyzing the energetics of the system.

Dividing (7.53) by $(\overline{u} - c)$ and separating the resulting equation into real and imaginary parts, we obtain

$$\frac{\partial^2\Psi_r}{\partial y^2} + \frac{1}{\rho_0}\frac{\partial}{\partial z^*}\left(\varepsilon\rho_0\frac{\partial\Psi_r}{\partial z^*}\right) - \left[k^2 - \delta_r\left(\partial\overline{q}/\partial y\right)\right]\Psi_r - \delta_i\partial\overline{q}/\partial y\Psi_i = 0 \tag{7.55}$$

$$\frac{\partial^2\Psi_i}{\partial y^2} + \frac{1}{\rho_0}\frac{\partial}{\partial z^*}\left(\varepsilon\rho_0\frac{\partial\Psi_i}{\partial z^*}\right) - \left[k^2 - \delta_r\left(\partial\overline{q}/\partial y\right)\right]\Psi_i + \delta_i\partial\overline{q}/\partial y\Psi_r = 0 \tag{7.56}$$

where

$$\delta_r = \frac{\overline{u} - c_r}{(\overline{u} - c_r)^2 + c_i^2}, \quad \text{and} \quad \delta_i = \frac{c_i}{(\overline{u} - c_r)^2 + c_i^2}$$

Similarly, dividing (7.54) through by $(\bar{u} - c)$ and separating into real and imaginary parts gives, for the boundary condition at $z^* = 0$,

$$\frac{\partial \Psi_r}{\partial z^*} + \frac{\partial \overline{u}}{\partial z^*}(\delta_i \Psi_i - \delta_r \Psi_r) = 0; \quad \frac{\partial \Psi_i}{\partial z^*} - \frac{\partial \overline{u}}{\partial z^*}(\delta_r \Psi_i + \delta_i \Psi_r) = 0 \tag{7.57}$$

Multiplying (7.55) by Ψ_i, (7.56) by Ψ_r, and subtracting the latter from the former yields

$$\begin{aligned} &\rho_0 \left[\Psi_i \frac{\partial^2 \Psi_r}{\partial y^2} - \Psi_r \frac{\partial^2 \Psi_i}{\partial y^2} \right] + \left[\Psi_i \frac{\partial}{\partial z^*} \left(\varepsilon \rho_0 \frac{\partial \Psi_r}{\partial z^*} \right) \right. \\ &\quad \left. - \Psi_r \frac{\partial}{\partial z^*} \left(\varepsilon \rho_0 \frac{\partial \Psi_i}{\partial z^*} \right) \right] - \rho_0 \delta_i (\partial \overline{q}/\partial y) \left(\Psi_i^2 + \Psi_r^2 \right) = 0 \end{aligned} \tag{7.58}$$

Using the chain rule of differentiation, (7.58) can be expressed in the form

$$\begin{aligned} &\rho_0 \frac{\partial}{\partial y} \left[\Psi_i \frac{\partial \Psi_r}{\partial y} - \Psi_r \frac{\partial \Psi_i}{\partial y} \right] + \frac{\partial}{\partial z^*} \left[\varepsilon \rho_0 \left(\Psi_i \frac{\partial \Psi_r}{\partial z^*} - \Psi_r \frac{\partial \Psi_i}{\partial z^*} \right) \right] \\ &\quad - \rho_0 \delta_i (\partial \overline{q}/\partial y) \left(\Psi_i^2 + \Psi_r^2 \right) = 0 \end{aligned} \tag{7.59}$$

The first term in brackets in (7.59) is a perfect differential in y; the second term is a perfect differential in z^*. Thus, if (7.59) is integrated over the y, z^* domain, the result can be expressed as

$$\begin{aligned} &\int_0^\infty \left[\Psi_i \frac{\partial \Psi_r}{\partial y} - \Psi_r \frac{\partial \Psi_i}{\partial y} \right]_{-L}^{+L} \rho_0 dz^* + \int_{-L}^{+L} \left[\varepsilon \rho_0 \left(\Psi_i \frac{\partial \Psi_r}{\partial z^*} - \Psi_r \frac{\partial \Psi_i}{\partial z^*} \right) \right]_0^\infty dy \\ &\quad = \int_{-L}^{+L} \int_0^\infty \rho_0 \delta_i \frac{\partial \overline{q}}{\partial y} \left(\Psi_i^2 + \Psi_r^2 \right) dy dz^* \end{aligned} \tag{7.60}$$

However, from (7.51) $\Psi_i = \Psi_r = 0$ at $y = \pm L$ so that the first integral in (7.60) vanishes. Furthermore, if Ψ remains finite as $z^* \to \infty$, the contribution to the second integral of (7.60) at the upper boundary vanishes. If we then use (7.57) to eliminate the vertical derivatives in this term at the lower boundary, (7.60) can be expressed as

$$c_i \left[\int_{-L}^{+L} \int_0^{\infty} \frac{\partial \overline{q}}{\partial y} \frac{\rho_0 |\Psi|^2}{|\overline{u} - c|^2} dy dz^* - \int_{-L}^{+L} \varepsilon \frac{\partial \overline{u}}{\partial z^*} \frac{\rho_0 |\Psi|^2}{|\overline{u} - c|^2} \bigg|_{z^*=0} dy \right] = 0 \qquad (7.61)$$

where $|\Psi|^2 = \Psi_r^2 + \Psi_i^2$ is the disturbance amplitude squared.

Equation (7.61) has important implications for the stability of quasi-geostrophic perturbations. For unstable modes, c_i must be nonzero, and thus the quantity in square brackets in (7.61) must vanish. Because $|\Psi|^2/|\overline{u} - c|^2$ is nonnegative, instability is possible only when $\partial \overline{u}/\partial z^*$ at the lower boundary and $(\partial \overline{q}/\partial y)$ in the whole domain satisfy certain constraints:

1. If $\partial \overline{u}/\partial z^*$ at $z^* = 0$ (which by thermal wind balance implies that the meridional temperature gradient vanishes at the boundary), the second integral in (7.61) vanishes. Thus, the first integral must also vanish for instability to occur. This can occur only if $\partial \overline{q}/\partial y$ changes sign within the domain (i.e., $\partial \overline{q}/\partial y = 0$ somewhere). This is referred to as the *Rayleigh necessary condition* and is another demonstration of the fundamental role played by potential vorticity. Because $\partial \overline{q}/\partial y$ is normally positive, it is clear that in the absence of temperature gradients at the lower boundary, a region of negative meridional potential vorticity gradients must exist in the interior for instability to be possible.
2. If $\partial \overline{q}/\partial y \geq 0$ everywhere, then it is necessary that $\partial \overline{u}/\partial z^* > 0$ somewhere at the lower boundary for $c_i > 0$.
3. If $\partial \overline{u}/\partial z^* < 0$ everywhere at $z^* = 0$, then it is necessary that $\partial \overline{q}/\partial y < 0$ somewhere for instability to occur. Thus, there is an asymmetry between westerly and easterly shear at the lower boundary, with the former more favorable for baroclinic instability.

The basic state potential vorticity gradient in (7.49) can be written in the form

$$\frac{\partial \overline{q}}{\partial y} = \beta - \frac{\partial^2 \overline{u}}{\partial y^2} + \frac{\varepsilon}{H} \frac{\partial \overline{u}}{\partial z^*} - \varepsilon \frac{\partial^2 \overline{u}}{\partial z^{*2}} - \frac{\partial \varepsilon}{\partial z^*} \frac{\partial \overline{u}}{\partial z^*}$$

Because β is positive everywhere, if ε is constant a negative basic state potential vorticity gradient can occur only for strong positive mean flow curvature (i.e., $\partial^2 \overline{u}/\partial y^2$ or $\partial^2 \overline{u}/\partial z^{*2} \gg 0$) or strong negative vertical shear ($\partial \overline{u}/\partial z^* \ll 0$). Strong positive meridional curvature can occur at the core of an easterly jet or on the flanks of a westerly jet. Instability associated with such horizontal curvature is referred to as *barotropic instability*. The normal baroclinic instability in midlatitudes is associated with mean flows in which $\partial \overline{q}/\partial y > 0$ and $\partial \overline{u}/\partial z^* > 0$ at the ground. Hence, a mean meridional temperature gradient at the ground is essential for the existence of such instability. Baroclinic instability can also be excited at the tropopause because of the rapid decrease of ε with height if there is a sufficiently strong easterly mean wind shear to cause a local reversal in the mean potential vorticity gradient.

7.4.3 The Eady Stability Problem

This section analyzes the structures (eigenfunctions) and growth rates (eigenvalues) for unstable modes in the simplest possible model that satisfies the necessary conditions for instability in a continuous atmosphere given in the previous subsection. For simplicity, we make the following assumptions:

- Basic state density constant (Boussinesq approximation).
- f-plane geometry ($\beta = 0$).
- $\partial \overline{u}/\partial z^* = \Lambda = \text{constant}$.
- Rigid lids at $z^* = 0$ and H.

These conditions are only a crude model of the atmosphere, but provide a first approximation for study of the dependence of vertical structure on horizontal scale and stability. Despite the zero mean potential vorticity in the domain, the Eady model satisfies the necessary conditions for instability discussed in the previous subsection because vertical shear of the basic state mean flow at the upper boundary provides an additional term in (7.61) that is equal and opposite to the lower boundary integral.

Using the aforementioned approximations, the quasi-geostrophic potential vorticity equation is

$$\left(\frac{\partial}{\partial t} + \overline{u}\frac{\partial}{\partial x}\right) q' = 0 \tag{7.62}$$

where the perturbation potential vorticity is given by

$$q' = \nabla_h \psi' + \varepsilon \frac{\partial^2 \psi}{\partial z^{*2}} \tag{7.63}$$

and $\varepsilon \equiv f_0^2/N^2$. The thermodynamic energy equation at the horizontal boundaries ($z^* = 0, H$) is

$$\left(\frac{\partial}{\partial t} + \overline{u}\frac{\partial}{\partial x}\right) T' = 0 \tag{7.64}$$

Letting

$$\begin{aligned} \psi'\left(x, y, z^*, t\right) &= \Psi\left(z^*\right) \cos ly \exp\left[ik\left(x - ct\right)\right] \\ \overline{u}\left(z^*\right) &= \Lambda z^* \end{aligned} \tag{7.65}$$

where as in the previous subsection $\Psi(z^*)$ is a complex amplitude and c a complex phase speed, and substituting from (7.65) into (7.62) we find that

$$\left(\overline{u} - c\right) q' = 0 \tag{7.66}$$

From (7.66) we see that either $q' = 0$ or $\overline{u} - c = 0$. Since $\overline{u} = \Lambda z^*$, $\overline{u} - c = 0$ allows for nonzero q' only at the level where the wave speed matches the flow speed. Moreover, since $\overline{u}$ is strictly real, the wave speed in this case must be as well, so this particular solution branch describes singular neutral modes (spikes of PV at the steering level of the wave). They are useful for describing the evolution of potential vorticity disturbances in the Eady model, but they do not describe instability. Therefore, unstable modes must have $q' = 0$, which from (7.63) implies that the vertical structure is given by the solution of the second-order differential equation

$$\frac{d^2\Psi}{dz^{*2}} - \alpha^2\Psi = 0 \tag{7.67}$$

where $\alpha^2 = \left(k^2 + l^2\right)/\varepsilon$. A similar substitution into (7.64) yields the boundary conditions

$$\left(\Lambda z^* - c\right) d\Psi/dz^* - \Psi\Lambda = 0, \quad \text{at } z^* = 0, H \tag{7.68}$$

valid for rigid horizontal boundaries ($w^* = 0$) at the surface ($z^* = 0$) and the tropopause ($z^* = H$).

The general solution of (7.67) can be written in the form

$$\Psi\left(z^*\right) = A\sinh\alpha z^* + B\cosh\alpha z^* \tag{7.69}$$

Substituting from (7.69) into the boundary conditions (7.68) for $z^* = 0$ and H yields a set of two linear homogeneous equations in the amplitude coefficients A and B:

$$-c\alpha A - B\Lambda = 0$$
$$\alpha(\Lambda H - c)(A\cosh\alpha H + B\sinh\alpha H) - \Lambda(A\sinh\alpha H + B\cosh\alpha H) = 0$$

As in the two-layer model, a nontrivial solution exists only if the determinant of the coefficients of A and B vanishes. Again, this leads to a quadratic equation in the phase speed c. The solution (see Problem 7.12) has the form

$$c = \frac{\Lambda H}{2} \pm \frac{\Lambda H}{2}\left[1 - \frac{4\cosh\alpha H}{\alpha H\sinh\alpha H} + \frac{4}{\alpha^2 H^2}\right]^{1/2} \tag{7.70}$$

Thus

$$c_i \neq 0 \quad \text{if} \quad 1 - \frac{4\cosh\alpha H}{\alpha H\sinh\alpha H} + \frac{4}{\alpha^2 H^2} < 0$$

and the flow is then baroclinically unstable. When the quantity in square brackets in (7.70) is equal to zero, the flow is said to be *neutrally stable*. This condition occurs for $\alpha = \alpha_c$ where

$$\alpha_c^2 H^2/4 - \alpha_c H\left(\tanh\alpha_c H\right)^{-1} + 1 = 0 \tag{7.71}$$

Using the identity

$$\tanh \alpha_c H = 2 \tanh\left(\frac{\alpha_c H}{2}\right) \Big/ \left[1 + \tanh^2\left(\frac{\alpha_c H}{2}\right)\right]$$

we can factor (7.71) to yield

$$\left[\frac{\alpha_c H}{2} - \tanh\left(\frac{\alpha_c H}{2}\right)\right]\left[\frac{\alpha_c H}{2} - \coth\left(\frac{\alpha_c H}{2}\right)\right] = 0 \qquad (7.72)$$

Thus, the critical value of α is given by $\alpha_c H/2 = /\coth(\alpha_c H/2)$, which implies $\alpha_c H \cong 2.4$. Hence, instability requires $\alpha < \alpha_c$ or

$$\left(k^2 + l^2\right) < \left(\alpha_c^2 f_0^2 / N^2\right) \approx 5.76 / L_R^2$$

where $L_R \equiv NH/f_0 \approx 1000$ km is the Rossby *radius of deformation* for a continuously stratified fluid—compare to λ^{-1} defined just below equation (7.16). For waves with equal zonal and meridional wave numbers ($k = l$), the wavelength AQ:1
of maximum growth rate turns out to be

$$L_m = 2\sqrt{2}\pi L_R / (H\alpha_m) \cong 5500 \text{ km}$$

where α_m is the value of α for which kc_i is a maximum.

Substituting this value of α into the solution for the vertical structure of the streamfunction (7.69) and using the lower boundary condition to express the coefficient B in terms of A, we can determine the vertical structure of the most unstable mode. As shown in Figure 7.10, trough and ridge axes slope westward with height, in agreement with the requirements for extraction of available potential energy from the mean flow. The axes of the warmest and coldest air, however, tilt eastward with height, a result that could not be determined from the two-layer model where temperature was given at a single level. Furthermore, Figures 7.10a and 7.10b show that east of the upper-level trough axis, where the perturbation meridional velocity is positive, the vertical velocity is also positive. Thus, parcel motion is poleward and upward in the region where $\theta' > 0$. Conversely, west of the upper-level trough axis parcel motion is equatorward and downward where $\theta' < 0$. Both cases are thus consistent with the energy-converting parcel trajectory slopes shown earlier in Figure 7.8.

Although the Eady model yields unstable solutions that resemble the baroclinic waves that dominate the statistics of midlatitude eddy fields, individual cyclone events are highly localized and often develop at a faster rate than described by the growth rate of the most unstable mode. Both issues are resolved by considering initial value problems for finite-amplitude, *localized*, upper-level initial disturbances, as are often observed to precede the development of surface cyclones. Figure 7.11 shows the development of a surface cyclone from a

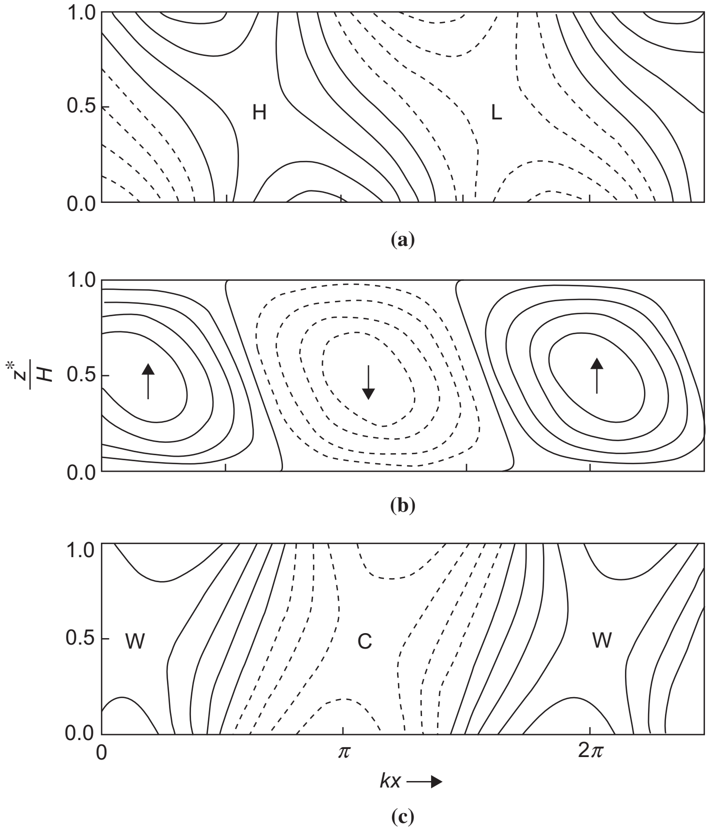

FIGURE 7.10 Properties of the most unstable Eady wave. (a) Contours of perturbation geopotential height; "H" and "L" designate ridge and trough axes, respectively. (b) Contours of vertical velocity; *up* and *down arrows* designate axes of maximum upward and downward motion, respectively. (c) Contours of perturbation temperature; "W" and "C" designate axes of warmest and coldest temperatures, respectively. In all panels 1 and 1/4 wavelengths are shown for clarity.

localized initial disturbance. Note that, after 48 hours, the full nonlinear solution resembles a mature extratropical cyclone, with warm air moving poleward and cold air moving equatorward around an area of low pressure. The linear solution for only the unstable growing modes approximates the full nonlinear solution and shows that the development may be explained by the projection of the initial disturbance onto only the unstable modes. Nonlinear effects relate to the poleward drift of the surface cyclone because of the interaction of the surface and upper-level PV anomalies and details of the development of the surface cold and warm fronts. Although the unstable modes are sufficient to explain the development of surface cyclones, it turns out that *transient* development is also possible, even when all the modes are neutral.

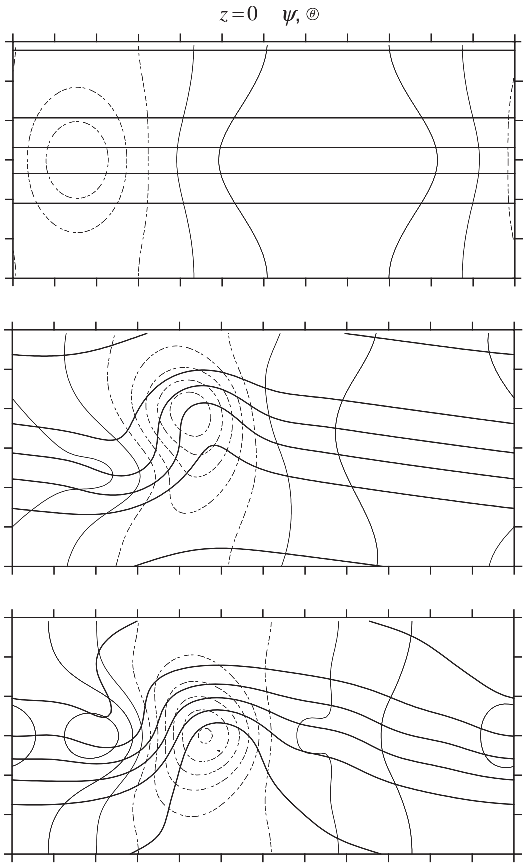

FIGURE 7.11 Development of a spatially localized disturbance in an idealized westerly jet stream. *Dashed lines* show pressure every 4 hPa and *solid lines* show potential temperature every 5 K. An initial surface disturbance (*top panel*) associated with an upper-level PV anomaly evolves into a well-developed extratropical cyclone 48 h later (*middle panel*). The linear solution for only the projection of the initial disturbance onto the unstable normal modes (*bottom panel*) captures most of the development of the full nonlinear solution. (*Adapted from Hakim, 2000. Copyright © American Meteorological Society. Reprinted with permission.*)

7.5 GROWTH AND PROPAGATION OF NEUTRAL MODES

As suggested earlier, baroclinic wave disturbances with certain favorable initial configurations may amplify rapidly even in the absence of baroclinic instability. Although the theory for the optimal initial perturbations that give rise to rapid transient growth is beyond the scope of this book, the main ideas can be exposed mathematically and illustrated with an example from the two-layer model.

A central concept for growth involves a metric, which is needed to measure the amplitude of disturbances; we call this measure a *norm*. A familiar example is the magnitude of a scalar z, $|z|$, which gives the absolute value for real-valued z. For complex-valued $z = a+ib$, the magnitude gives the length of a vector on the complex plane, as defined by $|z| = (z^*z)^{1/2} = (a^2+b^2)^{1/2}$, where the asterisk denotes a complex conjugate. For *functions*, we adopt a natural extension of this definition:

$$|f| = [\langle f, f\rangle]^{1/2} \tag{7.73}$$

where, for functions of a single independent variable, x,

$$\langle f, g\rangle = \int f^* g\, dx \tag{7.74}$$

is an *inner product* that gives a scalar result. In particular, for $g = f$, (7.74) reveals that $|f|^2$ gives the integral over f^*f, which is a continuous analog of the sum of squared scalar components for complex numbers discussed previously. We define *amplification* over a time interval as the ratio of the norm at the time of interest, t, to the norm at the initial time, t_0:

$$A = \frac{|f|_t}{|f|_{t_0}} \tag{7.75}$$

Consider the normal modes of the Eady model, which have the form (dropping the prime)

$$\psi = \Psi(z^*)\, e^{i\phi}\, e^{kc_it} \tag{7.76}$$

where $\phi = k(x - c_rt)$ and c_r and c_i are the real and imaginary parts of the phase speed, respectively. The amplification of a single normal mode, as defined by (7.75), for $t_0 = 0$ is given by

$$\left[\frac{\iint \Psi^* e^{-i\phi} e^{kc_it}\, \Psi e^{i\phi} e^{kc_it}\, dxdz}{\iint \Psi^* e^{-ikx}\, \Psi e^{ikx}\, dxdz}\right]^{1/2} = \left[e^{2kc_it} \frac{\iint \Psi^*\Psi\, dxdz}{\iint \Psi^*\Psi\, dxdz}\right]^{1/2} = e^{kc_it} \tag{7.77}$$

For neutral modes $c_i = 0$ and $A = 1$; otherwise, amplitude grows or decays exponentially depending on the sign of c_i. Note that, because of the space and time separation in (7.76), any function of the spatial structure of the normal modes (e.g., potential vorticity) amplifies at the same rate given by (7.77). This means that, for a single mode, the exponential growth found in (7.77) is independent of the norm.

Consider now the sum of two *neutral* modes, $\psi_1 + \psi_2$. In this case, amplification is given by

$$\left[\frac{\langle\psi_1+\psi_2, \psi_1+\psi_2\rangle_t}{\langle\psi_1+\psi_2, \psi_1+\psi_2\rangle_{t_0}}\right]^{1/2} = \left[\frac{\langle\psi_1, \psi_1\rangle_t + \langle\psi_2, \psi_2\rangle_t + 2\langle\psi_1, \psi_2\rangle_t}{\langle\psi_1, \psi_1\rangle_{t_0} + \langle\psi_2, \psi_2\rangle_{t_0} + 2\langle\psi_1, \psi_2\rangle_{t_0}}\right]^{1/2} \tag{7.78}$$

where we have used the fact that $\langle f, g\rangle = \langle g, f\rangle^*$. Since the modes are neutral, $\langle \psi_1, \psi_1\rangle$ and $\langle \psi_2, \psi_2\rangle$ are constants, and amplification is determined by the term

$$\langle \psi_1, \psi_2\rangle_t = e^{ik(c_1-c_2)t} \iint \Psi_1^* \Psi_2 \, dxdz \tag{7.79}$$

This shows that if the modes are *orthogonal in the chosen norm*—that is,

$$\iint \Psi_1^* \Psi_2 \, dxdz = 0 \tag{7.80}$$

then there is no amplification. On the other hand, if the modes are not orthogonal, then the amplitude fluctuates periodically proportional to the difference in the phase speeds of the modes. A physical interpretation is that, because the modes move relative to one another, there are times when the sum gives an upshear-tilted disturbance[3] and the amplitude of the sum increases. Eventually, the relationship changes so that the modes tilt downshear and the amplitude of the sum decreases. Therefore, the amplification effect is transient and depends on the chosen norm. In contrast, the unstable normal modes grow exponentially for all time, and measures of amplification do not depend on the norm.

7.5.1 Transient Growth of Neutral Waves

Consider now a specific example for the two-layer model of Section 7.2. If we neglect the β effect, let $U_m = 0$, and assume that $k^2 > 2\lambda^2$, the two-layer model has two oppositely propagating neutral solutions given by (7.24) with zonal phase speeds

$$c_1 = +U_T\mu; \quad c_2 = -U_T\mu \tag{7.81}$$

where

$$\mu = \left[\frac{k^2 - 2\lambda^2}{k^2 + 2\lambda^2}\right]^{1/2}$$

Then from (7.17) a disturbance consisting of these two modes can be expressed as

$$\psi_m = A_1 \exp\left[ik\left(x - c_1 t\right)\right] + A_2 \exp\left[ik\left(x - c_2 t\right)\right] \tag{7.82a}$$

$$\psi_T = B_1 \exp\left[ik\left(x - c_1 t\right)\right] + B_2 \exp\left[ik\left(x - c_2 t\right)\right] \tag{7.82b}$$

but from (7.18)

$$c_1 A_1 - U_T B_1 = 0; \quad c_2 A_2 - U_T B_2 = 0$$

[3] This interpretation is based on energy, which, as shown in Section 7.3.2, is proportional to ψ^2.

So that with the aid of (7.81)

$$B_1 = \mu A_1; \quad B_2 = -\mu A_2 \tag{7.83}$$

For an initial disturbance confined entirely to the upper level, it is easily verified that $\psi_m = \psi_T$ ($\psi_1 = 2\psi_m$ and $\psi_3 = 0$). Thus, initially $A_1 + A_2 = B_1 + B_2$, and substituting from (7.83) gives

$$A_2 = -A_1 \left[(1-\mu)/(1+\mu)\right]$$

Hence, if A_1 is real, the streamfunctions of (7.82a,b) can be expressed as

$$\begin{aligned}\psi_m(x,t) &= A_1\left[\cos\left[k\left(x-\mu U_T t\right)\right] - \frac{(1-\mu)}{(1+\mu)}\cos\left[k\left(x+\mu U_T t\right)\right]\right] \\ &= \frac{2\mu A_1}{(1+\mu)}\left[\cos kx \cos\left(k\mu U_T t\right) + \frac{1}{\mu}\sin kx \sin\left(k\mu U_T t\right)\right]\end{aligned} \tag{7.84a}$$

$$\begin{aligned}\psi_T(x,t) &= \mu A_1\left[\cos\left[k\left(x-\mu U_T t\right)\right] + \frac{(1-\mu)}{(1+\mu)}\cos\left[k\left(x+\mu U_T t\right)\right]\right] \\ &= \frac{2\mu A_1}{(1+\mu)}\left[\cos kx \cos\left(k\mu U_T t\right) + \mu \sin kx \sin\left(k\mu U_T t\right)\right]\end{aligned} \tag{7.84b}$$

The first forms on the right side in (7.84a,b) show that for small μ the barotropic mode initially consists of two waves of nearly equal amplitude that are 180° out of phase so that they nearly cancel, whereas the baroclinic mode initially consists of two very weak waves that are in phase.

As time advances, the two oppositely propagating barotropic modes begin to reinforce each other, leading to a maximum-amplitude trough 90° to the east of the initial trough at time $t_m = \pi/(2k\mu U_T)$. From (7.84) the baroclinic and barotropic modes at time t_m are then

$$\begin{aligned}(\psi_m)_{\max} &= 2A_1(1+\mu)^{-1}\sin kx \\ (\psi_T)_{\max} &= 2A_1\mu^2(1+\mu)^{-1}\sin kx\end{aligned} \tag{7.85a,b}$$

from which it is shown easily that

$$(\psi_1)_{\max} = 2A_1\left(1+\mu^2\right)(1+\mu)^{-1}\sin kx; \quad (\psi_3)_{\max} = 2A_1(1-\mu)\sin kx$$

so that for small μ the resulting disturbance is nearly barotropic. Thus, the initial disturbance not only amplifies but spreads in the vertical. The time for growth to maximum amplitude is inversely proportional to the basic state thermal wind; the maximum amplitude, however, depends only on the initial amplitude and the parameter μ.

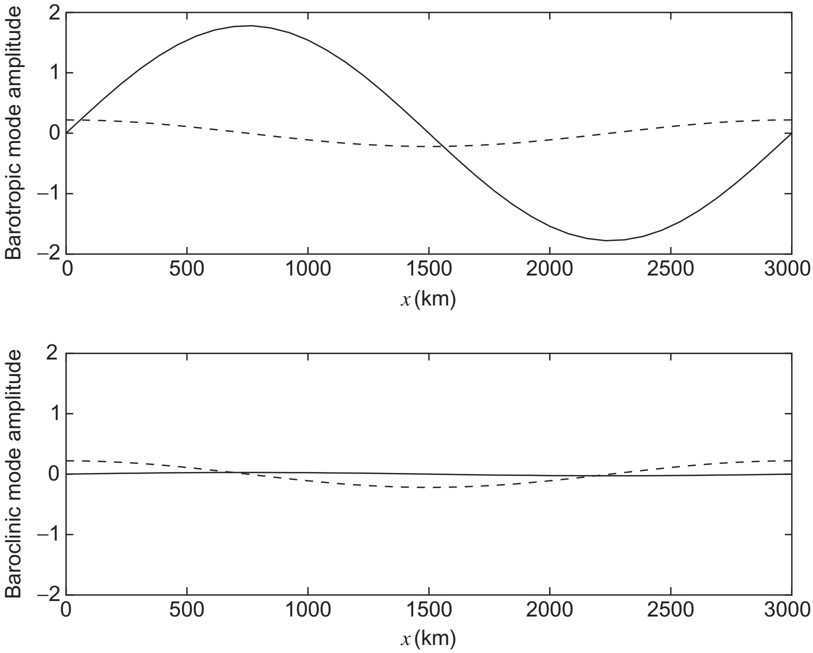

FIGURE 7.12 Zonal distribution of the amplitude of a transient neutral disturbance initially confined entirely to the upper layer in the two-layer model. *Dashed lines* show the initial distribution of the baroclinic and barotropic modes; *solid lines* show the distribution at the time of maximum amplification.

Figure 7.12 shows the initial and maximum amplitudes of the barotropic and baroclinic streamfunctions for $f_0 = 10^{-4}\ \mathrm{s}^{-1}$, $\sigma = 2 \times 10^{-6}\ \mathrm{m}^2\,\mathrm{Pa}^{-2}\,\mathrm{s}^{-2}$, $U_T = 35\ \mathrm{m\,s}^{-1}$, and a zonal wavelength of 3000 km. In this case, the amplitude of the barotropic disturbance increases by a factor of 8 in about 48 h. Although the most unstable normal mode for these conditions amplifies by a similar amount in less than 1 day, if the initial upper-level neutral disturbance has a velocity amplitude of a few meters per second, its growth on the time scale of a few days may dominate over a normal mode instability that grows exponentially from a much smaller initial perturbation.

As with normal mode baroclinic instability, the energy source for the transient amplification of the neutral modes is conversion of the available potential energy of the mean flow into disturbance potential energy by meridional temperature advection, followed immediately by conversion to disturbance kinetic energy by the secondary vertical circulation. This secondary circulation has a vertical velocity field that lags the upper-level streamfunction field by 90° phase. Maximum upward motion and lower-level convergence thus occur to the west of the initial upper-level ridge, and maximum downward motion and lower-level divergence occur west of the initial upper-level trough. Vorticity tendencies associated with this convergence and divergence pattern partly balance the eastward vorticity advection at the upper level and also act to produce a lower-level trough to the east of the initial upper-level trough and lower-level ridge to the east of the initial upper-level ridge. The result is that a pattern of nearly barotropic troughs and ridges develops 90° to the east of the initial trough and ridge pattern. Unlike normal mode instability, the growth in this case does not continue indefinitely. Rather, for a given value of μ the maximum growth occurs at the time for which $t_m = \pi/(2kU_T\mu)$. As the zonal wave number approaches the short-wave instability cutoff, the total amplification increases, but the amplification time also increases.

7.5.2 Downstream Development

It was noted in Section 7.2.2 that under some circumstances the zonal group velocity may exceed the zonal phase speed so that the energy of a wave group propagates faster than the individual wave disturbances. This dispersion effect is demonstrated for barotropic Rossby waves in Problem 5.15. The β effect is not necessary, however, for the development of new disturbances to occur downstream of the original wave disturbances on the synoptic scale. The two-layer channel model with constant Coriolis parameter can be used to demonstrate the process of dispersion and downstream development of neutral waves in a simple context.

Expressed in terms of wave frequency, the dispersion relation of (7.24) becomes

$$\nu = kU_m \pm k\mu U_T \tag{7.86}$$

where μ is defined below (7.81). The corresponding group velocity is then

$$c_{gx} = \frac{\partial \nu}{\partial k} = U_m \pm U_T\mu\left(1 + \frac{4k^2\lambda^2}{k^4 - 4\lambda^4}\right) \tag{7.87}$$

Comparison of (7.87) with (7.81) shows that relative to the mean zonal flow the group velocity exceeds the phase velocity by the factor in parentheses on the right side of (7.87) for both eastward- and westward-directed neutral modes. For example, if $k^2 = 2\lambda^2(1+\sqrt{2})$, the group velocity equals twice the phase speed, which is the situation shown schematically earlier in Figure 7.4.

Observations of baroclinic waves in the midlatitude storm tracks show clearly the downstream development of wave energy. For example, over the North Pacific ocean, the baroclinic wave phase speed is about 10 m s^{-1}, while the group speed is about 30^{-1} (Figure 7.13). As a result, the impact of extratropical cyclones that develop near the Asian coastline may be felt along the West Coast of North America in three days, even though the initial disturbance may take five days to reach the middle Pacific during its decay phase.

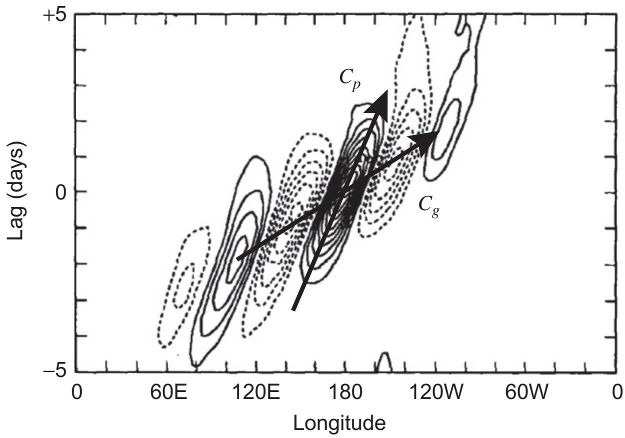

FIGURE 7.13 Time-series correlation of meridional wind as a function of longitude and time lag. Correlation is shown every 0.1 unit (i.e., a unitless number between −1 and 1), with the reference time series at 180. Results are averaged over 30 to 60°N latitude during winter. (*From Chang, 1993. Copyright © American Meteorological Society. Reprinted with permission.*)

SUGGESTED REFERENCES

Charney (1947) is the classic paper on baroclinic instability. The mathematical level is advanced, but Charney's paper contains an excellent qualitative summary of the main results that is very readable.

Hoskins, McIntyre, and Robertson (1985) discuss cyclogenesis and baroclinic instability from a potential vorticity perspective.

Pedlosky, *Geophysical Fluid Dynamics* (2nd ed.), contains a thorough treatment of normal mode baroclinic instability at a mathematically advanced level.

Pierrehumbert and Swanson (1995) review numerous aspects of baroclinic instability, including spatiotemporal development.

Vallis, *Atmospheric and Oceanic Fluid Dynamics: Fundamentals and Large-Scale Circulation*, covers topics in baroclinic instability similar to those considered here.

PROBLEMS

7.1. Show using (7.25) that the maximum growth rate for baroclinic instability when $\beta = 0$ occurs for

$$k^2 = 2\lambda^2\left(\sqrt{2} - 1\right)$$

How long does it take the most rapidly growing wave to amplify by a factor of e^1 if $\lambda^2 = 2 \times 10^{-12}\,\text{m}^{-1}$ and $U_T = 20\,\text{m s}^{-1}$?

7.2. Solve for ψ_3' and ω_2' in terms of ψ_1' for a baroclinic Rossby wave whose phase speed satisfies (7.23). Explain the phase relationship among ψ_1', ψ_3', ω_2' and in terms of the quasi-geostrophic theory. (Note that $U_T = 0$ in this case.)

7.3. For the case $U_1 = -U_3$ and $k^2 = \lambda^2$, solve for ψ_3' and ω_2' in terms of ψ_1' for marginally stable waves—that is, $\delta = 0$ in (7.21).

7.4. For the case $\beta = 0, k^2 = \lambda^2$, and $U_m = U_T$, solve for ψ_3' and ω_2' in terms of ψ_1'. Explain the phase relationships among ω_2', ψ_1', and ψ_3' in terms of the energetics of quasi-geostrophic waves for the amplifying wave.

7.5. Suppose that a baroclinic fluid is confined between two rigid horizontal lids in a rotating tank in which $\beta = 0$, but friction is present in the form of linear drag proportional to the velocity (i.e., $\mathbf{Fr} = -\mu\mathbf{V}$). Show that the two-level model perturbation vorticity equations in Cartesian coordinates can be written as

$$\left(\frac{\partial}{\partial t} + U_1\frac{\partial}{\partial x} + \mu\right)\frac{\partial^2 \psi_1'}{\partial x^2} - \frac{f}{\delta p}\omega_2' = 0$$

$$\left(\frac{\partial}{\partial t} + U_3\frac{\partial}{\partial x} + \mu\right)\frac{\partial^2 \psi_3'}{\partial x^2} + \frac{f}{\delta p}\omega_2' = 0$$

where perturbations are assumed in the form given in (7.8). Assuming solutions of the form (7.17), show that the phase speed satisfies a relationship similar to (7.21) with β replaced everywhere by $i\mu k$, and that as a result the condition for baroclinic instability becomes

$$U_T > \mu\left(2\lambda^2 - k^2\right)^{-1/2}$$

7.6. For the case $\beta = 0$ determine the phase difference between the 250- and 750-hPa geopotential fields for the most unstable baroclinic wave (see Problem 7.1). Show that the 500-hPa geopotential and thickness fields (ψ_m, ψ_T) are 90° out of phase.

7.7. For the conditions of Problem 7.6, given that the amplitude of ψ_m is $A = 10^7\,\text{m}^2\,\text{s}^{-1}$, solve the system (7.18) and (7.19) to obtain B. Let $\lambda^2 = 2.0 \times 10^{-12}\,\text{m}^{-2}$ and $U_T = 15\,\text{m}\,\text{s}^{-1}$. Use your results to obtain expressions for ψ_1' and ψ_3'.

7.8. For the situation of Problem 7.7, compute ω_2' using (7.28).

7.9. Compute the total potential energy per unit cross-sectional area for an atmosphere with an adiabatic lapse rate given that the temperature and pressure at the ground are $p = 10^5$ Pa and $T = 300$ K, respectively.

7.10. Consider two air masses at the uniform potential temperatures $\theta_1 = 320$ K and $\theta_2 = 340$ K that are separated by a vertical partition as shown in Figure 7.7. Each air mass occupies a horizontal area of 10^4 m^2 and extends from the surface ($p_0 = 10^5$ Pa) to the top of the atmosphere. What is the available potential energy for this system? What fraction of the total potential energy is available in this case?

7.11. For the unstable baroclinic wave that satisfies the conditions given in Problems 7.7 and 7.8, compute the energy conversion terms in (7.37) and (7.38) and thus obtain the instantaneous rates of change of the perturbation kinetic and available potential energies.

7.12. Starting with (7.62) and (7.64), derive the phase speed c for the Eady wave given in (7.70).

7.13. Unstable baroclinic waves play an important role in the global heat budget by transferring heat poleward. Show that for the Eady wave solution the poleward heat flux averaged over a wavelength,

$$\overline{v'T'} = \frac{1}{L}\int_0^L v'T'dx$$

is independent of height and is positive for a growing wave. How does the magnitude of the heat flux at a given instant change if the mean wind shear is doubled?

7.14. Assuming that the coefficient A in (7.69) is real, obtain an expression for the geostrophic streamfunction $\psi'(x, y, z^*, t)$ for the most unstable mode in the Eady stability problem for the case $k = l$. Use this result to derive an expression for the corresponding vertical velocity w^* in terms of A.

7.15. For the neutral baroclinic wave disturbance in the two-layer model given by (7.85a,b), derive the corresponding ω_2' field. Describe how the convergence and divergence fields associated with this secondary circulation influence the evolution of the disturbance.

7.16. For the situation of Problem 7.15, derive expressions for the conversion of zonal available potential energy to eddy available potential energy and the conversion of eddy available potential energy to eddy kinetic energy.

MATLAB Exercises

M7.1. By varying the input zonal wavelength in the MATLAB script **twolayer_model_1A.m**, find the shortest zonal wavelength for which the two-layer model is baroclinically unstable and the wavelength of maximum instability (i.e., most rapid growth rate) in the case where the basic state thermal wind is 15 m s^{-1}. The case given corresponds to the situation given in Section 7.2.1. The code of **twolayer_model_1B.m** differs only in that a finite meridional width is assumed with meridional wave number $m = \pi/(3000\,\text{km})$. Compare the zonal wavelengths for short-wave cutoff and for maximum growth rate for these two cases.

M7.2. Use the MATLAB script **twolayer_model_2A.m** to examine the transient growth associated with a disturbance that is initially entirely confined to the 250-hPa level. Let the basic state thermal wind be 25 m s^{-1}. By examining zonal wavelengths shorter than the instability cutoff determined in Exercise M7.1, find the zonal wavelength that gives the largest amplification of the disturbance. Repeat this exercise using the script **twolayer_model_2B.m**, which includes a meridional dependence with wave number $m = \pi/(3000\ \text{km})$. Note that the program will terminate if you choose a wavelength that is long enough to be baroclinically unstable. Discuss the vertical structure of the transiently growing stable modes. What sort of situation in the real atmosphere does this solution crudely model?

M7.3. The MATLAB script **twolayer_model_3b.m** shows the propagation of a wave packet composed of the sum of nine eastward propagating neutral waves of the two-layer model, ranging in wave number from 0.6 to 1.6 k, where $k = 2\pi/L$ and $L = 1850\,\text{km}$. Run the script and estimate from the animation the characteristic phase velocity and the characteristic group velocity for the cases of $U_T = 15$ and $30\,\mathrm{m\ s^{-1}}$.

M7.4. Suppose that a meridional dependence is included in the eddy fields in the two-layer model so that (7.17) becomes

$$\psi_m = A\cos(my)\, e^{ik(x-ct)}; \quad \psi_T = B\cos(my)\, e^{ik(x-ct)}$$

where $m = 2\pi/L_y$ and $L_y = 3000\,\mathrm{km}$. Determine the zonal wavelength of the most unstable wave. Solve for the fields ψ_m, ψ_T, and ω_2' and plot (x, y) cross-sections of these fields using the MATLAB script **contour_sample.m** as a template. *Hint:* The solutions in this case are similar to those of Problems 7.6 through 7.8 but with k^2 replaced by $k^2 + m^2$ everywhere.

M7.5. The MATLAB script **eady_model_1.m** shows vertical and meridional cross-sections of the solution for the Eady model (Section 7.4.3) for the most unstable wave mode at time $t = 0$. Modify this script to plot the solution for the Eady wave corresponding to the neutral stability condition given in (7.71). Explain the vertical structure in this case in terms of quasi-geostrophic theory.